Global Translational Medicine

ACCSCIENCE PUBLISHING

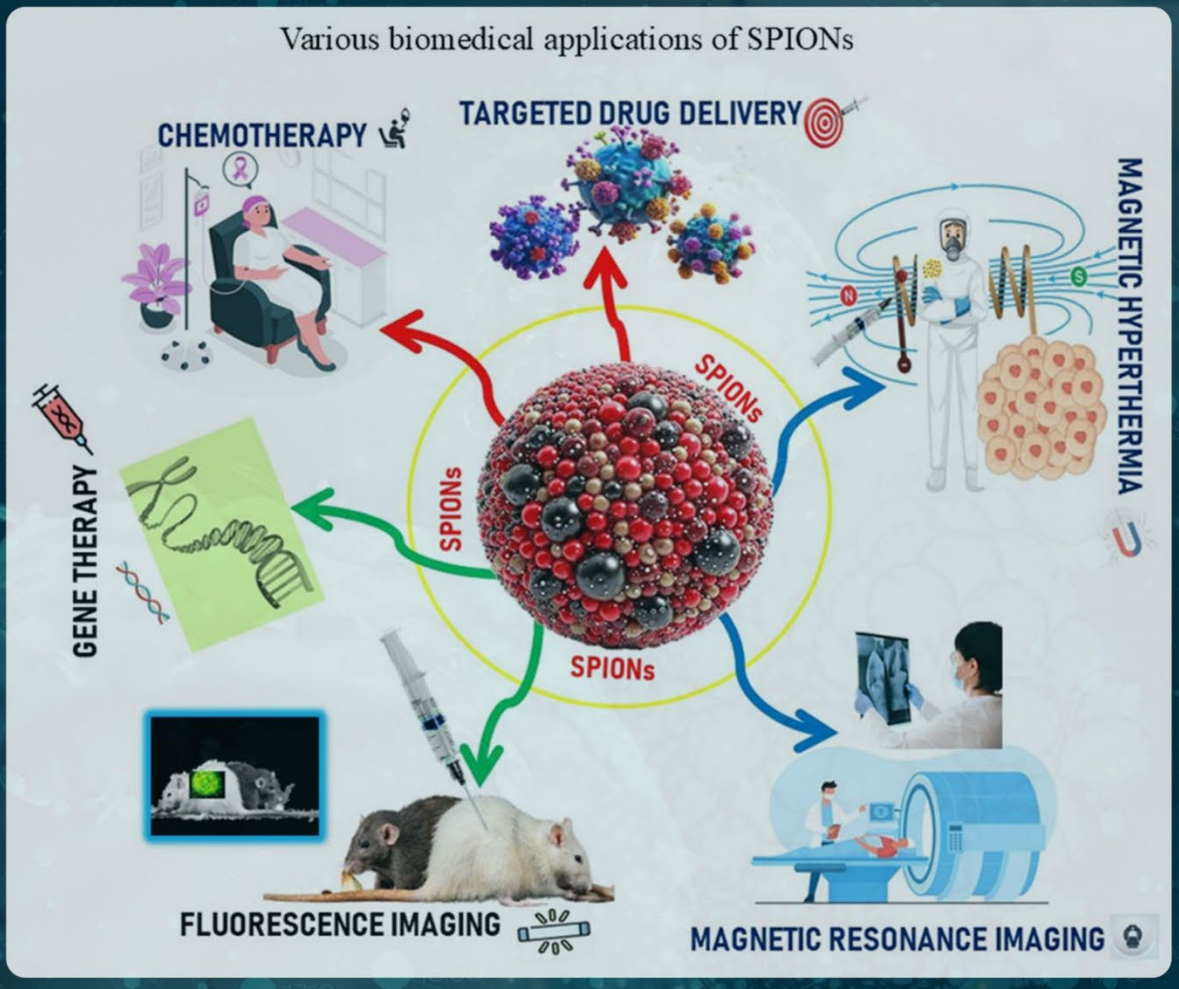

Superparamagnetic iron oxide nanoparticle-based nanosystems for cancer theranostics

ISSN: 3060-8600 (Print)
ISSN: 2811-0021 (Online)
Volume 4 · Issue 2
June 2025

Global Translational Medicine

Print ISSN: 3060-8600
Online ISSN: 2811-0021

Global Translational Medicine is a quarterly journal that focuses on medicine, biological sciences, and biomaterials engineering. *Global Translational Medicine* provides a platform to fill the gaps in preclinical and inter-disciplinary research, to promote clinical translation of scientific research results, and to contribute to the conception of new and improved preventive measures as well as diagnostic and therapeutic techniques of diseases.

About the Publisher

AccScience Publishing is a publishing company based in Singapore. We publish a range of high-quality, open-access, peer-reviewed journals and books from a broad spectrum of disciplines.

Contact Us

Managing Editor
gtm.office@accscience.sg

AccScience Publishing
9 Raffles Place, Republic Plaza 1 #06-00 Singapore 048619.

Volume 4 • Issue 2 • June 2025
ISSN 3060-8600 (print) ISSN 2811-0021 (online)

GLOBAL TRANSLATIONAL MEDICINE

ACCSCIENCE PUBLISHING

Access Science Without Barriers

GLOBAL TRANSLATIONAL MEDICINE

ISSN: 3060-8600 (print)
ISSN: 2811-0021 (online)

Editorial and Production Credits

Publisher: AccScience Publishing
Managing Editor: Lily Liu
Production Editor: Sharmila Velapasamy
Article Layout and Typeset: Sinjore Technologies (India)

For all advertising queries, contact gtm.office@accscience.sg.

Supplementary file

Supplementary files of articles can be obtained at https://accscience.com/journal/GTM/4/2.

About the Cover

An abstract illustration of human brain

Disclaimer

AccScience Publishing is not liable to the statements, perspectives, and opinions contained in the publications. The appearance of advertisements in the journal shall not be construed as a warranty, endorsement, or approval of the products or services advertised and/or the safety thereof. AccScience Publishing disclaims responsibility for any injury to persons or property resulting from any ideas or products referred to in the publications or advertisements. AccScience Publishing remains neutral with regard to jurisdictional claims in published maps and institutional affiliations.

Global Translational Medicine

Editorial Board

Assistant Editor

Youth Editorial Board Members

*Editorial Board Members as of June 19, 2025

ACCSCIENCE PUBLISHING

Volume 4 | Issue 2 | June 2025 | Page 1 – 108 |

Global Translational Medicine

https://accscience.com/journal/gtm

CONTENTS

ACCSCIENCE PUBLISHING

Global Translational Medicine

EDITORIAL

Adeno-associated virus as a powerful tool for gene therapy

Ling Yin*

Institute of Health and Medicine, Hefei Comprehensive National Science Center, Hefei, Anhui, China

(This article belongs to the *Special Issue: Gene Therapy Revolution in Cancer Immunology with Groundbreaking AAV Research*)

Gene therapy is a revolutionary new approach to treating genetic disorders by fixing errors in DNA, potentially with a single treatment.[1] The U.S. Food and Drug Administration (FDA) and European regulators were expected to approve up to 17 new gene therapies in 2024. These approvals include advances for rare diseases and even therapies that use cells to target illnesses more effectively.[2-4] One of the key tools for delivering these gene therapies is the adeno-associated virus (AAV), a type of virus that can insert corrected genes into specific tissues without causing strong immune responses. This technology has already helped restore vision for people with rare eye disorders and improve movement abilities for young children with severe muscle disease.[5]

AAV is a small, non-harmful virus discovered in the 1960s. It is employed to carry healthy genes into specific body tissues by virtue of several advantages, such as high specificity in cell targeting, long-lasting impact on the body, and minimal immune reactions.[6-8] This makes AAV the top choice for gene delivery in medical treatments. Four AAV therapies have already been approved in the U.S. to treat serious diseases such as certain eye and muscle disorders. AAV vectors present unique advantages, such as specific tissue tropism, high transduction efficiency, low immune responses, long-lasting gene expression, and staying unincorporated into the host chromosome, which make them the most popular viral gene delivery system in clinical trials to achieve long-term correction, addressing the unmet medical needs. Biallelic *RPE65* mutation-associated retinal dystrophy affects approximately 1,000 – 2,000 patients in the U.S. Biallelic mutation carriers are recognized for harboring a mutation in both copies of a particular gene.[9,10] Luxturna, an AAV2 vector for one-time gene therapy treatment of patients with established genetic vision loss due to Leber congenital amaurosis or retinitis pigmentosa, has become the first viral-based drug approved by the FDA in 2017.[11] After receiving treatment with Luxturna, patients with confirmed biallelic *RPE65* mutation-associated retinal dystrophy underwent vision restoration within several months. Children with spinal muscular atrophy (SMA) experience difficulty performing essential life functions and surviving past early childhood due to respiratory failure. Zolgensma, also known as AVXS-101, an AAV9 vector for one-time gene therapy treatment of pediatric SMA patients less than 2 years of age with biallelic mutations in the survival motor neuron 1 (*SMN1*) gene, was approved by the FDA in 2019.[12] After receiving treatment with Zolgensma, patients showed improvements in their ability to reach developmental motor milestones, such as head control and the ability to sit without support.

AAV's ability to transfer corrected genes directly into affected tissues without triggering severe immune reactions has opened doors for ground-breaking treatments. AAV vectors are widely applied in clinical delivery system due to their multiple unique advantages, as stated in the above, which allow for the successful delivery

***Corresponding author:**
Ling Yin
(lingyin@ihm.ac.cn)

Citation: Yin L. Adeno-associated virus as a powerful tool for gene therapy. *Global Transl Med*. 2025;4(2):1-2.
doi: 10.36922/GTM025120026

Received: March 17, 2025

Published online: April 4, 2025

and transfer of therapeutic genes in gene therapies for cancer, neurodegenerative diseases, retinal diseases, and COVID-19.[13-16] In light of our growing understanding of viral biology and the availability of diverse platforms, it is essential to optimize AAV vector delivery system in terms of capsid properties, production yield, packaging efficiency, immune response, biodistribution potential, and transduction safety, which are critical for the successful application and development of clinically approved therapy. Consequently, future research should focus on creating AI-driven tools for AAV capsid engineering and packaging capacity/immune response prediction methods evolving from the current basic programming to support the learning of more advanced concepts.

Conflict of interest

Ling Yin is the Guest Editor of this special issue. The author declared that he has no known competing financial interests or personal relationships that could have influenced the work reported in this paper.

References

1. Tang R, Xu Z. Gene therapy: A double-edged sword with great powers. *Mol Cell Biochem*. 2020;474(1-2):73-81.

   doi: 10.1007/s11010-020-03834-3

2. Rind DM. The FDA and gene therapy for duchenne muscular dystrophy. *JAMA*. 2024;331(20):1705-1706.

   doi: 10.1001/jama.2024.5613

3. Singh A, Irfan H, Fatima E, Nazir Z, Verma A, Akilimali A. Revolutionary breakthrough: FDA approves CASGEVY, the first CRISPR/cas9 gene therapy for sickle cell disease. *Ann Med Surg* (*Lond*). 2024;86(8):4555-4559.

   doi: 10.1097/MS9.0000000000002146

4. Anguela XM, High KA. Hemophilia b and gene therapy: A new chapter with etranacogene dezaparvovec. *Blood Adv.* 2024;8(7):1796-1803.

   doi: 10.1182/bloodadvances.2023010511

5. Gardin A, Ronzitti G. Current limitations of gene therapy for rare pediatric diseases: Lessons learned from clinical experience with AAV vectors. *Arch Pediatr.* 2023;30(8S1):8S46-8S52.

   doi: 10.1016/S0929-693X(23)00227-0

6. Naso MF, Tomkowicz B, Perry WL 3rd, Strohl WR. Adeno-associated virus (AAV) as a vector for gene therapy. *BioDrugs*. 2017;31(4):317-334.

   doi: 10.1007/s40259-017-0234-5

7. Asaad W, Volos P, Maksimov D, *et al.* AAV genome modification for efficient AAV production. *Heliyon.* 2023;9(4):e15071.

   doi: 10.1016/j.heliyon.2023.e15071

8. Tan F, Dong Y, Qi J, Yu W, Chai R. Artificial intelligence-based approaches for AAV vector engineering. *Adv Sci (Weinh).* 2025;12(9):e2411062.

   doi: 10.1002/advs.202411062

9. Maguire AM, Bennett J, Aleman EM, Leroy BP, Aleman TS. Clinical perspective: Treating rpe65-associated retinal dystrophy. *Mol Ther.* 2021;29(2):442-463.

   doi: 10.1016/j.ymthe.2020.11.029

10. Alsalloum A, Gornostal E, Mingaleva N, *et al.* A comparative analysis of models for AAV-mediated gene therapy for inherited retinal diseases. *Cells*. 2024;13(20):1706.

    doi: 10.3390/cells13201706

11. Pierce EA, Bennett J. The status of RPE65 gene therapy trials: Safety and efficacy. *Cold Spring Harb Perspect Med.* 2015;5:a017285.

    doi: 10.1101/cshperspect.a017285

12. Ogbonmide T, Rathore R, Rangrej SB, *et al.* Gene therapy for spinal muscular atrophy (SMA): A review of current challenges and safety considerations for onasemnogene abeparvovec (Zolgensma). *Cureus*. 2023;15(3):e36197.

    doi: 10.7759/cureus.36197

13. Yang H, Qing K, Keeler GD, *et al.* Enhanced transduction of human hematopoietic stem cells by AAV6 vectors: Implications in gene therapy and genome editing. *Mol Ther Nucleic Acids.* 2020;20:451-458.

    doi: 10.1016/j.omtn.2020.03.009

14. Yin L, Keeler GD, Zhang Y, *et al.* AAV3-mirna vectors for growth suppression of human hepatocellular carcinoma cells *in vitro* and human liver tumors in a murine xenograft model *in vivo*. *Gene Ther*. 2021;28:422-434.

    doi: 10.1038/s41434-020-0140-1

15. Zhu P, Dyka F, Ma X, *et al.* Disease mechanisms of x-linked cone dystrophy caused by missense mutations in the red and green cone opsins. *FASEB J.* 2021;35(10):e21927.

    doi: 10.1096/fj.202101066R

16. Glazkova DV, Bogoslovskaya EV, Urusov FA, *et al.* Generation of sars-cov-2 mouse model by transient expression of the human ace2 gene mediated by intranasal administration of aav-hace2. *Mol Biol (Mosk).* 2022;56:705-712.

    doi: 10.1134/S0026893322050065

ACCSCIENCE PUBLISHING

Global Translational Medicine

REVIEW ARTICLE

Revolutionizing drug response prediction: An unmet requirement for patients unresponsive to precision medicine

Chen Yeh*, Shu-Ti Lin, Andre Baranski, and Sharon Yeh

OncoDxRx, Los Angeles, California, United States of America

Abstract

Precision cancer therapies frequently fail due to tumors' evolving clonal diversity rather than drug efficacy. Even when initial treatment succeeds, resistance often emerges, leading to relapse. Clinicians then find themselves in the same cycle of repeating the process of testing a new drug until therapeutic exhaustion. The cycle escalates with each new treatment until no further options are available. The real-life experience of precision therapy will undeniably lead to an upgrade – from biomarker testing to drug response prediction – accordingly to favor more effective treatment options, more clinical benefit, and more patient coverage to include non-responders. While biomarker tests (or companion diagnostics) advance precision medicine by identifying only a fraction of patients as responders, drug response prediction aims to expand treatment options – particularly for non-responders – by tailoring personalized therapies to optimize outcomes while minimizing side effects. Artificial intelligence-driven approaches (e.g., deep learning and predictive modeling) leverage large datasets to generate these predictions. However, such systems remain experimental, not yet ready for clinical use. Patient-derived gene expression-informed anticancer drug efficacy (PGA) is the ultimate answer to the unmet clinical need for a quick turnaround and cost-efficient drug response prediction technology. With PGA, therapeutic non-responders now are able to benefit from more drug options than ever before. Since the technology is fitted with patient testing, gene activity detection, data mapping, drug matching, and efficacy ranking capabilities, clinicians can be quickly notified of potentially effective drugs, winning the decisive time for decision-making.

Keywords: Drug response prediction; Precision medicine; Biomarker testing; Patient-derived gene expression-informed anticancer drug efficacy; Non-responders

***Corresponding author:**
Chen Yeh
(cyeh.oncodxrx@gmail.com)

Citation: Yeh C, Lin S, Baranski A, Yeh S. Revolutionizing drug response prediction: An unmet requirement for patients unresponsive to precision medicine. *Global Transl Med*. 2025;4(2):3-11. doi: 10.36922/gtm.5091

Received: October 8, 2024

Revised: January 18, 2025

Accepted: February 24, 2025

Published online: March 7, 2025

1. Introduction

Cancer remains one of the most life-threatening diseases globally, with an estimated 20 million new cases and 10 million deaths annually.[1] The World Health Organization projects a 60% increase in the global cancer burden by 2040, with substantial health, social, and financial impacts.[1] The economic burden alone is expected to reach $25.2 trillion between 2020 and 2050.[1] Traditional treatments such as surgery, radiation therapy, chemotherapy, and immunotherapy are currently available but often fall short in addressing intrinsic genetic abnormalities unique to each patient. This has led to

the development of precision medicine, which leverages patients' genomic information to provide targeted diagnostics and personalized therapeutics. This innovative approach aims to offer more effective treatments by focusing on the specific genetic makeup of each individual's cancer.

New precision drugs based on the exact DNA mutations that drive the cancer are needed to help the millions of patients diagnosed with some form of cancer each year. Where available, targeted therapy or immunotherapy has been the standard of care to treat cancer; however, only 20–30% of cancer patients will be qualified and this practice has left out an approximately 70–80% of patients due to their ineligibility (or negative biomarker testing), making precision oncology incomplete and inefficient. Most significantly, two persons might have the same type of cancer, but their diseases can behave differently and respond differently to the same treatment. That is why we desperately need a precision and personalized tool for drug response prediction, beyond traditional biomarker tests or companion diagnostics, and beyond the responder population.

We should no longer focus on a 60° angle between targeted therapy and the patient responders dictated by the guidelines; instead, we should constantly look around with a 360° spectrum for not only actionable DNA alterations but also drug response prediction technologies for non-responders. The idea would be the patient comes in and then gets an answer about alternative treatment options if not qualified for targeted therapy or immunotherapy, and we could get patients into the system immediately so that they could get the right lifesaving medicines. The broader the treatment options, the more it will benefit patients.

A new data network that integrates cutting-edge research on the molecular makeup of diseases with clinical data on individual patients could revolutionize the classification of diseases, ultimately enhancing diagnosis and treatment. The resulting "precision medicine" would define diseases based on their underlying molecular causes and other factors, in addition to their traditional physical signs and symptoms. The ability to exploit the actionable information gathered from tumor genomics to provide reliable and verifiable drug response prediction changed the dynamic of molecular diagnostics, as well as precision therapeutics. This review highlights the rapidly evolving landscape, exciting new developments and key challenges in drug response prediction with a particular focus on the most recent systems in predicting drug efficacy in various settings. With the advent of state-of-the-art technologies such as liquid biopsy, coupled with genomic and transcriptomic profiling and machine learning/modeling, we now have the opportunity to transform the drug response prediction and drug repurposing process to ultimately reach every patient without creating too much of a burden on the healthcare system.

2. Precision drug development: Too few and too long

Over a century of relentless research, and yet, cancer still ranks among the top causes of death.[1] Recent breakthroughs in treatment are promising, but there is a long way to go for these scientific advancements to translate into meaningful clinical outcomes. Astonishingly, only about 3% of oncology drugs ever reach the market.[2] Even then, many offer minimal improvements to patient lifespan or quality of life.[3,4] The pharmaceutical industry's ultimate mission is to deliver safe and effective drugs, but the escalating costs and high failure rates pose significant challenges. Developing a drug can cost up to $2.6 billion and can take up to 15 years, with a staggering 90% of drugs failing during clinical trials.[4]

These failures can generally be split into three categories: (i) incomplete understanding of underlying biology: genomic and transcriptomic data often fail to reveal cancer's full complexity, leading to partial insights into tumor biology; and (ii) incorrect drug targets: some cancer drugs act on unintended targets. Clinical trial analyses show cases where off-target effects lead to efficacy but also to toxicity and side effects[5]; (iii) lack of effective biomarkers: this limits the ability to identify and stratify patients, making it difficult to monitor treatment responses in clinical settings.

The gap between animal and human translation, alongside ethical efforts to reduce animal testing, has driven the industry toward earlier testing with patient-relevant cell-based models such as tumor xenografts, primary tumor cells, and cancer cell lines. Progress is further bolstered by advanced and more physiologically relevant 3D organoid and spheroid cultures. Highly sensitive analytical techniques have greatly enhanced the predictive accuracy of these models.[6-8] However, despite initiatives to mitigate risks in drug development, relying on the same tools and methods will not likely yield innovative, first- or best-in-class targets or transformative advancements.

3. Precision drugs are only for responders

Oncology became the leading therapy area globally in 2010 and since then has spectacularly increased its value over the past decade. In 2020, it is still the leading therapy area by size and growth. Innovation has fueled this phenomenal growth with the sustained launch of diverse medicines, most of which are targeted with various mechanisms of action. As we have developed a deeper understanding of

the underlying biology and natural history of oncology, more sophisticated therapies have emerged with a clear shift toward precision medicine.

Biomarker testing involves examining genes, proteins, and other targets-of-interest (known as biomarkers or tumor markers) to gather information about cancer. Each individual's cancer presents a unique pattern of biomarkers, some of which can influence the effectiveness of specific cancer treatments. Coupled with the rise of precision medicine, oncology has also seen biomarker tests not just entering the mainstream but also shifting the way decisions are made. Undoubtedly, the rise in genomic information is also a driver of this paradigm shift. The use of biomarkers is at the core of the precision medicine movement to provide the right therapy to the right patient population.[9] As valuable as it is to use genetic information to prescribe the right drugs to the right patients, there are multiple challenges that come with it. New targeted therapies with biomarkers do not always fit in every cancer patient, they can make the treatment landscape more complex, and cause patient coverage to shrink and fragment, thus overwhelming healthcare professionals.

Biomarkers have become an essential part of the treatment paradigm and the decision-making process for many tumor types.[9,10] In a global healthcare environment where we see widespread cost containment measures, it is important for payers and other key stakeholders to identify patient subgroups who will benefit from certain drugs. It is certainly invaluable for the patients receiving cancer therapies to have this reassurance that the therapy they are receiving is targeting the specific mutation underlying their illness.

The overall success of this segment does not mean that all precision therapies with biomarkers are set to thrive. Typical challenges to overcome include benefiting small patient subgroups (as responders), low response rates, evolving resistance, disease relapse, and therapy exhaustion.

4. Emerging drug response prediction trends

The discovery of precision drugs and the customization of cancer therapy remain a daunting task. The hallmark of precision medicine is to tailor more effective diagnostic and anti-cancer therapy to each individual patient. Although biomarker tests (or companion diagnostics) offer unprecedented capabilities, they ultimately qualify the minority of patients for precision medicine, while excluding the majority. Precision medicine can no longer solely count on superiority in the field of biomarker testing. As a gap-filler for biomarker testing, drug response prediction is another core element of precision medicine. Drug response prediction is about using genomic and digital methods to forecast how patients will react to certain medicines. It involves looking at various types of data sources, such as genomics or transcriptomics, drug classes, and preclinical and clinical datasets, to predict how well a patient will respond to a particular drug. The integration of precision medicine in cancer treatment is on the rise, driven by multiple factors. This shift significantly enhances the potential for accurate drug response prediction in the years to come (Figure 1).

The increasing global cancer incidence is a key factor driving the development and treatment prediction of precision medicines for oncological disorders. According to the American Cancer Society, approximately 2 million new cases are expected to be diagnosed in the United States in 2023. This highlights a critical need for more effective and targeted treatments to address the global burden of cancer. Personalized healthcare, which tailors treatment to an individual's unique genetic makeup, has significantly improved the quality of life for cancer patients. The favorable outcomes of precision oncology have led to a higher demand for such customized drugs and spurred the development of drug response prediction pipelines, such as biomarker testing. Companion diagnostics play a key role in identifying genetic mutations in cancer patients and determining those most likely to respond to precision medicines being evaluated in clinical trials. These tests not only increase the success rate of clinical trials but also streamline regulatory approval for these drugs, creating lucrative opportunities for the growth of precision oncology and drug response prediction markets.

5. The challenges of drug response prediction

Over the recent years, scientific and clinical communities have developed various drug response prediction strategies, in addition to biomarker testing, often consisting of *in silico* data mining, pooling, modeling, regression, classification, and training with digital algorithm computation (Figure 2). There are still key limitations that need to be addressed: (i) low patient coverage: Targeted therapy or immunotherapy has saved countless lives but only 20 – 30% of patients are eligible for the treatment. Further, the average response rates to these precision therapies are not high, again around 20 – 30%.[10] Predicting which drugs would benefit those non-responders could significantly help this desperate population; (ii) inadequate technologies: despite the promising potential of deep machine learning in evaluating drug response through genomic data, it faces significant challenges. These include a lack of technical

Figure 1. The key drivers for drug response prediction market. The increasing prevalence of cancer and the pressing need for early diagnosis and intervention are fueling the demand for drug response prediction technologies. Accurate drug response prediction can help identify personalized gene signatures linked to effective drugs, enabling early intervention and better patient outcomes.

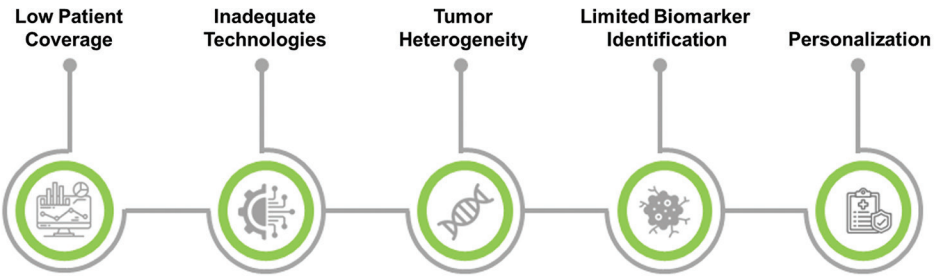

Figure 2. Current challenges associated with drug response prediction methodologies

expertise, large gaps when translating findings to real-world patients, and the production of inaccurate results; (iii) clonal heterogeneity also poses a problem, as precision medicine in oncology relies on accurately characterizing the molecular profile of individual tumors at the start of treatment. However, tumor profiles are dynamic, and targeting the dominant clone can lead to the emergence of resistant subclones; (iv) limited biomarker identification is another hurdle, as precision medicine depends on reliable cancer biomarkers to track disease progression. The collection of high-quality genomic data for these biomarkers is challenging, resulting in a shortage of clinically validated biomarkers for predicting and monitoring outcomes in patients receiving targeted drugs; (v) personalization adds further complexity, as regulatory compliance demands stringent safety and efficacy standards for targeted drugs, which require rigorous clinical trials involving diverse patient populations with specific cancer-associated genetic mutations. These standards are often difficult to meet, posing a significant barrier to the development and implementation of precision medicines. Most significantly, all *in silico* drug response prediction algorithms apply one-size-fits-all approaches (i.e., population-wide approach).

6. *In silico* drug response prediction models

Translational precision medicine consists of key areas such as multi-omics profiling of patients, digital biomarker discovery, and model-based data integration and artificial intelligence (AI). Therefore, it is not far-fetched to imagine that the advancement of machine learning is having a significant impact on precision medicine. Drug response prediction based on the genomic or transcriptomic profile of a cancer patient is one of the hallmarks of precision oncology. Despite improvements in *in silico* deep learning approaches for drug response prediction, there is still an urgent need to upgrade from "one-size-fits-all" digital models to technologies that could truly offer high accuracy as well as interpretable predictions for real-world real-life applications, especially in the non-responder population. Recent advancements in deep learning have played a crucial role in aiding scientists to develop drug response prediction models. These machine training computation techniques contribution to this field is significant, but they all missing vital clinical validation, a key step to translate pre-clinical findings to clinical utility (Table 1).

The field of machine learning, particularly deep neural networks (DNNs), has been propelled by the surge in big data, enhanced computing power, and cloud storage across various sectors, including both industrial and academic.[11-17] In medicine, DNNs positively impact three key areas: enabling clinicians to interpret data rapidly and accurately, enhancing connectivity and reducing medical errors within health systems, and empowering patients to process their

Table 1. A characteristic comparison of drug response prediction methodologies: The PGA technology versus top-ranking *in silico* deep-learning models

Methods	Data sources	Data computation algorithms	Resolution	Proof-of-concept testing cohorts	Applications	Clinical validation	Year (Reference)
PGA	CCLE; GDSC; CTRP v2; TCGA; GEO; EMBL-EBI scRNA-Seq datasets; and real-life patient samples	Proprietary *in vitro* and *in silico* data acquisition and analytics	At the individual patient level	30 real-life cancer patients with lung cancer	Drug efficacy prediction; drug repurposing	Yes	2024[11]
CODE-AE	CCLE; GDSC; DepMap; TCGA	Self-supervised training of the encoder	One-size-fits-all pipeline	*In silico* cell line and tumor datasets	Drug response prediction	No	2022[12]
HQNN	GDSC	Hybrid quantum machine learning model	One-size-fits-all pipeline	*In silico* cell line datasets	Drug response prediction	No	2023[13]
SubCDR	GDSC; COSMIC	Subcomponent-guided deep learning method	One-size-fits-all pipeline	*In silico* cell line datasets	Drug response prediction	No	2023[14]
GPDRP	CCLE; GDSC; PubChem	Graph neural networks with graph transformers and deep neural networks	One-size-fits-all pipeline	*In silico* cell line datasets	Drug response prediction	No	2023[15]
MMDRP	CTRP v2; DepMap	Multi-modal deep learning	One-size-fits-all pipeline	*In silico* cell line datasets	Drug response prediction	No	2024[16]
DBDNMF	CCLE; GDSC	Deep neural matrix factorization; latent representations	One-size-fits-all pipeline	*In silico* cell line datasets	Drug response prediction	No	2024[17]

Abbreviations: CCLE: Cancer Cell Line Encyclopedia; COSMIC: Catalogue of Somatic Mutations in Cancer; CTRP: the Cancer Therapeutics Response Portal; DepMap: the Dependency Map; EMBL-EBI: the European Molecular Biology Laboratory-European Bioinformatics Institute; GDSC: the Genomics of Drug Sensitivity in Cancer; GEO: Gene Expression Omnibus; PubChem: the Public Chemical database; TCGA: The Cancer Genome Atlas; PGA: Patient-derived Gene expression-informed Anticancer drug efficacy; CODE-AE: Context-aware deconfounding autoencoder, HQNN: Hybrid quantum neural networks; GPDRP: Graph and gene pathway-based drug response prediction; MMDRP: Multi-modal drug response prediction; DBDNMF: Dual branch deep neural matrix factorization.

own data, thereby improving their outcomes and quality of life. For cancer, which remains a leading cause of death globally, the integration of precision medicine – through multi-omics data analysis and computational techniques like DNNs – has led to the rise of precision oncology.

Traditional machine learning models often assume that training and testing data come from the same distribution, but this does not hold true for many real-world scenarios, including precision oncology. Preclinical resources, such as cell lines, lack a tumor microenvironment and an immune system, making them quite different from patient data. To build a more accurate model for patients, we need to combine large preclinical datasets with smaller clinical datasets. Deep neural networks address this using knowledge from a large, data-rich source domain to enhance prediction accuracy in a smaller target domain. In precision oncology, preclinical data serves as the source domain, while patient data is the target domain. However, this multi-layer translation is challenging due to the small-scale and high-dimensional nature of patient datasets.

The wealth of data in pre-clinical pharmacogenomics has facilitated the development of machine learning methods to predict drug sensitivity both *in vitro* and *in vivo*. We categorized these cutting-edge drug response predictors by data sources, computational algorithms, resolution, proof-of-concept testing cohorts, applications, and clinical validation (Table 1). Data on cell lines with drug sensitivity were the most common and effective input source, with many methods trained on datasets such as CCLE, GDSC, CTRPv2, and DepMap. An emerging trend is incorporating drug structures, such as PubChem representations of drug molecules. Other potential inputs include drug interactions and toxicity.

Our research demonstrated that deep learning-based models for drug response prediction generally outperformed traditional machine learning models. Some deep-learning models have achieved high accuracy when predicting drug responses for drug-cell line pairs. However, these models still face huge challenges and gaps in translation toward real patients. A successful deep-learning model in drug response prediction will

likely depend on the effective combination of real-world real-time data with learned representations and carefully selected manual features. It is, therefore, crucial to harness the potential of deep learning-based models before conducting clinical studies.

In summary, deep-learning models often function as black-box models, needing more human interfaces, which make decision-making challenging. It is hard to fix variations in biology that show high-degree of heterogeneity between patients, tumors, and their microenvironment. Future researches should incorporate strategies for enhancing their generalizability and interpretability.

7. A gene-to-drug renaissance

Precision oncology is the use of omics data to tailor therapy for an individual cancer patient; however, only 10% of patients actually benefit from precision therapy today.[18,19] Improving drug response prediction in the rest 90% non-responders will significantly benefit many more cancer patients. It is no longer viable for companies to load up their instruments with bespoke capabilities that individually detect and identify actionable biomarkers to benefit only the responders. The urgent need now is for a trainable platform that can quickly and accurately predict drug efficacy for those patient non-responders who have been excluded from precision medicine.

PGA technology is the world-first gene-to-drug platform, offering high-value-added diagnostic and therapeutic solutions.[11] For drug response prediction, PGA combines the high-resolution cell-free messenger RNA (mRNA) profiling with gene expression mapping dedicated to identify a patient-unique signature. Based on this *in vitro* configuration, combining *in silico* digital curation, data fusion, and computation ensures accurate identification of potential hits (after screening of more than 700 Food and Drug Administration-approved, clinical trial, and investigational drugs). This unprecedented combination of *in vitro* and *in silico* approaches allows PGA to effectively map and identify effective drugs at the individual patient level, providing a significant boost to improve treatment outcome in precision oncology, especially for those patients with limited treatment options (Figure 3).

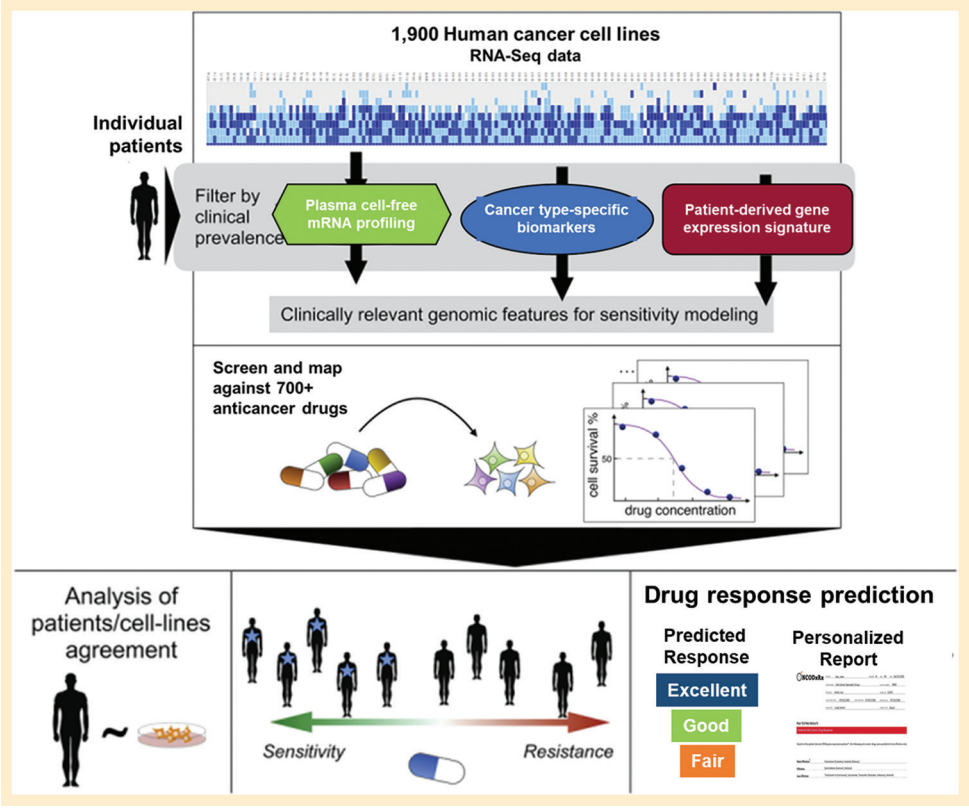

Figure 3. Overview of PGA data acquisition, fusion, transformation, and translation analyses. Prospective and retrospective gene expression data from various cohorts of cell lines, single-cell transcriptomics, primary tumors, and real-world patients were analyzed to identify clinically relevant, cancer type-specific, and patient-derived signatures. The unique signature was further used for *in silico* drug screening and mapping to identify top-ranking anticancer drugs which the patient will most likely respond to.
Abbreviation: PGA: Patient-derived gene expression-informed anticancer drug efficacy.

PGA is designed to improve therapeutic efficacy among the increasingly prevalent patient non-responders. The key to its effectiveness lies in the genetic signature of the patient, which is meticulously generated to maximize the predictive power of drug efficacy in real time, thereby increasing the chances of successful therapeutic intervention. Unlike traditional biomarker testing for DNA mutation detection, which only reflects tumor itself, the mRNA expression signature is designed to represent both tumor and non-tumor microenvironment, maximizing the accuracy of drug efficacy prediction even without a biomarker test.[11]

Having the PGA gene-to-drug technology is essential to treatment selection and decision-making as an extended option to patients who are not responders and had exhausted other treatment options. Necessity for such a technology could mean that the progressive disease is in place and that previous efforts to destroy the tumor have been unsuccessful. In the end, if none of that works, we have PGA test which will actually allow clinicians to direct the treatment strategy to other tumor targets and pathways.

8. Conclusion and future perspectives

The management of cancer has improved in recent years, with targeted therapy and immunotherapy gradually complementing chemotherapy and radiotherapy. Despite the promise of these precision treatments for treating cancer, but a non-responsiveness case would catapult clinicians back into the cycle, figuring out other therapeutic alternatives. Approximately 70 – 80% of cancer patients will be disqualified for or fail to respond to precision medicine, and designing a predictive tool of drug response remains a significant unmet need in this population. Other than doing imaging, performing a physical examination, and clinically monitoring the patient, there is no effective companion tool to gauge drug efficacy in a particular patient.

Studies have proposed neural network deep learning, machine learning or AI training models as potential predictors of drug response. However, none of these *in silico* attempts have been clinically tested. There is a huge realistic gap between the availability and the applicability of these models. On the contrary, the transformative PGA test takes plasma samples from patients, extracts and profiles cell-free mRNA, obtains patient-derived gene expression signatures, which are then used to screen, match, and catalog potentially effective drugs. Results from *in vitro* tests are combined with drug databases to power *in silico* predictive models, pinpointing the drugs to which a specific patient will have good responses.

Cancer treatments are complex, especially when they are combined, like using chemotherapeutic drugs and immunotherapy together, making it difficult to accurately mirror real-world conditions for testing the efficacy of treatment plans. The first-ever patient-tailored PGA approach can work with the complexity of more complicated combination therapy, with the hope to improve the response rates of patients that are currently left out of targeted therapy due to the lack of actionable mutations or become unresponsive to current treatments.

Drug response prediction has undeniably transformed precision oncology, enabling tailored cancer care that aligns with each patient's unique genetic profile. This advancement has paved the way for more effective and personalized treatment strategies, ultimately improving patient outcomes. The growing interest and demand of more effective and durable therapies have enabled quick transition of drug response prediction tests from the bench to bedside. Despite advancements in precision therapies, many patients remain unresponsive due to the complex nature of the human genome. Scientists are still in the early stages of decoding genetic data and translating it into actionable information. Therefore, there is a critical need for diagnostic technology that can leverage a patient's unique genetic data to make accurate therapeutic predictions for each individual non-responder.

The breakthrough PGA technology no longer focuses on a 60-degree angle between targeted therapy and the patient responders dictated by the guidelines; instead, it constantly looks around with a 360° spectrum for identifying not only disease-relevant DNA sequences but also strategies to integrate liquid biopsy, gene expression, and drug response prediction, for use in the non-responder patients. The future will tell, but the low patient eligibility and poor response rates of precision medicine could serve for clinicians as a wake-up call for having alternative and reliable drug response prediction tools. Indeed, it was a lack of both drug efficacy and patient benefit the medical community experienced that prompted the invention of the PGA technology. Although biomarker tests offer unprecedented capabilities, they ultimately qualify the minority of patients for precision medicine, while excluding the majority. Precision medicine can no longer solely count on superiority in the field of biomarker testing, and we should not solely focus on precision therapy, as any other important, viable treatment options available are worth explored too. The broader the treatment options, the more it will benefit patients.

Although precision medicine appears to be promising in future, the success will be primarily determined by the utilization of drug response prediction tools to capitalize on the growth trends and meet demands from the non-responder population.

Acknowledgments

None.

Funding

None.

Conflict of interest

The authors declare no conflicts of interest.

Author contributions

Conceptualization: Chen Yeh
Visualization: Shu-Ti Lin, Sharon Yeh
Writing–original draft: Chen Yeh, Andre Baranski
Writing–review & editing: All authors

Ethics approval and consent to participate

Not applicable.

Consent for publication

Not applicable.

Availability of data

Not applicable.

References

1. World Health Organization. *Cancer Fact Sheet*. World Health Organization; 2022. Available from: https://www.who.int/news-room/fact-sheets/detail/cancer [Last accessed on 2024 Aug 13].
2. Wong CH, Siah KW, Lo AW. Corrigendum: Estimation of clinical trial success rates and related parameters. *Biostatistics.* 2018;20(2):366-366.

   doi: 10.1093/biostatistics/kxy072
3. Davis C, Naci H, Gurpinar E, Poplavska E, Pinto A, Aggarwal A. Availability of evidence of benefits on overall survival and quality of life of cancer drugs approved by European Medicines Agency: Retrospective cohort study of drug approvals 2009-13. *BMJ.* 2017;359:j4530.

   doi: 10.1136/bmj.j4530
4. Kim C, Prasad V. Cancer drugs approved on the basis of a surrogate end point and subsequent overall survival: An analysis of 5 years of US Food and Drug Administration Approvals. *JAMA Intern Med.* 2015;175(12):1992-1994.

   doi: 10.1001/jamainternmed.2015.5868
5. Lin A, Giuliano CJ, Palladino A, *et al*. Off-target toxicity is a common mechanism of action of cancer drugs undergoing clinical trials. *Sci Transl Med.* 2019;11(509):eaaw8412.

   doi: 10.1126/scitranslmed.aaw8412
6. Idrisova KF, Simon HU, Gomzikova MO. Role of patient-derived models of cancer in translational oncology. *Cancers* (*Basel*). 2022;15(1):139.

   doi: 10.3390/cancers15010139
7. Bashor CJ, Hilton IB, Bandukwala H, Smith DM, Veiseh O. Engineering the next generation of cell-based therapeutics. *Nat Rev Drug Discov*. 2022;21:655-675.

   doi: 10.1038/s41573-022-00476-6
8. Kim J, Koo BK, Knoblich JA. Human organoids: Model systems for human biology and medicine. *Nat Rev Mol Cell Biol*. 2020;21:571-584.

   doi: 10.1038/s41580-020-0259-3
9. Yeh C. Enabling real-world data to accelerate the development of innovative cancer biomarkers. *Glob Med Genet.* 2023;10:97-100.

   doi: 10.1055/s-0043-1768993
10. Haslam A, Kim MS, Prasad V. Updated estimates of eligibility for and response to genome-targeted oncology drugs among US cancer patients, 2006-2020. *Ann Oncol.* 2021;32(7):926-932.

    doi: 10.1016/j.annonc.2021.04.003
11. Yeh C, Lin ST, Lai HC. A transformative technology linking patient's mRNA expression profile to anticancer drug efficacy. *Onco.* 2024;4(3):143-162.

    doi: 10.3390/onco4030012
12. He D, Liu Q, Wu Y, Xie L. A context-aware deconfounding autoencoder for robust prediction of personalized clinical drug response from cell-line compound screening. *Nat Mach Intell.* 2022;4:879-892.

    doi: 10.1038/s42256-022-00541-0
13. Sagingalieva A, Kordzanganeh M, Kenbayev N, Kosichkina D, Tomashuk T, Melnikov A. Hybrid quantum neural network for drug response prediction. *Cancers* (*Basel*). 2023;15(10):2705.

    doi: 10.3390/cancers15102705
14. Liu X, Zhang W. A subcomponent-guided deep learning method for interpretable cancer drug response prediction. *PLoS Comput Biol.* 2023;19(8):e1011382.

    doi: 10.1371/journal.pcbi.1011382
15. Yang Y, Li P. GPDRP: A multimodal framework for drug response prediction with graph transformer. *BMC Bioinformatics.* 2023;24:484.

    doi: 10.1186/s12859-023-05618-0
16. Taj F, Stein LD. MMDRP: Drug response prediction and biomarker discovery using multi-modal deep learning.

Bioinform Adv. 2024;4(1):vbae010.

doi: 10.1093/bioadv/vbae010

17. Liu H, Wang F, Yu J, *et al*. DBDNMF: A dual branch deep neural matrix factorization method for drug response prediction. *PLoS Comput Biol.* 2024;20(4):e1012012.

doi: 10.1371/journal.pcbi.1012012

18. Pfohl U, Pflaume A, Regenbrecht M, *et al*. Precision oncology beyond genomics: The future is here-it is just not evenly distributed. *Cells.* 2021;10(4):928.

doi: 10.3390/cells10040928

19. Malone ER, Oliva M, Sabatini PJB, Stockley TL, Siu LL. Molecular profiling for precision cancer therapies. *Genome Med.* 2020;12:8.

doi: 10.1186/s13073-019-0703-1

ACCSCIENCE PUBLISHING

Global Translational Medicine

REVIEW ARTICLE

Perspectives on the small ribonucleic acid drugs for pancreatic cancer

Qingqing Zhou[1], Guoan Shen[2], Huaying Li[2], Haimei Chen[1], and Chang Liu[1]*

[1]Department of Bioinformatics, Institute of Medicinal Plant Development, Chinese Academy of Medical Sciences, Peking Union Medical College, Beijing, China

[2]Department of Research & Development, Beijing Young Lingzhi Health Industry Research Institute Co., Ltd, Beijing, China

Abstract

Pancreatic cancer (PC) remains one of the most lethal forms of cancer. Unfortunately, existing drugs for PC would cause significant side effects, and the tumor may develop resistance to these treatments. Therefore, there is an urgent need to develop new drugs to provide more treatment options for PC patients. Compared to traditional protein-targeted and DNA-based drugs, ribonucleic acid (RNA)-based therapies have gained significant attention in recent years due to their unique physicochemical and physiological properties. Various strategies have been developed to enhance the metabolic stability and intracellular delivery of small RNA drugs, making them a key focus in cancer drug development in recent years. To explore the therapeutic potential of small RNA drugs in PC, an overview of the status of small RNA drug development is provided, including 17 approved small RNA drugs and 43 small RNA drug candidates in clinical trials. In addition, genetic factors involved in PC progression are examined, identifying 17 protein-coding genes and 15 *microRNA* genes. Finally, six strategies for developing small RNA drugs for PC are discussed.

Keywords: Small ribonucleic acid drugs; Pancreatic cancer; Drug target

***Corresponding author:**
Chang Liu
(cliu@implad.ac.cn)

Citation: Zhou Q, Shen G, Li H, Chen H, Liu C. Perspectives on the small ribonucleic acid drugs for pancreatic cancer. *Global Transl Med*. 2025;4(2):12-30. doi: 10.36922/gtm.8247

Received: December 27, 2024

Revised: February 26, 2025

Accepted: March 6, 2025

Published online: March 19, 2025

1. Introduction

Pancreatic cancer (PC) remains one of the deadliest cancers globally, with a 5-year survival rate significantly lower than that of many other cancers,[1] such as lung cancer,[2] colorectal cancer,[3] and ovarian cancer.[4] Despite significant advances in cancer treatment in recent years, the treatment of PC remains extremely challenging,[5] particularly in completely eliminating residual tumor cells and circulating tumor cells.[6] Traditional treatment approaches, such as surgery, chemotherapy, and radiotherapy, not only lead to severe side effects but also fail to meet the needs of all patients. As a result, novel and more effective drugs are required to enhance survival rates and mitigate side effects.[7] Due to the limited therapeutic options available, the research focus has shifted toward innovative approaches to overcoming PC's inherent resistance to treatment and aggressive nature.

At present, ribonucleic acid (RNA)-based drugs are emerging as a promising therapeutic avenue.[8] Small RNAs, such as microRNA (miRNA) mimics and small interfering RNA (siRNA), precisely regulate the expression of tumor-associated protein-coding and *miRNA* genes to achieve therapeutic effects. The key advantage of small RNA

drugs lies in their ability to target sites that traditional drugs cannot reach, with higher specificity and fewer side effects. Despite their enormous potential, applying small RNAs in clinical settings remains challenging. Small RNA molecules are highly susceptible to degradation by nucleases in the body, and they struggle to penetrate cell membranes effectively due to their relatively large size. Although the development of RNA drugs is confronted with unprecedented challenges, numerous strategies have been developed to enhance RNA metabolic stability and intracellular delivery,[9] including nanoparticle carriers, liposomes, and viral vectors. With continued advancements in these technologies, small RNA drugs hold promise as a new and effective treatment for PC and other malignant tumors.

This article provides a brief overview of the current state of PC treatment and the development of small RNA drugs, including 17 approved small RNA drugs and 43 small RNA drugs currently in clinical trials. Subsequently, the genetic factors involved in the progression of PC are explored, summarizing 17 protein-coding genes and 15 *miRNA* genes that could serve as targets for small RNA drugs. Finally, six strategies for the development of small RNA drugs are discussed.

2. PC

2.1. PC introduction

PC is a malignant tumor that originates from the pancreatic ductal epithelium and acinar cells, often referred to as the "king of cancers" in the medical community. The exact cause of its onset is not yet fully understood, but studies suggest that factors such as long-term smoking, poor dietary habits, high body mass index, and chronic pancreatic damage may increase the risk of developing PC. In recent years, the incidence of PC has risen significantly, more than two-fold over the past 30 years.[10] Even more concerning, projections indicate that by 2040, PC will surpass colorectal cancer to become the second leading cause of cancer-related deaths, behind only lung cancer.[11]

PC is notorious for its difficult prognosis, which is driven by several factors.[12] First, PC is difficult to detect in its early stages due to its tendency to grow around nerves and blood vessels. In addition, it often metastasizes to distant sites early, which makes radical surgical resection unsuccessful in most patients.[13] Second, patients with advanced PC exhibit significant resistance to most conventional treatment methods, including chemotherapy, radiation, and molecularly targeted therapy. Finally, PC displays multiple genetic and epigenetic alterations and has a complex, dense tumor microenvironment, which not only makes it difficult to develop specific drugs but also prevents effective drug delivery. All these factors contribute to an overall 5-year survival rate of <7% for PC patients.

2.2. The main treatment methods for PC

The current treatment of PC primarily includes surgical treatment, radiation therapy, chemotherapy, interventional therapy, and best supportive care. Chemotherapy remains the main treatment option for metastatic PC patients. Here, the categories, principles, and side effects of six existing PC drugs are summarized, including gemcitabine, nab-paclitaxel, 5-fluorouracil (5-FU), leucovorin, irinotecan, and oxaliplatin (Table 1). Among these six drugs, gemcitabine is the most studied chemotherapy for PC.[14] Gemcitabine is a cytosine nucleoside analog that can be incorporated into replicative DNA to inhibit DNA synthesis. After entering the body, gemcitabine is converted by deoxycytidine kinase into gemcitabine diphosphate and triphosphate, which are active drug metabolites that have multiple inhibitory effects on DNA synthesis.[15]

For a long time, single-agent gemcitabine treatment was the standard treatment regimen for advanced PC.[15] However, gemcitabine had significant limitations as a monotherapy for advanced PC, with the biggest drawback being its short half-life. A higher dosage was required to maintain an effective concentration. However, high-dose administration inevitably causes severe side effects in patients, such as leukopenia, thrombocytopenia, anemia, and gastrointestinal reactions. Given these limitations in monotherapies, the clinical communities have increasingly turned their attention to combination therapy. In the past decade, two new combination therapies have emerged as first-line treatment options for patients with advanced PC. The first was a combination of 5-FU, leucovorin, irinotecan, and oxaliplatin, known as FOLFIRINOX.[16] PRODIGE 4/ACCORD 11 was a clinical trial involving 342 French patients, in which FOLFIRINOX was administered fortnightly to previously untreated, functionally intact metastatic PC patients (Eastern Tumor Cooperative group performance status 0 – 1) and compared with gemcitabine monotherapy.[16] This study highlighted the superior efficacy of FOLFIRINOX across all clinically significant parameters.[17] Consequently, FOLFIRINOX has become the preferred first-line treatment for patients; however, its severe side effects require that patients be in good physical condition.

The second combination therapy combined gemcitabine with nab-paclitaxel,[18] a 130-nm paclitaxel formulation bound to albumin particles. An international phase III study involving 861 patients with metastatic PC was conducted, in which participants were randomly assigned to receive either gemcitabine alone or gemcitabine + nab-

Table 1. Categories, principles, and side effects of existing chemotherapy drugs for PC

Drug name	Category	Mechanisms of action	Side effects
Gemcitabine	Cytosine nucleoside derivative	Its main metabolites penetrate DNA inside cells, interfering with DNA synthesis and inhibiting ribonucleotide reductase.	Leukopenia, thrombocytopenia, anemia, and gastrointestinal reactions.
Nab-paclitaxel	Paclitaxel nanodrug-targeted formulation	Paclitaxel is a natural anticancer agent that inhibits DNA unwinding, thereby suppressing tumor cell proliferation and metastasis.	Bone marrow suppression.
5-FU	Antimetabolic drug	Inhibits thymidylate synthase, suppressing DNA synthesis.	Bone marrow suppression, leading to reduced white blood cells and platelets.
Leucovorin	Antidote to folic acid antagonists	Enhances the antitumor effect of 5-FU	Gastrointestinal discomfort at high doses.
Irinotecan	DNA topoisomerase I inhibitor	Blocks DNA replication and inhibits RNA synthesis, specifically during the S-phase.	Gastrointestinal discomfort at high doses.
Oxaliplatin	DNA crosslinker	Platinum atoms form crosslinks with DNA, disrupting replication and transcription.	Neurotoxicity.

Abbreviations: PC: Pancreatic cancer; 5-FU: 5-Fluorouracil.

paclitaxel.[18] The results showed that patients receiving the combination therapy demonstrated superior outcomes, leading to the Food and Drug Administration (FDA) approval of nab-paclitaxel for PC in 2014.

In general, there are no established universal guidelines for second-line treatments and beyond for PC. The choice of therapy typically depends on factors such as the patient's performance status, the presence of "actionable" targets, and the availability of suitable clinical trials.

3. Genetic factors involved in PC development

3.1. Proteins involved in the development of PC

Seventeen protein targets for PC are shown in Table 2. These targets can be categorized into three major groups according to their mechanisms of action.

The first group focuses on inhibiting tumor invasiveness and metastasis. PC develops due to the accumulation of multiple genetic alterations, including mutations in tumor suppressor genes, oncogenes, and chromosomal abnormalities. These changes may arise gradually through a multistep process or suddenly in a single catastrophic event.[19,20] As a result of these mutational processes, tumors acquire numerous random bystander mutations that contribute to tumor initiation, progression, metastasis, and resistance to therapy. Whole-exome sequencing studies have revealed several recurrent mutations that impact the function of critical oncogenes and tumor suppressors, including Kirsten rat sarcoma viral oncogene homolog (KRAS),[21] tumor protein p53,[22] cyclin-dependent kinase inhibitor 2A,[23] SMAD family member 4,[24] ring finger protein 43,[25] and F-box and WD repeat domain containing 7.[26] The KRAS protein functions as a molecular switch, which is activated in response to upstream epidermal growth factor receptor and regulated downstream mitogen-activated protein kinase 1 (MAPK) and PI3K/mTOR pathways, ultimately controlling cell proliferation, differentiation, and survival. *KRAS* gene mutations are particularly common in solid tumors and have long been a focus of precision therapy. In addition, the classic targets with abnormal mutations associated with the invasiveness and metastasis of PC also include matrix metallopeptidase 2 (MMP2),[27] Ras-responsive element binding protein 1 (RREB1),[28] nuclear factor-kappa B (NF-κB),[29] ribonucleotide reductase regulatory subunit M2,[30] and signal transducer and activator of transcription 3 (STAT3).[31] In addition to known classical mutations, a recent study found that ubiquitin-specific peptidase 15 (USP15) acts in a haplodeficient manner, where the loss of USP15 or SR-related CTD-associated factor 1 leads to reduced inflammatory tumor necrosis factor-alpha, transforming growth factor beta, and interleukin-6 responses and increased sensitivity to poly-ADP ribose polymerase inhibitors and gemcitabine.[32] All these abnormal mutated genes represent potential targets for small RNA drug development (Table 2).

The second group of genetic factors is related to enhancing the sensitivity of PC cells to chemotherapy drugs. Another challenge in the development of new drugs for PC is their resistance to chemotherapy.[33] The transport, activation, and metabolism of gemcitabine are regulated by a wide range of enzymes, meaning that drug resistance can arise through various mechanisms, as almost all metabolic processes involving gemcitabine contribute to resistance.[14] The intracellular transport of gemcitabine is mainly mediated by human equilibrative nucleoside

Table 2. List of potential mRNA targets for small RNA drug development against PC

Number	Group	Target name	Effects of this target in PC development	Potential application of this target in PC treatment	Current stage in small RNA drug development
1	Group 1: Inhibiting tumor invasiveness and metastasis	KRAS	Promote invasiveness and liver metastasis in PC	Downregulates KRAS expression to inhibit invasiveness and metastasis	Clinical research
2		TP53		Upregulates TP53 expression to inhibit invasiveness and metastasis	
3		STAT3		Downregulates STAT3 expression to inhibit invasiveness and metastasis	
4		EGFR		Downregulates EGFR expression to inhibit invasiveness and metastasis	
5		RRM2		Downregulates RRM2 expression to inhibit invasiveness and metastasis	
6		RREB1		Downregulates RREB1 expression to inhibit invasiveness and metastasis	Pre-clinical research
7		CDKN2A		Downregulates CDKN2A expression to inhibit invasiveness and metastasis	
8		SMAD4		Downregulates SMAD4 expression to inhibit invasiveness and metastasis	
9		RNF43		Downregulates RNF43 expression to inhibit invasiveness and metastasis	
10		FBXW7		Downregulates FBXW7 expression to inhibit invasiveness and metastasis	
11		MMP2		Downregulates MMP2 expression to inhibit liver metastasis	
12		NF-κB		Downregulates NF-κB expression to inhibit invasiveness and metastasis	
13		USP15		Downregulates USP15 expression to inhibit invasiveness and metastasis	
14	Group 2: Enhancing sensitivity of PC cells to chemotherapy drugs	hENT1	Mediate intracellular transport of gemcitabine	Upregulates hENT1 expression to enhance sensitivity of PC patients to gemcitabine	Pre-clinical research
15		MRP	Mediate efflux of a series of chemotherapy drugs such as gemcitabine	Downregulates MRP expression to enhance sensitivity of PC patients to gemcitabine	
16		DPD	Breaks down 5-FU into dihydrofluorouracil	Downregulates DPD expression to enhance sensitivity of PC patients to 5-FU	
17	Group 3: Improving the tumor microenvironment	P4HA1	Leads to accumulation of collagen fibers in the tumor microenvironment	Downregulates P4HA1 expression to decrease collagen fiber accumulation	Pre-clinical research

Abbreviations: PC: Pancreatic cancer; KRAS: Kirsten rat sarcoma viral oncogene homolog; TP53: Tumor protein p53; STAT3: Signal transducer and activator of transcription-3; EGFR: Epidermal growth factor receptor; RRM2: Ribonucleotide reductase regulatory subunit M2; RREB1: Ras-responsive element-binding protein 1; CDKN2A: Cyclin-dependent kinase inhibitor 2A; SMAD4: SMAD family member 4; RNF43: Ring finger protein 43; FBXW7: F-box and WD repeat domain containing 7; MMP2: Matrix metallopeptidase 2; NF-κB: Nuclear factor kappa-light-chain-enhancer of activated B cells; USP15: Ubiquitin-specific peptidase 15; hENT1: Human equilibrative nucleoside transporter 1; MRP: Multidrug resistance-associated protein; DPD: Dihydropyrimidine dehydrogenase; P4HA1: Prolyl 4-hydroxylase subunit alpha 1; 5-FU: 5-fluorouracil.

transporters (hENTs). Previous studies have shown that high expression of hENT1 is linked to improved overall survival and disease-free survival in PC patients.[34] The expression level of hENT1 may serve as a prognostic marker for PC patients undergoing gemcitabine chemotherapy.[35] Therefore, hENT1 activity is an important determinant of cancer cell susceptibility to gemcitabine, and its deficiency or decreased activity may contribute to gemcitabine resistance.[34] In addition, multidrug resistance protein (MRP) is a type of ATP-binding cassette transporters that mediate the efflux of various chemotherapy drugs, such as gemcitabine, thus reducing intracellular drug concentration and promoting drug resistance.[36] In pancreatic ductal adenocarcinoma (PDAC), MRP1 and

MRP5 are major transporters of gemcitabine efflux, and their expression is induced by gemcitabine in a time- and dose-dependent manner in PDAC cell lines.[37]

In addition to gemcitabine, another commonly used chemotherapy agent is 5-FU. By incorporation of DNA, RNA, or both, 5-FU accumulates in cells, leading to increased cytotoxicity and, eventually, cell death. However, due to its low intracellular stability, most 5-FU is easily broken down into dihydrofluorouracil by dihydropyrimidine dehydrogenase (DPD) in the liver, which affects drug sensitivity and resistance. Therefore, DPD may be a potential therapeutic target.[38] The combination of cisplatin with other nucleophiles *in vivo* can lead to drug resistance, but the mechanism of oxaliplatin resistance remains unclear. In this review, small RNA drugs may target enzymes that cause chemical resistance, and their combination with chemical drugs may help improve this resistance. However, the combination of the two drugs may lead to drug interactions, toxic side effects, and other potential risks. Further research is needed to overcome these challenges.

The last group of genetic factors is related to improving the tumor microenvironment. One of the biggest challenges in the development of new drugs for PC is the complexity of its tumor microenvironment.[39] PC is characterized by a dense stroma, hypoxia, limited blood vessels, and strong immunosuppressive activity. Composed of pancreatic stellate cells, cancer-associated fibroblasts, immune cells, and extracellular matrix components, this environment not only promotes tumor growth and invasion but also contributes to resistance against chemotherapy and other anticancer treatments. The dense fibrotic reaction in the stroma and changes in the tumor's immune environment are considered the main reasons for the failure of current PC treatments.[40] However, a recent study from the University of Rome in Italy found that the increased invasiveness of PDAC linked to metabolic disorders is associated with the accumulation of collagen fibers, driven by the enhanced activity of Prolyl 4-hydroxylase subunit alpha-1 (P4HA1).[41] Under conditions of metabolic imbalance, P4HA1 promotes the hydroxylation of collagen proline, strengthens collagen contraction, and inhibits the infiltration of PDAC.[41] This suggests that P4HA1 plays a role in matrix deposition during PC development and could serve as a potential target for small RNA drug development.

3.2. miRNAs involved in the development of PC

Previous studies have shown that some miRNAs are abnormally expressed under disease conditions and become important factors in disease occurrence and development. In this review, 15 miRNA targets for PC are summarized in Table 3. These targets can be categorized into two major groups based on their expression levels in PC.

One group includes eight miRNAs whose expression was downregulated. Li *et al.*[42] identified the role of the entire miR-200 miRNA family in gemcitabine-resistant PDAC cells, primarily through the reversal of epithelial-mesenchymal transition. In addition, it was proposed that upregulation of miR-34 might partially restore the tumor-suppressive function of p53 in p53-deficient human PC cells.[43] Overexpression of miR-143 or miR-145 downregulated KRAS and RREB1, as well as a series of genes in the MAPK signaling cascade, thereby achieving an inhibitory effect on PC.[44] The persistent activation of NF-κB, a key regulator of important genes that influence various cellular processes, was also recognized as a contributor to the aggressive behavior of PC.[45] Previous studies showed that overexpression of miR-146a diminished the invasiveness of PC cells, which was accompanied by a reduction in NF-κB expression.[46] In primary PC, STAT3 is activated and plays a role in several physiological processes.[21] Yan *et al.*[47] demonstrated that miR-20a modulated STAT3 at the post-transcriptional level, leading to a reduction in cell proliferation and invasion in pancreatic carcinoma. In addition, dual-luciferase assays demonstrated that miR-130b directly targeted STAT3, a result that was further confirmed by the inverse expression of miR-130b and STAT3 in PC specimens.[48] Zou *et al.*[49] found that overexpression of miR-29c could inhibit hepatic metastasis of PC in the nude mouse orthotopic transplantation model. Xu *et al.*[50] studied gemcitabine-resistant PC cells and found that miR-497 inhibited cell proliferation, decreased the percentage of cells in the S-phase, and targeted fibroblast growth factor-2 and its receptor-1. Overexpression of miR-497 inhibited tumor growth *in vivo*. miR-137 is also a tumor suppressor that inhibits the proliferation and invasion of cancer cells through targeting multiple oncogenes.[51]

The second group of miRNAs had abnormally elevated expression in PC. As early as 2008, some researchers used *miRNA* gene chips to screen the differentially expressed miRNAs in pancreatic tumor tissues and normal pancreatic tissues, as well as in PC cells and normal pancreatic cells and found that miR-181 and miR-214 were specifically expressed in PC.[52] In addition, miR-21, as an oncogene in human cancer, promoted cancer progression by enabling evasion of host immune surveillance in PC.[53] Wang *et al.*[54] also found that the expression of miR-155 in tumor tissues of PC patients was higher than in the adjacent normal tissues. Furthermore, miRNAs with abnormally elevated expression in PC include miR-221/miR-222,[55] miR-29a,[56]

Table 3. List of potential miRNA targets for small RNA drug development in current PC research

Number	Group	Target name	Roles of miRNAs in pancreatic cancer	Type of drug to be developed
1	Group 1: miRNAs expressed at a suppressed level in PC	miR-200 family	Reverse EMT and inhibits the invasion and metastasis of PC	miR-200 mimics
2		miR-34	Restores the tumor-suppressive function of p53 in p53-deficient human PC cells	miR-34 mimics
3		miR-143/miR-145	Downregulate KRAS, RREB1, and MAPK signaling genes and inhibit PC progression	miR-143/miR-145 mimics
4		miR-146a	Downregulates NF-κB expression and inhibits PC progression	miR-146a mimics
5		miR-20a/miR-130b	Downregulate STAT3 expression and inhibit PC progression	miR-20a/miR-130b mimics
6		miR-29c	Inhibits PC cell metastasis and invasion by downregulating MMP2	miR-29c mimics
7		miR-497	Inhibits the proliferation of gemcitabine-resistant PC cells	miR-497 mimics
8		miR-137	Inhibits the proliferation and invasion of cancer cells by targeting multiple oncogenes	miR-137 mimics
9	Group 2: miRNAs with abnormally elevated expression in PC	miR-181	Contributes to chemoresistance in PC by inactivating the Hippo signaling pathway	miR-181 inhibitor
10		miR-21	Promotes cancer to evade host immune surveillance and accelerates PC progression	miR-21 inhibitor
11		miR-214	Accelerates the proliferation and differentiation of PC cells	miR-214 inhibitor
12		miR-155	Promotes the growth and metastasis of PC cells by inhibiting SHIP1	miR-155 inhibitor
13		miR-221/222	Accelerate PC progression through the regulation of matrix metalloproteinases	miR-221/222 inhibitor
14		miR-29a	Promotes PC growth by inhibiting tristetraprolin	miR-29a inhibitor
15		miR-210	Mediates the occurrence of EMT in PC cells induced by HIF-1α under hypoxia	miR-210 inhibitor

Abbreviations: PC: Pancreatic cancer; miR: miRNA; EMT: Epithelial-mesenchymal transition; KRAS: Kirsten rat sarcoma viral oncogene homolog; RREB1: Ras-responsive element-binding protein 1; MAPK: Mitogen-activated protein kinase; NF-κB: Nuclear factor kappa-light-chain-enhancer of activated B cells; STAT3: Signal transducer and activator of transcription-3; MMP2: Matrix metallopeptidase 2; SHIP1: Src homology 2 domain-containing inositol-5-phosphatase 1; HIF-1α: Hypoxia-inducible factor 1-alpha.

and miR-210.[57] All these miRNAs can be targeted by miRNA inhibitors.

Finally, a search of the Web of Science database using the keywords "Pancreatic cancer" and "miRNA" identified a total of 1,726 articles, which were analyzed for annual publication volume (Figure 1). The bibliometric analysis found that, in recent years, the number of published research papers on RNA drugs has been increasing (Figure 1). Numerous studies on the transcriptional level of PC have shown that the dual regulatory network of miRNA and transcription factors plays an important role in the formation and progression of PC. Therefore, investigating the relationship and interaction mechanisms between miRNA and traditional treatment of PC may provide new insights for the development of small RNA drugs. Finally, interactions between miRNAs could represent another emerging field for further exploration.

4. Small RNA drugs

4.1. Mechanisms of action of small RNA drugs

Small RNA is a class of non-coding RNAs typically ranging from 20 to 30 nucleotides in length. Current research and development on small RNA drugs have focused on four types, including miRNA mimics, siRNA, antisense oligonucleotides (ASOs), and aptamers.

Previous studies have shown that miRNAs regulate a substantial portion of the human transcriptome.[58] The intricate nature of miRNA regulation is highlighted by the ability of a single miRNA to target hundreds of distinct mRNAs, whereas multiple miRNAs can also coordinate the regulation of the same mRNA.[59] The classical mechanism by which miRNAs exert their effects involves binding to the 3' untranslated region (UTR) of target mRNAs, leading to either their degradation or the inhibition of their translation (Figure 2A).[60] This process requires miRNA

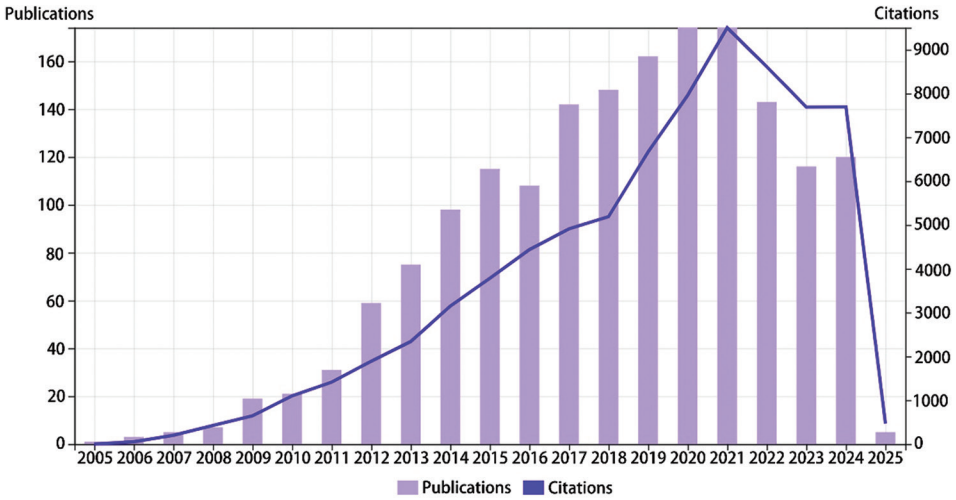

Figure 1. The number of research papers published from 2005 to 2025, retrieved from the Web of Science database using the keyword "Pancreatic cancer" and "microRNA"

binding to an Argonaute (AGO) protein, which serves as the central component of the RNA-induced silencing complex (RISC). Once incorporated into the AGO protein, the miRNA guides RISC to bind a complementary target mRNA, resulting in translational repression or degradation of the targeted mRNA. In addition to binding to the 3' UTR, miRNAs can also inhibit protein expression by interacting with coding sequences or the 5'UTR of mRNAs.

RNA interference (RNAi) is a natural process that promotes the degradation of target mRNA, thereby silencing gene expression[61] (Figure 2B). When long-chain double-stranded RNA is cleaved by Dicer, a member of the ribonuclease (RNase) III family, siRNA duplexes are produced. Subsequently, the siRNA is incorporated into the RISC. Inside the RISC, the siRNA interacts with the AGO2 component, causing the duplex to unwind and leading to the degradation of the sense strand. The antisense strand, which is complementary to the target mRNA, then guides the RISC complex to the target mRNA.

ASO is a single-stranded oligonucleotide with three mechanisms of action.[62] The first is based on the RNase H1-mediated mRNA degradation mechanism. ASO specifically targets RNA molecules, leading to the formation of ASO-RNA heteroduplexes, which serve as substrates for RNase enzymes in the cytoplasm, as depicted in Figure 2C.[63] Once the ASO-RNA heteroduplexes are formed, RNases initiate RNA degradation within these structures. The design of gapmer ASOs is particularly innovative. It features a central region composed of unmodified nucleotides, which plays a crucial role in facilitating RNase H1 activity. Meanwhile, the flanking regions consist of modified nucleotides that enhance ASO binding affinity to the target RNA and improve resistance against enzymatic degradation. Notably, most drugs approved by the U.S. FDA exert their antisense effects through RNase-mediated mechanisms.[64]

The second mechanism of action of ASOs is based on steric hindrance, which blocks key regions of mRNA, thereby affecting its maturation or translation into proteins. For example, Bennett and Swayze.[65] found that an ASO targeting the mRNA sequence leads to translational arrest by either inhibiting its interaction with the 40S ribosomal subunit or preventing the assembly of the 40S and 60S ribosomal subunits (Figure 2C).

The third mechanism of action of ASOs involves blocking alternative splicing (Figure 2C).[66] Dhuri *et al.*[62] found that ASOs can target the splicing regulatory regions of pre-mRNA and bind to them in a complementary manner. After binding, steric hindrance is generated, which inhibits or promotes the binding of splicing factors to regulatory regions, thereby affecting spliceosome assembly and generating different mRNA isoforms.

Aptamers are structured oligonucleotide sequences (RNA or DNA) obtained through an *in vitro* screening technique called Systematic Evolution of Ligands by Exponential Enrichment.[67] Due to their unique tertiary structures, aptamers can recognize target molecules through their three-dimensional conformations and exhibit high binding affinities (Figure 2D). The small and flexible structures of aptamers enable them to bind to smaller targets or hidden domains that antibodies cannot access.[68] The applications of aptamers have been extensively described. Interested readers are encouraged to refer to relevant literature.[68,69]

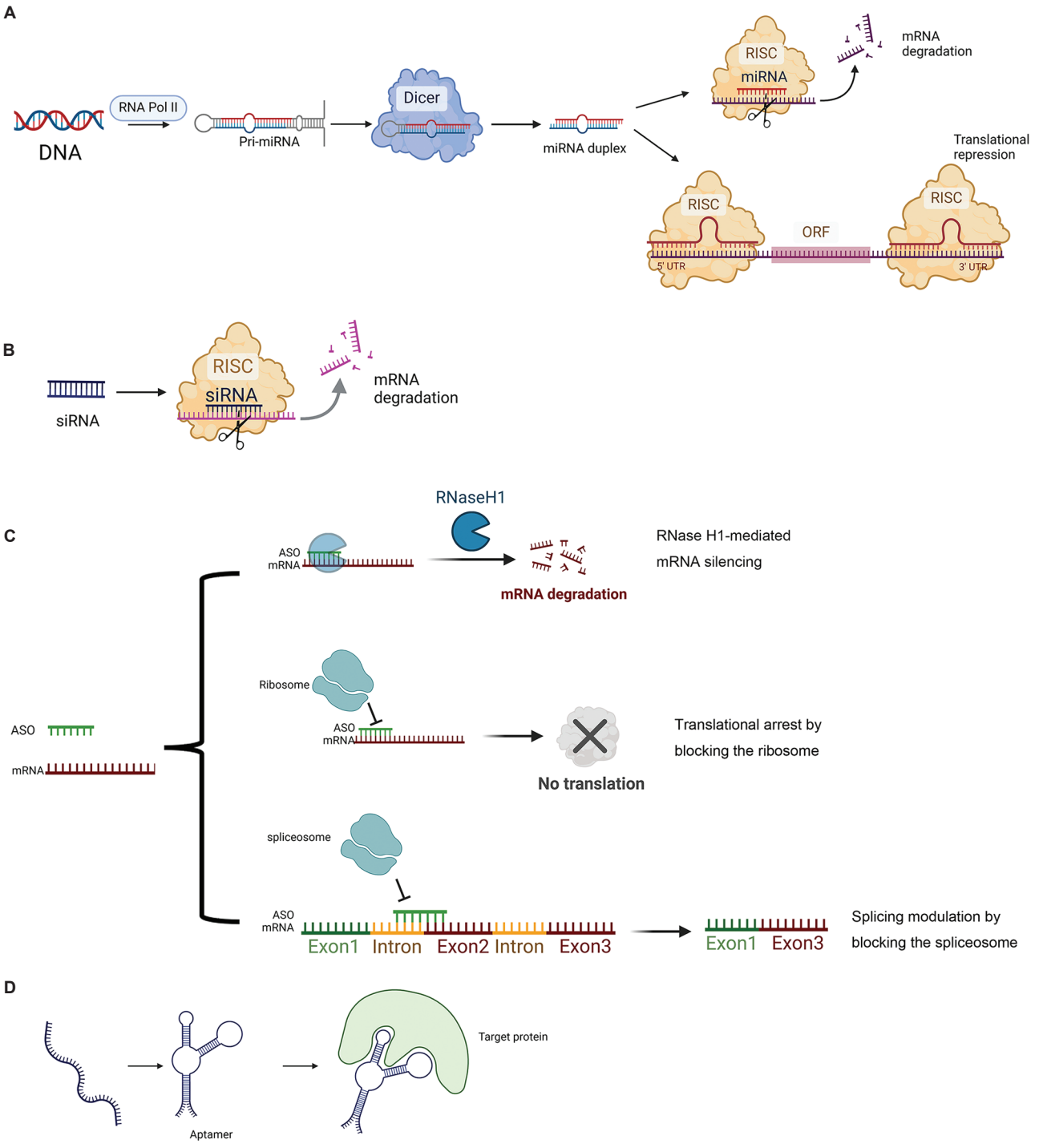

Figure 2. Schematic diagram of the mechanisms of action of different types of small RNA drugs, including miRNA, siRNA, ASO, and aptamer. (A) miRNAs exert their effects by binding to the 3′ UTR, 5′ UTR, or ORF of target mRNAs, which leads to either mRNA degradation or inhibition of mRNA translation. (B) siRNAs exert their effects by binding to the ORF of target mRNAs, which leads to mRNA degradation. (C) In the first scenario, ASO specifically target RNA molecules, leading to the formation of ASO-RNA heteroduplexes. These heteroduplexes serve as substrates for RNase enzymes located in the cytoplasm. Once the ASO-RNA heteroduplexes are formed, RNases initiate the degradation process of the RNA within these structures. In the second scenario, ASOs bind to the target mRNA sequence, leading to translational arrest by inhibiting its interaction with the 40S ribosomal subunit or preventing its assembly on the 40S or 60S ribosomal subunit. In the third scenario, a gene with three exons (exon 1, 2, and 3) and two introns is shown. An ASO binds to the junction of the intron and exon2, blocking the action of spliceosome and causing exon 2 to be spliced out along with the introns. As a result, the mature mRNA lacks exon 2. (D) Aptamers recognizes target molecules through their three-dimensional conformations and have high binding affinities. Abbreviations: siRNA: Small interfering RNA; ASO: Antisense oligonucleotide; UTR: Untranslated region; ORF: Open reading frame; RNase: Ribonuclease; miRNA: MicroRNA.

Table 4. Currently approved small RNA drugs

Number	Name	Type	Indications	Target	Responsible company	Year approved
1	Patisiran	siRNA	Familial amyloidotic polyneuropathy	hATTR	Alnylam Pharmaceuticals	2018 (America, Europe)
2	Givosiran		Acute hepatic porphyrias	ALAS1	Alnylam Pharmaceuticals	2019 (America), 2020 (Europe), 2021 (Japan)
3	Lumasiran		Primary hyperoxaluria type 1	HAO1	Alnylam Pharmaceuticals	2020 (America, Europe)
4	Inclisiran		Familial hypercholesterolemia	PCSK9	Alnylam Pharmaceuticals, Novartis AG	2020 (Europe)
5	Vutrisiran		Amyloidosis polyneuropathy	TTR	Alnylam Pharmaceuticals	2022 (America)
6	Nedosiran		Primary hyperoxaluria type 1	LDH	NovoNordisk	2023 (America)
7	Fomivirsen	ASO	Cytomega-lovirus retinitis	Cytomegalovirus	CIBA Vision Corp	1999 (Brazil)
8	Mipomersen		Familial hypercholesterolemia	APOB gene	Kastle Therapeutics	2013 (Argentina)
9	Nusinersen		Spinal muscular atrophy	SMN2	Biogen	2016 (America), 2019 (China)
10	Eteplirsen		Duchenne Muscular Dystrophy	Dystrophin gene exon 51	Sarepta Therapeutics	2016 (America)
11	Inotersen		Familial Amyloidotic Polyneuropathy	hATTR	Akcea Therapeutics; PTC Therapeutics	2018 (America)
12	Volanesorsen		Familial chylomicronemia syndrome	APOC3	Akcea Therapeutics; PTC Therapeutics	2019 (Europe)
13	Golodirsen		Duchenne muscular dystrophy	Dystrophin gene exon 53	Sarepta Therapeutics	2019 (America)
14	Viltolarsen		Duchenne muscular dystrophy	Dystrophin gene exon 53	Viltepso	2020 (Japan, America)
15	Casimersen		Duchenne muscular dystrophy	Dystrophin gene exon 45	Sarepta Therapeutics	2021 (America)
16	Tofersen		Amyotrophic lateral sclerosis	SOD1	Biogen, lonis	2023 (America) 2024 (China)
17	Pegaptanib	Aptamer	Wet age-related macular degeneration	VEGF	Bausch Health; Pfizer lnc	2012 (America), 2006 (Europe)

Abbreviations: siRNA: Small interfering RNA; ASO: Antisense oligonucleotide; hATTR: Hereditary transthyretin amyloidosis; ALAS1: 5'-aminolevulinate synthase 1; HAO1: Hydroxyacid oxidase 1; PCSK9: Proprotein convertase subtilisin/kexin type 9; TTR: Transthyretin; LDH: Lactate dehydrogenase; APOB: Apolipoprotein B; SMN2: Survival motor neuron 2; APOC3: Apolipoprotein C-III; SOD1: Superoxide dismutase 1; VEGF: Vascular endothelial growth factor.

4.2. Research status of small RNA drugs

The development of RNA therapeutics has reached several milestones, including the first application of ASOs (1978), the discovery of RNAi (1998), the approval of the first ASO drug (1998), the approval of the first RNA aptamer drug (2004), and the approval of the first siRNA drug (2018).[70]

By January 2025, 14 small RNA drugs had been approved by the US FDA for treating various human diseases. These include RNA aptamers (e.g., pegaptanib),[71,72] ASOs (e.g., mipomersen, eteplirsen, nusinersen, inotersen, casimersen, viltolarsen, tofersen, and golodirsen),[73-79] and siRNAs (e.g., patisiran, lumasiran, vutrisiran, nedosiran, and givosiran)[80-83] (Table 4). In addition, other small RNA drugs have been approved for marketing outside the USA, including volanesorsen,[79] fomivirsen,[84] and inclisiran[85,86] (Table 4). The mechanisms of action of these three types of small RNA drugs are shown in Figure 2.

The approved drugs mainly target rare diseases such as spinal muscular atrophy, Duchenne muscular dystrophy

(DMD), and familial amyloidotic polyneuropathy (Table 4).

The development of these small RNA drugs is predominantly led by six companies, including Alnylam (https://www.alnylam.com), Ionis (https://www.ionispharma.com), Sarepta (https://www.sarepta.com), Arrowhead (https://www.arrowheadpharma.com), Sirnaomics (https://www.sirnaomics.com), and Ruibo (https://www.ribobio.com).

Alnylam, a pioneer in the field of RNAi, has successfully commercialized multiple drugs, including patisiran, givosiran, lumasiran, and inclisiran. The company has developed a proprietary N-acetylgalactosamine (GalNAc) delivery system that efficiently delivers siRNA to liver tissue. At present, Alnylam's research pipeline covers multiple therapeutic areas, including rare diseases, metabolic diseases, cardiovascular diseases, and central nervous system disorders.

Ionis is a leader in ASO therapeutics and has successfully commercialized multiple drugs, including nusinersen, inotersen, volanesorsen, and eplontersen. The company has developed proprietary chemical modification technologies that enhance the stability, targeting, and therapeutic efficacy of ASOs. At present, Ionis' research pipeline covers multiple therapeutic areas, including rare diseases, metabolic diseases, cardiovascular diseases, and neurological disorders.

Similarly, Sarepta is a leader in the treatment of DMD, with three marketed ASO drugs, including eteplirsen, golodirsen, and casimersen. In addition to DMD, Sarepta's research pipeline focuses on other rare diseases, including Limb-Girdle muscular dystrophy.

Arrowhead focuses on the development and commercialization of RNAi-based technologies, with currently marketed drugs including vutrisiran and givosiran. The company has developed proprietary targeted delivery platforms, including TRiM™ (Targeted RNAi Molecule) and Dynamic Polyconjugate technologies, which enhance the stability, targeting, and therapeutic efficacy of siRNA. Arrowhead's research pipeline spans multiple therapeutic areas, including rare diseases, metabolic disorders, cardiovascular diseases, and liver diseases.

Sirnaomics has developed a proprietary peptide nanoparticle delivery platform to enhance the stability, targeting, and therapeutic efficacy of siRNA. The company focuses on common diseases, including cancer, fibrotic diseases, and metabolic disorders. In addition, they utilize a unique dual-targeting delivery technology to enhance treatment efficacy. Although Sirnaomics currently has no marketed drugs, its research direction and technology hold significant potential for future development.

Ruibo Biotech has developed its proprietary RIBO-GalSTAR delivery technology, which significantly enhances the liver-targeting efficiency of siRNA. The company's research efforts focus on metabolic diseases, cardiovascular diseases, and liver disorders. While Ruibo Biotech has yet to bring a drug to market, its rapidly advancing pipeline demonstrates substantial potential for future growth and development.

As of January 2025, in addition to the 17 approved drugs, 44 small RNA drug candidates are in clinical trials. Details of these drug candidates are shown in Table 5. These include 25 siRNA drugs, 10 ASO drugs, six miRNA mimics, and three miRNA inhibitors. These small RNA drug candidates cover a wide range of diseases, including genetic disorders (such as primary hyperoxaluria types 1 and 2, hemophilia A and B, and familial hypercholesterolemia), cardiovascular diseases (hypertension, atherosclerosis, and heart failure), liver diseases (hepatitis B, non-alcoholic steatohepatitis, and hepatocellular carcinoma), ocular diseases (dry eye disease with Sjögren syndrome, elevated intraocular pressure, diabetic macular edema, and wet age-related macular degeneration), cancers (PC, solid tumor cancers, and hematologic malignancies), and kidney diseases (acute kidney injury), among others.

In summary, small RNA drugs are highly active in clinical trials and cover a wide range of disease areas, demonstrating their immense potential. With continuous advancements in delivery systems, siRNA drugs currently lead the field, whereas ASO and miRNA technologies are also advancing rapidly. Interestingly, no miRNA-based drugs have reached the market, and many have been discontinued during clinical trials. This may be due to the inherent complexity of miRNAs, which typically target multiple sites, making it challenging to precisely define their mechanisms of action. As a result, ensuring patient safety remains a significant challenge in the clinical development of miRNA therapeutics.

4.3. Advantages and challenges of small RNA drugs

RNA-based therapies offer three key advantages. First, small RNA drugs can target both protein-coding and non-coding genes, enabling precise regulation of gene expression, thus offering broad therapeutic potential. Second, the design and synthesis of small RNA drugs are rapid, allowing them to quickly advance into pre-clinical and clinical studies. The accumulated knowledge from prior research in RNA characterization continues to expedite this process. Third, small RNA drugs can exert sustained effects on cells, potentially achieving long-term therapeutic outcomes with a single dose. For instance, recent clinical trials have demonstrated that siRNAs drugs

Table 5. List of small RNA drugs in clinical trials

Number	Clinical trial number	Type	Drug candidate name	Target name	Targeted disease	Status
1	NCT00689065	siRNA	CALAA-01	RRM2	Solid tumor cancers	Phase 1
2	NCT04202354	siRNA	ARO-HSD	Unknown	NASH	Phase 1
3	NCT04169711	siRNA	ALN-HSD	Unknown	NASH	Phase 1
4	NCT04565718	siRNA	ARO-HIF2	HIF2α	HCC	Phase 1
5	NCT00499590	siRNA	Bevasiranib	VEGF	AMD	Phase 1
6	NCT02110563	siRNA	DCR-MYC	MYC	Hematological malignancy	Phase 1
7	NCT04936035	siRNA	Zilebesiran (ALN-AGT01)	AGT	Mild-to-moderate hypertension	Phase 2
8	NCT03365947	siRNA	ARO-HBV (JNJ-3989)	HBV	Hepatitis B	Phase 2
9	NCT04832971	siRNA	ARO-ANG3	ANGPTL3	Mixed dyslipidemia	Phase 2
10	NCT02963311	siRNA	ALN-PCSSC	PCSK9	Homozygous familial hypercholesterolemia	Phase 2
11	NCT02250612	siRNA	SYL040012	ADRB2	Elevated intraocular pressure	Phase 2
12	NCT01965106	siRNA	QPI-1007	Caspase2	Acute primary angle closure glaucoma	Phase 2a
13	NCT01445899	siRNA	PF-0423655	Unknown	Diabetic macular edema, choroidal neovascularization, diabetic	Phase 2
14	NCT05637255	siRNA	SYL1801	Unknown	Wet AMD	Phase 2
15	NCT04669808	siRNA	Cotsiranib (STP705)	TGF-β1, COX-2	Hypertrophic scarring	Phase 2
16	NCT04012099	siRNA	cp-asiRNA	Unknown	Prevention of hypertrophic scarring	Phase 2a
17	NCT02030275	siRNA	RXI-109	CTGF	Hypertrophic scarring	Phase 2
18	NCT01676259	siRNA	siG12D-LODER	KRAS G12D	Pancreatic cancer	Phase 2
19	NCT03974113	siRNA	Fitusiran	AT3	Hemophilia A and B	Phase 2
20	NCT02610296	siRNA	Teprasiran (I5NP, QPI-1002)	p53	Acute kidney injury	Phase 3
21	NCT04042402	siRNA	DCR-PHXC	LDHA	Primary hyperoxaluria type 1,2	Phase 3
22	NCT03549871	siRNA	ALN-AT3SC	AT3	Hemophilia A and B	Phase 3
23	NCT02319005	siRNA	ALN-TTRSC	TTR	Transthyretin-mediated amyloidosis	Phase 3
24	NCT03108664	siRNA	Tivanisiran (SYL1001)	TRPV1	Dry eye disease with Sjögren syndrome	Phase 3
25	NCT04288856	ASO	BIIB078	C9orf72	Amyotrophic lateral sclerosis	Phase 1
26	NCT02981602	ASO	IONIS-HBVRx	HBV	Hepatitis B	Phase 1
27	NCT03421353	ASO	AZD9150	STAT3	Solid tumor cancers	Phase 2
28	NCT00062244	ASO	Oblimersen	BCL-2	Hematological malignancy	Phase 2
29	NCT04855045	ASO	Sepofarsen	CEP290	Hereditary retinal diseases	Phase 2
30	NCT04023552	ASO	TQJ230	Unknown	Cardiovascular disease and lipoprotein (a)	Phase 3
31	NCT04136171	ASO	Eplontersen	TTR	ATTR-CM	Phase 3
32	NCT05185843	ASO	Olezarsen	APOC3	Familial chylomicronemia syndrome	Phase 3
33	NCT05139810	ASO	Tominersen	HTT	Huntington's Disease	Phase 3
34	NCT05139810	ASO	ION363	Unknown	Amyotrophic lateral sclerosis	Phase 3
35	NCT02369198	miR-16	TargomiRs	Unknown	Recurrent malignant pleural mesothelioma and non-small cell lung cancer	Phase 1
36	NCT01829971	miR-34	MRX34	miR-34	Liver cancer and lymphoma	Phase 1
37	NCT03601052	miR-29	Remlarsen	miR-29	History of keloid scars	Phase 1
38	NCT03603431	microRNA-92 inhibitors	MRG-110	miR-92	Myocardial infarction	Phase 1

(*Contd*...)

Table 5. (*Continued*)

Number	Clinical trial number	Type	Drug candidate name	Target name	Targeted disease	Status
39	NCT03373786	miR-21 inhibitors	RG-012	miR-21	Alport syndrome	Phase 1
40	NCT03713320	miR-155	Cobomarsen	miR-155	CTCL and MF subtype	Phase 2
41	NCT04675996	miR-193a-3p	INT-1B3	Unknown	Advanced solid tumors	Phase 2
42	NCT02508090	miR-122 inhibitors	Miravirsen	miR-122	Hepatitis C virus	Phase 2
43	NCT05953831	miR-132 inhibitors	CDR132L	miR-132	Heart failure	Phase 2

Source: Data obtained from https://clinicaltrials gov.
Abbreviations: siRNA: Small interfering RNA; ASO: Antisense oligonucleotide; RRM2: Ribonucleotide reductase regulatory subunit M2; HIF2α: Hypoxia-inducible factor 2 alpha; MYC: MYC proto-oncogene; AGT: Angiotensinogen; HBV: Hepatitis B virus; ANGPTL3: Angiopoietin-like 3; PCSK9: Proprotein convertase subtilisin/kexin type 9; ADRB2: Adrenoceptor beta 2; TGF-β1: Transforming growth factor beta 1; COX-2: Cyclooxygenase-2; CTGF: Connective tissue growth factor; KRAS G12D: Kirsten rat sarcoma viral oncogene homolog with G12D mutation; AT3: Antithrombin III; LDHA: Lactate dehydrogenase A; TTR: Transthyretin; TRPV1: Transient receptor potential vanilloid-1; C9orf72: Chromosome 9 open reading frame 72; STAT3: Signal transducer and activator of transcription-3; BCL-2: B-cell lymphoma 2; CEP290: Centrosomal protein 290; APOC3: Apolipoprotein C3; HTT: Huntingtin; NASH: Nonalcoholic steatohepatitis; HCC: Hepatocellular carcinoma; AMD: Age-related macular degeneration; ATTR-CM: Transthyretin amyloid cardiomyopathy; CTCL: Cutaneous T-cell lymphoma; MF: Mycosis fungoides.

effectively suppress proprotein convertase subtilisin/kexin type 9 gene expression, resulting in sustained reductions in low-density lipoprotein cholesterol levels for up to 6 months post-treatment.[87] This long-lasting effect is particularly beneficial for patients who may not undergo frequent treatments.

Despite these advantages, small RNA drugs also have three key disadvantages. First, targeted delivery remains a major challenge. However, significant progress has been made in developing various delivery platforms. Evidence from recently approved RNA-based drugs and ongoing clinical trials suggests that RNA therapies can be delivered to the liver with high efficiency. However, effective delivery to non-liver tissues and organs remains a significant challenge. Future research will need to focus on developing strategies to enhance RNA delivery to these targeted tissues.

Second, the synthesis and purification of small RNA drugs are complex and costly. The need for chemical modifications and specialized delivery systems further increases manufacturing expenses, making RNA drugs among the most expensive medications on the market.[88,89] While automation has improved the chemical synthesis and purification processes, the production of large quantities of synthetic RNA for animal studies, clinical trials, and large-scale medical use remains logistically and economically challenging.

Third, artificial modifications of RNA raise concerns regarding their impact on RNA folding, activity, and safety compared to naturally occurring RNA.[90,91] At present, more clinical data are needed to assess the long-term risks associated with these modifications. Further advancements in RNA therapeutics will depend on improvements in RNA design, the development of more efficient delivery systems, and the refinement of targeted technologies to ensure therapeutic efficacy while minimizing off-target effects and immunogenicity.

4.4. Chemical modification and delivery of small RNA drugs

A significant challenge in developing RNA-based drugs is preventing degradation by serum RNases while enabling RNA molecules to cross the membranes of target cells, ensuring sufficient intracellular delivery to elicit pharmacological effects. Certain chemical modifications can greatly enhance the metabolic stability and pharmacokinetic properties of RNA,[90,92-94] making them more viable as drug candidates.

Modifications to the phosphate backbone, ribose ring, and 3'- and 5'-ends of RNA can improve substrate specificity, enhance nuclease resistance, and facilitate targeted delivery. In addition, these modifications can reduce toxicity and immune responses.[95] The modification of the phosphorothioate backbone was the first widely adopted modification in ASOs, in which one of the non-bridging oxygen atoms in the internucleotide phosphate group is replaced with sulfur.[96] This modification increases the hydrophobicity of ASO molecules, enhances resistance to phosphodiesterases, improves cellular uptake, and strengthens binding to serum proteins, thereby improving bioavailability.[96] The 2'-fluoro (2'-F) and 2'-O-methyl (2'-

O-Me) modifications mimic the biophysical characteristics of the 2'-hydroxyl (2'-OH) group, which stabilize siRNAs against RNases while preventing activation of innate immune receptors. Consequently, nearly all therapeutic siRNAs in clinical trials incorporate either 2'-F or 2'-O-Me modifications.[97]

Moreover, RNA drugs can now be actively delivered to target cells or tissues through encapsulation or formulation with specific materials, as well as through viral vectors, plasmid DNAs, or intact cells.[98-101]

Advancements in nanotechnology and materials science provide promising solutions to the challenges of oligonucleotide drug delivery, particularly in facilitating intracellular delivery across biological barriers and membranes. Key advantages of nanoparticle drug delivery systems include the ability to customize biophysics and biological properties for precise delivery. RNA-delivering nanoparticles can be synthesized in various forms.[102] One strategy involves encapsulating RNA inside lipid bilayers with a positively charged surface, forming lipid nanoparticles that protect RNA and extend its half-life. Patisiran is an example of an RNA drug utilizing this lipid nanoparticle-based delivery system, and many other RNA drugs in clinical trials employ similar formulations for delivery.[103] Another approach involves blending negatively charged RNAs with positively charged polymers.[100] Since the liver is the primary organ responsible for filtering nanoparticles, a significant portion of nanoparticle-based RNA therapies has been designed to target liver-related diseases.[104]

A prominent approach for RNA drug delivery involves the use of conjugates. By binding to specific receptors on cell surfaces, conjugates facilitate the targeted delivery of covalently attached RNA molecules. A well-known conjugate in RNA therapy is GalNAc, which specifically targets the hepatocyte-specific asialoglycoprotein receptor.[105] Givosiran, based on GalNAc conjugate technology, is the first FDA-approved RNA drug. Compared to nanoparticle-based delivery systems, conjugate-based delivery requires fewer excipient materials, thereby reducing the risk of toxicity. With the continuous development of new technologies, microrobots also hold significant potential for the delivery system of small RNA drugs.[106]

4.5. Other emerging topics in small RNA drugs

Monoclonal antibodies (mAbs) are well-established therapeutic agents due to their high specificity and sensitivity to extracellular targets. They have also been employed in the targeted delivery of small-molecule drugs, as demonstrated by antibody-drug conjugates, which enable precise delivery of chemotherapeutic agents to tumor cells while minimizing toxicity to healthy tissues and cells.[107] Similarly, antibody-oligonucleotide conjugates (AOCs) have also been shown to facilitate the targeted delivery of oligonucleotides to specific tissues and cells, expanding their therapeutic applications beyond the liver.[108] These molecules consist of an antibody linked to an oligonucleotide through a linker, offering a flexible and customizable approach. The antibody targets a cell type of interest specifically, which enables the oligonucleotide to reach and regulate a disease-associated gene.

In 2019, Avidity launched the first AOC drug, AOC 1001, a transferrin receptor 1 (TfR1)-targeted mAb conjugated with anti-myotonic dystrophy type 1 (DM1) protein kinase siRNA for the treatment of DM1, which entered Phase I clinical trials in November 2021.[109] Recently, Avidity's AOC drug, AOC 1044, a TfR1-targeted mAb for DMD disease with anti-DMD phosphorodiamidate morpholino oligomer, received FDA fast track and orphan drug status, further boosting the enthusiasm for AOC development. AOCs are typical combinatorial innovations and have great potential in the future.

5. Development of small RNA drugs for PC

To date, two clinical trials of siRNA-based therapies for PC have been reported. The first therapy, siG12D-LODER, is a biodegradable polymer matrix containing siRNA targeting KRAS G12D, a mutation in *KRAS* gene. siG12D-LODER has been studied in a dose-escalation Phase I trial involving 15 patients, showing a high safety and tolerability profile, with no instances of dose-limiting toxicity.[110] In 2018, this study advanced to a Phase 2 clinical trial to evaluate the response rate of siG12D-LODER in patients with unresectable or borderline resectable PC.[110] The second therapy, CALAA-01, was developed to inhibit tumor growth and/or shrink tumors. CALAA-01 contained a siRNA that can suppress the expression of the M2 subunit of ribonucleotide reductase, thereby reducing tumor growth.[111] In particular, the CALAA-01 siRNA was encapsulated in a stabilized nanoparticle to shield it from nuclease degradation (Table 5).[111]

In addition to siRNA, the therapeutic use of ASO and miRNA mimics has also been developed for cancer treatment, including PC. AZD9150 is an ASO drug that has been under clinical investigation for patients with advanced solid tumors. In August 2024, it completed its Phase 2 clinical trial, demonstrating preliminary anti-tumor activity. INT-1B3 is a lipid nanoparticle-formulated miRNA (miR-193a-3p) mimic developed for therapeutic intervention in oncology. Pre-clinical work suggested that the mechanism of action of INT-1B3 involves

multiple targets, including the inhibition of tumor cell proliferation, metastasis, and migration, disruption of the cell cycle, induction of apoptosis, modulation of the tumor microenvironment, and enhancement of T cell-mediated immune responses.[112]

6. Discussion

In recent years, numerous studies have provided detailed insights into the extensive alterations of small RNA in cancer.[113] Large international cancer consortiums, such as The Cancer Genome Atlas[114] and the Cancer Cell Line Encyclopedia,[115] have mapped the miRNA landscape in over 10,000 patient samples and more than 1,000 cancer cell lines from various cancer types. These large-scale datasets have offered an unprecedented opportunity to explore the functional roles of miRNAs and their mechanisms of action. Given the intricate nature of miRNA expression regulation, a key challenge lies in determining whether miRNA dysregulation is a driving factor in disease progression or merely a result of the disease development. Some miRNAs function as oncogenes or tumor suppressors depending on the tumor type, stage, and tumor microenvironment. This underscores the importance of elucidating miRNA functions in a context-dependent manner.[116,117]

In this review, six strategies have been proposed to develop small RNA drugs specifically aimed at PC. The first strategy is to target mRNAs involved in PC development, including KRAS, NF-κB, and MMP2. Furthermore, ASOs, siRNAs, and miRNA mimics can be designed to downregulate the mRNA expression of these genes. The second strategy is to design aptamers that bind to proteins involved in PC development and inhibit their activity. These proteins include KRAS, NF-κB, and MMP2. The third strategy is to design miRNA inhibitors to target miRNAs that promote PC initiation and metastasis, thereby downregulating their expression, such as miR-181, miR-21, and miR-155. The fourth strategy is to design miRNA mimics to restore the expression levels of tumor-suppressive miRNAs that inhibit PC progression, such as miR-200, miR-34, and miR-143 (Table 3). The fifth strategy focuses on targeting genes associated with chemotherapy resistance in PC. For example, siRNAs, ASOs, and miRNA mimics can be designed to target hENT1, MRP, and *DPD* genes. This strategy is intended to be used in combination with other chemotherapy drugs. Finally, the sixth strategy involves targeting genes that modulate the tumor microenvironment, such as P4HA1. All these targets are summarized in Tables 2 and 3.

With the continuous advancement of technology, these strategies are expected to facilitate the development of effective treatments for PC.

7. Conclusion

This review summarizes the current status of drug therapy for PC and the research progress on small RNA drugs. Six strategies are proposed for developing small RNA drugs against PC.

Acknowledgments

None.

Funding

The study was supported by the National Natural Science Foundation of China (81872966), the CAMS Innovation Fund for Medical Sciences (CIFMS) (2021-1-I2M-022), the Provincial Special Project for Construction of Innovation Demonstration Area at Chenzhou City under the National Sustainable Development Plan (2023sfq04), and the National Science and Technology Fundamental Resources Investigation Program of China (2018FY100705). The funders had no role in the study design, data collection, analysis, publication decision, or manuscript preparation.

Conflict of interest

The authors declare they have no competing interests.

Author contributions

Conceptualization: Chang Liu, Haimei Chen
Writing – original draft: Qingqing Zhou
Writing – review & editing: Chang Liu, Huaying Li, Guoan Shen

Ethics approval and consent to participate

Not applicable.

Consent for publication

Not applicable.

Availability of data

Not applicable.

References

1. Vincent A, Herman J, Schulick R, Hruban RH, Goggins M. Pancreatic cancer. *Lancet*. 2011;378(9791):607-620.

   doi: 10.1016/s0140-6736(10)62307-0

2. Luo YH, Luo L, Wampfler JA, *et al*. 5-year overall survival in patients with lung cancer eligible or ineligible for screening according to US PREVENTIVE SERVICES TASK FORCE criteria: A prospective, observational cohort study. *Lancet Oncol*. 2019;20(8):1098-1108.

   doi: 10.1016/s1470-2045(19)30329-8

3. Wang R, Lian J, Wang X, *et al*. Survival rate of colorectal cancer in China: A systematic review and meta-analysis. *Front Oncol*. 2023;13:1033154.

doi: 10.3389/fonc.2023.1033154

4. Maleki Z, Vali M, Nikbakht HA, *et al*. Survival rate of ovarian cancer in Asian countries: A systematic review and meta-analysis. *BMC Cancer*. 2023;23(1):558.

doi: 10.1186/s12885-023-11041-8

5. Wang Z, Liu Z, Qu J, Sun Y, Zhou WJAMM. Role of natural products in tumor therapy from basic research and clinical perspectives. *Acta Mater Med*. 2024;3:163-206.

doi: 10.15212/AMM-2023-0050

6. Padillo-Ruiz J, Suarez G, Pereira S, *et al*. Circulating tumor cells enumeration from the portal vein for risk stratification in early pancreatic cancer patients. *Cancers* (*Basel*). 2021;13(24):6153.

doi: 10.3390/cancers13246153

7. Bu LL, Yan J, Wang Z, *et al*. Advances in drug delivery for post-surgical cancer treatment. *Biomaterials*. 2019;219:119182.

doi: 10.1016/j.biomaterials.2019.04.027

8. Crooke ST, Witztum JL, Bennett CF, Baker BF. RNA-targeted therapeutics. *Cell Metab*. 2019;29(2):501.

doi: 10.1016/j.cmet.2019.01.001

9. Yu AM, Choi YH, Tu MJ. RNA drugs AND RNA targets for small molecules: Principles, progress, and challenges. *Pharmacol Rev*. 2020;72(4):862-898.

doi: 10.1124/pr.120.019554

10. Siegel RL, Giaquinto AN, Jemal A. Cancer statistics, 2024. *CA Cancer J Clin*. 2024;74(1):12-49.

doi: 10.3322/caac.21820

11. Rahib L, Smith BD, Aizenberg R, Rosenzweig AB, Fleshman JM, Matrisian LM. Projecting cancer incidence and deaths to 2030: The unexpected burden of thyroid, liver, and pancreas cancers in the United States. *Cancer Res*. 2014;74(11): 2913-2921.

doi: 10.1158/0008-5472.Can-14-0155

12. Siegel RL, Miller KD, Wagle NS, Jemal A. Cancer statistics, 2023. *CA A Cancer J Clin*. 2023;73(1):17-48.

doi: 10.3322/caac.21763

13. Kleeff J, Korc M, Apte M, *et al*. Pancreatic cancer. *Nat Rev Dis Primers*. 2016;2(1):16022.

doi: 10.1038/nrdp.2016.22

14. Zeng S, Pöttler M, Lan B, Grützmann R, Pilarsky C, Yang H. chemoresistance in pancreatic cancer. *Int J Mol Sci*. 2019;20(18):4504.

doi: 10.3390/ijms20184504

15. Sarvepalli D, Rashid MU, Rahman AU, *et al*. Gemcitabine: A review of chemoresistance in pancreatic cancer. *Crit Rev Oncog*. 2019;24(2):199-212.

doi: 10.1615/CritRevOncog.2019031641

16. Conroy T, Desseigne F, Ychou M, *et al*. FOLFIRINOX versus gemcitabine for metastatic pancreatic cancer. *New Engl J Med*. 2011;364(19):1817-1825.

doi: 10.1056/NEJMoa1011923

17. Gourgou-Bourgade S, Bascoul-Mollevi C, Desseigne F, *et al*. Impact of FOLFIRINOX compared with gemcitabine on quality of life in patients with metastatic pancreatic cancer: Results from the PRODIGE 4/ACCORD 11 randomized trial. *J Clin Oncol*. 2013;31(1):23-29.

doi: 10.1200/jco.2012.44.4869

18. Von Hoff DD, Ervin T, Arena FP, *et al*. Increased survival in pancreatic cancer with nab-paclitaxel plus gemcitabine. *New Engl J Med*. 2013;369(18):1691-1703.

doi: 10.1056/NEJMoa1304369

19. Hruban RH, Goggins M, Parsons J, Kern SE. Progression model for pancreatic cancer. *Clin Cancer Res*. 2000;6(8): 2969-2972.

20. Notta F, Chan-Seng-Yue M, Lemire M, *et al*. A renewed model of pancreatic cancer evolution based on genomic rearrangement patterns. *Nature*. 2016;538(7625):378-382.

doi: 10.1038/nature19823

21. Corcoran RB, Contino G, Deshpande V, *et al*. STAT3 plays a critical role in KRAS-induced pancreatic tumorigenesis. *Cancer Res*. 2011;71(14):5020-5029.

doi: 10.1158/0008-5472.Can-11-0908

22. Mello SS, Flowers BM, Mazur PK, *et al*. Multifaceted role for p53 in pancreatic cancer suppression. *Proc Natl Acad Sci U S A*. 2023;120(10):e2211937120.

doi: 10.1073/pnas.2211937120

23. Doyle A, Kubler MM, Harris AC, *et al*. The impact of CDKN2A mutations on overall survival in pancreatic adenocarcinoma. *J Clin Oncol*. 2019;37(4_suppl):278-278.

doi: 10.1200/JCO.2019.37.4_suppl.278

24. Xia X, Wu W, Huang C, *et al*. SMAD4 and its role in pancreatic cancer. *Tumour Biol*. 2015;36(1):111-119.

doi: 10.1007/s13277-014-2883-z

25. Xu Y, Lin Z, Ji Y, *et al*. Pan-cancer analysis identifies RNF43 as a prognostic, therapeutic and immunological biomarker. *Eur J Med Res*. 2023;28(1):438.

doi: 10.1186/s40001-023-01383-1

26. Ishii N, Araki K, Yokobori T, *et al*. Reduced FBXW7 expression in pancreatic cancer correlates with poor prognosis and chemotherapeutic resistance via accumulation of MCL1. *Oncotarget*. 2017;8(68):112636-112646.

doi: 10.18632/oncotarget.22634

27. Ellenrieder V, Alber B, Lacher U, *et al*. Role of MT-MMPs and MMP-2 in pancreatic cancer progression. *Int J Cancer*. 2000;85(1):14-20.

doi: 10.1002/(sici)1097-0215(20000101)85:1<14:aid-ijc3>3.0.co;2-o

28. Hui B, Ji H, Xu Y, *et al*. RREB1-induced upregulation of the lncRNA AGAP2-AS1 regulates the proliferation and migration of pancreatic cancer partly through suppressing ANKRD1 and ANGPTL4. *Cell Death Dis*. 2019;10(3):207.

doi: 10.1038/s41419-019-1384-9

29. Silke J, O'Reilly LA. NF-κB and pancreatic cancer; Chapter and verse. *Cancers* (*Basel*). 2021;13(18):4510.

doi: 10.3390/cancers13184510

30. Du Z, Zhang Q, Xiang X, *et al*. RRM2 promotes liver metastasis of pancreatic cancer by stabilizing YBX1 and activating the TGF-beta pathway. *iScience*. 2024;27(10):110864.

doi: 10.1016/j.isci.2024.110864

31. Li R, Liu R, Xu Y, *et al*. Suppressing pancreatic cancer survival and immune escape via nanoparticle-modulated STING/STAT3 axis regulation. *Bioconjug Chem*. 2024;35(11):1815-1822.

doi: 10.1021/acs.bioconjchem.4c00379

32. Martinez S, Wu S, Geuenich M, *et al*. *In vivo* CRISPR screens reveal SCAF1 and USP15 as drivers of pancreatic cancer. *Nat Commun*. 2024;15(1):5266.

doi: 10.1038/s41467-024-49450-3

33. Gu A, Li J, Li MY, Liu Y. Patient-derived xenograft model in cancer: Establishment and applications. *MedComm* (*2020*). 2025;6(2):e70059.

doi: 10.1002/mco2.70059

34. Raffenne J, Nicolle R, Puleo F, *et al*. hENT1 testing in pancreatic ductal adenocarcinoma: Are we ready? A multimodal evaluation of hENT1 status. *Cancers* (*Basel*). 2019;11(11):1808.

doi: 10.3390/cancers11111808

35. Elander NO, Aughton K, Ghaneh P, *et al*. Expression of dihydropyrimidine dehydrogenase (DPD) and hENT1 predicts survival in pancreatic cancer. *Br J Cancer*. 2018;118(7):947-954.

doi: 10.1038/s41416-018-0004-2

36. Arana MR, Altenberg GA. ATP-binding cassette exporters: Structure and mechanism with a focus on P-glycoprotein and MRP1. *Curr Med Chem*. 2019;26(7):1062-1078.

doi: 10.2174/0929867324666171012105143

37. Kohan HG, Boroujerdi M. Time and concentration dependency of P-gp, MRP1 and MRP5 induction in response to gemcitabine uptake in Capan-2 pancreatic cancer cells. *Xenobiotica*. 2015;45(7):642-652.

doi: 10.3109/00498254.2014.1001809

38. Adamska A, Elaskalani O, Emmanouilidi A, *et al*. Molecular and cellular mechanisms of chemoresistance in pancreatic cancer. *Adv Biol Regul*. 2018;68:77-87.

doi: 10.1016/j.jbior.2017.11.007

39. Gu A, Li J, Qiu S, *et al*. Pancreatic cancer environment: From patient-derived models to single-cell omics. *Mol Omics*. 2024;20(4):220-233.

doi: 10.1039/d3mo00250k

40. Zhang Y, Xu M. Research advances in the mechanism of tumor microenvironment in pancreatic cancer and related targeted therapy. *J Clin Hepatol*. 2022;38(4):965-968.

doi: 10.3969/j.issn.1001-5256.2022.04.046

41. Cencioni C, Malatesta S, Vigiano Benedetti V, *et al*. The GLP-1R agonist semaglutide reshapes pancreatic cancer associated fibroblasts reducing collagen proline hydroxylation and favoring T lymphocyte infiltration. *J Exp Clin Cancer Res*. 2025;44(1):18.

doi: 10.1186/s13046-024-03263-w

42. Li Y, VandenBoom TG 2nd, Kong D, *et al*. Up-regulation of miR-200 and let-7 by natural agents leads to the reversal of epithelial-to-mesenchymal transition in gemcitabine-resistant pancreatic cancer cells. *Cancer Res*. 2009;69(16):6704-6712.

doi: 10.1158/0008-5472.Can-09-1298

43. Ji Q, Hao X, Zhang M, *et al*. MicroRNA miR-34 inhibits human pancreatic cancer tumor-initiating cells. *PLoS One*. 2009;4(8):e6816.

doi: 10.1371/journal.pone.0006816

44. Kent OA, Fox-Talbot K, Halushka MK. RREB1 repressed miR-143/145 modulates KRAS signaling through downregulation of multiple targets. *Oncogene*. 2013;32(20):2576-2585.

doi: 10.1038/onc.2012.266

45. Fujioka S, Sclabas GM, Schmidt C, *et al*. Function of nuclear factor kappaB in pancreatic cancer metastasis. *Clin Cancer Res*. 2003;9(1):346-354.

46. Li Y, Vandenboom TG 2nd, Wang Z, *et al*. miR-146a suppresses invasion of pancreatic cancer cells. *Cancer Res*. 2010;70(4):1486-1495.

doi: 10.1158/0008-5472.Can-09-2792

47. Yan H, Wu J, Liu W, *et al*. MicroRNA-20a overexpression inhibited proliferation and metastasis of pancreatic carcinoma cells. *Human Gene Ther*. 2010;21(12):1723-1734.

doi: 10.1089/hum.2010.061

48. Zhao G, Zhang JG, Shi Y, *et al*. MiR-130b is a prognostic marker and inhibits cell proliferation and invasion in

pancreatic cancer through targeting STAT3. *PLoS One*. 2013;8(9):e73803.

doi: 10.1371/journal.pone.0073803

49. Zou Y, Li J, Chen Z, *et al*. miR-29c suppresses pancreatic cancer liver metastasis in an orthotopic implantation model in nude mice and affects survival in pancreatic cancer patients. *Carcinogenesis*. 2015;36(6):676-684.

doi: 10.1093/carcin/bgv027

50. Xu J, Wang T, Cao Z, *et al*. MiR-497 downregulation contributes to the malignancy of pancreatic cancer and associates with a poor prognosis. *Oncotarget*. 2014;5(16):6983-6993.

doi: 10.18632/oncotarget.2184

51. Li L, He Z, Zhu C, *et al*. MiR-137 promotes anoikis through modulating the AKT signaling pathways in pancreatic cancer. *J Cancer*. 2020;11(21):6277-6285.

doi: 10.7150/jca.44037

52. Zuo H. *MicroRNA Expression in Pancreatic Cancer*. China: Sun Yat-sen University; 2008.

53. Li R, Hu Y, Hou S. An exploration of oral-gut pathogens mediating immune escape of pancreatic cancer via miR-21/PTEN axis. *Front Microbiol*. 2022;13:928846.

doi: 10.3389/fmicb.2022.928846

54. Wang J, Guo J, Fan H. MiR-155 regulates the proliferation and apoptosis of pancreatic cancer cells through targeting SOCS3. *Eur Rev Med Pharmacol Sci*. 2019;23(12):5168-5175.

doi: 10.26355/eurrev_201906_18181

55. Xu Q, Li P, Chen X, *et al*. miR-221/222 induces pancreatic cancer progression through the regulation of matrix metalloproteinases. *Oncotarget*. 2015;6(16):14153-14164.

doi: 10.18632/oncotarget.3686

56. Sun XJ, Liu BY, Yan S, *et al*. MicroRNA-29a promotes pancreatic cancer growth by inhibiting tristetraprolin. *Cell Physiol Biochem*. 2015;37(2):707-718.

doi: 10.1159/000430389

57. Lian M, Mortoglou M, Uysal-Onganer P. Impact of hypoxia-induced miR-210 on pancreatic cancer. *Curr Issues Mol Biol*. 2023;45(12):9778-9792.

doi: 10.3390/cimb45120611

58. Lewis BP, Burge CB, Bartel DP. Conserved seed pairing, often flanked by adenosines, indicates that thousands of human genes are microRNA targets. *Cell*. 2005;120(1):15-20.

doi: 10.1016/j.cell.2004.12.035

59. Bartel DP. Metazoan MicroRNAs. *Cell*. 2018;173(1):20-51.

doi: 10.1016/j.cell.2018.03.006

60. Shang R, Lee S, Senavirathne G, Lai EC. microRNAs in action: Biogenesis, function and regulation. *Nat Rev* 10.1038/s41576-023-00611-y *Genet*. 2023;24(12):816-833.

doi: 10.1038/s41576-023-00611-y

61. Alshaer W, Zureigat H, Al Karaki A, *et al*. siRNA: Mechanism of action, challenges, and therapeutic approaches. *Eur J Pharmacol*. 2021;905:174178.

doi: 10.1016/j.ejphar.2021.174178

62. Dhuri K, Bechtold C, Quijano E, *et al*. Antisense oligonucleotides: An emerging area in drug discovery and development. *J Clin Med*. 2020;9(6):2004.

doi: 10.3390/jcm9062004

63. Wu H, Lima WF, Zhang H, Fan A, Sun H, Crooke ST. Determination of the role of the human RNase H1 in the pharmacology of DNA-like antisense drugs. *J Biol Chem*. 2004;279(17):17181-17189.

doi: 10.1074/jbc.M311683200

64. Yin W, Rogge M. Targeting RNA: A transformative therapeutic strategy. *Clin Transl Sci*. 2019;12(2):98-112.

doi: 10.1111/cts.12624

65. Bennett CF, Swayze EE. RNA targeting therapeutics: Molecular mechanisms of antisense oligonucleotides as a therapeutic platform. *Ann Rev Pharmacol Toxicol*. 2010;50:259-293.

doi: 10.1146/annurev.pharmtox.010909.105654

66. Passini MA, Bu J, Richards AM, *et al*. Antisense oligonucleotides delivered to the mouse CNS ameliorate symptoms of severe spinal muscular atrophy. *Sci Transl Med*. 2011;3(72):72ra18.

doi: 10.1126/scitranslmed.3001777

67. Chai C, Xie Z, Grotewold E. SELEX (systematic evolution of ligands by exponential enrichment), as a powerful tool for deciphering the protein-DNA interaction space. *Methods Mol Biol*. 2011;754:249-258.

doi: 10.1007/978-1-61779-154-3_14

68. Zhang Y, Lai BS, Juhas M. Recent advances in aptamer discovery and applications. *Molecules*. 2019;24(5):941.

doi: 10.3390/molecules24050941

69. Khan S, Hussain A, Fahimi H, *et al*. A review on the therapeutic applications of aptamers and aptamer-conjugated nanoparticles in cancer, inflammatory and viral diseases. *Arab J Chem*. 2022;15(2):103626.

doi: 10.1016/j.arabjc.2021.103626

70. Kim YK. RNA therapy: Rich history, various applications and unlimited future prospects. *Exp Mol Med*. 2022;54(4):455-465.

doi: 10.1038/s12276-022-00757-5

71. Gragoudas ES, Adamis AP, Cunningham ET Jr., Feinsod M,

Guyer DR. Pegaptanib for neovascular age-related macular degeneration. *N Engl J Med*. 2004;351(27):2805-2816.

doi: 10.1056/NEJMoa042760

72. Gryziewicz L. Regulatory aspects of drug approval for macular degeneration. *Adv Drug Deliv Rev*. 2005;57(14):2092-2098.

doi: 10.1016/j.addr.2005.09.009

73. Morrow T. For patients who inherit homozygous familial hypercholesterolemia, 2 new treatments available. *Manag Care*. 2013;22(3):47-48.

74. Stein CA. Eteplirsen approved for duchenne muscular dystrophy: The FDA faces a difficult choice. *Mol Ther*. 2016;24(11):1884-1885.

doi: 10.1038/mt.2016.188

75. Syed YY. Eteplirsen: First global approval. *Drugs*. 2016;76(17):1699-1704.

doi: 10.1007/s40265-016-0657-1

76. Ottesen EW. ISS-N1 makes the first FDA-approved drug for spinal muscular atrophy. *Transl Neurosci*. 2017;8:1-6.

doi: 10.1515/tnsci-2017-0001

77. Keam SJ. Inotersen: First global approval. *Drugs*. 2018;78(13):1371-1376.

doi: 10.1007/s40265-018-0968-5

78. Saad FA, Siciliano G, Angelini C. Advances in dystrophinopathy diagnosis and therapy. *Biomolecules*. 2023;13(9):1319.

doi: 10.3390/biom13091319

79. Chen W, Xu J, Wu Y, *et al*. The potential role and mechanism of circRNA/miRNA axis in cholesterol synthesis. *Int J Biol Sci*. 2023;19(9):2879-2896.

doi: 10.7150/ijbs.84994

80. Wood H. FDA approves patisiran to treat hereditary transthyretin amyloidosis. *Nat Rev Neurol*. 2018;14(10):570.

doi: 10.1038/s41582-018-0065-0

81. Scott LJ. Givosiran: First approval. *Drugs*. 2020;80(3): 335-339.

doi: 10.1007/s40265-020-01269-0

82. Gang X, Liu F, Mao J. Lumasiran for primary hyperoxaluria type 1: What we have learned? *Front Pediatr*. 2022;10:1052625.

doi: 10.3389/fped.2022.1052625

83. Keam SJ. vutrisiran: First approval. *Drugs*. 2022;82(13):1419-1425.

doi: 10.1007/s40265-022-01765-5

84. Perry CM, Balfour JA. Fomivirsen. *Drugs*. 1999;57(3):375-380; discussion 381.

doi: 10.2165/00003495-199957030-00010

85. Frampton JE. Inclisiran: A review in hypercholesterolemia. *Am J Cardiovasc Drugs*. 2023;23(2):219-230.

doi: 10.1007/s40256-023-00568-7

86. Lamb YN. Inclisiran: First approval. *Drugs*. 2021;81(3):389-395.

doi: 10.1007/s40265-021-01473-6

87. Fitzgerald K, White S, Borodovsky A, *et al*. A highly durable RNAi therapeutic inhibitor of PCSK9. *N Engl J Med*. 2017;376(1):41-51.

doi: 10.1056/NEJMoa1609243

88. Simoens S, Huys I. Market access of Spinraza (Nusinersen) for spinal muscular atrophy: Intellectual property rights, pricing, value and coverage considerations. *Gene Ther*. 2017;24(9):539-541.

doi: 10.1038/gt.2017.79

89. Burgart AM, Magnus D, Tabor HK, *et al*. Ethical challenges confronted when providing nusinersen treatment for spinal muscular atrophy. *JAMA Pediatr*. 2018;172(2):188-192.

doi: 10.1001/jamapediatrics.2017.4409

90. Ho PY, Yu AM. Bioengineering of noncoding RNAs for research agents and therapeutics. *Wiley Interdiscip Rev RNA*. 2016;7(2):186-197.

doi: 10.1002/wrna.1324

91. Yu AM, Batra N, Tu MJ, Sweeney C. Novel approaches for efficient *in vivo* fermentation production of noncoding RNAs. *Appl Microbiol Biotechnol*. 2020;104(5):1927-1937.

doi: 10.1007/s00253-020-10350-3

92. Bramsen JB, Kjems J. Development of therapeutic-grade small interfering RNAs by chemical engineering. *Front Genet*. 2012;3:154.

doi: 10.3389/fgene.2012.00154

93. Khvorova A, Watts JK. The chemical evolution of oligonucleotide therapies of clinical utility. *Nat Biotechnol*. 2017;35(3):238-248.

doi: 10.1038/nbt.3765

94. Yu AM, Jian C, Yu AH, Tu MJ. RNA therapy: Are we using the right molecules? *Pharmacol Ther*. 2019;196:91-104.

doi: 10.1016/j.pharmthera.2018.11.011

95. Wan WB, Seth PP. The medicinal chemistry of therapeutic oligonucleotides. *J Med Chem*. 2016;59(21):9645-9667.

doi: 10.1021/acs.jmedchem.6b00551

96. Eckstein F. Phosphorothioates, essential components of therapeutic oligonucleotides. *Nucleic Acid Ther*. 2014;24(6):374-387.

doi: 10.1089/nat.2014.0506

97. Setten RL, Rossi JJ, Han SP. The current state and future directions of RNAi-based therapeutics. *Nat Rev Drug*

Discov. 2019;18(6):421-446.

doi: 10.1038/s41573-019-0017-4

98. Tibbitt MW, Dahlman JE, Langer R. Emerging frontiers in drug delivery. *J Am Chem Soc*. 2016;138(3):704-717.

doi: 10.1021/jacs.5b09974

99. Dowdy SF. Overcoming cellular barriers for RNA therapeutics. *Nat Biotechnol*. 2017;35(3):222-229.

doi: 10.1038/nbt.3802

100. Kaczmarek JC, Kowalski PS, Anderson DG. Advances in the delivery of RNA therapeutics: From concept to clinical reality. *Genome Med*. 2017;9(1):60.

doi: 10.1186/s13073-017-0450-0

101. Kowalski PS, Rudra A, Miao L, Anderson DG. Delivering the messenger: Advances in technologies for therapeutic mRNA delivery. *Mol Ther*. 2019;27(4):710-728.

doi: 10.1016/j.ymthe.2019.02.012

102. Donahue ND, Acar H, Wilhelm S. Concepts of nanoparticle cellular uptake, intracellular trafficking, and kinetics in nanomedicine. *Adv Drug Deliv Rev*. 2019;143:68-96.

doi: 10.1016/j.addr.2019.04.008

103. Kulkarni JA, Cullis PR, van der Meel R. Lipid nanoparticles enabling gene therapies: From concepts to clinical utility. *Nucleic Acid Ther*. 2018;28(3):146-157.

doi: 10.1089/nat.2018.0721

104. Lorenzer C, Dirin M, Winkler AM, Baumann V, Winkler J. Going beyond the liver: Progress and challenges of targeted delivery of siRNA therapeutics. *J Control Release*. 2015;203:1-15.

doi: 10.1016/j.jconrel.2015.02.003

105. Huang X, Leroux JC, Castagner B. Well-defined multivalent ligands for hepatocytes targeting via asialoglycoprotein receptor. *Bioconju Chem*. 2017;28(2):283-295.

doi: 10.1021/acs.bioconjchem.6b00651

106. Wang J, Liao ZX. Research progress of microrobots in tumor drug delivery. *Food Med Homology*. 2024;1(2):9420025.

doi: 10.26599/FMH.2024.9420025

107. Khongorzul P, Ling CJ, Khan FU, Ihsan AU, Zhang J. Antibody-drug conjugates: A comprehensive review. *Mol Cancer Res*. 2020;18(1):3-19.

doi: 10.1158/1541-7786.Mcr-19-0582

108. Benizri S, Gissot A, Martin A, Vialet B, Grinstaff MW, Barthélémy P. Bioconjugated oligonucleotides: Recent developments and therapeutic applications. *Bioconjug Chem*. 2019;30(2):366-383.

doi: 10.1021/acs.bioconjchem.8b00761

109. Mullard A. Antibody-oligonucleotide conjugates enter the clinic. *Nat Rev Drug Discov*. 2022;21(1):6-8.

doi: 10.1038/d41573-021-00213-5

110. Varghese AM, Ang C, Dimaio CJ, Javle MM, O'Reilly EMJJoCO. A phase II study of siG12D-LODER in combination with chemotherapy in patients with locally advanced pancreatic cancer (PROTACT). *J Clin Oncol*. 2020;38(15_Suppl):TPS4672.

doi: 10.1200/JCO.2020.38.15_suppl.TPS4672

111. Zuckerman JE, Gritli I, Tolcher A, *et al*. Correlating animal and human phase Ia/Ib clinical data with CALAA-01, a targeted, polymer-based nanoparticle containing siRNA. *Proc Natl Acad Sci U S A*. 2014;111(31):11449-11454.

doi: 10.1073/pnas.1411393111

112. Duurland CL, Gunst T, den Boer HC, *et al*. INT-1B3, an LNP formulated miR-193a-3p mimic, promotes anti-tumor immunity by enhancing T cell mediated immune responses via modulation of the tumor microenvironment and induction of immunogenic cell death. *Oncotarget*. 2024;15:470-485.

doi: 10.18632/oncotarget.28608

113. Zhang Z, Zhang J, Diao L, Han L. Small non-coding RNAs in human cancer: Function, clinical utility, and characterization. *Oncogene*. 2021;40(9):1570-1577.

doi: 10.1038/s41388-020-01630-3

114. Weinstein JN, Collisson EA, Mills GB, *et al*. The cancer genome atlas pan-cancer analysis project. *Nat Genet*. 2013;45(10):1113-1120.

doi: 10.1038/ng.2764

115. Ghandi M, Huang FW, Jané-Valbuena J, *et al*. Next-generation characterization of the cancer cell line encyclopedia. *Nature*. 2019;569(7757):503-508.

doi: 10.1038/s41586-019-1186-3

116. Dhawan A, Scott JG, Harris AL, Buffa FM. Pan-cancer characterisation of microRNA across cancer hallmarks reveals microRNA-mediated downregulation of tumour suppressors. *Nat Commun*. 2018;9(1):5228.

doi: 10.1038/s41467-018-07657-1

117. Ding L, Lan Z, Xiong X, *et al*. The dual role of MicroRNAs in colorectal cancer progression. *Int J Mol Sci*. 2018;19(9):2791.

doi: 10.3390/ijms19092791

ACCSCIENCE PUBLISHING

Global Translational Medicine

REVIEW ARTICLE

Superparamagnetic iron oxide nanoparticle-based nanosystems for cancer theranostics

Jnanranjan Panda[1]* and Dipanwita Das[2]

[1]Faculty of Science, Sri Sri University, Cuttack, Odisha, India

[2]Department of Physics, Jadavpur University, Kolkata, West Bengal, India

(This article belongs to the *Special Issue: Recent advances in targeted therapy and immunotherapy for lung cancer*)

Abstract

The advancement of nanotechnology in the biomedical field has garnered growing interest due to the diverse physical properties of nanoparticles (NPs) and their potential applications in cancer theranostics. Although various nanodrug delivery systems, such as polymeric, lipid-based, and gold NPs, are available, superparamagnetic iron oxide NPs (SPIONs) have attracted significant attention due to their multifunctionality, biocompatibility, ease of surface functionalization, and responsiveness to external magnetic fields, enabling both cancer diagnostics and drug delivery applications. This review provides an overview of SPIONs as a powerful theranostic tool in cancer treatment. It also focuses on the synthesis and stabilization of SPIONs, discussing various protection and stabilization strategies using both organic coatings (synthetic and natural polymers) and inorganic coatings (such as silica and gold), as well as liposomes. In addition, the review highlights targeted biomedical applications of SPIONs, including magnetic resonance imaging, hyperthermia, and drug delivery. Finally, it also addresses the challenges and limitations of SPIONs, as well as their future perspective in clinical translation in cancer theranostics.

Keywords: Iron oxide nanoparticles; Synthesis methods; Stabilization; Cancer theranostics

***Corresponding author:**
Jnanranjan Panda
(jnanranjanpanda.phys.rs@jadavpuruniversity.in)

Citation: Panda J, Das D. Superparamagnetic iron oxide nanoparticle-based nanosystems for cancer theranostics. *Global Transl Med*. 2025;4(2):31-50. doi: 10.36922/gtm.8464

Received: January 8, 2025

1st revised: February 20, 2025

2nd revised: February 27, 2025

3rd revised: March 4, 2025

Accepted: March 4, 2025

Published online: March 21, 2025

1. Introduction

Over the past decade, nanomaterials and nanotechnology have received significant attention in cancer theranostics, as well as in cancer diagnosis and treatment, due to their unique physicochemical properties at the nanoscale.[1-3] Among the various nanoparticles (NPs), superparamagnetic iron oxide NPs (SPIONs), such as magnetite (Fe_3O_4) and hematite (γ-Fe_2O_3), have garnered substantial attention due to their favorable magnetic properties, low toxicity, biocompatibility, high chemical stability, and ease of surface functionalization.[4-7] SPION-based materials have emerged at the forefront of cancer research due to their potential to provide a comprehensive theranostic approach – serving both as imaging agents for early tumor detection and as drug carriers for targeted drug delivery – thus addressing many of the significant limitations associated with current therapeutic approaches.

Cancer, with a startling global death rate, has recently been identified as one of the most fatal illnesses. According to the 2022 report from the International Agency for Research

on Cancer, 20 million new cancer cases were diagnosed worldwide, resulting in 9.7 million cancer-related fatalities.[8] Among all cancer types, lung cancer remains the most diagnosed, representing 12.4% of all cancer diagnoses, followed by breast cancer, which accounts for 11.6% of total cases and is the most commonly diagnosed cancer among women in both developed and developing countries.[8] In India alone, more than 1.41 million new cancer cases were reported in 2022, with carcinoma responsible for 910,000 deaths and breast cancer being the leading cause of death. These statistics highlight the limitations of current cancer treatment modalities and underscore the need for the development of early cancer detection and more effective therapeutic approaches.

Despite the use of multimodal treatment strategies – including surgery, radiation therapy, and chemotherapy – that improve outcomes in patients with locally advanced cancer,[6,7] chemotherapy remains the primary option once cancer cells begin to metastasize.[6,7] However, conventional chemotherapy has significant disadvantages, particularly the severe adverse effects it causes in patients. As a result, one of the most challenging aspects of cancer treatment is delivering anticancer drugs to cancer cells while minimizing damage to healthy tissues. Similarly, traditional imaging modalities, such as magnetic resonance imaging (MRI) and X-ray computed tomography, also have inherent limitations due to the use of radioactive materials, high costs, low sensitivity, and limited tissue penetration depth. Given these drawbacks, novel and more efficient theranostic strategies incorporating highly sensitive probes must be developed for early and precise cancer detection.

In this context, nanomedicine has emerged at the forefront of cancer research due to its potential to provide a comprehensive theranostic approach, significantly impacting the global economy.[2-4] Various nanostructures, such as polymeric liposomes, gold (Au) NPs, and SPIONs, have been reported for target-specific drug delivery systems.[9-11] In particular, chemotherapeutic agents with poor solubility and less absorption capacity are encapsulated or integrated into these nanostructures. However, the effectiveness of these NPs in drug delivery applications depends on their shape, size, and other biophysical and chemical properties. A comparison table of different NP-based formulations is provided in Table 1. Although all nanostructures have both advantages and disadvantages, SPION-based nanostructures offer a versatile platform for loading various chemotherapeutic agents, enhancing the effectiveness of cancer treatment. At room temperature, SPIONs exhibit superparamagnetism when the particle size is smaller than 30 nm. When the applied external magnetic field is removed, this property is characterized by the absence of hysteresis, showing no remanence or coercivity and enabling the material to be used as a contrast agent for MRI, a widely used medical imaging tool. Under the influence of a magnetic field, SPION-based materials exhibit strong paramagnetic behavior, with high susceptibility and saturation magnetization.[1,7] SPION-based systems can be further enhanced to deliver a variety of cytotoxic anticancer drugs (e.g., doxorubicin [DOX] and docetaxel) specifically to tumor sites using an external magnetic field while minimizing side effects on healthy tissues.[12-14] Furthermore, SPION-based magnetic systems can induce heat when exposed to an external magnetic field, making them a potential candidate for magnetic hyperthermia (MHT) treatment, a promising tool for localized tumor ablation. The versatility of SPION-based systems makes them highly efficient in serving a dual purpose in cancer theranostics.

According to the literature, various synthesis strategies, such as coprecipitation, hydrothermal/solvothermal methods, thermal decomposition, sonochemical techniques, and microemulsion methods, have been used to prepare high-quality SPIONs. However, SPIONs without proper surface modification tend to aggregate, which reduces both their magnetic properties and colloidal stability, limiting their application in magnetic targeting, MRI, and hyperthermia.[7,15] By introducing appropriate surface modification strategies, such as organic or inorganic coatings, it is possible to enhance their biocompatibility and colloidal stability, preventing particle agglomeration and improving targeting capabilities. As per the literature, various synthesis strategies such as coprecipitation, hydrothermal/solvothermal, thermal decomposition, sonochemical, and microemulsion techniques have been used to prepare high-quality SPIONs. However, SPIONs without proper surface modification can have a tendency to aggregate by reducing both magnetic properties and colloidal stability by limiting their application in magnetic targeting, MRI, and hyperthermia. However, by introducing appropriate surface modification strategies, such as organic or inorganic coatings to the surfaces of SPIONs, one can enhance the biocompatibility and colloidal stability by preventing particle agglomeration as well as targeting capabilities.[1,7] Furthermore, the incorporation of other NPs, such as Au and Ag, can further enhance the functionality of SPIONs and expand their range of applications. For instance, integrating Au NPs can provide plasmonic features to SPIONs, making them a promising candidate for both MRI and photothermal therapy.[7] Similarly, the integration of Ag NPs imparts antimicrobial properties, broadening the biomedical applications of SPIONs. Moreover, proper surface coatings on SPIONs create multifunctional nanoformulations that

Table 1. Comparison of SPIONs with other nanoparticles-based drug delivery systems

Criteria	SPIONs	Gold NPs	Polymeric NPs	Liposome
Composition	Iron-oxide (Fe_3O_4 or Fe_2O_3)	Gold (Au)	Biodegradable polymers (e.g., PLGA, PCL)	Phospholipid bilayer
Size range	1 – 100 nm	1 – 100 nm	10 – 1,000 nm	50 – 500 nm
Magnetic properties	Superparamagnetic and can be manipulated using external magnetic fields	None	None	None
Biocompatibility	Generally biocompatible with proper surface modification	Biocompatible with proper surface functionalization	Biodegradable and biocompatible, depending on the polymer used	High, especially for lipids
Drug release mechanism	Magnetically controlled release	Surface charge and functionalization can control the release	pH, temperature, or enzymatic triggers	pH, temperature, or enzymatic triggers
Targeted drug delivery	Magnetic targeting via external magnetic fields	Passive or active targeting	Active targeting via surface functionalization	Passive or active targeting
Advantages	Magnetic targeting; high drug loading; easy monitoring with MRI	Easy synthesis; surface modification for targeted delivery	Controlled and sustained release; customizable	High encapsulation efficiency; versatile formulation
Disadvantages	Possible toxicity due to iron accumulation; requires external magnetic field	Stability issues; potential cytotoxicity at high concentrations	Complex synthesis and potential cytotoxicity from polymers	Instability in blood; drug leakage
Applications	Cancer therapy; imaging; MRI	Cancer therapy; vaccine delivery; gene delivery	Cancer therapy; gene therapy; immunotherapy	Drug delivery; diagnostic imaging; gene therapy

Abbreviations: MRI: Magnetic resonance imaging; NPs: Nanoparticles; PLGA: Poly (lactic-co-glycolic) acid; PCL: Polycaprolactone; SPIONs: Superparamagnetic iron oxide nanoparticles.

can be used for both tumor imaging and cancer treatment. These formulations can improve the water solubility of the anticancer drugs, prolong the drug's circulation time in the bloodstream, and reduce rapid renal excretion.[1,7] This nanoformulation also enhances cell-specific drug accumulation and allows for controlled drug activation at the tumor site, thereby reducing the adverse effects typically associated with anticancer treatments.[8-11]

This review explores the development of high-quality SPIONs using various synthesis techniques for cancer theranostic applications. Furthermore, it examines the challenges associated with the clinical feasibility of SPIONs, particularly their use as contrast agents for cancer detection and treatment. A schematic representation of SPIONs, illustrating their synthesis, stabilization strategy, and key features, is presented in Figure 1.

2. Synthesis of SPIONs

Over the years, significant efforts have focused on synthesizing SPIONs with desirable physicochemical properties for biomedical purposes. The major challenge lies in producing stable, phase-pure, monodispersed SPIONs with the optimal size and high crystallinity to ensure the best pharmacokinetic behavior. These characteristics also play a crucial role in enhancing MRI contrast. Another challenge is developing simple purification techniques to replace complex methods such as magnetic filtering or ultracentrifugation. SPIONs can be synthesized through both hydrolytic and non-hydrolytic routes, each offering distinct advantages and limitations. Table 2 compares their key features, including solvents, reaction conditions, and environmental impact.

Various approaches have been developed to efficiently produce high-quality, water-dispersible, and biocompatible SPIONs. Common methods include chemical coprecipitation, microemulsion, hydrothermal/solvothermal, thermal decomposition, and sonochemical techniques, as summarized in Table 3.

2.1. Chemical coprecipitation method

Black iron oxide (Fe_3O_4) NPs are produced through this straightforward synthesis technique, which involves reducing ferric and ferrous salts in a 2:1 ratio at temperatures ranging from 70°C to 90°C in an alkaline environment (pH 9 – 14).[16,17] Massart[18] was the first scientist to employ this synthesis approach. The particle size and morphology of the synthesized NPs depend on: (i) The type of salts used, such as chlorides, sulfates, and

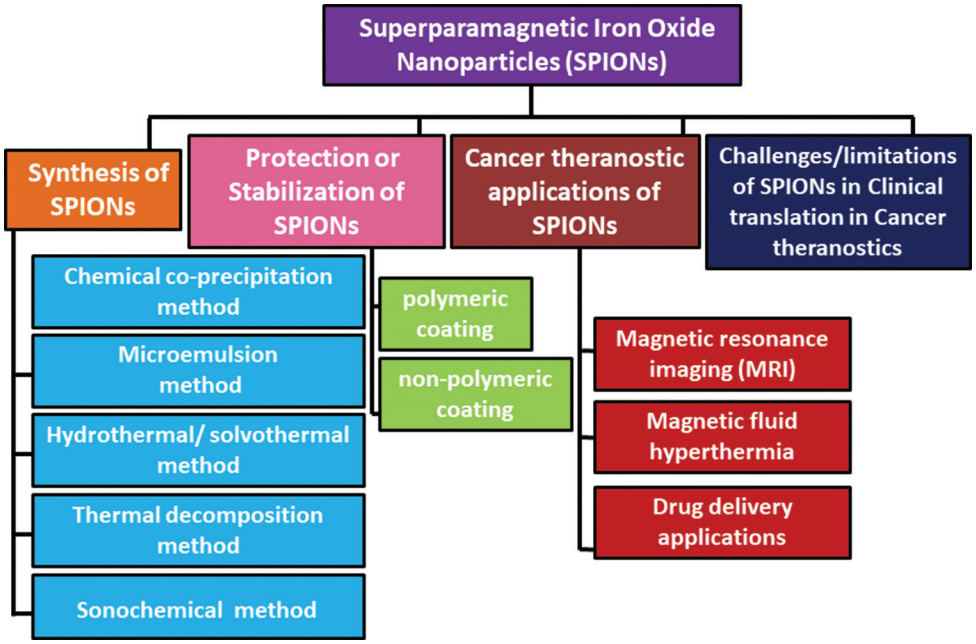

Figure 1. Schematic representation of SPIONs, showing their synthesis, stabilization strategy, and key features as discussed in the manuscript
Abbreviation: SPIONs: Superparamagnetic iron oxide nanoparticles.

Table 2. Comparison of superparamagnetic iron oxide nanoparticles synthesis through hydrolytic and non-hydrolytic routes

Feature	Hydrolytic route	Non-hydrolytic route
Solvent	Water-based	Organic solvents
Reaction temperature	Low to moderate	High
Control over size and shape	Limited	Better
Crystallinity	Lower	Higher
Ease of synthesis	Easier	More complex
Environmental impact	More eco-friendly	Involves toxic solvents

nitrates; (ii) the ferric cation (Fe^{3+}) to ferrous cation (Fe^{2+}) stoichiometric ratio; (iii) the reaction temperature; and (iv) the pH of the solution. Challenges associated with this method include potential oxidation or reduction of iron salts, leading to unstable Fe_3O_4 NPs with high polydispersity and broad particle size distribution.[16-18] The surface charge can be tuned by adjusting pH and ionic strength, but the NPs tend to be highly reactive and need immediate coating. The surface of SPIONs can be easily modified by adding stabilizers such as natural or synthetic polymers, surfactants, or biomolecules. Due to their low crystallinity and broader particle size distribution, Fe_3O_4 NPs exhibit a lower saturation magnetization value (30 – 50 emu/g) compared to their bulk counterparts (92 emu/g).[17] Despite this, SPIONs synthesized by this method are suitable for use as MRI contrast agents and in drug delivery applications due to their biocompatibility and ease of surface functionalization. However, these NPs are less suitable for hyperthermia application due to their lower crystallinity nature and weaker magnetic properties.

2.2. Microemulsion method

A microemulsion is a thermodynamically stable and isotropic dispersion consisting of two immiscible liquids (oil and water), stabilized by suitable surface-active agents.[16,17] Two common systems for synthesizing SPIONs are water-in-oil (W/O) and oil-in-water microemulsions. Different types of surface-stabilizing agents are used in the synthesis of SPIONs. The hydrophilic and hydrophobic components of these coatings are critical for stabilizing the NPs and influencing their physicochemical properties. Among these methods, the water-in-oil microemulsion technique is widely employed to produce SPIONs with a narrow size distribution and desired physical characteristics. The size and shape of the NPs can be precisely controlled by adjusting the concentrations of the iron precursor, surfactant, and solvents. The material produced using this technique is suitable for MRI contrast enhancement and targeted drug delivery. However, this technique is expensive and difficult to scale up for clinical translation.

2.3. Hydrothermal/Solvothermal method

The hydrothermal synthesis technique, less commonly explored than coprecipitation, can produce high-quality

Table 3. Comprehensive review of commonly used methods for superparamagnetic iron oxide nanoparticle synthesis

Synthesis method	Coprecipitation	Microemulsion	Hydrothermal	Thermal Decomposition	Sonochemical
Solvent	Water	Organic solvent	Water-ethanol	Organic solvent	Organic solvent
Reaction condition	Organic solvent	20 – 50°C	High temperature and high pressure	High Temperature	Room temperature
Duration	Minutes	Hours	Hours	Hours–days	Minutes
Particle size and size distribution	5 – 20 nm, broad	2 – 20, narrow	20 – 200 nm, narrow	4 – 20 nm, narrow	5 – 15 nm, narrow
Shape control	Not good	Good	Very good	Very good	Good
Saturation magnetization (emu/g)	Moderate (30 – 60)	Moderate (40 – 60)	High (60 – 80)	Very High (70 – 90)	Moderate (45 – 65)
Dispersity profile	Polydisperse	Relatively monodisperse	Monodisperse	Monodisperse	Monodisperse
Yield	Scalable	Low	Medium	Scalable	Medium

Note: Information are derived from Hu *et al.*,[7] Lu *et al.*[17].

SPIONs in aqueous solutions (hydro) or organic solvents (solvo) using a Teflon-lined stainless steel autoclave at temperatures ranging from 130 to 250°C for 8 – 72 h under 0.3 – 4 MPa pressure.[7,17] This method produces a clear, homogeneous solution by dissolving ferric chloride, sodium acetate, and polyethylene glycol (PEG) in ethylene glycol, followed by constant stirring for 30 min. The autoclave is then filled with the resultant solution, sealed, and heated to 200°C for 8 – 72 h. In this process, PEG serves as the surfactant to prevent particle aggregation, sodium acetate as the electrostatic stabilizer, ethylene glycol as the solvent, and ferric chloride ($FeCl_3$) as the precursor.[19] The controlled reaction parameters yield highly monodispersed NPs with uniform shapes. The surface charge can be adjusted by varying the choice of solvent and precursor. The SPIONs can be further functionalized by coating them with polymers or silica to enhance their water dispensability or hydrophilicity. This functionalization is more controllable than in the thermal decomposition method, although the synthesis process is more complex than the coprecipitation method. SPIONs produced using this route are versatile for applications in MRI, hyperthermia, and drug delivery. A schematic figure illustrating magnetic drug targeting under the application of an external magnetic field is presented in Figure 2.

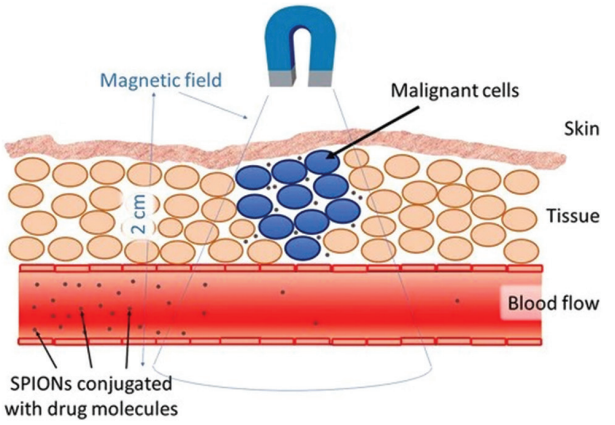

Figure 2. Diagram illustrating magnetic drug targeting under the control of an external magnetic field. Reproduced from Shabatina *et al.*[13]. Copyright 2020 Authors.
Abbreviation: SPIONs: Superparamagnetic iron oxide nanoparticles.

2.4. Thermal decomposition method

The thermal decomposition method is an effective technique for synthesizing high-quality, monodispersed Fe_3O_4 NPs with smaller sizes and high crystallinity, outperforming other synthesis methods.[17] This approach involves the decomposition of organometallic precursors, such as tris(acetylacetonato) iron(III) ($Fe[acac]_3$) and iron (III) cupferronate ($Fe[cup]_3$), in high-boiling organic solvents in the presence of stabilizing surfactants like oleic acid. Precise control over reagent ratios and reaction conditions is crucial for achieving the desired nanoparticle size and morphology. For instance, Yang *et al.*[20] successfully synthesized monodispersed Fe_3O_4 nanocubes (6.5 – 30 nm) by thermally decomposing ferric acetate in a mixture of 1,2-hexadecanediol, oleic acid, oleylamine, and benzyl ether at 200°C. The SPIONs produced using this technique are monodispersed and require ligand exchange for aqueous dispersion. SPIONs synthesized by this method are excellent for MRI, multimodal imaging, and MHT due to higher crystallinity and superior magnetic properties. However, they require additional surface modifications to improve biocompatibility for biomedical applications. Despite its advantages, the thermal decomposition method faces limitations in biomedical applications due to the requirement for high

temperatures, the use of toxic reagents, and the poor water solubility of the resulting NPs.

2.5. Sonochemical method

The sonochemical synthesis method is an efficient and adaptable technique for producing monodispersed SPIONs with a narrow size distribution using high-intensity ultrasonic waves. This technique relies on acoustic cavitation, where microbubbles develop, expand, and collapse in a liquid, generating shock waves that trigger chemical reactions as well as extremely high local temperatures (up to 5000 K) and pressures (up to 1000 atm).[21] This method is faster and more energy-efficient compared to other traditional methods. Surface functionalization can be achieved by introducing surfactants or polymers during the synthesis process.

3. Protection or stabilization of SPIONs

Stability is a crucial requirement for nearly all types of biomedical applications of SPIONs. Uncoated NPs are prone to agglomeration and cluster formation as they attempt to minimize their high surface area-to-volume ratio, leading to reduced colloidal stability and diminished functionality. Coating the surface of SPIONs not only improves their colloidal stability but also offers a protective barrier against oxidation. Furthermore, selecting an appropriate coating enables functionalization, allowing the attachment of specific molecules or functional groups to tailor the NP's properties for a wide range of applications (Figure 3).

3.1. Stabilization of SPIONs with polymer coating

SPIONs can be coated using synthetic polymers, such as PEG, polyvinyl alcohol (PVA), and poly(D, L-lactic-co-glycolic acid) (PLGA) to improve hydrophilicity, reduce protein adsorption, and minimize immune system recognition. This coating also allows SPIONs to circulate in the bloodstream for extended periods by preventing agglomeration and enhancing colloidal stability through steric hindrance. Among these, PEG, a biodegradable polymer widely used in biomedical applications, offers numerous advantages for SPION coating. Its hydrophilic, biocompatible, and non-toxic nature makes it particularly effective for NP functionalization. The presence of PEG on the NP surface imparts stealth properties and hydrophilicity, helping to maintain prolonged blood circulation.[14,22] In addition, PEG coating enhances the NPs' ability to cross cell membranes due to its solubility in both polar and non-polar solvents, as well as its high permeability. PEG is an ideal choice for biomedical applications because it demonstrates outstanding solubility and stability in aqueous solutions and maintains its stability in physiological saline.

Similarly, PLGA, renowned for its exceptional biocompatibility and biodegradability, is extensively studied in biomedical applications, including drug delivery and MRI.[14] Its polymeric scaffold provides high drug-loading efficiency, making it particularly effective for carrying significant amounts of hydrophobic drugs.

PVA, a hydrophilic, biocompatible, and biodegradable polymer, is commonly used for NP functionalization.[23,24] PVA coating significantly improves the colloidal stability of NPs by preventing aggregation and ensuring uniform dispersion in aqueous and other solutions.[16,25] The hydroxyl groups in PVA also enable further functionalization, allowing the attachment of biomolecules, drugs, or targeting agents, making it highly versatile for biomedical applications. Moreover, PVA coating serves as a protective barrier, shielding cells from direct exposure to the iron oxide core and reducing cytotoxic effects.

Dextran, a biocompatible and neutral polysaccharide, is widely used for coating SPIONs and has found extensive applications in areas such as MRI imaging of the liver and cancer treatment.[16,25] Its coating enhances colloidal stability and prolongs the blood circulation time of SPIONs, making them highly suitable for *in vivo* applications.[22] Natural polymers such as dextran have been successfully used in clinical applications like *Feridex* due to their excellent biocompatibility.

Chitosan is a hydrophilic, biocompatible, and non-toxic copolymer (poly-aminosaccharide) composed of 2-amino-2-deoxy-β-D-glucan units linked through glycosidic bonds.[16,30] Due to its amine and hydroxyl groups, chitosan is widely utilized in pharmaceutical applications. Its coating properties prevent the agglomeration of NPs and enable functionalization of their surfaces, enabling the attachment of biological entities such as drugs and proteins, making it highly favorable for drug delivery applications.[26]

Polymeric liposomes composed of amphiphilic octadecyl-quaternized lysine-modified chitosan (OQLCS), PEGylated OQLCS, and folate-conjugated OQLCS, can be used in combination with SPIONs to improve their biocompatibility and bioavailability while avoiding non-specific uptake of NPs by healthy tissues. In this system, SPIONs are either encapsulated within or attached to polymeric liposomes. In addition, this system enables surface functionalization by facilitating the attachment of targeting ligands, such as antibodies and peptides, for specific cell targeting. This nanocomposite system combines imaging capabilities for diagnosis and drug delivery applications into one platform. However, stability remains a concern, as liposomes can degrade over time. An additional challenge is that high SPION loading could destabilize the liposome structure.

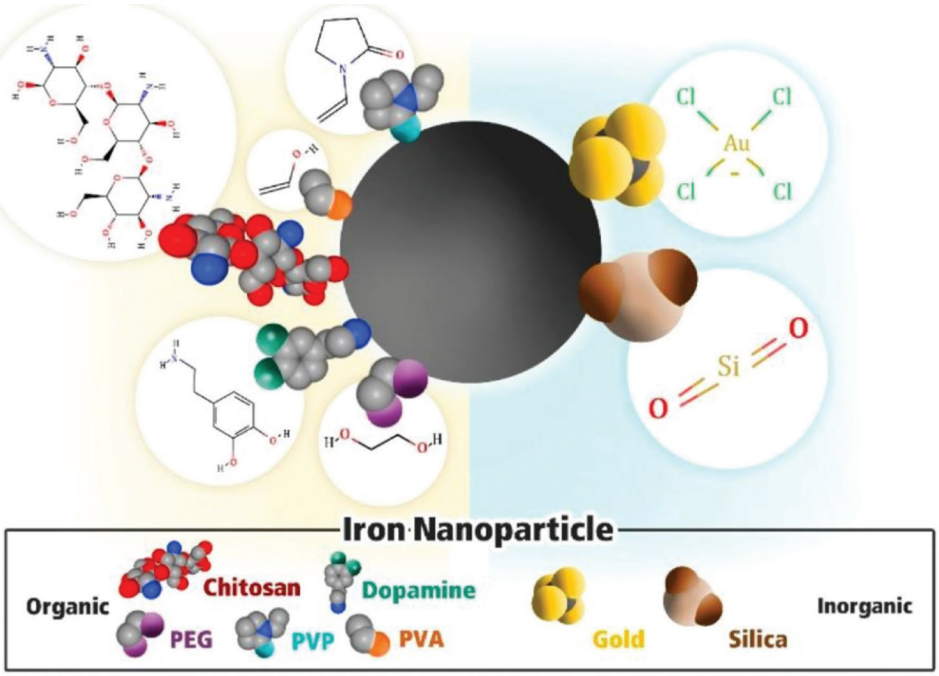

Figure 3. Various surface functionalizations of super paramagnetic iron oxide nanoparticles. Reproduced from Gambhir *et al.*[22] Copyright 2022 Authors. Abbreviations: PEG: polyethylene glycol; PVA: Polyvinyl alcohol; PVP: Polyvinylpyrrolidone.

3.2. Stabilization of SPIONs within non-polymeric coating

SPIONs stabilized by polymers are often unstable in air and can be easily affected by acidic solutions, which negatively impact their magnetic properties. As a result, non-polymeric or inorganic coatings are frequently preferred over polymeric coatings to achieve superior colloidal stability, enhanced functionality, and improved biocompatibility. This method involves creating a protective layer of inorganic material around the SPION core, which helps prevent aggregation, reduce surface oxidation, and provides a flexible platform for further functionalization. Among the various non-polymeric coating materials, silica and Au are the most widely studied and utilized due to their unique advantages and proven effectiveness.

Silica coating on SPIONs is a well-established technique that enhances their stability, functionality, and biocompatibility.[27,28] The silica layer protects against oxidation, prevents particle aggregation and provides a chemically versatile surface for further modifications. In addition, due to its hydrophilic nature, silica facilitates the binding of various biological ligands. The silica coating stabilizes SPIONs by shielding magnetic dipole interactions, while its negative charge enhances coulombic repulsion between particles, improving colloidal stability.[23,29] Silica coatings also improve cellular uptake and reduce toxicity by creating a strong protective layer that prevents iron ion leakage, which could otherwise cause oxidative stress. The rigid silica shell enhances stability, preventing particle agglomeration and ensuring dispersibility in different pH environments, such as the acidic conditions found in tumor microenvironments. However, a major limitation of this approach is the difficulty in achieving a uniform silica shell thickness. Inconsistent coating thickness can result in irregular magnetic fields, potentially leading to uneven heating in MHT applications.

The integration of SPIONs, either coated with Au NPs or decorated with Au shell, offers several benefits, including enhanced stability, improved biocompatibility, and the ability to functionalize the surface with a variety of biomolecules or ligands, making them suitable for targeted drug delivery and bio-imaging applications. These nanohybrid systems combine the unique optical and chemical characteristics of Au with the magnetic properties of SPIONs. Au coating also improves MRI contrast and provides surface plasmon resonance for optical detection, enabling dual-mode imaging. The synergistic effects of these systems allow for combined MHT and photothermal therapy. Figure 4 shows spike-like Au shell crystals coated onto the surface of SPIONs, with the planes of both Fe_3O_4 and Au crystals visible in the composite's powder X-ray diffraction pattern. The composite material was used for *in vivo* MRI/computed tomography imaging of tumors, as shown in Figure 5.

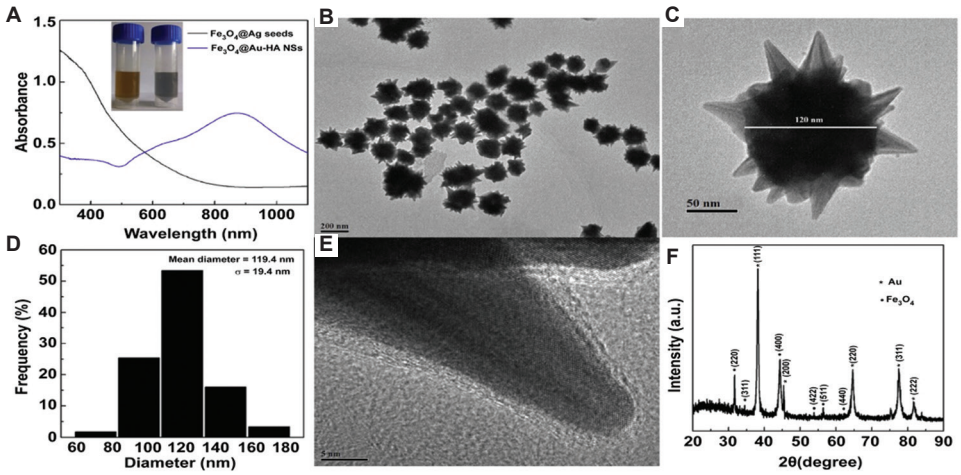

Figure 4. (A) Absorbance spectra (B and C) transmission electron microscopy image, (D) size distribution histogram, (E) high-resolution transmission electron microscopy image, and (F) X-ray diffraction pattern of the hyaluronic acid-modified Fe_3O_4@Au core/shell nanostars. Reproduced with permission from Li *et al.*[35] Copyright 2014 Elsevier.

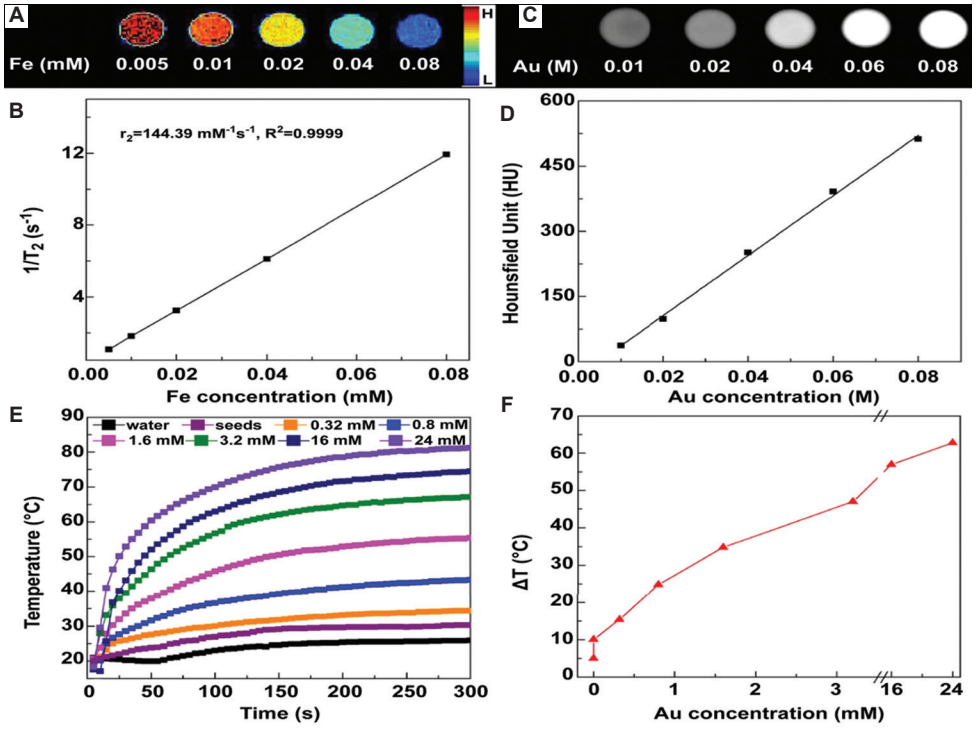

Figure 5. (A) Color (spin-spin) T_2-weighted magnetic resonance images and (B) linear fitting of $1/T_2$ of hyaluronic acid-modified Fe_3O_4@Au core/shell nanostars (Fe_3O_4@Au-HA NSs) at different iron (Fe) concentrations. (C) Computed tomography images and (D) X-ray attenuation intensity of Fe_3O_4@Au-HA NSs with different Au concentrations. (E) Temperature elevation of water and the aqueous solution of Fe_3O_4@Ag seeds ([Fe] = 0.972 mm) or Fe_3O_4@Au-HA NSs at varying gold (Au) concentrations under the irradiation of a 915 nm laser with a power density of 1.2 W/cm^2 as a function of irradiation time. (F) Temperature change (ΔT) of an aqueous suspension of Fe_3O_4@Au-HA NSs with different Au concentrations over a period of 300 s.
Note: The color bar, ranging from red to blue, in panel A indicates the gradual decrease of magnetic resonance signal intensity. Reproduced with permission from Li *et al.*[35] Copyright 2014 Elsevier.

However, there are some drawbacks associated with this coating. The Au layer can reduce the magnetic properties of the underlying SPION core, as Au is non-magnetic. As a result, the overall magnetic behavior of the composite may be compromised compared to bare SPIONs, potentially limiting their effectiveness in cancer theranostics applications.[30] Moreover, achieving a stable and uniform Au coating is challenging due to differences in the surface

properties of Au and SPIONs, which can affect the long-term stability and consistency of the Au shell.[31,32]

The integration of SPIONs with Ag offers several advantages. By combining SPIONs with Ag NPs or an Ag shell, these coatings can be functionalized with biomolecules to improve cell interactions. In addition, the antimicrobial properties of Ag can be beneficial for cancer therapy with antimicrobial effects. However, the Ag coating can reduce the magnetic properties of SPIONs, which may diminish MRI contrast. Ag toxicity at high doses and stability issues further limit their biomedical applications. A comparison of different types of coatings with SPIONs and their stability in biological environments is provided in Table 4.

4. Cancer theranostic applications of SPIONs

In the last few decades, SPIONs have been extensively investigated for numerous biomedical applications, including as contrast agents in MRI, magnetic fluid hyperthermia agents, and drug delivery systems. Their unique magnetic properties enable a wide range of applications in both diagnostics and therapeutics, making them a cornerstone of modern biomedical research and clinical practices.[7,23] This section provides a detailed explanation of these approaches, along with their current limitations and recent developments.

4.1. MRI

Significant advancements have been made in medical imaging technology for disease diagnosis with the introduction of non-invasive techniques such as MRI.[33,34] The use of SPIONs as contrast agents for MRI applications has become one of the most significant and rapidly advancing areas in medical imaging. MRI contrast agents improve sensitivity by shortening the T_1 (spin-lattice) and T_2 (spin-spin) relaxation times of protons, thereby enhancing tissue distinction. T_1 reduction brightens images, while T_2 reduction darkens them. The effectiveness

Table 4. A detailed comparison of different types of coatings for SPIONs

Coating type	Biocompatibility	Stability in biological environments	Advantages	Disadvantages
Synthetic polymers	(i) Improve hydrophilicity and minimize immune responses (ii) Reduce cytotoxicity and improve cellular uptake	(i) Offers good stability in physiological conditions (pH, temperature)	(i) Good dispersion in biological fluids	(i) Can accumulate in organs like the liver and spleen (ii) Can lead to long-term toxicity
Natural polymers	(i) Well-tolerated by the body, with lower immune reactions. (ii) Biodegradable and more environmentally friendly	(i) Moderate stability in some biological environments (ii) Degradation rates depend on the polymer used	(i) Biodegradable (ii) Low toxicity (iii) Compatible with various biological systems	(i) May degrade too quickly in certain environments (ii) Limited control over polymer degradation and particle size
Lipids	(i) Biocompatible (ii) Well tolerated by cells	(i) Good stability in physiological environments (ii) Protects SPIONs from aggregation in serum	(i) Biodegradable (ii) Low toxicity (iii) Compatible with various biological systems	(i) Lipid degradation over time (ii) Low drug loading capacity
Silica coatings	(i) Biocompatible and non-toxic (ii) Can be functionalized for drug delivery, improving cellular uptake	(i) Excellent stability in physiological conditions (ii) Remain stable for prolonged periods in the bloodstream	(i) High surface area for functionalization (ii) Easy to modify with ligands for targeting	(i) Cause inflammation if not properly functionalized (ii) May aggregate in certain conditions
Gold coatings	(i) Biocompatible with low toxicity (ii) Easily modified for targeting specific cells or tissues	(i) Stable under physiological conditions, resistant to oxidation (ii) Maintain shape and size over time	(i) High surface stability (ii) Excellent surface modification options for drug delivery (iii) Non-toxic and non-inflammatory	(i) Potential for aggregation in biological fluids (ii) Expensive (iii) Limited biodegradability
Silver	(i) Mild cytotoxicity at high concentrations (ii) Functionalized with biomolecules to improve cell interaction	(i) Can improve colloidal stability (ii) Prone to oxidation	(i) Good colloidal stability (ii) Good surface modification	(i) Potential cytotoxicity at higher concentrations (ii) Reduced magnetic properties of SPIONs (iii) Silver ion release may cause toxicity over time

Abbreviation: SPIONs: Superparamagnetic iron oxide nanoparticles.

of a contrast agent is measured by its r_1 (for T_1) or r_2 (for T_2) relaxivity. There are two main types of contrast agents: positive contrast agents, which mainly shorten T_1 for bright images, and negative contrast agents, which primarily shorten T_2, leading to darker images that are effective for distinguishing between healthy and diseased tissues.

4.1.1. SPIONs as spin-spin MRI contrast agents

Recent studies have shown that SPIONs with particle sizes smaller than 20 nm are widely used as negative contrast agents.[36] The MRI signal contrast of SPIONs is higher than that of paramagnetic contrast agents, such as gadolinium Gd(III) and manganese Mn(II) based complexes, due to the higher transverse relaxivity of SPIONs (r_2 value) compared to their longitudinal relaxivity (r_1 value). In addition, SPIONs exhibit chemical stability, biocompatibility, and biodegradability under *in vivo* conditions, as they integrate into the bloodstream as normal iron ions. Building on their exceptional magnetic properties and the significant influence of SPIONs on T_2 relaxation times, numerous candidates have been developed for use as negative contrast agents in MRI. Several iron oxide-based imaging probes, including ferumoxides (Feridex/Endorem), ferucarbotran (Resovist/Supravist), ferumoxtran-10 (Sinerem/Combidex), ferumoxsil (Lumirem/Gastromark), and ferristene (Abdoscan), have been developed and evaluated in clinical trials.

Ferumoxides, developed by Guerbet, were the first commercially available dextran-coated SPIONs with a hydrodynamic size of 40 – 150 nm.[37,38] They were approved by the United States Food and Drug Administration (FDA) in 1996 for use in Europe, specifically for imaging liver tumors. However, Ferridex was withdrawn from the market in 2011 due to its severe side effects and lack of demand.

Resovist, developed by Bayer Healthcare, consists of carboxydextran-coated SPIONs with a hydrodynamic size of 60 – 80 nm and was used for liver imaging. It is considered a standard contrast agent in the development of magnetic particle imaging.[37,39] Supravist, another carboxydextran-coated SPION formulation with a hydrodynamic size of 20 – 25 nm, was developed for longer circulation times, with T_1 and T_2 properties. However, it has not been marketed for clinical use, and the formulation was discontinued in 2008 due to reports of severe allergic reactions.

Developed by AMAG Pharmaceuticals, ferumoxtran comprises dextran-coated SPIONs with a hydrodynamic size of 20 – 50 nm.[37,40] Initially used for prostate cancer lymph node metastasis imaging, the FDA issued a safety alert in 2008, warning of the potential risk of serious allergic reactions. Consequently, the manufacturing company voluntarily withdrew Combidex from the United States market.

Ferumoxytol, another candidate, comprises polyglucose sorbitol carboxymethyl ether-coated SPIONs with a hydrodynamic size of 20 – 40 nm. It was developed to address iron deficiency anemia in patients with chronic kidney disease.[37,41] However, ferumoxytol was associated with side effects, leading the FDA to issue a black box warning due to the risk of serious allergic reactions. Despite these limitations, ferumoxytol remains one of the few SPION formulations still in use today, both for its intended purpose and off-label as an MRI angiography agent in patients who cannot receive Gd-based contrast agents.

Ferucarbotran (Sienna+/Magtrace), consisting of carboxydextran-coated SPIONs with a hydrodynamic size of 59 nm, was developed by Endomagnetics Ltd. for sentinel lymph node identification.[37] To the best of our knowledge, these products have not been used for imaging applications yet.

Other notable mentions include formulations used as oral gastrointestinal contrast agents, such as ferumoxsil (marketed as GastroMARK in Europe and Lumirem in the United States) and ferristene (Abdoscan®). These SPION-based formulations, coated with insoluble materials – silica for ferumoxsil (~300 nm core size) and polystyrene for ferristene (~3,500 nm core size) – are considered safe and effective.[37] Ferumoxsil remains the only SPION approved by the FDA for imaging applications, specifically for gastrointestinal and bowel contrast.

Although some formulations have been associated with side effects, ongoing advancements continue to focus on developing more effective SPION-based formulations for improved cancer imaging and diagnosis applications. Although some formulations have been associated with side effects, ongoing advancements aim to develop more effective SPION-based formulations for enhanced cancer imaging and diagnostic applications.

Numerous efforts have been made to enhance the sensitivity of cancer cell diagnosis. One strategy involves increasing the relaxivity of SPIONs to achieve more sensitive MRI applications. Ding *et al.*[42] synthesized laponite-stabilized SPIONs using a coprecipitation synthesis route and observed that the T_2 relaxivity of the synthesized NPs (475.9/mM/s) was almost twice as high as that of bare Fe_3O_4 NPs (247.6/mM/s). They observed that laponite-stabilized SPIONs successfully lowered the MRI signal intensity of tumors following intravenous injection, in addition to acting as a contrast agent for MRI of cancer cells *in vitro*. In another study, Zhao *et al.*[43] fabricated concave octopod-shaped Fe_3O_4 NPs using a

thermal decomposition synthesis route. By optimizing the morphology of the SPIONs, they achieved a high M_s value along with an ultrahigh transverse relaxivity value (679.3 ± 30/mM/s). Their study showed that the synthesized SPIONs could serve as high-performance T_2 contrast agents for in vivo MRI and early tumor detection. Zhu *et al.*[44] synthesized polyethyleneimine-coated SPIONs via mild reduction and used them as cross-linkers to create Fe_3O_4 NP-loaded γ-polyglutamic acid nanogels (152.3 nm, relaxivity 171.1/mM/s) using a double emulsion method. The nanocomposite showed potential as an MRI contrast agent for cancer cells *in vitro* and *in vivo*. Li *et al.*[45] produced two distinct SPIONs with a size of 15 – 16 nm using the hydrothermal synthesis method, preparing polyethyleneimine-coated Fe_3O_4 NPs modified with fluorescein isothiocyanate and hyaluronic acid with two different molecular weights. They stated that the generated NPs might serve as useful probes for both *in vitro* and *in vivo* targeted MR imaging of cancer cells.

4.1.2. SPIONs as spin-lattice MRI contrast agents

Spin-lattice, also known as positive contrast in MRI, refers to a substance's ability to reduce the longitudinal relaxation time of nearby water protons. This results in enhanced signal intensity and a brighter appearance in T_1-weighted images, improving contrast and aiding in the visualization of anatomical structures. The spin canting effect, arising from the incomplete alignment of spins in surface atoms, is recognized as the primary cause of the reduced magnetization observed in small-sized iron oxide NPs (IONPs).[7,46] Consequently, the strong surface spin canting effect in ultrasmall Fe_3O_4 NPs (with a diameter of less than 5 nm) leads to their lower magnetization, making them suitable for use as T_1 MRI contrast agents. The challenges associated with using SPIONs as T_2 contrast agents have driven the search for nanomaterials capable of providing T_1 contrast in MRI, offering enhanced brightness while maintaining favorable physicochemical properties.

Luo *et al.*[47] developed ultrasmall Fe_3O_4 NPs functionalized with arginylglycylaspartic acid for targeted T_1-weighted MRI imaging of gliomas. The Fe_3O_4 NPs, with an average size of 2.7 nm, were synthesized through a solvothermal technique and stabilized using sodium citrate. The NPs were subsequently conjugated to a PEG-linked arginylglycylaspartic acid peptide through 1-ethyl-3-(3-dimethylaminopropyl)carbodiimide coupling chemistry. This nanoformulation demonstrated high efficiency as a nanoprobe for targeted T_1-weighted positive MRI, both in glioma cells in vitro and in vivo.

Bhavesh *et al.*[48] developed dextran-coated, ultrasmall IONPs with a particle size of 2.5 nm using a microwave synthesis technique. These NPs were demonstrated to be effective for fluorescence imaging and high-quality T_1-weighted MRI. Their in vivo performance was evaluated through magnetic resonance angiography in mice. Remarkably, the NPs exhibited partial excretion through the liver and kidneys, which was attributed to their hydrodynamic diameter being close to the renal clearance threshold. Achieving renal clearance with IONPs is particularly important for applications requiring repeated dosing or the incorporation of radioactivity, as it helps reduce excessive radiation exposure to healthy tissues.

Wei *et al.*[49] reported the synthesis of ultrasmall IONPs with a size of 4 nm. The small size of these NPs facilitated efficient renal elimination, thereby avoiding prolonged hepatic accumulation, which is often associated with an increased risk of iron overload. Furthermore, the NPs generated a positive signal in traditional MRA, showcasing their potential for *in vivo* imaging applications.

Zhou *et al.*[50] developed small Gd-ion-embedded SPIONs, which showed enhanced T_1 magnetic resonance contrast in the heart, kidneys, and bladder 10 min after injection. They observed that the Gd species affected the spin alignment in Fe_3O_4 NPs, leading to a fully spin-canted structure. While the signals in the kidneys and bladder increased over time, the cardiac signal declined.

4.1.3. SPIONs as dual mode (spin-lattice–spin-spin) MRI contrast agents

Although each imaging modality has unique advantages and limitations, no single imaging technique can provide comprehensive disease information.[51,52] The integration of combined imaging technologies has significantly enhanced data reconstruction and visualization, providing more detailed diagnostic insights into disease progression. To further improve diagnostic precision, SPION-based contrast agents have been developed for simultaneous T_1- and T_2-weighted MRI.

Paramagnetic Gd complexes are widely used as MRI contrast agents because they shorten the T1 relaxation time of water protons, making tissues or cells appear bright in images. However, Gd(III) complexes must be encapsulated with proteins or liposomes to be effectively delivered *in vivo*, as free Gd ions are highly toxic to biological systems.[7] Other challenges of Gd(III) complexes *in vivo* include: (i) Short lifespan, (ii) poor cellular uptake, (iii) limited distribution in the bloodstream, which restricts their use to molecular imaging, and (iv) the potential to induce nephrogenic systemic fibrosis.

One strategy to minimize the long-term toxicity associated with Gd-based contrast agents is the development of new chelation systems for stable Gd^3

loading. Alternatively, selecting ultrasmall Fe_3O_4 NPs with excellent T_1 contrast performance and biocompatibility offers a promising alternative. Consequently, for dual-mode T_1-/T_2-weighted MRI, addressing the long-term toxicity risks posed by Gd^{3+} release remains a critical consideration.

For instance, Bae *et al.*[53] developed Gd^{3+}-labeled Fe_3O_4 NPs for dual-mode MRI. First, they synthesized oleic acid-coated Fe_3O_4 NPs using the thermal decomposition method and modified in an organic solvent with a mixture of 3,4-dihydroxy-L-phenylalanine-conjugated methoxy PEG and dopamine, both of which form strong coordination bonds with the Fe_3O_4 NP surfaces. The NPs were subsequently functionalized with diethylene triamine pentaacetic acid, a chelating ligand for paramagnetic Gd^{3+} ions. The resulting nanoformulation demonstrated the ability to enhance the surrounding water proton signals in T_1-weighted MR images while also inducing significant signal reduction in T_2-weighted MR images. This dual functionality of the nano-formulations enables both T_1- and T_2-weighted MRI of the targeted tissue site.

4.2. MHT

Another promising application of SPIONs is in hyperthermia therapy, which involves the thermal treatment of cancerous cells.[54,55] In this treatment, SPIONs are concentrated in the cancerous tissue (via intravenous injection or targeted delivery) and are made to resonate in response to an alternating magnetic field, transferring energy from the magnetic field to the surrounding tissue as heat. By applying an alternating magnetic field of sufficient intensity and optimal frequency, the temperature of the cancerous tissue can be raised to 40 – 42°C, selectively destroying the malignant cells, as tumor cells are more heat-sensitive compared to healthy tissue. This technique has been used to treat various types of cancer, including prostate, brain, breast, and liver cancers. Moreover, studies have suggested that MHT could serve as an alternative or complementary approach to current cancer therapies, such as in combination therapies, where it may be combined with other treatments to induce tumor regression or necrosis of cancerous cells. In an alternating magnetic field, heating occurs due to both hysteresis and relaxation losses. In ferromagnetic NPs, hysteresis loss is the primary contributor to MHT, while in superparamagnetic NPs; relaxation loss plays the dominant role.

When SPIONs are exposed to an alternating magnetic field, they generate power dissipation due to the orientational relaxation of particles undergoing thermal fluctuations within a viscous medium. The heating capacity of SPIONs is quantified by the specific absorption rate (SAR), which represents the heating power per unit mass of the dissipating material. The SAR of SPIONs is influenced by factors such as their phase composition, size, morphology, and magnetic anisotropy.[56] It also depends on the characteristics of the alternating magnetic field, including its amplitude and frequency.

Gilchrist *et al.* conducted the first hyperthermia experiment with SPIONs in 1957.[57,58] However, the first clinical trial using SPIONs for prostate cancer treatment was introduced by Jordan *et al.* in 1993.[57] Later, Ghosh *et al.*[59] developed oleic acid- and PEG-capped Fe_3O_4 NPs using the coprecipitation method and demonstrated that the temperature increased to 42.1°C at an NP concentration of 1 mg/mL under an applied frequency of 265 kHz and a current of 550 A. The hyperthermia effectiveness of these NPs was further validated through the treatment of MCF-7 breast cancer cells.

Hayashi *et al.*[60] synthesized cysteine-modified magnetite NPs using the thiol-ene click reaction, achieving an average SAR of 156 W/g under an alternating magnetic field with an amplitude of 100 Oe and a frequency of 230 kHz. Furthermore, they demonstrated the NPs' ability to enhance T_2-weighted MRI contrast.

Espinosa *et al.*[61] synthesized 20 nm Fe_3O_4 nanocubes using the thermal decomposition method and exposed the magnetic nanocube suspension to an AC magnetic field (25 mT) at a frequency of 520 kHz, as well as to a near-infrared spectroscopy laser (808 nm) with a power density of 0.3 W/cm². They observed that the Fe_3O_4 nanocubes exhibited a high specific loss power of up to 5,000 W/g, as shown in Figure 6. The tumor temperature increased from 33°C to 40°C when exposed to either the AC magnetic field or laser irradiation, and further rose to 50°C when subjected to both treatments simultaneously, demonstrating a synergistic tumor therapeutic effect.

Despite their potential, Fe_3O_4 NPs for hyperthermia treatment face significant challenges in clinical applications, primarily due to the requirement for high NP concentrations.[7,54] To address this limitation, a synergistic approach is desirable to reduce the dose of Fe_3O_4 NPs while enhancing therapeutic efficacy. For example, Fe_3O_4 NPs can be encapsulated within the core of liposomes using a reverse-phase evaporation method. The resulting magnetic liposomes, with an average size of 150 nm and a high Fe content (approximately 2,400 NPs per liposome), have been shown to generate a substantial temperature increase under the influence of an AC magnetic field, making them promising for hyperthermia therapy in tumor treatment.[62] Similar to MRI contrast agents, most MHT heat mediators reported to date are based on SPIONs, with typical SAR values ranging from 10 W/g to 200 W/g.[63] While numerous

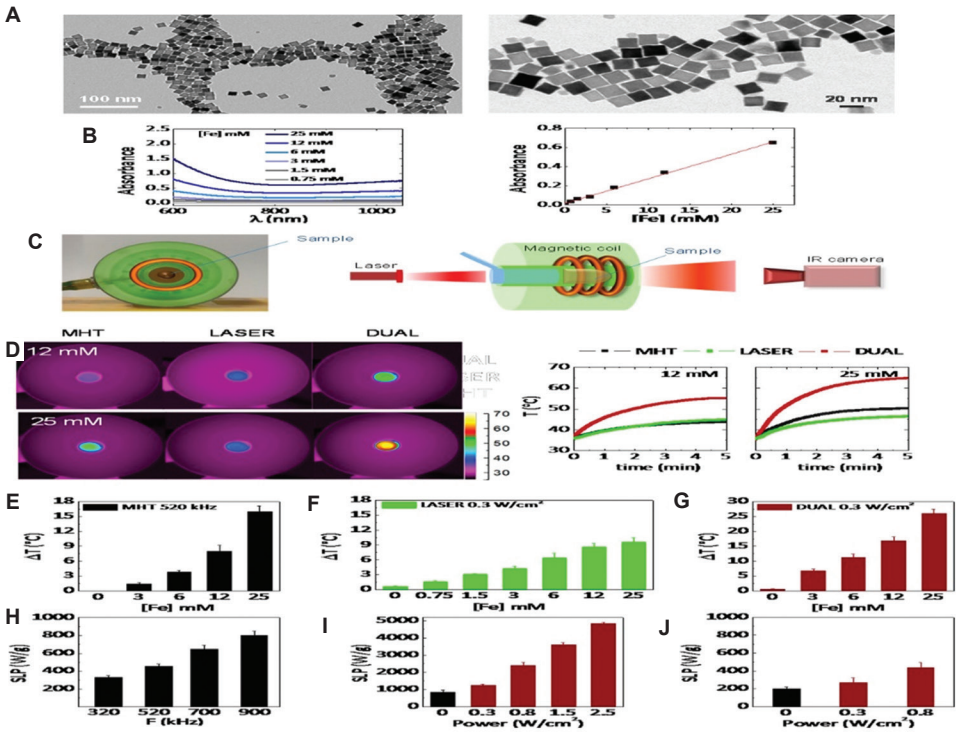

Figure 6. (A and B) Transmission electron microscopy micrographs. (B) Absorbance spectra of magnetic iron oxide nanocubes (IONCs). (C) Schematic of the experimental setup for combined hyperthermia experiments. (D) Temperature elevation curves of IONCs at the same iron concentrations ([Fe] = 12 or 25 mM), measured inside the coil setup magnetic hyperthermia (MHT) at 520 kHz, 25 mT; laser at 0.3 W/cm^2. (E) MHT at 520 kHz. (F) Laser at 0.3 W/cm^2. (G) Dual mode heating capacity of IONCs. (H) Specific loss power (SLP) as a function of frequency with a magnetic field of 2 Mt. (I) Near-infrared spectroscopy laser power in dual mode. (J) Heating capacity of 9 nm IONPs in dual mode. Reproduced with permission from Espinosa *et al.*[61] Copyright 2016 American Chemical Society.

in vitro studies on MHT have been conducted, the therapy remains in the pre-clinical stage, with only a few reports involving human patients.[64]

4.3. Drug delivery applications

One of the major challenges in drug delivery is the poor absorption of hydrophobic drugs, while another challenge involves achieving site-specific targeting of drugs to diseased sites. Magnetic drug delivery using NP-based techniques offers a promising solution to these issues by enhancing the therapeutic efficacy and biocompatibility of drugs.[65] The concept of "magnetic drug delivery" using SPIONs as drug carriers was first proposed in the late 1970s by Widder *et al.*[66] and Senyei *et al.*[67] In this approach, therapeutic agents are either encapsulated within or attached to SPIONs using a protective polymeric layer. These NPs are then guided to the diseased site using an external magnetic field. The core of the NPs is typically superparamagnetic to ensure responsiveness to the magnetic field, while the surrounding polymeric layer provides stability, protection, and suitability for *in vivo* applications. This polymeric coating also facilitates conjugation with biological ligands for improved tumor specificity and extends the circulation time of SPIONs in the bloodstream, thereby increasing their half-life. A variety of anticancer drugs, including cisplatin, methotrexate, daunorubicin, DOX, and paclitaxel, have been successfully loaded onto the organic or inorganic scaffolds of surface-modified SPIONs for drug delivery applications. In magnetic drug delivery systems, the application of an external magnetic field allows the magnetic nanocarriers to bypass the reticuloendothelial system, ensuring targeted delivery of anticancer drugs to the desired site. Magnetic targeting refers to the targeting of SPIONs to a specific tumor site by applying an external magnetic field, which can be achieved using either passive or active strategies.[68,69] Passive targeting is considered one of the key targeting techniques for targeting, where the free accumulation of nanoformulations at the tumor site enhances both cancer diagnosis and MRI detection.[70,71] Angiogenesis, or the formation of new blood vessels, is a most common phenomenon in cancer cells, leading to the formation of abnormal, leaky vessels. Passive targeting does not use specific ligands for tumor-specific receptors. As a result, the distribution of the nanoformulations is

highly non-specific and is driven by the leaky blood vessels of the tumor cells. In addition, tumor cells have limited lymphatic drainage. Once the nanoformulations enter the tumor tissue through leaky vasculature, they tend to remain due to ineffective lymphatic drainage. This phenomenon is known as the enhanced permeability and retention effect.[70,72] Unfortunately, at low doses, nanoformulations may not produce satisfactory results in tumor targeting, while higher doses required for effectiveness can lead to toxicity. To overcome this challenge, active targeting was developed. This approach involves modifying the surface of nanoformulations with tumor-specific ligands, such as folic acid, hyaluronic acid, lactobionic acid, peptides, and antibodies. This is typically a multistep process that includes the adhesion of coating or targeting molecules to the NPs, followed by drug loading. Drug loading can be achieved through various methods, such as covalent conjugation or physical adsorption.

One of the earliest clinical trials and drug release studies was carried out by Widder *et al.*,[66] who coated human serum albumin microspheres with SPIONs and loaded them with the anticancer drug DOX. Subsequent studies by Alexiou *et al.*[73] explored the use of SPIONs to deliver epidoxorubicin.

Kim *et al.*[74] prepared DOX-loaded PLGA-coated SPIONs using a single emulsion-evaporation technique and studied them for simultaneous cancer-targeted imaging and targeted drug delivery. Similarly, Basuki *et al.*[75] developed polymer-stabilized SPIONs by linking DOX through a pH-responsive imine bond and reported that these nanoformulations have potential applications in both diagnosis and therapy.

Panda *et al.*[14] developed a PLGA–PEG-based SPIONs nanocarrier by attaching the anticancer drug docetaxel and reported that this approach holds significant potential for cell-specific targeting of docetaxel, enabling effective treatment of breast cancer. Likewise, Ling *et al.*[76] developed PLGA-based SPIONs functionalized with PEG for the delivery of docetaxel to prostate cancer cells, reporting that the nanoformulation could be used for both tumor imaging and drug delivery treatment.

As with other cancers, SPION-based formulations have emerged as a potent tool for lung cancer theranostics due to their favorable magnetic properties, such as superparamagnetism and biocompatibility. Reczyńska *et al.*[77] modified the surface of SPIONs by coating them with a silica layer and evaluated their compatibility with both lung cancer cells (A549) and normal cells (BEAS-2B), reporting that these SPION-based carriers have the potential to be used in lung cancer treatment.

Horvat *et al.*[78] synthesized PIONs containing core-cross-linked polymer micelles and evaluated their anticancer efficacy against a lung cancer cell line model. Their report showed that the prepared formulation could be a promising option for lung cancer treatment.

Wang *et al.*[79] synthesized epidermal growth factor receptor-targeted, PEG-coated SPIONs and evaluated their targeting capability and cytotoxicity in H460 human lung cancer cells, as well as in nude rat models bearing lung cancer xenografts. They reported that the prepared nanoformulations could enhance MRI sensitivity and improve the tumor-targeting efficacy in a clinically developed rat xenograft model.

Finally, the FDA-approved nanomedicines, along with their uses and date of approval, are presented in Table 5.

5. Challenges and limitations of SPIONs in clinical translation for cancer theranostics

Despite significant progress in utilizing SPIONs for cancer theranostics, several challenges and limitations must be addressed before these NPs can be effectively used as probes for diagnostic and therapeutic applications in clinical settings.

5.1. Toxicity and biocompatibility

Uncoated SPIONs can generate reactive oxygen species, which may lead to cellular damage. While coatings made from natural, synthetic polymer, or inorganic materials improve biocompatibility, the long-term effects of SPIONs in the human body remain unclear. In addition, it is critical to address challenges related to their long-term stability and the potential of accumulation in organs such as the spleen and liver. Such accumulation could pose risks to healthy tissues and hinder their clinical utility. Therefore, evaluating and optimizing the potential toxicity of SPIONs, especially when used at high concentrations or over prolonged periods, is necessary for ensuring their safety in clinical applications.

5.2. Clearance and bio-distribution

SPIONs are cleared from the body by the mononuclear phagocyte system, where they tend to accumulate in the spleen and liver. This accumulation can limit their effectiveness in targeting tumors. Achieving prolonged circulation time without rapid clearance remains a challenge, especially for passive targeting strategies. Although SPIONs have been approved by the FDA, a comprehensive understanding of the pharmacokinetic profiles and bio-distribution of these materials requires thorough investigation to ensure their safety and effectiveness in clinical applications.

Table 5. Nanomedicines approved by the United States Food and Drug Administration

Product name	Nanoparticle type	Company	Approved use	Date of approval
Doxil/Caelyx	Lipid based (PEGylated liposomal doxorubicin)	Johnson & Johnson	Kaposi's sarcoma, ovarian cancer, and multiple myeloma	1995
Myocet	Lipid-based (non-PEGylated liposomal doxorubicin)	Teva Pharmaceutical Industries	Metastatic breast cancer	2000
Onivyde	Lipid-based (liposomal irinotecan)	Ipsen Pharmaceuticals	Metastatic pancreatic cancer	2015
Vyxeos	Lipid-based (liposomal daunorubicin and cytarabine)	Jazz Pharmaceuticals	Acute myeloid leukemia	2017
Eligard	Polymeric (Atrigel® sustained-release delivery system)	Tolmar	Treatment of advanced prostate cancer	2002
Abraxane	Protein-bound (albumin-bound paclitaxel)	Celgene (a Bristol Myers Squibb company)	Lung cancer, metastatic breast cancer, metastatic pancreatic cancer	2005
GastroMARK/ Lumirem	SPIONs	AMAG Pharmaceuticals	Oral contrast agent for MRI of the gastrointestinal tract	1996 (Presently discontinued from the market)
Feridex I.V./ Endorem	SPIONs	AMAG Pharmaceuticals	Intravenous contrast agent for MRI of liver lesions	1996 (Presently discontinued from the market)
Resovist/Cliavist	SPIONs	Schering AG	Contrast-enhanced MRI of the liver	2001
Feraheme/ ferumoxytol	SPIONs	AMAG Pharmaceuticals	Primarily approved for the treatment of iron deficiency anemia in adult patients with chronic kidney disease; now explored as an MRI contrast agent	2009
Verigene® System	Gold NPs	Nanosphere (now part of Luminex Corporation)	Diagnostic system for rapid detection of infectious pathogens and genetic variations	2007
Datroway	Antibody-drug conjugate	AstraZeneca and Daiichi Sankyo	Treatment of advanced breast cancer in patients who have received prior treatment	2025

Note: Information obtained from Mitchell *et al.*,[9] Pellico *et al.*,[37] Hundt *et al.*,[38] Fortuin *et al.*,[40] Nguyen *et al.*,[41], Patra *et al.*,[80], FDA[81].
Abbreviations: I.V.: Intravenously; MRI: Magnetic resonance imaging; NPs: Nanoparticles; PEG: Polyethylene glycol; SPIONs: Superparamagnetic iron oxide nanoparticles.

5.3. Stability

SPIONs are prone to aggregation, which reduces their effectiveness in circulation. To maintain their functionality, proper surface modifications are needed to achieve colloidal stability. In addition, variations in physiological pH can lead to the aggregation of SPION or loss of their functionality, further complicating their use in clinical settings.

5.4. Imaging and monitoring

Although SPIONs are frequently used as MRI contrast agents, their imaging sensitivity is not as high as that of some other contrast agents, such as Gd-based agents. Tracking SPIONs in real-time within the body remains challenging, which complicates treatment monitoring and dosage optimization.

5.5. MHT

For MHT therapy, SPIONs must generate sufficient heat upon exposure to an alternating magnetic field. However, achieving uniform heat distribution at the tumor site remains a significant challenge. To ensure efficient heating and uniform heat distribution, high SPION dosages may be required, which could raise concerns about toxicity.

5.6. Tumor penetration and targeting efficiencies

NPs accumulate at tumor sites due to the enhanced permeability and retention effect, which can vary significantly among different cancer types and patients. Tumor localization can be improved through active targeting using ligands or antibodies; however, this approach may lead to immunological reactions and off-target effects.

5.7. Combination therapies

Integrating SPIONs with other treatment methods, such as chemotherapy, immunotherapy, or radiation therapy, requires careful optimization and an understanding of synergistic effects, dosage schedules, and possible drug interactions.

5.8. Clinical translation and ethical hurdles

Although preclinical studies have shown encouraging results, clinical trials are necessary to evaluate the safety, effectiveness, and long-term outcomes of SPION-based therapies. Regulatory licensing or approval procedures for SPION-based medicines are stringent due to concerns about long-term retention in the body, clearance pathways, and potential unforeseen adverse effects. Therefore, navigating these regulatory and approval processes is necessary to bring these treatments into clinical practice.

5.9. Scalability

Variations in synthesis techniques lead to inconsistencies in size, surface coating, and magnetic properties, which hampers the reproducibility of SPIONs. As a result, producing SPIONs on a large scale while adhering to good manufacturing practices remains expensive and technically challenging.

5.10. Limited clinical success compared to other nanocarriers

Although the FDA has approved polymeric NPs (such as Abraxane) and liposomes (like Doxil), SPION-based treatments are still in the experimental stage due to issues with toxicity and clearance pathways.

6. Conclusion and future perspective

This review summarizes the synthesis, surface stabilization, and advancements in Fe_3O_4 NPs, which are emerging as versatile platforms for multimodal tumor imaging and drug delivery. The presence of active functional groups on Fe_3O_4 NPs allows for the conjugation of biological and therapeutic molecules, thereby enhancing their versatility. Recent developments in Fe_3O_4 NP synthesis and modification have expanded their potential for effective theranostic applications. In addition, when combined with other treatments, SPION-based nanoplatforms show great promise for imaging-guided cancer therapy and MHT-enhanced treatments. However, as with all advancements, some SPION-based formulations face limitations, such as insufficient renal clearance and the risk of side effects due to iron overload. Nevertheless, ongoing research is actively addressing the long-term effects of SPIONs on biological systems, striving to overcome these obstacles and fully unlock the potential of SPION-based technologies. Once these challenges are addressed, multifunctional SPIONs could be further developed for theranostics of various diseases, paving the way for their application in translational medicine in the near future.

Acknowledgments

Jnanranjan Panda gratefully acknowledges Faculty of Science, Sri Sri University, Cuttack, India. The authors also thank Dr. Bhabani Sankar Satapathy, GITAM School of Pharmacy, Hyderabad campus, Telangana, India, for his fruitful discussions during the preparation of the manuscript.

Funding

None.

Conflict of interest

The authors declare no competing interests.

Author contributions

Conceptualization: Jnanranjan Panda
Writing – original draft: All authors
Writing – review & editing: All authors

Ethics approval and consent to participate

Not applicable.

Consent for publication

Not applicable.

Availability of data

Not applicable.

References

1. Lee N, Yoo D, Ling D, Cho MH, Hyeon T, Cheon J. Iron oxide based nanoparticles for multimodal imaging and magneto responsive therapy. *Chem Rev*. 2015;115:10637-10638.

   doi: 10.1021/acs.chemrev.5b00112.

2. Gao J, Gu H, Xu B. Multifunctional magnetic nanoparticles: Design, synthesis, and biomedical applications. *Acc Chem Res*. 2009;42(8):1097-1107.

   doi: 10.1021/ar9000026

3. Panda J, Ghouri K, Sarkar R, Tudu B. Fabrication and characterization of self-assembled zinc ferrite nanospheres for biomedical applications. *Appl Phys A*. 2022;128(4):1-9.

   doi: 10.1007/s00339-022-05456-6

4. Hao R, Xing R, Xu Z, Hou Y, Gao S, Sun S. Synthesis, functionalization, and biomedical applications of

multifunctional magnetic nanoparticles. *Adv Mater*. 2010;22:2729-2742.

doi: 10.1002/adma.201000260

5. Poller JM, Zaloga J, Schreiber E, *et al.* Selection of potential iron oxide nanoparticles for breast cancer treatment based on *in vitro* cytotoxicity and cellular uptake. *Int J Nanomedicine*. 2017;12:3207-3220.

doi: 10.2147/IJN.S132369

6. Panda J, Satapathy BS, Sarkar R, Tudu B. A zinc ferrite nanodrug carrier for delivery of docetaxel: Synthesis, characterization, and *in vitro* tests on C6 glioma cells. *J Microencapsul*. 2022;39(2):136-144.

doi: 10.1080/02652048.2022.2053757

7. Hu Y, Mignani S, Majoral JP, Shen M, Shi X. Construction of iron oxide nanoparticle-based hybrid platforms for tumor imaging and therapy. *Chem Soc Rev*. 2018;47:1874-1900.

doi: 10.1039/c7cs00657h

8. Bray F, Laversanne M, Sung H, *et al.* Global cancer statistics 2022: GLOBOCAN estimates of incidence and mortality worldwide for 36 cancers in 185 countries. *CA Cancer J Clin*. 2024;74(3):229-263.

doi: 10.3322/caac.21834

9. Mitchell MJ, Billingsley MM, Haley RM, Wechsler ME, Peppas NA, Langer R. Engineering precision nanoparticles for drug delivery. *Nat Rev Drug Discov*. 2021;20:101-124.

doi: 10.1038/s41573-020-0090-8

10. Caster JM, Patel AN, Zhang T, Wang A. Investigational nanomedicines in 2016: A review of nanotherapeutics currently undergoing clinical trials. *Wiley Interdiscip Rev Nanomed Nanobiotechnol*. 2017;9:1416-1425.

doi: 10.1002/wnan.1416

11. Panda J, Satapathay BS, Mishra A, Biswal B, Sahoo PK. *Potential of Ferrite-Based Nanoparticles for Improved Cancer Therapy: Recent Progress and Challenges Ahead. Applications of Ferrites.* London: Intech Open; 2023. p. 1-18.

doi: 10.5772/intechopen.1002346

12. Cui Y, Zhang M, Zeng F, Jin H, Xu Q, Huang Y. Dual-targeting magnetic PLGA nanoparticles for codelivery of paclitaxel and curcumin for brain tumor therapy. *ACS Appl Mater Interfaces*. 2016;8:32159-32169.

doi: 10.1021/acsami.6b10175

13. Shabatina TI, Vernya OI, Shabatin VP, Melnikov MY. Magnetic nanoparticles for biomedical purposes: Modern trends and prospects. *Magnetochemistry*. 2020;6:30.

doi: 10.3390/magnetochemistry6030030

14. Panda J, Satapathy BS, Majumder S, Sarkar R, Mukherjee B, Tudu B. Engineered polymeric iron oxide nanoparticles as potential drug carrier for targeted delivery of docetaxel to breast cancer cells. *J Magn Magn Mater*. 2019;485:165-173.

doi: 10.1016/j.jmmm.2019.04.058

15. Fatima H, Charinpanitkul T, Kim KS. Fundamentals to apply magnetic nanoparticles for hyperthermia therapy. Nanomaterials *(*Basel*). 2021;11:1203.*

doi: 10.3390/nano11051203

16. Demirer GS, Okur AC, Kizilel S. Synthesis and design of biologically inspired biocompatible iron oxide nanoparticles for biomedical application. *J Mater Chem B*. 2015;3:7831-7849.

doi: 10.1039/c5tb00931f

17. Lu AH, Salabas EL, Schuth F. Magnetic nanoparticles: Synthesis, protection, functionalization, and application. *Angew Chem Int Ed*. 2007;46:1222-1244.

doi: 10.1002/anie.200602866

18. Massart R. Preparation of aqueous magnetic liquids in alkaline and acidic media. *IEEE Trans Magn.* 1981;17:1247-1248.

doi: 10.1109/TMAG.1981.1061188

19. Wang X, Zhuang J, Peng Q, Li Y. A general strategy for nanocrystal synthesis. *Nature*. 2005;437:121-124.

doi: 10.1038/nature03968

20. Yang H, Ogawa T, Hasegawa D, Takahashi M. Synthesis and magnetic properties of monodisperse magnetite nanocubes. *J Appl Phys.* 2008;103:07D526.

doi: 10.1063/1.2833820

21. Dolores R, Raquel S, Adianex GL. Sonochemical synthesis of iron oxide nanoparticles loaded with folate and cisplatin: Effect of ultrasonic frequency. *Ultrason Sonochem*. 2014;23:39-398.

doi: 10.1016/j.ultsonch.2014.08.005

22. Gambhir RP, Rohiwal SS, Tiwari AP. Multifunctional surface functionalized magnetic iron oxide nanoparticles for biomedical applications: A review. *Appl Surf Sci Adv*. 2022;11:100303.

doi: 10.1016/j.apsadv.2022.100303

23. Laurent S, Forge D, Port M, *et al.* Magnetic iron oxide nanoparticles: Synthesis, stabilization, vectorization, physicochemical characterizations, and biological applications. *Chem Rev*. 2008;108:2064-2110.

doi: 10.1021/cr068445e

24. Sairam M, Naidu BV, Nataraj SK, Sreedhar B, Aminabhavi TM. Poly(vinyl alcohol)-iron oxide nanocomposite membranes for pervaporation dehydration of isopropanol, 1,4-dioxane and tetrahydrofuran. *J Membr Sci*. 2006;283:65-73.

doi: 10.1016/j.memsci.2006.06.013

25. McCarthy JR, Weissleder R. Multifunctional magnetic nanoparticles for targeted imaging and therapy. *Adv Drug Deliv Rev*. 2008;60(11):1241-1251.

doi: 10.1016/j.addr.2008.03.014

26. Belessi V, Zboril R, Tucek J, Mashlan M, Tzitzios VK, Petridis D. Ferrofluids from magnetic-chitosan hybrids. *Chem Mater*. 2008;20:3298-3305.

doi: 10.1021/cm702990t

27. Wu W, He Q, Jiang C. Magnetic iron oxide nanoparticles: Synthesis and surface functionalization strategies. *Nanoscale Res Lett*. 2008;3:397-415.

doi: 10.1007/s11671-008-9174-9

28. Bruce IJ, Sen T. Surface modification of magnetic nanoparticles with alkoxysilanes and their application in magnetic bio separation. *Langmuir*. 2005;21:7029-7035.

doi: 10.1021/la050553t

29. Ding HL, Zhang YX, Wang S, Xu JM, Xu SC, Li GH. Fe_3O_4 @SiO_2 Core/Shell nanoparticles: The silica coating regulations with a single core for different core sizes and shell thicknesses. *Chem Mater*. 2012;24:4572-4580.

doi: 10.1021/cm302828d

30. Lin J, Zhou WL, Kumbhar A, *et al.* Gold-coated iron (Fe@Au) nanoparticles: Synthesis, characterization, and magnetic field-induced self-assembly. *J Solid State Chem*. 2001;159:26-31.

doi: 10.1006/jssc.2001.9117

31. Yu H, Chen M, Rice PM, Wang SX, White RL, Sun S. Dumbbell-like bi-functional Au-Fe_3O_4 nanoparticles. *Nano Lett*. 2005;5:379-382.

doi: 10.1021/nl047955q

32. Wang L, Luo J, Maye MM, *et al.* Iron oxide-gold core-shell nanoparticles and thin film assembly. *J Mater Chem*. 2005;15:1821-1832.

doi: 10.1039/B501375E

33. Lapusan R, Borlan R, Focsan M. Advancing MRI with magnetic nanoparticles: A comprehensive review of translational research and clinical trials. *Nanoscale Adv*. 2024;6:2234-2259.

doi: 10.1039/d3na01064c

34. Liao Z, Wang H, Lv R, *et al.* Polymeric liposomes-coated superparamagnetic iron oxide nanoparticles as contrast agent for targeted magnetic resonance imaging of cancer cells. *Langmuir*. 2011;27:3100-3105.

doi: 10.1021/la1050157

35. Li J, Hu Y, Yang J, *et al.* Hyaluronic acid-modified Fe3O4@Au core/shell nanostars for multimodal imaging and photothermal therapy of tumors. *Biomaterials*. 2015;38:10-21.

doi: 10.1016/j.biomaterials.2014.10.065

36. Jun YW, Huh YM, Choi YS, *et al.* Nanoscale size effect of magnetic nanocrystals and their utilization for cancer diagnosis via magnetic resonance imaging. *J Am Chem Soc*. 2005;127:12387-12391.

doi: 10.1021/ja0422155

37. Pellico J, Cabello JR, Herranz F. Radiolabeled iron oxide nanomaterials for multimodal nuclear imaging and positive contrast magnetic resonance imaging (MRI): A review. *ACS Appl Nano Mater*. 2023;6:20523-20538.

doi: 10.1021/acsanm.3c04269

38. Hundt W, Petsch R, Helmberger T, Reiser M. Signal changes in liver and spleen after endorem administration in patients with and without liver cirrhosis. *Eur Radiol*. 2000;10:409-416.

doi: 10.1007/s003300050067

39. Reimer P, Balzer T. Ferucarbotran (resovist): A new clinically approved RES-specific contrast agent for contrast enhanced MRI of the liver: Properties, clinical development, and applications. *Eur Radiol*. 2003;13:1266-1276.

doi: 10.1007/s00330-002-1721-7

40. Fortuin AS, Brüggemann R, van der Linden J, *et al.* Ultra-small superparamagnetic iron oxides for metastatic lymph node detection: Back on the block. *Wiley Interdiscip Rev Nanomed Nanobiotechnol*. 2018;10:e147.

doi: 10.1002/wnan.1471

41. Nguyen KL, Yoshida T, Kathuria-Prakash N, *et al.* Multicenter safety and practice for off-label diagnostic use of ferumoxytol in MRI. *Radiology*. 2019;293:554-564.

doi: 10.1148/radiol.2019190477

42. Ding L, Wang R, Hu Y, *et al.* Folic acid-modified Laponite®-stabilized Fe3O4 nanoparticles for targeted T2-weighted MR imaging of tumour. *Appl Clay Sci*. 2020;186:105447.

doi: 10.1016/j.clay.2020.105447

43. Zhao Z, Zhou Z, Bao J, *et al.* Octapod iron oxide nanoparticles as high-performance T contrast agents for magnetic resonance imaging. *Nat Commun*. 2013;4:2266.

doi: 10.1038/ncomms3266

44. Zhu J, Peng C, Sun W, *et al.* Formation of iron oxide nanoparticle-loaded γ-polyglutamic acid nanogels for MR imaging of tumors. *J Mater Chem B*. 2015;3:8684-8693.

doi: 10.1039/C5TB01854D

45. Li J, Zheng L, Cai H, *et al.* Polyethyleneimine-mediated synthesis of folic acid-targeted iron oxide nanoparticles for *in vivo* tumor MR imaging. *Biomaterials*. 2013;4:8382-8392.

doi: 10.1016/j.biomaterials.2013.07.070

46. Coey JMD. Noncollinear spin arrangement in ultrafine ferrimagnetic crystallites. *Phys Rev Lett*. 1971;27:1140-1142.

doi: 10.1103/PhysRevLett.27.1140

47. Luo Y, Yang J, Yan Y, *et al.* RGD-functionalized ultrasmall iron oxide nanoparticles for targeted T_1-weighted MR imaging of gliomas. *Nanoscale*. 2015;7:14538-14546.

doi: 10.1039/C5NR04003E

48. Bhavesh R, Lechuga-Vieco AV, Ruiz-Cabello J, Herranz F. T1-MRI fluorescent iron oxide nanoparticles by microwave assisted synthesis. *Nanomaterials*. 2015;5:1888-1890.

doi: 10.3390/nano5041880

49. Wei H, Bruns OT, Kaul MG, *et al.* Exceedingly small iron oxide nanoparticles as positive MRI contrast agents. *Proc Natl Acad Sci U S A*. 2017;114:2325-2330.

doi: 10.1073/pnas.1620145114

50. Zhou Z, Zhao Z, Zhang H, Wang Z, Chen X, Wang R, *et al*. Interplay between longitudinal and transverse contrasts in Fe3O4 nanoplates with (111) exposed surfaces. *ACS Nano.* 2013;7:3287-3296.

doi: 10.1021/nn5038652

51. Taboada E, Rodríguez R, Roig A, Oró J, Roch A, Muller RN. Relaxometric and magnetic characterization of ultrasmall iron oxide nanoparticles with high magnetization. Evaluation as potential T1 magnetic resonance imaging contrast agents for molecular imaging. *Langmuir.* 2007;23:4583-4588.

doi: 10.1021/la063415s

52. Sun Y, Zheng Y, Ran H, *et al*. Superparamagnetic PLGA-iron oxide microcapsules for dual-modality US/MR imaging and high intensity focused US breast cancer ablation. *Biomaterials*. 2012;33:5854-5864.

doi: 10.1016/j.biomaterials.2012.04.062

53. Bae KH, Kim YB, Lee Y, *et al.* Bioinspired synthesis and characterization of gadolinium-labeled magnetite nanoparticles for dual contrast t1- and T2-weighted magnetic resonance imaging. *Bioconjug Chem*. 2010;21:505-512.

doi: 10.1021/bc900424u

54. Johannsen M, Gneveckow U, Eckelt L, *et al.* Clinical hyperthermia of prostate cancer using magnetic nanoparticles: Presentation of a new interstitial technique. *Eur Urol*. 2007;52:1653-1662.

doi: 10.1080/02656730500158360

55. Guardia P, Di Corato R, Lartigue L, *et al.* Water-soluble iron oxide nanocubes with high values of specific absorption rate for cancer cell hyperthermia treatment. *ACS Nano.* 2012;6:3080-3091.

doi: 10.1021/nn2048137

56. Chastellain M, Petri A, Gupta A, Rao KV, Hofmann H. Superparamagnetic silica-iron oxide nanocomposites for application in hyperthermia. *Adv Eng Mater*. 2004;6:235-241.

doi: 10.1002/adem.200300574

57. Johannsen M, Thiesen B, Jordan A, Wust P. Magnetic nanoparticle hyperthermia for prostate cancer. *Int J Hyperthermia.* 2010;26:790-795.

doi: 10.3109/02656731003745740

58. Gordon AC, Lewandowski RJ, Salem R, Day DE, Omary RA, Larson AC. Localized hyperthermia with iron oxide-doped yttrium microparticles: Steps towards image-guided thermoradiotherapy in liver cancer. *J Vasc Interv Radiol*. 2014;25:397-404.

doi: 10.1016/j.jvir.2013.10.022

59. Ghosh R, Pradhan L, Devi YP, *et al.* Induction heating studies of Fe_3O_4 magnetic nanoparticles capped with oleic acid and polyethylene glycol for hyperthermia. *J Mater Chem*. 2011;21:13388-13398.

doi: 10.1039/C1JM10092K

60. Hayashi K, Ono K, Suzuki H, *et al.* One-pot biofunctionalization of magnetic nanoparticles via thiolene click reaction for magnetic hyperthermia and magnetic resonance imaging. *Chem Mater*. 2010;22:3768-3772.

doi: 10.1021/cm100810g

61. Espinosa A, Di Corato R, Kolosnjaj-Tabi J, Flaud P, Pellegrino T, Wilhelm C. The duality of iron oxide nanoparticles in cancer therapy: Amplification of heating efficiency by magnetic hyperthermia and photothermal bimodal treatment. *ACS Nano.* 2016;10:2436-2446.

doi: 10.1021/acsnano.5b07249

62. Corato D, Béalle G, Kolosnjaj-Tabi J, *et al.* Combining magnetic hyperthermia and photodynamic therapy for tumor ablation with photoresponsive magnetic liposomes. *ACS Nano.* 2015;9:2904-2916.

doi: 10.1021/nn506949t

63. Fortin JP, Wilhelm C, Servais J, Ménager C, Bacri JC, Gazeau F. Size-sorted anionic iron oxide nanomagnets as colloidal mediators for magnetic hyperthermia. *J Am Chem Soc*. 2007;129:2628-2635.

doi: 10.1021/ja067457e

64. Landeghem V, Maier-Hauff FK, Jordan K, *et al.* Post-mortem studies in glioblastoma patients treated with thermotherapy using magnetic nanoparticles. *J Neurooncology*. 2007;81:53-60.

doi: 10.1016/j.biomaterials.2008.09.044

65. Kandasamy G, Maity D. Recent advances in superparamagnetic iron oxide nanoparticles (SPIONs) for *in vitro* and *in vivo* cancer nanotheranostics. *Int J Pharm*. 2015;496:191-218.

doi: 10.1016/j.ijpharm.2015.10.058

66. Widder K, Senyei AE, Scarpelli DG. Magnetic microspheres: A model system of site specific drug delivery *in vivo*. *Proc Soc Exp Biol Med*. 1978;158:141-146.

doi: 10.3181/00379727-158-40158

67. Senyei AE, Widder K, Czerlinski G. Magnetic guidance of drug-carrying microspheres. *J Appl Phys.* 1978;49:3578-3583.

doi: 10.1063/1.325219

68. Price PM, Mahmoud WE, Al-Ghamdi AA, Bronstein LM.

Magnetic drug delivery: Where the field is going. *Front Chem*. 2018;6:619-626.

doi: 10.3389/fchem.2018.00619

69. Bhuyan T, Singh AK, Dutta D, Unal A, Ghosh SS, Bandyopadhyay D. Magnetic field guided chemotaxis of Mushbots for targeted anticancer therapeutics. *ACS Biomater Sci Eng*. 2017;3:1627-1640.

doi: 10.1021/acsbiomaterials.7b00086

70. Mai BT, Fernandes S, Balakrishnan PB, Pellegrino T. Nanosystems based on magnetic nanoparticles and thermoorph responsive polymers: An update and future perspectives. *Acc Chem Res*. 2018;51:999-1013.

doi: 10.1021/acs.accounts.7b00549

71. Chen Z, Kankala RK, Long L, Xie S, Chen A, Zou L. Current understanding of passive and active targeting nanomedicines to enhance tumor accumulation. *Coord Chem Rev*. 2023;481:215051.

doi: 10.1016/j.ccr.2023.215051

72. Wahajuddin, Arora S. Superparamagnetic iron oxide nanoparticles: Magnetic nanoplatforms as drug carriers. *Int J Nanomed*. 2012;7:3445-3471.

doi: 10.2147/IJN.S30320

73. Alexiou C, Arnold W, Klein RJ, *et al.* Locoregional cancer treatment with magnetic drug targeting. *Cancer Res*. 2000;60:6641-6648.

74. Kim J, Lee JE, Lee JH, *et al.* Designed fabrication of a multifunctional polymer nanomedical platform for simultaneous cancer- targeted imaging and magnetically guided drug delivery. *Adv Mater*. 2008;20:478-483.

doi: 10.1002/adma.200701726

75. Basuki JS, Duong HTT, Macmillan A, *et al.* Using fluorescence lifetime imaging microscopy to monitor theranostic nanoparticle uptake and intracellular doxorubicin release. *ACS Nano.* 2013;7:10175-10189.

doi: 10.1021/nn404407g

76. Ling Y, Wei K, Luo Y, Gao X, Zhong S. Dual docetaxel/superparamagnetic iron oxide loaded nanoparticles for both targeting magnetic resonance imaging and cancer therapy. *Biomaterials*. 2011;32:7139-7150.

doi: 10.1016/j.biomaterials.2011.05.089

77. Reczyńska K, Marszałek M, Zarzycki A, *et al.* Superparamagnetic iron oxide nanoparticles modified with silica layers as potential agents for lung cancer treatment. Nanomaterials. 2020;*10*:1076.

doi: 10.3390/nano10061076

78. Horvat NK, Chocarro S, Marques O, *et al.* Superparamagnetic iron oxide nanoparticles reprogram the tumor microenvironment and reduce lung cancer regrowth after crizotinib treatment. *ACS Nano.* 2024;18:11025-11041.

doi: 10.1021/acsnano.3c08335

79. Wang ZL, Qiao RR, Tang NG, *et al.* Active targeting theranostic iron oxide nanoparticles for MRI and magnetic resonance-guided focused ultrasound ablation of lung cancer. *Biomaterials*. 2017;127:25-35.

doi: 10.1016/j.biomaterials.2017.02.037

80. Patra JK, Das G, Fraceto LF, *et al.* Nano based drug delivery systems: Recent developments and future prospects. *J Nanobiotechnol*. 2018;16(71):1-33.

doi: 10.1186/s12951-018-0392-8

81. Available from: https://www.fda.gov/drugs/resources-information-approved-drugs/fda-approves-datopotamab-deruxtecan-dlnk-unresectable-or-metastatic-hr-positive-her2-negative-breast cancer [Last accessed on 2025 Jan 17].

ACCSCIENCE PUBLISHING

Global Translational Medicine

PERSPECTIVE ARTICLE

YeeZzzy does it: Using Kanye West's tweets to identify sleep and emotional disturbances through digital rest-activity rhythms analysis

Matthew J. Reid[1]*, Darlynn M. Rojo-Wissar[2,3], Michelle Mei[1], Moira Differding[4], Michael T. Smith[1], and Michael G. Smith[5]

[1]Department of Psychiatry and Behavioral Sciences, Johns Hopkins University School of Medicine, Baltimore, MD, United States of America

[2]Department of Psychiatry and Human Behavior, Alpert Medical School of Brown University, Providence, Rhode Island, United States of America

[3]Bradley/Hasbro Children's Research Center, E.P. Bradley Hospital, East Providence, Rhode Island, United States of America

[4]Department of Epidemiology, Johns Hopkins Bloomberg School of Public Health, Baltimore, Maryland, United States of America

[5]Department of Occupational and Environmental Medicine, School of Public Health and Community Medicine, University of Gothenburg, Gothenburg, Västra Götaland, Sweeden

Abstract

One of the greatest challenges faced by precision medicine is the identification of biomarkers capable of detecting clinically meaningful change at the individual level, not just among large-scale population studies. To this end, the high-volume nature of an individual's social media data could be leveraged with single-user precision to monitor sleep patterns and tweet content to determine emotional state. However, there is a lack of established methods to detect and estimate sleep and mood using social-media activity. We present here a new approach (digital rest-activity rhythms analysis) to using social media to track both sleep and mood, with potential applications to mental health monitoring and prevention. Our proof-of-concept showed that the emotional content of a single user's tweets (Kanye West "@Ye") were influenced by sleep disturbances inferred from usage over a 2-year period. We herein provide an ethical and theoretical-framework of how to proceed among this sensitive yet potentially fruitful field.

Keywords: Sleep; Twitter; Social media; Depression; Emotion; Mood

***Corresponding author:**
Matthew J. Reid
(mreid27@jhmi.edu)

Citation: Reid MJ, Rojo-Wissar DM, Mei M, Differding M, Smith MT, Smith MG. YeeZzzy does it: Using Kanye West's tweets to identify sleep and emotional disturbances through digital rest-activity rhythms analysis. *Global Transl Med.* 2025;4(2):51-57.
doi: 10.36922/gtm.5176

Received: October 17, 2024

Revised: December 7, 2024

Accepted: December 13, 2024

Published online: January 9, 2025

1. Introduction

One of the greatest challenges faced by the field of precision medicine is the identification of biomarkers capable of detecting clinically meaningful change at the individual level, not just among large-scale population studies. To this end, the evermore present social mediaverse provides unparalleled access to ecologically valid databases of digital biomarkers that could be leveraged with single-user precision to support mental health care by monitoring use patterns and emotional state. An illustrative study[1] published in *Science* demonstrated the presence of circadian rhythmicity in the emotional content

of "Tweets" with positive emotionality declining and negative emotion increasing with progression of the day. Despite these early advancements, further investigation into how social media use can be used to study sleep-wake behaviors has been remarkably scant, in part due to a lack of established methods to detect and estimate sleep using social media activity.

In an elegant effort, Roenneberg[2] used tweets to estimate sleep opportunity by analyzing the circadian rhythmicity of a single social media account (~6.5 h in the case of Donald Trump). However, links between these digital rest-activity rhythms (dRARs) and clinically or socially relevant indices, such as the emotional content of tweets, were not examined, potentially due to the complexities involved in integrating these dRARs with the highly complex yet rich nature of tweet contents. Extending this work, we developed a methodological process to examine the relationship between a user's sleep-wake patterns and the daytime emotional content of their tweets. As these tools are ultimately intended for use at the level of the individual user, here we present proof-of-concept data from a single user (Kanye West "@Ye") to identify periods of sleep disturbance, based on a user's habitual sleep window and evaluated their impact on next-day emotional state.

1.1. An individual-level proof of concept: Introducing dRARs analysis

As demonstrated by Roenneberg,[2] case studies of high-volume Twitter ("*X*.com") users may represent such a means through which meaningful longitudinal data can be validated. In this analysis, 1868 tweets were extracted from the user profile of Kanye West (available at www.twitter.com/@Ye) across 258 days using the Twitter.com application programming interface and a custom programming script written in Python. To approximate nocturnal from diurnal tweets, data were mean-averaged across the period, and a sliding window function applied to determine the least active 5 h (L5 index) of the 24-h period, a common method used to determine the nadir of circadian quiescence and define the "nocturnal" window. We subsequently identified days in which @Ye's tweets were preceded by Twitter activity during the previous nocturnal window and derived the number of tweets during that window, as well as the total number of nocturnal tweets over the previous 7 days (Supplement File for detailed methods).

The most frequently adopted approach to study Twitter and other social media content is sentiment analysis. Sentiment analysis offers a low-dimensional representation of emotion by integrating several complex word valences into one measure of relative positive/negative emotion, ranging from –1 (negative) to 0 (neutral), to +1 (positive). However, this approach conflates positive and negative emotion into a single dimension, assuming their conditional dependence. This assumption departs from the substantial body of literature, indicating that positive and negative emotion are independent dimensions that are differentially affected by sleep loss and circadian trajectories.[3] Therefore, in accordance with the previous study[1] which explored circadian aspects of emotional tweet content, we also derived measures of positive and negative affect for each tweet using a natural language processing (NLP) model (Linguistic Enquiry and Word Count [LIWC] analysis[4]), using the "positive emotion" and "negative emotion" output variables which give an overall positivity and negativity score for each tweet based on a validated linguistic dictionary of 6400 words. We subsequently calculated mean positive and negative affect across hourly and monthly bins to assess circadian and seasonal effects. Models were conducted with Zero-Inflated Poisson (ZIP) regression controlling for time and month of each tweet to limit confounding. In separate sensitivity analyses, we also tested the relationship of time and month with positive and negative emotion using ZIP regression to test main and interaction effects of hour, month, and affect (positive vs. negative), both to serve as a validation check for their pre-specified inclusion as covariates, and to test the sensitivity of the model to detect known effects observed at the population level in a single user. Finally, we visualized data using a double plot, adapted from a common method used in circadian actigraphy research, along with semantic networks for the emotional constructs identified by the LIWC analysis (Figure 1).

Our model confirmed findings[1] at the population level that tweets fluctuate significantly across the 24-h cycle with positive emotion declining with the progression of the day ($P < 0.001$), whilst negative emotion increased and peaked towards the evening ($P < 0.001$) (Figure 1). Next, we tested the effect of nocturnal tweeting on next-day emotional tweet content whilst controlling for time-of-day of the daytime tweets, month, and the tweet-word count, to mitigate their potential confounding impact (Table S1). Our models demonstrated that increased nocturnal tweeting was significantly associated with negative emotional content of tweets the following day (Bonferroni-corrected $P \leq 0.001$) and was also linked to significantly reduced positive emotion the following day (Bonferroni-corrected $P \leq 0.001$). When examining tweets across the previous week, increased nocturnal tweeting was also significantly associated with decreased positive emotional content (Bonferroni-corrected $P = 0.041$), but not with negative emotional content (Bonferroni-corrected $P = 0.432$).

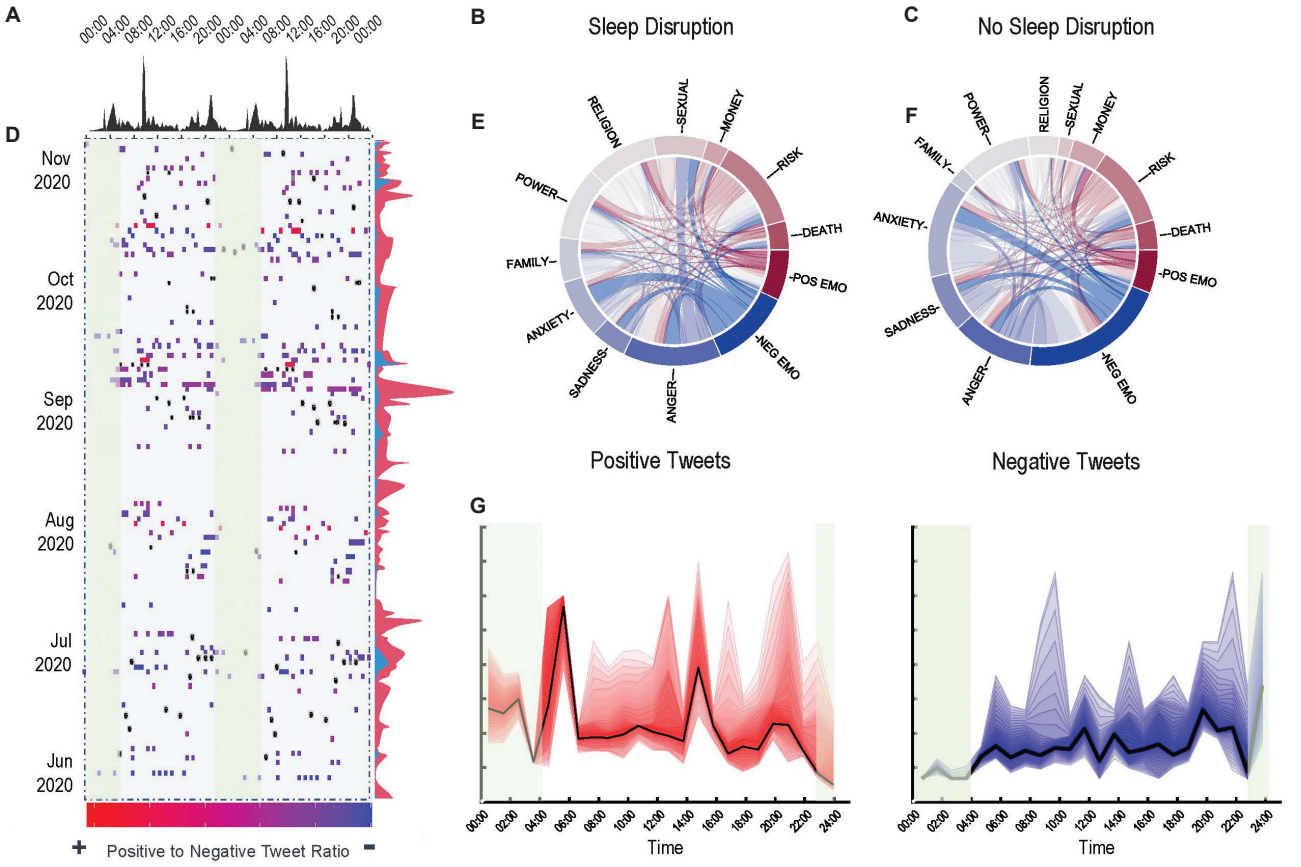

Figure 1. Visualization of emotional tweet content. (A) Daily tweet frequency in 20-min bins across the 24-h day, averaged from 258 days of Twitter data and 1868 tweets. (B and C) The semantic network of principally weighted emotional constructs during days which were preceded by known nocturnal tweeting, versus those in which no nocturnal tweeting was present. (D) Double plot visualizes the relative emotional ratio of positive to negative content of tweets in each 20-min bin across the 24-h day across a representative sample period from June to November 2020, with red indicating more positive content, blue more negative content, and purple about the same amount of positive and negative content (see color bar key on horizontal axis). Gray squares indicate the presence of tweets which were timestamped but were omitted from sleep-linguistic analyses. (E and F) Positive and negative valences of tweets when plotted as a function of the average 24-h period. As positive emotion was much more prominent than negative emotion, the y-axis depicts relative units to facilitate comparisons of circadian trajectories, as opposed to relative magnitudes. Shaded error bars indicate 95% confidence intervals of the relative values. (G) Represents the frequency of positive (in red) tweet content overlaid with the relative frequency (horizontal axis) (in arbitrary units scaled 0 – 1) of negative (in blue) tweet content per day across the assessment period (vertical axis).
Note: The nocturnal period (L5 window) from 23:00 to 04:00 is shaded in light green.

These data show that previous nights' nocturnal tweeting is associated with a decrease in positive tweet content the following day (defined as the period outside the L5 window: 23:00 – 04:00), whilst negative tweet content remains stable. These observations align with previous social media studies[1] and causal sleep-disruption studies[3,5] in humans, which report blunting of positive emotion and modest or no increases in negative emotion, suggesting our methods may be sensitive to detecting both sleep-determined emotional-state and circadian effects on emotion. Broadly, these findings give credence to the notion that sleep disturbance results in a generalized "negative emotional-bias" even when assessed through naturalistic observations of a single user. Nevertheless, it should be noted that whilst dRARs do allow us to estimate maximal sleep opportunities, sleep cannot be definitively inferred from nocturnal digital quiescence, and should not be considered a surrogate marker for sleep.

2. Potential applications and implementation of dRARs in mental health care

Our method (dRARs analysis) has the advantage of leveraging real-world data which reflects an individual's unprompted and spontaneous thoughts and feelings, and are sensitive to change on this individual level, making them ideal candidates for deployment as digital biomarkers, and mobile health interventions. Although continuous social media monitoring poses ethnical concerns, automated

text-mining algorithms could be applied benevolently to identify individuals susceptible to emotional distress from circadian and sleep-related disruption, which could facilitate the administration of "Just-In-Time Adaptive Interventions,"[6] or signpost to appropriate support. One of the reasons that existing suicide prevention approaches have had limited impact on suicide rates is that prevention interventions are too slow for the dynamic temporal nature of suicide ideation, which fluctuates in real-time. In particular, during the night, when suicide risk is substantially elevated and support mechanisms are scare, social media monitoring could provide timely and ecological support in the form of counseling, or referral to 24-h telehealth services when it is most needed. These interventions may complement or even integrate with automated harm-prevention mechanisms present on social media sites, such as "pop-ups" offering support resources whenever a user's activity is flagged due to the use of keywords associated with suicide. Nevertheless, the implementation of these methods presents a number of methodological and legal challenges, which we discuss over the proceeding sections.

3. Methodological challenges

3.1. Determining validation and alignment with circadian rhythms

Much in the same manner that wearable devices which track sleep must be compared against gold-standard metrics of sleep, examinations of how sleep estimates from dRARs align with predetermined benchmarks for accuracy must be conducted, by assessing their synchronicity with well-defined biological (e.g., circadian), environmental (e.g., night/day or light/dark) or social rest-activity (e.g., work-leisure) rhythms when measured using techniques commonly held as accurate assays of these rhythms. For instance, determination of the peak of dRARs activity relative to one's dim light melatonin onset peak could provide a window into alignment with endogenous biological rhythms. Most relevant are comparisons with 24-h waist-actigraphy (a gold-standard for rest-activity rhythms [RAR] assessments), which would represent a logical next-step in this validation pipeline and necessitate comparison of how accurately measurements of L5 and M10 (most active 10/24 h) align between dRARs and movement RARs. Such validation studies should employ standardized approaches and recommended guidelines (for further details see Smith *et al.* [2018][7]) for traditional RAR assessment in performing these comparisons. Crucially, as we demonstrated this approach on a single user, generalizability of these findings is limited, and should only be considered as a proof-of-concept of the method. Large-scale studies are required to assess the stability of intra-individual interactions between dRARs and emotional tweet content across a larger and diverse population.

From a translational perspective, future studies may consider assessment of clinical validity among known "at-risk" populations as all the lexicons used in NLP methods such as sentiment analysis and LIWC are based on healthy individuals. Once the goal of these methodologies becomes the identification of clinically salient emotional distress, one must consider the extent to which we can consider these normative datasets to be valid. We recommend the development of lexicons based on distinct clinical populations (e.g., major depressive disorder, generalized anxiety disorder), which may maximize the sensitivity of these models. Moreover, language by nature differs drastically among cultures, and societies. Therefore, it is important to consider whether models trained using one particular language be transferred to another, as well as whether these models perform equally well across different populations. Equally important is the question of how differences in language are perceived across different genders, ethnic identities, races, and cultures, and how their relationship with the 24-h cycle should be considered. Given that certain cultures, ethnicities, and genders communicate emotion much more readily than others, it is critical to consider how conspicuous language should be before it is considered to be indicative of emotional distress. Nevertheless, obtaining this demographic information from social media may prove unreliable, due to the limited nature of the source data (a user's profile). Much in the same way that disorder-specific models may contribute toward increased precision for the detection of emotional distress, models which adapt to the differences in sleep behaviors (e.g., chronotype, bi-phasic sleeping or siesta cultures) may prove beneficial. However, consideration of how to considerately integrate these data with other sources of demographic meta-data must first be addressed.

3.2. Defining sleep window with minimal datapoints

Perhaps the most salient methodological challenge associated with deriving RARs from social media use is the continuity and completeness of the data. Thorough sensitivity analyses to determine both the minimum amount of data are required to accurately determine rhythms, as well as the precision points at which further data brings no further gain in model accuracy. These parameters should be determined to ensure the credibility of predictions, as well as protection against unnecessary exposure of data when it is not necessary to inform models. Although the present study focused exclusively on social

media activity as its data source, it should be noted that the proposed methods are by no means limited to these data. For better or worse, activities of daily living increasingly rely on the use of smartphones or mobile applications,[8,9] all of which have potential to inform models used to train predictive dRARs. Moreover, a significant portion of individuals report using their phone immediately before going to bed (e.g., checking social media or emails, setting alarms, plugging a phone into a charging socket) and immediately again on awaking (e.g., to cancel an alarm).[10,11] On the other hand, individuals are increasingly encouraged to avoid devices before bed[12,13] which may bias estimations of a user's least active (L5) periods. Nevertheless, triangulating data from multiple digital sources within a user's digital device network (e.g., app usage, screen inactivity) in an increasingly digital world could yield a remarkably accurate digital fingerprint of the user's bed and rise time patterns, over time helping to build a highly intelligent model of the user's dRARs, and flag any deviations from normative cycles.

4. Ethical and legal challenges

Who should be the gatekeeper of information obtained on real-time emotional state and vulnerability? The social media platforms themselves, or some form of health liaison agency with links to mental health services? One must consider whether such organizations have the necessary infrastructure to support such a large-scale repository of what could reasonably be considered patient health information. Social media networks are notoriously susceptible to cyber-attacks, and assessments would first need to be made to verify that security systems meet the clinical standards. Furthermore, a new data governance system must be established to ensure proper safekeeping of data and their transfer to clinical liaison services. Proper data governance is also essential to prevent the commoditization of these potentially rich and revealing data. Given the growing use of behavioral economics to create individually targeted advertisement campaigns, it would be naïve to assume that these data have no financial value, or even that they are not already being used in such a way. Information on a user's sleep habits, or level of sleep disruption, would likely be an extremely valuable asset to commercial organizations promoting sleep medications or supplements, much like information on positive or negative emotional states would be financially incentivizing to myriad facets of the highly lucrative field of mental wellness. Permitting modular adjustments to data visibility (e.g., preventing timestamps of posts from being visible) could be one potential solution to addressing some aspects of this dilemma. However, the prevention of emotional word content being used by third parties or internal algorithms is far more challenging. Furthermore, given that many environmental aspects such as latitude, longitude, altitude, and light exposure, have potential to influence both sleep and emotion, one must weigh the potential benefits of including geographical coordinates into predictive models against the clear and present threat of monitoring users' locations.

4.1. Tending to the ethical and legal landscape of social media monitoring

Although a great deal of research development stands in the way of any form of real-world implementation, earnest exploration of the ethical and legal landscape of such advancements is certainly warranted. Principally, consideration of how the use of social media data to monitor an individual's sleep behaviors of emotional well-being aligns with the basic ethical principles upheld by medicine requires addressing. For instance, where does the responsibility of technology devised to monitor health behaviors and emotional well-being end? In the process of monitoring emotional word content, do we also uphold a responsibility to monitor other behaviors which may be perceived as threatening (e.g., abuse, terrorism) to others. One could easily draw comparisons with analogs among the medical field, such as incidental findings of structural abnormalities which occur during MRI scans.

Assuming consent is deemed a requirement, the stage and source at which consent is obtained presents another challenge. For instance, should this take place at the terms-and-conditions level of the end-user platform, in essence permitting monitoring of all users, or should there be an independent opt-in process external to these initial terms and conditions, either allowing users to opt-in or opt-out. Once entertaining the realms of informed consent, the age at which one is considered competent of consent or assent becomes an immediately pertinent factor. Most social media platforms permit adolescent users, typically below the age of what most healthcare systems would be considered medically autonomous. Should these users be omitted from monitoring on the grounds of inability to consent, or should consent be sought through legal guardians? Whilst ethically straightforward and defensible on the grounds of consent, omitting adolescents and those under the age of legal consent entirely from the process has the potential to create an age-group disparity in the availability of preventative health measures. One must also, of course, take into account the fact that adolescents are those most likely to be: (1) high-volume users, (2) likely to convey

emotional distress on social media, as well as (3) those at greatest risk for sleep and circadian disruption as well as the development of preventable mental illness. Under this consideration, perhaps the benefits may outweigh the risks in this age group, and thus, cost-benefit analyses should be performed.

5. Conclusion

This paper presents the feasibility of methods to leverage the digital rhythms of social media users (dRARs) for the benefit of monitoring sleep and emotional well-being. Future work requires a multidisciplinary approach through parallel lines of investigation spanning scientific, digital, medical, and philosophical disciplines. The work we present here represents a modest step in the roadmap we outline in this paper, and we outline several recommendations for key questions to facilitate and stimulate future work in this arena. Importantly, several vital questions with more provocative and wide-reaching implications need to be overcome to bridge the gap between proof-of-concept and implementation.

Acknowledgments

None.

Funding

None.

Conflict of interest

The authors declare that they have no competing interests.

Author contributions

Conceptualization: Matthew J. Reid
Writing–original draft: Matthew J. Reid
Writing–review & editing: All authors

Ethics approval and consent to participate

Not applicable.

Consent for publication

Not applicable.

Availability of data

Data are available publicly on Twitter (officially known as X).

References

1. Golder SA, Macy MW. Diurnal and seasonal mood vary with work, sleep, and daylength across diverse cultures. *Science.* 2011;333(6051):1878-1881.

   doi: 10.1126/science.1202775

2. Roenneberg T. Twitter as a means to study temporal behaviour. *Curr Biol.* 2017;27(17):R830-R832.

   doi: 10.1016/j.cub.2017.08.005

3. Finan PH, Quartana PJ, Remeniuk B, *et al*. Partial sleep deprivation attenuates the positive affective system: Effects across multiple measurement modalities. *Sleep.* 2017;40(1):zsw017.

   doi: 10.1093/sleep/zsw017

4. Tausczik YR, Pennebaker JW. The psychological meaning of words: LIWC and computerized text analysis methods. *J Lang Soc Psychol.* 2010;29(1):24-54.

   doi: 10.1177/0261927X09351676

5. Reid MJ, Omlin X, Espie CA, Sharman R, Tamm S, Kyle SD. The effect of sleep continuity disruption on multimodal emotion processing and regulation: A laboratory-based, randomised, controlled experiment in good sleepers. *J Sleep Res.* 2023;32(1):e13634.

   doi: 10.1111/jsr.13634

6. Nahum-Shani I, Smith SN, Spring BJ, *et al*. Just-in-time adaptive interventions (JITAIs) in mobile health: Key components and design principles for ongoing health behavior support. *Ann Behav Med.* 2018;52(6):446-462.

   doi: 10.1007/s12160-016-9830-8

7. Smith MT, McCrae CS, Cheung J, *et al*. Use of actigraphy for the evaluation of sleep disorders and circadian rhythm sleep-wake disorders: An American Academy of Sleep Medicine clinical practice guideline. *J Clin Sleep Med.* 2018;14(7):1231-1237.

   doi: 10.5664/jcsm.7230

8. Araujo T, Wonneberger A, Neijens P, de Vreese C. How much time do you spend online? Understanding and improving the accuracy of self-reported measures of internet use. *Commun Methods Meas.* 2017;11(3):173-190.

   doi: 10.1080/19312458.2017.1317337

9. Vanden Abeele M, Beullens K, Roe K. Measuring mobile phone use: Gender, age and real usage level in relation to the accuracy and validity of self-reported mobile phone use. *Mobile Media Commun.* 2013;1(2):213-236.

   doi: 10.1177/2050157913477095

10. Levenson JC, Shensa A, Sidani JE, Colditz JB, Primack BA. Social media use before bed and sleep disturbance among young adults in the United States: A nationally representative study. *Sleep.* 2017;40(9):zsx113.

    doi: 10.1093/sleep/zsx113

11. Shin JC, Kim J, Grigsby-Toussaint D. Mobile phone interventions for sleep disorders and sleep quality:

Systematic review. *JMIR Mhealth Uhealth.* 2017;5(9):e7244.

doi: 10.2196/mhealth.7244

12. Brown TM, Brainard GC, Cajochen C, *et al.* Recommendations for daytime, evening, and nighttime indoor light exposure to best support physiology, sleep, and wakefulness in healthy adults. *PLoS Biol.* 2022;20(3):e3001571.

doi: 10.1371/journal.pbio.3001571

13. Gubin D, Danilenko K, Stefani O, *et al.* Blue light and temperature actigraphy measures predicting metabolic health are linked to melatonin receptor polymorphism. *Biology* (*Basel*). 2024;13(1):22.

doi: 10.3390/biology13010022

ACCSCIENCE PUBLISHING

Global Translational Medicine

ORIGINAL RESEARCH ARTICLE

Luminal α-glucosidase inhibition improves insulin sensitivity and modulates glycemic and lipid profiles in obese rats with type 2 diabetes mellitus

Orien L. Tulp[1]* and Syed A. A. Rizvi[2,3]

[1]Department of Medicine, University of Science, Arts and Technology, Montserrat, British West Indies, United Kingdom

[2]Department of Biomedical Sciences, College of Biomedical Sciences, Larkin University, Miami, Florida, United States of America

[3]Division of Clinical and Translational Research, Larkin Community Hospital, Miami, Florida, United States of America

Abstract

Atherogenic plasma lipid and glycemic profiles are commonly observed in obesity and adult-onset type 2 diabetes mellitus (T2DM) and may improve following therapeutic intervention. The effects of the luminal α-glucosidase inhibitor miglitol (MIG) on carbohydrate digestion and plasma lipid profiles were evaluated in adult male obese spontaneously hypertensive and diabetes-prone/Ntul//-*cp* rats, a genetic model that develops early-onset obesity and T2DM independently of diet. Rats were fed either a nutritionally complete diet (formulated by the United States Department of Agriculture) containing 54% sucrose as the carbohydrate component (control) or the same diet supplemented with MIG at 150 mg/kg of diet admixture *ad libitum* for <8 weeks. MIG treatment resulted in a ~15% decrease in energy intake ($p<0.05$), net weight gain ($p<0.05$), and a 14% decrease in adiposity ($p<0.05$), along with significant decreases in fasting glucose, insulin, and glycated hemoglobin ($p<0.05$). In addition, MIG reduced the glucose area under the curve by 20% ($p<0.05$), triglycerides by 15% ($p<0.05$), and the total cholesterol, α-lipoprotein (low-density lipoprotein), and β-lipoprotein (high-density lipoprotein) fractions by 20% ($p<0.05$, all comparisons). MIG regimen also led to decreases in liver glucokinase, malic enzyme, and glucose-6-phosphate dehydrogenase ($p<0.05$). In conclusion, these results suggest that therapeutic α-glucosidase inhibition through MIG improves multiple insulin-related atherogenic parameters and may serve as a useful adjunct in the long-term clinical management of plasma lipid and glycemic profiles in the glucose-intolerant states of obesity and T2DM.

Keywords: Obesity; Type 2 diabetes mellitus; Miglitol; α-glucosidase activity; Glycemic parameters; Lipid profiles; Liver enzymes; Spontaneously hypertensive and diabetes-prone/Ntul//-*cp* rat

***Corresponding author:**
Orien L. Tulp
(o.tulp@usat.edu)

Citation: Tul OL, Rizvi SAA. Luminal α-glucosidase inhibition improves insulin sensitivity and modulates glycemic and lipid profiles in obese rats with type 2 diabetes mellitus. *Global Transl Med*. 2025;4(2):58-70. doi: 10.36922/gtm.6501

Received: November 22, 2024

1st revised: August 1, 2024

2nd revised: February 5, 2025

Accepted: February 21, 2025

Published online: March 26, 2025

1. Introduction

Recent reports indicate that the prevalence of obesity and type 2 diabetes mellitus (T2DM) now affects up to one-sixth of the population in some Westernized countries.

The common pathophysiological sequelae of obesity and T2DM are approaching epidemic proportions, with no clear preventative or therapeutic solutions on the horizon.[1-4] As recently as 2021, the Centers for Disease Control and Prevention estimated that over 38 million adults in the United States of America had diabetes, representing more than 14% of the population, with over 90% of these cases being a mix of diagnosed and undiagnosed T2DM – the most common form of diabetes worldwide, affecting over 800 million individuals.[4,5] Dietary, medication, and lifestyle changes remain the hallmark of conventional therapeutic approaches to treat the diabetes element of obesity, aimed at improving glycemic markers. Unfortunately, present approaches to reducing the burden of obesity and T2DM, although well-intentioned, are often less than fully successful. The common clinical sequelae of obesity and T2DM, arising from long-standing dietary and lifestyle factors, may have been largely asymptomatic before diagnosis, making them not immediately reversible. Long-held dietary and lifestyle habits can be difficult to change, and even when modifications are made, the pathophysiologic progression of typical sequelae may be firmly established, with incomplete reversibility occurring over the weeks or months following the initiation of therapeutic measures. While glycemic improvement may begin shortly after the implementation of dietary or luminal therapeutic interventions, restoration of plasma lipid profiles typically takes longer and resolves more gradually, requiring long-term interventions to normalize. In addition, once systemic inflammation and advanced states of atheroma and vascular plaque have developed, full recovery, including atheromatous reversal, may be difficult to achieve.[5,6]

Chronic elevations in plasma lipid profiles are common observations in obesity and T2DM, contributing to the progression of cardiovascular disorders often associated with these conditions.[1-4] In addition, chronic hyperinsulinemia contributes to systemic inflammation in the central nervous system and other tissues, adding to the pathophysiologic burden of the disorder.[4-6] Thus, implementing therapeutic measures to reduce inflammation and decrease elevated triglycerides, total cholesterol, and low-density lipoprotein cholesterol (LDL-C) is considered essential and desirable for long-term treatment goals, often requiring prolonged intervention to achieve satisfactory progress.[2]

The industrialization of the food supply chain has introduced dietary changes in industrialized populations, including a greater abundance of commercially processed foods. While many processed foods retain nutritional qualities, they often contain excess salts and preservatives not typically found in fresher, whole foods. Although the convenience of table-ready, manufactured foods may seem advantageous to modern families, over the long term, they may be less healthful than the traditional, wholesome "home-cooked" meals of past generations.[1,7] The influx of high-fructose corn syrup (HFCS) sweeteners, for example, has resulted in a four- to five-fold increase in fructose intake, now approaching the generally accepted safe levels of 80 – 100 mg/day. This intake comprises up to 20% or more of daily caloric intake for many individuals consuming processed foods and beverages.[8] The excess consumption of HFCS-containing foods and beverages may further disrupt optimal metabolic pathways in glycolysis and substrate oxidation.[8] Healthful dietary changes are often challenging to implement in a population accustomed to the convenience and prevalence of industrialized food choices, where the inclusion of lipids and sweeteners, along with the ease of meal preparation, adds to their palatability, popularity, and convenience.[3-8] In addition, the modernization of the food supply's macronutrient and micronutrient composition may not be adequate to address chronic insulin resistance and associated systemic inflammation common in obese and T2DM states.[7] Moreover, once diagnosed, diabetes treatment is typically long-term and may continue for the remainder of a patient's life.[6-8]

The magnitude and duration of the insulin response to a meal are generally proportional to the type, quality, and quantity of the carbohydrates consumed. The compound 1,5 dideoxy-1,5-[(2-hydroxyethyl) imino]-D glucitol (generic name: Miglitol [MIG]; marketed as Glyset®) is an established competitive inhibitor of luminal starch digestion, acting within the brush border α-glucosidase receptor domains of the small intestine.[9-13] Once the compound competitively binds to the glucosidase receptor domains, it effectively delays the rate-limiting process of starch digestion into absorbable monosaccharide units, thereby reducing subsequent luminal glucose uptake from the gastrointestinal tract.[9] Unlike some other α-glucosidase inhibitors, MIG is fully or nearly fully absorbed in the small intestine but escapes hepatic P-450 metabolism and conjugation, being cleared by the kidneys without further metabolism within a few hours of ingestion.[9] As the typical intestinal starch digestive process occurs rapidly, the generation of monosaccharide units is the rate-limiting step in glucose uptake. Post-ingestive glycemic excursions are proportional to the rate of dietary post-ingestive α-glucosidase activity. Dietary sources of fructose may result from the luminal digestion of sucrose into its constituent glucose and fructose monosaccharide units or from free fructose contained in foods and beverages. However, fructose uptake occurs more slowly than glucose,

as it is transported through specialized monosaccharide transporters (glucose transporter [GLUT] 1, GLUT2, and GLUT5) located along the basolateral epithelial membrane of the brush border in the gut and liver.[10] Unlike glucose, fructose uptake occurs through insulin-independent GLUT transporters. In addition, fructose uptake is a saturable, rate-limiting process with a more restrictive Michaelis-Menten constant for uptake than glucose, thereby delaying and prolonging immediate glycemic and insulinogenic responses beyond those typically encountered after a calorically equivalent non-fructose carbohydrate meal. Numerous physicochemical factors, including diet composition, can also influence interactions with brush border enzymes, affecting the efficiency of digestive activities. Specifically, dietary fibers, gums, pectin, and plant-derived phytochemicals can protect against glycemic excursions by impeding direct access to brush border enzymatic actions. These food constituents can effectively decrease the rate and efficiency of luminal brush border digestion, leading to a corresponding attenuation of glycemic and secondary insulinogenic responses – a well-established benefit of dietary fiber content.[7] The addition of natural and pharmacologic inhibitors of α-glucosidase activity can further attenuate insulinogenic and glycemic responses without compromising the net digestion or absorption of monosaccharides, nutrients, or micronutrients more distally in the gastrointestinal tract.[9-12]

Characteristic of luminal carbohydrate digestive enzymes, α-glucosidase activity is greatest in the proximal regions of the upper intestinal tract and decreases progressively as the digestive contents move distally.[9] As the rates of luminal carbohydrate digestion decrease, the generation of absorbable monosaccharide units also occurs more slowly, resulting in less pronounced fluctuations in plasma glucose and insulin concentrations following carbohydrate ingestion and digestion. As glycemic excursions are attenuated, plasma insulin requirements may plateau, typically at a lower level, as less insulin is needed to facilitate immediate peripheral monosaccharide uptake, oxidation, and disposal.[9,10] The extended nature of the fructose-induced insulinogenic response may trigger a shift in insulin-stimulated secondary actions, including lipogenesis, glycogenesis, and modulation of plasma insulin concentrations during the late post-prandial period. Thus, the insulin-lowering effect of α-glucosidase activity, whether as a monotherapy or combined therapy, may be enhanced in the presence of inhibitors of luminal starch digestion.[9,11-15] In addition, because the physiological half-life of insulin receptor activity typically extends considerably longer than that of starch digestion and subsequent monosaccharide uptake and oxidation, downstream improvements in biochemical pathways related to intermediary metabolism and lipogenesis are likely to follow.[13-15] Thus, dietary supplements or additives that extend the process of luminal digestion of starches and absorption of simple carbohydrates, thereby delaying the rate of glucose uptake, present an interesting prospect for modulating downstream physiological events, including their effects on appetite, satiety factors, plasma insulin activation, and the metabolic effects of insulin on lipogenesis and cholesterol production.[9-11] The improvements in glycemic responses would likely elicit favorable changes in other hormonal activities commonly associated with glycemic responses, including thyroidal, sympathetic, and possibly glucocorticoid interactions.

The insulinogenic actions exert numerous downstream effects on key parameters of intermediary metabolism in peripheral tissues, including modulation of glucose oxidation, protein synthesis and degradation (protein turnover), carbohydrate oxidation and storage, and lipogenesis, all of which are pertinent to this study.[16-18] Glucose readily enters glycolysis in peripheral tissues, providing substrates for glycogen deposition, as well as reducing equivalents for mitochondrial high-energy phosphate generation. In contrast, fructose, once absorbed by liver or intestinal tissues, is converted to fructose-1-phosphate and adenosine diphosphate, which then splits into two trioses (dihydroxyacetone phosphate and glyceraldehyde), both of which can serve as preferential substrates for *de novo* insulin-stimulated lipogenesis.[17] In addition, adenosine diphosphate undergoes further degradation to adenosine monophosphate and inosine monophosphate, and may eventually degrade to uric acid. Uric acid is less soluble in plasma than inosine monophosphate, has limited capacity for competitive renal secretion, and may form painful gouty lesions due to inflammatory uric acid crystallization in tissues over time when plasma concentrations exceed solubility levels.[17] The purpose of the present investigation was to determine the effects of partial luminal α-glucosidase inhibition through the inclusion of MIG as a controlled dietary admixture on plasma glycemic and lipid profiles. These studies were conducted using an animal model where early-onset obesity, hyperinsulinemia, insulin resistance, and T2DM develop in the obese phenotype due to the autosomal recessive inheritance of the *-cp* trait, with an age of onset during early adolescence.[16,18-20] Due to this genetic predisposition, T2DM develops reproducibly in the obese offspring of both genders, independent of high-fat diets or other dietary extremes. Furthermore, once expressed, the pathophysiologic stigmata of obesity and T2DM persist.[16-19] As noted, the epigenetic expression of obesity and the subsequent progression to T2DM occur

through the expression of an autosomal recessive trait, and are soon accompanied by the commonly observed progression of chronic pathophysiologic sequelae, including abnormalities in plasma cholesterol levels and lipid profiles. Preliminary observations suggest that the development of hyperglycemia and hyperinsulinemia in T2DM is less severe in females than in males. F1 hybrids with the non-diabetic LA/Ntul//-*cp* strain exhibit what appears to be a genetic dilution of obesity-linked T2DM, although the obese phenotype remains. Thus, the T2DM in this strain occurs reproducibly with normal, otherwise healthful diets, in contrast to high-fat diets or other dietary extremes used to induce diabetic symptoms, as has been employed in other strains of obese rodents, resembling the inheritance patterns of obesity and T2DM in humans.[17-26]

The congenic spontaneously hypertensive and diabetes-prone (SHR)/Ntul//-*cp* rat model was developed in the small animal genetics unit by Hansen at the National Institutes of Health (NIH) by incorporating the -*cp* trait from the Koletsky rat into a longevity-prone NIH (N) strain of unknown origin.[20] This step was followed by crossing the N-*cp* (NIH) strain with the SHR rat, with 12 or more cycles of backcrossing. This level of backcrossing was deemed sufficient to establish a congenic status, ensuring that 99.9% or more of the original genome remained authentic while preserving the SHR and -*cp* traits. In this model, all offspring are deemed genetically identical, and 25% of the offspring of breeding pairs heterogenous for the -*cp* trait will inherit the trait. The hypertensive trait is preserved only in the lean phenotype, while T2DM develops soon after weaning as a recessive trait in the obese phenotype. The newly developed SHR/N-*cp* strain also retains the albino coat characteristic of the donor SHR strain, but not the agouti coat of the LA/N-cp strain. In contrast, the F1 hybrids retain elements of both coat characteristics. Both phenotypes exhibit significantly reduced lifespans due to complications of T2DM compared to their longevity-prone NIH (N) heritage.[18] The independent contributions of the obesity and T2DM traits may be further assessed in the non-diabetic LA/Ntul-*cp* and SHR/Ntul//-*cp* strains, where T2DM has not been observed in the LA/Ntul//-*cp* strain to date, regardless of the diets offered.[17-20] Thus, the purpose of this investigation is to determine the efficacy of therapeutic luminal inhibition of α-glucosidase activity through MIG on established insulin-linked parameters of metabolism, including glycemic and lipid profiles, in a unique congenic animal model of early-onset obesity and T2DM, in the absence of other confounding variables. In this animal model, the onset of comorbidities associated with obesity and T2DM occurs soon after weaning in the obese phenotype of the strain. These conditions develop spontaneously due to an unknown mechanism, presumed to be linked to a genetic predisposition, independent of dietary or environmental factors.

2. Materials and methods

Two groups of congenic obese male SHR/Ntul//-*cp* rats (*n*=8 rats/group) were housed under standard laboratory conditions, including a temperature of 21 – 22°C, 50% relative humidity, and a reverse light cycle (darkness from 0800 to 2000 daily) in adjacent hanging steel cages with individual occupancy. The animals were fed Purina Chow and provided with house water *ad libitum* from weaning to 8 weeks of age, at which point early stages of obesity and T2DM were clearly established, with glycosuria and T2DM confirmed. It is noteworthy that, in this animal model, the onset of obesity and T2DM occurs spontaneously soon after weaning due to a genetic predisposition, likely resulting from a Tyr763Stop mutation in the extracellular domain of the leptin receptor, and is independent of specific dietary or environmental interactions.[26] Thus, the specific metabolic pathways involved in the progression to the metabolic sequelae of obesity and T2DM are currently unclear, beyond their genomic origin. All rats demonstrated glycosuria, confirmed by test strips, by 8 weeks of age, which persisted thereafter (Urine Glucose Test Strips, OneStep). At 8 weeks of age, the rats were switched to a semi-purified control diet developed by the Carbohydrate Nutrition Laboratories of the United States Department of Agriculture.[20] This diet contained 54% carbohydrate as sucrose, 20% protein (equal parts casein and lactalbumin), 5.9 % cellulose, 16% fat (equal parts beef tallow, lard, corn oil, and hydrogenated coconut oil), along with 3.1% the American Institute of Nutrition vitamin salt mix, and 1% Teklad vitamin fortification mix (control diet). The energy content of the diet was calculated to provide 48.2% of calories from carbohydrates, 33.3% from fats, and 18.5% from protein, yielding 4.4 kcal/gram as described elsewhere.[20-27] The semi-purified diet was fed *ad libitum* for up to 8 weeks. In addition, the control diet was fortified with 150 mg of the α-glucosidase inhibitor (MIG) per kg of diet (equivalent to ~2.5 mg MIG/rat/day) and was fed to the α-glucosidase inhibitor treatment group for up to 8 weeks. Thus, both treatment groups consumed diets with the same proportions of essential nutrients and caloric density, with or without MIG. Body weights were monitored periodically throughout the study as an indicator of wellness. At the end of the study, rats were fasted overnight, and blood was obtained through tail bleeding into heparinized tubes for plasma glucose and insulin area under the glucose tolerance curve (AUC) through a glucose oxidase method (250 mg/kg body weight, through gavage) on a YSI glucose analyzer and in-house radioimmunoassay, respectively.[28,29] Insulin

resistance, computed as homeostatic model assessment (HOMA), was determined as described by Wallace *et al.*[30] Glycated hemoglobin (hemoglobin A1C [HbA1c], gamma-hydroxybutyric acid) and lipid analysis were also performed. Plasma triglycerides, cholesterol, and the α-lipoprotein (LDL and β-lipoprotein high-density lipoprotein [HDL]) fractions were determined spectrophotometrically (Beckman AU480, United States of America) following affinity chromatographic separation, according to the procedure of Bentzen *et al.*, and triglycerides were measured by the enzymatic method of Bucolo and David, with all reagents acquired from Fischer Scientific (United States of America) and prepared on-site.[31,32] Measures of glycolytic enzyme activity, including glucokinase, malic enzyme, and glucose-6-phosphate dehydrogenase, were determined spectrophotometrically and expressed as micro moles of product produced per minute per mg of protein per liver in a sucrose-ethylenediaminetetraacetic acid-phosphate buffered liver homogenate, as described by Freeland.[33] Tissue protein content was determined as described by Lowry *et al.*[34,35] Data were analyzed using standard statistical procedures, including the application of Page's L test for trend analysis with corrections for covariates, where statistical significance through the *t*-test was suggestive but not confirmatory.[36,37] The study was approved by the Institutional Animal Care and Use Committee, University of Science Arts and Technology (approval number: 2016/009).

3. Results

Initial and final body weights, net weight gain, and dietary energy intake of rats over the 8-week observation period are depicted in Figures 1-6. Daily energy intake is depicted in Figure 1, which shows that control animals consumed more energy per day from week 1 to week 8. The cumulative energy intake over the 8 weeks is presented in Figure 2, confirming that the net energy intake during the observation period was greater in the control compared to the MIG group. Specifically, these data indicate that the net energy intake of control rats was approximately 13% greater overall than that of the MIG-fed rats over the 8-week period (Figure 2, left grouped bars). Additionally, there was a modest improvement in feed efficiency for the MIG regimen (Figure 2, right grouped bars). The effects

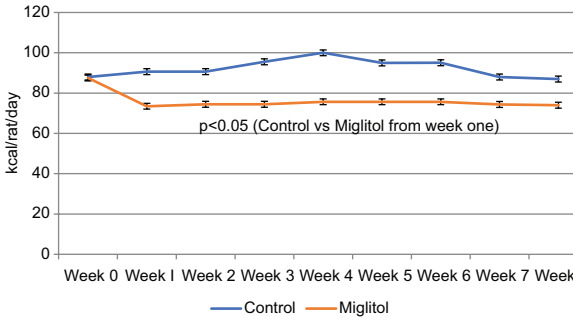

Figure 1. Effect of miglitol on weekly food intake in obese type 2 diabetes mellitus rats. Data are presented as mean ± 1 standard error of the mean (n=6–8 rats/group). p<0.05 for control versus miglitol from week 1 to week 8. (Students *t*-test, individual comparisons: Control vs. miglitol).

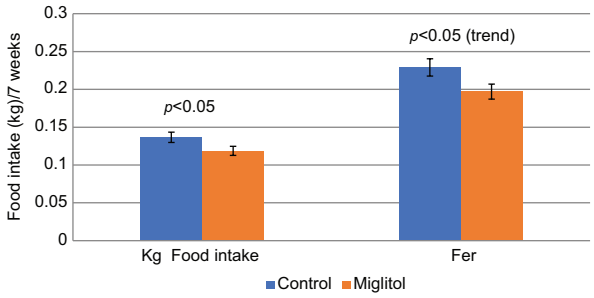

Figure 2. Effect of α-glucosidase inhibitor miglitol on net energy intake and feed efficiency ratio. Data are expressed as mean ± 1 standard error of the mean (n=8 rats/group). p<0.05 through Student's *t*-test; p<0.05 (trend) through Page's L test for trend analysis.
Abbreviation: Fer: Feed efficiency ratio.

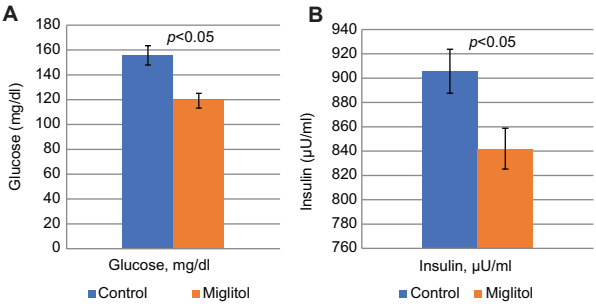

Figure 3. Effect of miglitol on fasting glucose (A) and insulin (B) at the end of the study. Data are presented as mean ± 1 standard error of the mean (n=6 rats/group). p<0.05 (Student's *t*-test). This resulted in a modest 5% decrease in the mean homeostatic model assessment score from 2.6 ± 0.1 (control) to 2.4 ± 0.1 (miglitol) (p > 0.05).

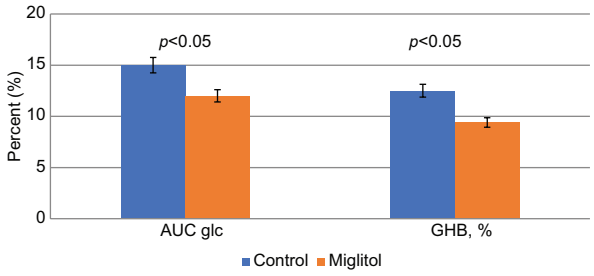

Figure 4. Effect of miglitol on glycemic parameters at 15 weeks of age. Data are expressed as mean ± 1 standard error of the mean (n=6 – 8 rats/group). p<0.05 as determined by Student's *t*-test.
Abbreviations: AUC glc: Area under the glucose tolerance curve; GHB: Glycated hemoglobin.

of MIG on fasting glucose and insulin levels at 15 weeks of age are shown in Figure 3A and B, respectively. These results indicate that MIG treatment was associated with lower fasting glucose and insulin concentrations by the end of the study. The AUC for glucose during a 120-minute oral glucose tolerance test after 7 weeks of treatment is depicted in Figure 4. The AUC for MIG-treated rats was approximately 20% lower than that of control rats, consistent with the energy intake data from the same timeframe. The HOMA score showed only a modest decrease, indicating that while insulin resistance was slightly improved, it remained present after the drug treatment (values are provided in the legend of Figure 3A and B). The improvement in glycated hemoglobin percentage (right grouped bars, Figure 4), while still above the normal range, reflects a 24% reduction following <8 weeks of MIG treatment. This result is highly significant and suggests that MIG is effective in lowering fasting insulin concentrations and controlling post-prandial glycemic responses to feeding. In addition, as rodents are generally considered grazers rather than meal eaters, the observed reduction in the AUC for glucose is even more noteworthy given the short duration of the study. It is likely that a longer duration of MIG treatment could lead to further improvements in HbA1c levels. This is an important consideration, as glycated hemoglobin shifts the oxygen saturation curve of hemoglobin to the left, thereby impairing oxygen release from the glycated molecules. This, in turn, decreases the net efficiency of oxygen delivery to myoglobin, where it would typically contribute to oxidative metabolism. The effects of MIG on liver glycolytic enzyme activity are shown in Figure 5. These data indicate that glucokinase and malic enzyme activity were lower in rats fed the MIG regimen, while the levels of glucose-6-phosphate in MIG-fed rats showed only a significant trend, consistent with improvements in insulin-related elements of glycolytic and lipogenic activity.

The body weights and weight gain are depicted in Figure 6. The initial weights were similar between the treatment groups (left grouped bars: 263 ± 11 g vs. 263 ± 12 g). In addition, the final body weights of the control rats were modestly (~6%) greater than those of the MIG-fed rats, with a final mean weight gain that was 12% lower than that of the control group. Notably, the weight gain per gram of protein consumed was similar in both groups (mean weight gain/gram protein consumed = 8.65 ± 0.18 g/g in the control group vs. 8.74 ± 0.21 g/g in the MIG-fed rats), suggesting, though not conclusively, an improved energy utilization in the MIG group ($p > 0.05$). Thus, the α-glucosidase inhibitor MIG resulted in modestly (~12 – 13%) lower rates of weight gain and similarly lower final body weights over the 8 weeks of observation (control vs. MIG final body weight: $p<0.05$ through trend analysis;

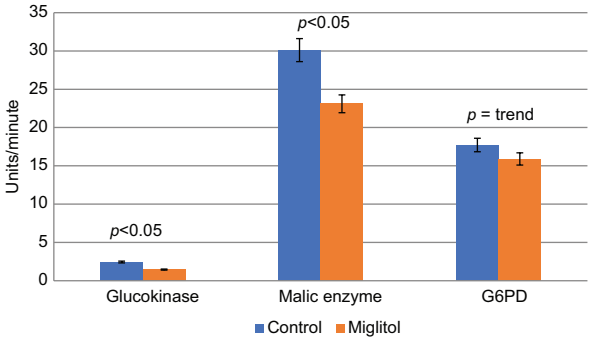

Figure 5. Effects of miglitol on glycolytic enzyme parameters at 15 weeks of age. Data are presented as mean ± 1 standard error of the mean (n=6 rats/group), recorded in units where 1 unit=z1 μmol/minute/mg protein of liver homogenate. $p<0.05$ through Student's t-test; trend = Page's L test for trend analysis.
Abbreviation: G6PD: Glucose-6-phosphate dehydrogenase.

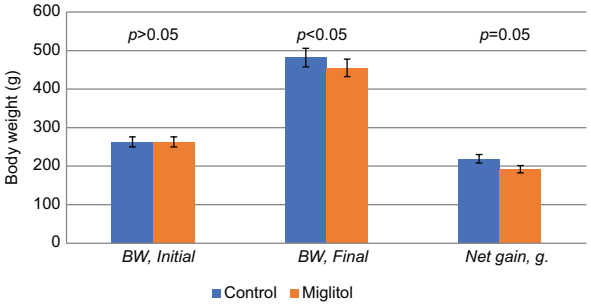

Figure 6. The body weights (BW) of rats. Data are expressed as mean ± 1 standard error of the mean (n=8 rats/group). $p<0.05$ as indicated by Student's t-test. Thus, the mean weight gain per gram of protein consumed was proportionate to protein intake: 8.6561 g gain/g protein consumed in the MIG group versus 8.7532 g gain/g protein consumed in the control group.

control vs. net gain: $p<0.05$ through trend analysis). The energy intake of rats is depicted in Figure 6, showing that the energy intake of control rats over the entire course of the study was 13% greater than that of the MIG-treated animals ($p<0.05$, Student's t-test). Consequently, the net efficiency of weight gain over the study period was similar between the two groups and generally proportional to nutrient intake.

The effects of MIG on adipose tissue depots are displayed in Figure 7, where MIG treatment (bars on the right of each group) was associated with a 15% decrease in the sum of the epididymal, retroperitoneal, and dorsal adipose tissue depots. However, not all individual adipose tissue depots in the control group, as shown in the left bars, exhibited proportional decreases. The most significant reduction in depot mass was observed in the retroperitoneal depot, while the epididymal and dorsal depots displayed only modest decreases in both groups. The dorsal depot and the

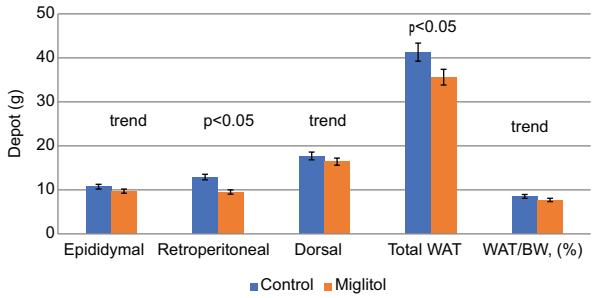

Figure 7. Effect of miglitol on adipose tissue mass at 15 weeks of age. Data are presented as mean ± 1 standard error of the mean (n=6 – 8 rats/group). p<0.05 for retroperitoneal and total white adipose tissue depots. Epididymal, dorsal, and percent white adipose tissue (WAT)/body weight (BW) showed a trend (p<0.05) as determined by Page's L test for trend analysis.

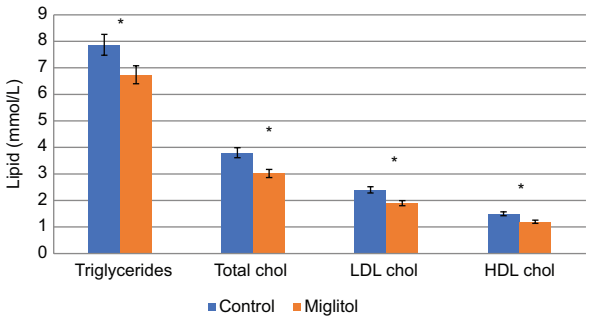

Figure 8. Effect of miglitol on lipid parameters at 15 weeks of age. Data are expressed as mean ± 1 standard error of the mean (n=6 – 8 rats/group). *p<0.05, determined by Student's t-test.
Abbreviations: CHOL: Cholesterol; HLD: High-density lipoproteins; LDL: Low-density lipoprotein.

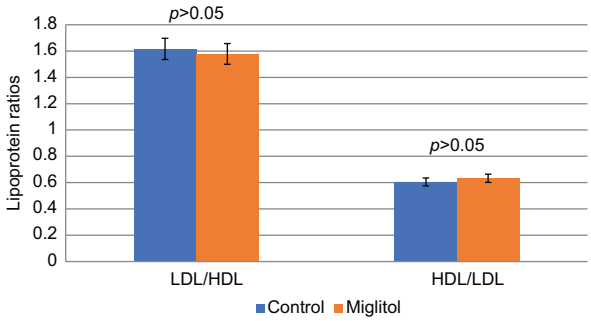

Figure 9. Effect of miglitol on lipoprotein fraction ratios at 15 weeks of age. Data are presented as mean ± 1 standard error of the mean (n=6 – 8 rats/group). p > 0.05 for all comparisons, determined by Student's t-test.
Abbreviations: HLD: High-density lipoproteins; LDL: Low-density lipoprotein.

white adipose tissue (WAT): Body weight ratio showed only a downward trend following MIG treatment, suggesting depot-specific effects (visceral vs. non-visceral depots) on lipid accretion. When the sum of the WAT depots was expressed as a percentage of body weight, the net decrease in WAT mass in the MIG-treated rats (represented by the bars on the right side of grouped bars in Figure 8) averaged 10% of final body weight and 18.5% of weight gain. Thus, the cumulative reduction in total combined WAT mass was similar in magnitude to the decreases observed in net energy intake and weight gain.

The effects of luminal α-glucoside inhibition on plasma triglycerides and total cholesterol concentrations are depicted in Figure 8. α-glucosidase inhibition resulted in approximately a 20% decrease in total plasma concentrations of triglycerides, cholesterol, and lipoprotein cholesterol fractions after <8 weeks of dietary and pharmacologic treatment. In addition, the final concentrations of both LDL and the HDL fractions were reduced by an average of ~18 – 20% following α-glucosidase inhibition, with the effects nearly evenly distributed across both LDL and HDL fractions. Furthermore, the LDL/HDL and HDL/LDL lipoprotein ratios displayed in Figure 9 indicate that, while the pharmacologic treatment with MIG to inhibit luminal α-glucosidase activity improved all lipid fractions, it had no significant effect on lipoprotein ratios. This suggests that the effects of the α-glucosidase inhibitor agent were uniformly distributed across all triglyceride and lipoprotein fractions, consistent with a global improvement in insulin action on lipid and cholesterol biosynthesis and metabolism.

4. Discussion

In the present study, feeding an admixture of MIG in a high-carbohydrate, nutritionally complete diet to obese T2DM rats for up to 8 weeks resulted in decreases in energy intake, weight gain, adiposity, key glycemic parameters, and improvements in plasma lipid profiles, despite only modest decreases in insulin resistance.[30] The reductions in weight gain and depot-specific adiposity associated with α-glucosidase inhibition were generally proportional to the decrease in total energy intake over the duration of the study duration and suggested favorable contributions from gastrointestinal satiety factors due to the delayed digestion of the dietary carbohydrate. Luminal digestion of sucrose occurs rapidly in the brush border projections, primarily located in the proximal regions of the duodenum, where the greatest activity of the glucosidase enzymes is found Glucosidase activity gradually decreases as the food moves distally along the small intestine.[9,10] Any residual carbohydrate that may remain undigested in the small intestine can likely become energy substrates for the colonic microbiota; however, under normal digestive conditions, little carbohydrate typically escapes digestion. Regardless of where the carbohydrate digestion occurs in the small intestine, the luminal uptake of monosaccharide moieties is straightforward, accounting for the magnitude and duration of the increase in plasma glucose following a

carbohydrate meal. As sucrose was the only carbohydrate in the research diet, luminal glucosidases would normally digest sucrose completely within the first 30 to 45 min post-prandially, depending on meal size, with subsequent luminal absorption of fructose. Thus, any delay in luminal carbohydrate digestion is expected to decrease the magnitude and intensity of glycemic excursions, including plasma glucose and insulin levels, following a carbohydrate-containing meal. The significant reduction in the AUC for glucose, along with the modest improvement in HOMA, provides further evidence of MIG's efficacy in modulating carbohydrate digestion in the upper regions of the small intestine, soon after gastric emptying. This likely occurs secondary to decreases in plasma insulin concentrations. Further support for improvements in insulin sensitivity is provided by the decreases in glucokinase, an enzyme that functions as the β-cell sensor for insulin release in response to rising plasma glucose levels, and in malic enzyme and glucose-6- phosphate dehydrogenase, which contributes to lipogenesis by catalyzing NADPH generation. The availability of NIDPH is essential for *de novo* fatty acid biosynthesis in the liver and adipose tissue.[17,33-38] Furthermore, improved insulin sensitivity may help reduce oxidative stress and enhance protein utilization efficiency.[17,22-38]

Given that T2DM, in association with obesity, overweight conditions, and metabolic syndrome, are emerging as one of the most prevalent metabolic disorders globally, it is imperative that a productive, cost-effective therapeutic strategy be developed and implemented to effectively address these conditions.[1-7] At present, more than a third of the population in Western societies is affected by overweight or obesity, with a high prevalence of T2DM among those with metabolic syndrome.[4] Treatment of T2DM and obesity is often lifelong, imposing a significant burden on healthcare resources due to the large number of patients with comorbidities associated with the disorder and the extended duration of their treatment. Discontinuation of an effective treatment strategy typically leads to relapse within weeks to months, often accompanied by the return of previous comorbidities.[1-6]

The prevalence of obesity and T2DM has placed an enormous economic burden on healthcare systems in many communities.[1-4] These disorder also contributes to economic losses in workplace productivity, as individuals may struggle to meet their workplace obligations in a timely or effective manner due to illnesses linked to obesity and T2DM.[1-3] The industrialization of food processing and distribution has enhanced food safety, but it has also led to changes in dietary preferences and nutritional practices, differing from those of past generations.[6,7] These changes, along with greater food availability, have inadvertently made it more challenging for individuals to maintain energy balance in a more sedentary society. In addition, modernized biological energy- and labor-saving innovations in daily life—common in Western nations—may also be significant contributors. Today's home and workplace efficiency standards allow more time for leisure and relaxation, reducing the physical exertion experienced by past generations. Given these factors, it is important to explore novel approaches to address the emerging trends in disordered energy balance and their contributions to pathophysiological sequelae, which may, at least in part, result from technological advancements. While no single strategy has yet been proven effective in addressing the obesity and T2DM dilemma, several relevant animal models have been developed, including the SHR/Ntul//-*cp* rat, the LA/Ntul//-*cp* rat, the Wistar Fatty Rat, the Zucker fatty rat, and others.[18,21-25] These models provide insights into effective environmental and pharmacological strategies and help further elucidate the pathophysiological mechanisms involved in the epigenetic expression of traits that contribute to obesity and T2DM.

The consumption of high carbohydrate, calorically dense, and high-glycemic-index diets, which are common in Western societies, is often contraindicated in obesity and T2DM as these diets are often associated with unwelcome elevations in weight gain, adiposity, fasting plasma lipid levels, and other stigmata of obesity and T2DM.[1-3,8] Present therapeutic strategies often include lifestyle changes, such as adopting a healthier diet, which typically emphasizes complex carbohydrates, modest fat intake, and adequate fiber and micronutrient consumption, combined with increased physical activity. The cumulative dietary and lifestyle changes are intended to lead to a lower-calorie, lower-glycemic index diet, which better matches an individual's energy requirements and helps maintain a neutral energy balance. Incorporating starch-blocking agents such as acarbose, MIG, or other natural inhibitors of starch digestion may complement a lower-glycemic-index, high-fiber diet.[1-3] These agents may help produce lasting weight loss with corresponding improvements in the common pathophysiological stigmata of obesity and T2DM, potentially contributing to improvements in the individual's metabolic profile. Luminal modulation of carbohydrate digestion and monosaccharide absorption through α-glucosidase inhibitors, combined with naturally occurring food components (often from vegetarian sources), may also have similar effects on α-glucosidase activity.[9] Considering that the primary mechanism of action of most α-glucosidase and sucrase inhibitors is competitive inhibition, typically limited to the luminal brush border region with little to no post-

ingestive absorption or systemic distribution, the risk of hepatic or other organ toxicity is minimal. MIG, the focus of this study, is a complex oligosaccharide that acts as a competitive, reversible inhibitor of membrane-bound intestinal α-glucoside hydrolase activity.[9,25-29] Luminal modulators of starch digestion, including acarbose and MIG, have been found to be useful agents in treating mild to moderate T2DM.[9,21-25] In a previous animal study lasting less than 8 weeks with the MIG analog acarbose, HbA1c, and glycemic responses demonstrated improvement toward normalization over time.[9] The results of this study are also consistent with previous clinical findings in the Wistar Fatty Rat and further confirm that an 8-week trial of feeding a highly palatable, high carbohydrate, sucrose-laden diet to obese adult Wistar Fatty Rats with well-established T2DM is sufficient to induce improvements in glycemic parameters, including reductions in excess adiposity and weight gain. The metabolic similarity in the development of insulin resistance between the obese phenotypes of the Wistar fatty rat, SHR/Ntul//-*cp* rats, and other similar models contributes to the development of the obese and T2DM phenotype in these animal models. All these models demonstrated significant improvements in glycemic parameters when treated with the glucosidase inhibitor regimen, including a reduction in chronic hyperphagia commonly associated with the obese phenotype.[9,10,38] As reported by Boque *et al.*,[41] when lean male Wistar rats were fed a similar high-carbohydrate diet, an increase in fasting triglyceride concentrations was observed. In the present study, the MIG treatment was associated with improvements in glycemic parameters, plasma triglycerides, total cholesterol, LDL-cholesterol, and HDL cholesterol fractions, as well as a reduction in sucrose-linked weight gain, a decrease in the glucose AUC, and a reduction in HbA1c levels.

Because only animals of the obese-T2DM phenotype were included in this study, it was not possible to determine whether the final weight and metabolic profiles would have been similar to those of their lean littermates if they had been fed similar diets over the 8-week duration of the observations. However, as the obese rats were already significantly heavier than their lean littermates at the beginning of the study (average lean = 235 ± 6 g vs. obese = 264 ± 19 g at 8 weeks of age; $p<0.05$), and the T2DM characteristics were well-established, it is likely that longer treatment would have been necessary for full resolution. This is especially relevant as hyperinsulinemia and atheroma development typically begins soon after weaning in this and other similar strains.[8-26,38,39] In the present study, the decreases in net energy intake and weight gain averaged 15% following the MIG feeding regimen, indicating a favorable correlation between the dietary impact and metabolic sequelae, with no apparent rebound effects, metabolic complications, or adverse side effects. Indeed, during necropsy, no pathophysiological aberrations were observed in the MIG-treated animals. An earlier study also observed a similar pattern of decreased food intake when the glucosidase inhibitor acarbose was fed as an admixture to lean and obese non-diabetic rats, resulting in comparable improvements in glycemic responses, adiposity, and plasma lipid parameters.[40] The evidence from the present study suggests that the dietary regimen linked improvements in glucose AUC, HbA1c, lipid profiles, and weight gain, consistent with improvements in insulin action in peripheral tissues, including skeletal muscle and adipose tissue, which are major sources of peripheral insulin resistance in obesity and T2DM.[41,42]

Although not studied in the present investigation, the contributions of inflammatory cytokines, including tumor necrosis factor-alpha, interleukin-6, C-reactive protein, and nuclear factor kappa B, were not determined. Numerous studies in rodents and cell cultures have linked elevated plasma lipids and fatty acids to the generation of inflammatory markers, which are associated with endothelial dysfunction, a common issue in T2DM and its comorbidities.[43-47] While the molecular mechanisms of these cytokines remain unclear, insulin resistance is commonly observed when levels of monocyte-derived inflammatory cytokines are elevated, contributing to the risk for T2DM. Given that T2DM is one of the most common metabolic disorders worldwide, cost-effective agents such as MIG could decrease plasma lipid levels, improve glycemic status, and reduce the trend toward greater adiposity. These pharmacological benefits could make MIG a valuable treatment, similar to the well-established anti-inflammatory and cholesterol-lowering effects of statins on cardiovascular diseases, which are now widely prescribed with minimal side effects.[48] Future studies of α-glucosidase inhibitors could determine whether such a regimen could prevent or delay the onset of T2DM and its sequelae in both humans and animals, as prevention is generally preferred over long-term management.

In summary, improvements in plasma lipid and glycemic profiles in the obese and T2DM phenotype of this and other strains following luminal glucosidase inhibition have been clearly established despite only modest improvements in insulin resistance as assessed by HOMA analysis. Without treatment, increases in biochemical markers for free radicals are consistent with atherogenic lipid profiles, including elevations in serum triglycerides, cholesterol, and LDL-cholesterol fractions, which are indicative of senescent, atherogenic alterations in the vascular intima.[4-6] Although the glycemic and lipid

parameters improved but did not completely normalize in the obese and T2DM rats following the MIG treatment, it is likely that a longer treatment duration would have resulted in a more complete recovery. Although a conclusive determination of the physiological mechanism for the lipid-lowering effects could not be made in this study, the insulin-linked parameters suggest improved insulin sensitivity and insulinogenic actions in peripheral tissues, including the liver. This conclusion is supported by the partial recovery of HbA1c in MIG-treated rats. Notably, the glycation reaction is considered irreversible and non-enzymatic, correlated with average plasma glucose concentrations. Once the glycation reaction has occurred, it is dependent on the typical 4-month lifespan of the normal erythrocyte. Furthermore, the MIG-treated rats exhibited an approximate 60% recovery in glucose AUC after only 8 weeks of study, and the hepatic glycolytic and lipogenic enzymes studied all showed improvements following MIG treatment. Thus, had the study been extended to several months, the HbA1c levels would likely have decreased closer to those observed in non-diabetic animals, around 7% or less, as laboratory rats tend to eat more frequently than other mammalian species.

The determination of HbA1c levels is considered a reliable marker for monitoring clinical diabetes therapy and was an important aspect of assessing the effectiveness of α-glucosidase inhibition on luminal monosaccharide generation and insulinogenic action in peripheral tissues in the present study. Thus, α-glucosidase inhibitors are deemed a useful clinical approach for attenuating the insulin-dependent, hyperglycemic sequelae of the obese and T2DM phenotype in this strain and support their potential usefulness in treating T2DM in humans.[41,42,49,50] In conclusion, while the effects of MIG and other luminal glucosidase inhibitors on lipid parameters have sometimes been inconclusive, these differences are likely due to variations in experimental models, patient populations, duration of pre-existing illness, dosages, and agents employed, and the duration of the treatment regimens. The improvements noted in the present study are likely attributable to an improved economy of insulin sensitivity, glucose utilization, and lipid metabolism in peripheral tissues.

5. Conclusion

The short-term administration of a modest dosage of the α-glucosidase inhibitor MIG, in the presence of a high glycemic index sucrose-enriched diet, was found to be effective in attenuating excess weight gain and increases in plasma cholesterol, LDL-cholesterol, and HDL-cholesterol concentrations in adult male obese SHR/Ntul//-*cp* rats. These findings are consistent with typical dietary recommendations for the consumption of complex carbohydrate and fiber-rich diets for a variety of glucose-intolerant conditions. Furthermore, they suggest that MIG, when administered as a dietary admixture, may serve as a useful therapeutic adjunct in the treatment of obesity and T2DM, potentially alleviating chronic systemic inflammation and pathophysiologic sequelae associated with the obese-diabetic state. Moreover, the clinical effectiveness of luminal glucosidase inhibitors on lipid parameters may be enhanced by the addition of a cholesterol-lowering agent or other therapeutic adjuncts, as demonstrated in multiple clinical trials. The clinical efficacy of MIG has now been demonstrated in numerous clinical trials, supporting its effectiveness in treating obesity-associated T2DM.[38-42,49,50] While a direct correlation between rodent and human studies cannot be made from the present investigation, the remarkable similarity in carbohydrate metabolism and digestive processes between rodents and humans lends credibility to the notion that the characteristics of T2DM and its pathophysiologic comorbidities combined with the metabolic effects of MIG, are demonstrably similar in both species. Thus, the results of this investigation support the concept of luminal modulation of starch digestion as a pharmacotherapeutic adjunct for the treatment of obesity, T2DM, and insulin resistance conditions.

Acknowledgments

None.

Funding

None.

Conflict of interest

The authors declare that they have no competing interests.

Author contributions

Conceptualization: Orien L. Tulp
Formal analysis: All authors
Investigation: Orien L. Tulp
Methodology: Orien L. Tulp
Writing – original draft: All authors
Writing – review & editing: All authors

Ethics approval and consent to participate

The research ethics committee of the University of Science, Arts, and Technology approved the study. It was also approved by the Institutional Animal Care and Use Committee (Approval Number: 2016/009; 2024).

Consent for publication

Not applicable.

Availability of data

Raw data can be obtained from the corresponding author upon reasonable request.

Further disclosure

An early shortened preliminary version of this paper was released on Preprints and can be found at: doi: 10.20944/preprints202411.1127.v1

References

1. Kelly T, Yang CS, Reynolds K, He J. Global burden of obesity in 2005 and projections to 2030. *Int J Obes (Lond)*. 2008;32(9):1431-1437.

   doi: 10.1038/ijo.2008.102

2. Aggarwal R, Ostrominski JW, Vaduganathan M. Prevalence of cardiovascular-kidney-metabolic syndrome stages in US adults, 2011-2020. *JAMA*. 2024;331:1858-1860.

   doi: 10.1001/jama.2024.6892

3. Njoloma I, Lewis N, Sainvil F, *et al*. A primer on hypertension and the racial/ethnic disparities in diagnosis and management. A comprehensive overview. *Int J Family Clin Med*. 2021;5(6):229-239.

4. Available from: https://www.cdc.gov/diabetes/php/data-research/index.html; https://www.who.int/news-room/fact-sheets/detail/diabetes [Last accessed on 2025 Mar 25].

5. Soták M, Clark M, Suur BE, Börgeson E. Inflammation and resolution in obesity. *Nat Rev Endocrinol.* 2025;21:45-61.

   doi: 10.1038/s41574-024-01047-y

6. Wiley CD, Campisi J. The metabolic roots of senescence: mechanisms and opportunities for intervention. *Nat Metab*. 2021;3(10):1290-1301.

   doi: 10.1038/s42255-021-00483-8

7. Malik A, Erginkaya Z, Erten H, editors. *Health and Safety Aspects of Food Processing Technologies*. Ch. 1-23. Germany: Springer Publications; 2020.

   doi: 10.1007/978-3-030-24903-8

8. Bray GA. Energy and fructose from beverages sweetened with sugar or high-fructose corn syrup pose a health risk for some people. *Adv Nutr*. 2013;4:220-225.

   doi: 10.3945/an.112.002816

9. Assefa ST, Yang EY, Chae SY, *et al.* Alpha glucosidase inhibitory activities of plants with focus on common vegetables. *Plants (Basel)*. 2020;9(1):2-19.

   doi: 10.3390/plants9010002

10. Douard V, Ferraris RP. Regulation of the fructose transporter GLUT5 in health and disease. *Am J Physiol Endocrinol Metab*. 2008;295:E227-E237.

    doi: 10.1152/ajpendo.90245.2008

11. Leonhardt W, Hanefeld M, Fischer S, Schulze J. Efficacy of alpha-glucosidase inhibitors on lipids in NIDDM subjects with moderate hyperlipidemia. *Eur J Clin Invest*. 1994;24 Suppl 3:45-49.

    doi: 10.1111/j.1365-2362.1994.tb02256.x

12. Monami M, Vitale V, Ambrosio ML, *et al*. Effects on lipid profile of dipeptidyl peptidase 4 inhibitors, pioglitazone, acarbose, and sulfonylureas: Meta-analysis of placebo-controlled trials. *Adv Ther*. 2012;29(9):736-746.

    doi: 10.1007/s12325-012-0045-5

13. Leonhardt W, Hanefeld M, Fischer S, Schulze J, Spengler M. Beneficial effects on serum lipids in noninsulin dependent diabetics by acarbose treatment. *Arzneimittelforschung*. 1991;41(7):735-738.

14. Hoffmann J, Spengler M. Efficacy of 24-week monotherapy with acarbose, metformin, or placebo in dietary-treated NIDDM patients: The Essen-II study. *Am J Med*. 1997;103(6):483-490.

    doi: 10.1016/s0002-9343(97)00252-0

15. Chiasson JL, Naditch L, Miglitol Canadian University Investigator Group. The synergistic effect of miglitol plus metformin combination therapy in the treatment of type 2 diabetes. *Diabetes Care*. 2001;24:989-994.

    doi: 10.2337/diacare.24.6.989

16. Tulp OL. Biometry, adiposity and mechanism of protein sparing growth in congenic preobese LA/Ntul//-*cp* rats. *Br J Healthc Med Res*. 2023;10:364-374.

    doi: 10.14738/bjhmr.103.14969

17. Granner DK, Mayes PA, Murray RK, *et al*. *Harpers Illustrated Biochemistry*. New York: McGraw-Hill Publications; 2012.

18. Tulp OL. Characteristics of thermogenesis, obesity, and longevity in the LA/Ntul//–*cp* rat. *ILAR J*. 1990;32(3):32-39.

19. Greenhouse DD. New Models of genetically obese rats for studies of diabetes, heart disease, and complications of obesity. *ILAR J.* 1990;32(3):1-3.

20. Hansen CT. The development of the SHR/N and LA/N-cp rat strains. In: *NER Models of Genetically Obese Rats for Studies in Diabetes, Heart Disease, and Complications of Obesity*. Bethesda, MD, USA: NIH Publication, Division of Research Services, Veterinary Resources Branch; 1988. p. 7-10.

21. Jing AI, Wang N, Yang M, Du ZM, Zhang YC, Yang BF. Development of Wistar rat model of insulin resistance. *World J Gastroenterol.* 2005;11(24):3675-3679.

    doi: 10.3748/wjg.v11.i24.3675

22. Ikeda H, Matsuo T. A new genetically obese hyperglycemic rat (Wistar fatty). *Diabetes*. 1981;30:1045-1050.

doi: 10.2337/diabetes.30.12.1045

23. Zucker LM, Zucker TF. Fatty, a new mutation in the rat. J Heredity. 1961;52(6):275-278.

doi: 10.1093/oxfordjournals.jhered.a107093

24. Peterson RG, Little LA, Neel MA. WKY Fatty rat as a model of obesity and non-insulin-dependent diabetes mellitus. *ILAR J*. 1990;32(3):13-15.

doi: 10.1093/ilar.32.3.13

25. Russell JC, Koeslag DG. Jcr: LA-corpulent Rat: A strain with spontaneous vascular and myocardial disease. *ILAR J*. 1990;32(3):27-32.

doi: 10.1093/ilar.32.3.27

26. Wu-Peng XS, Chua SC, Okada N, Liu SM, Nicolson M, Leibel RL. Phenotype of the obese Koletsky (f) rat due to Tyr763Stop mutation in the extracellular domain of the leptin receptor (Lepr): Evidence for deficient plasma-to-CSF transport of leptin in both the Zucker and Koletsky obese rat. *Diabetes*. 1997;46(3):513-518.

doi: 10.2337/diab.46.3.513

27. Michaelis OE IV, Ellwood KC, Tulp OL, Greenwood MR. Effect of feeding sucrose or starch diets on parameters of glucose tolerance in the LA/N-corpulent rat. *Nutr Res*. 1986;6:95-99.

doi: 10.1016/s0271-5317(86)80203-2

28. Raabo E, Terkilden TC. On the enzymatic determination of blood glucose. *Scand J Clin and Lab Invest*. 1960;12:402-407.

doi: 10.3109/00365516009065404

29. Hales CN, Randle PJ. Immunoassay of insulin and insulin antibody precipitate. *Biochem J*. 1963;88:137-146.

doi: 10.1042/bj0880137

30. Wallace TM, Levy JC, Mathews DR. Use and abuse of HOMA modeling. *Diabetes Care*. 2004;27(6):1487-1495.

doi: 10.2337/diacare.27.6.1487

31. Bentzen CJ, Acuff AJ, Marachal MA, Volk ME. Direct determination of lipoprotein cholesterol distribution with microscale affinity chromatography columns. *Clin Chem*. 1982;28(7):1451-1456.

32. Bucolo G, David H. Determination of cholesterol lipoproteins via affinity chromatography. *Clin Chem*. 1973;4:476-481.

33. Freeland RA. Effect of starvation on rat liver enzymes. *J Nutr*. 1987;91:489-495.

doi: 10.1093/jn/91.4.489

34. Lowry OH, Rosebrogh NJ, Farr AL, Randall RJ. Measurement of proteins in tissues. *J Biol Chem*. 1951;193:265-275.

35. Matschinsky FM, Wilson DF. The Central role of glucokinase in glucose homeostasis: A perspective 50 years after demonstrating the presence of the enzyme in islets of Langerhans. *Front Physiol*. 2019;10:148.

doi: 10.3389/fphys.2019.00148

36. Nie N, Hull CH, Jenkins K, Sternbrunner K, Bent D. *Statistical Package for the Social Sciences*. 2nd ed. New York: McGraw Hill.

37. Page EB. Ordered hypothesis for multiple treatments: A significance test for linear ranks. *J Am Stat Assoc*. 1963;58(301):216-230.

doi: 10.1080/01621459.1963.10500843

38. Chang GG, Tong L. Structure and function of malic enzymes, a new class of oxidative decarboxylases. *Biochemistry*. 2003;42:12721-12733.

doi: 10.1021/bi035251+

39. Chou BS, Shiau SY. Optimal dietary lipid level for growth of juvenile hybrid tilapia, *Oreochromis niloticus* X *Oreochromis aureus*. *Aquaculture*. 1996;143(2):185-195.

doi: 10.1016/0044-8486(96)01266-5

40. Sugimoto S, Nakajima H, Kosaka K, Hosoi H. Review: Miglitol has potential as a therapeutic drug against obesity. *Nutr Metab.* 2015;12:51.

doi: 10.1186/s12986-015-0048-8

41. Boque N, Campion J, Paterman L, *et al*. Influence of dietary macronutrient composition on adiposity and cellularity of different fat depots in Wistar rats. *J Physiol Biochem*. 2009;65(4):387-395.

doi: 10.1007/BF03185934

42. Scott LJ, Spencer CM. Miglitol: A review of its therapeutic potential in type 2 diabetes mellitus. *Drugs*. 2000;59(3):521-549.

doi: 10.2165/00003495-200059030-00012

43. Coniff RF, Shapiro JA, Robbins D, *et al*. Reduction of glycosylated hemoglobin and postprandial hyperglycemia by acarbose in patients with NIDDM. A placebo-controlled dose-comparison study. *Diabetes Care*. 1995;18(6):817-824.

doi: 10.2337/diacare.18.6.817

44. Hanefeld M, Fischer S, Schulze J, *et al*. Therapeutic potentials of acarbose as first-line drug in NIDDM insufficiently treated with diet alone. *Diabetes Care*. 1991;14(8):732-737.

doi: 10.2337/diacare.14.8.732

45. Lee J, Lee S, Zhang H, *et al*. Interaction of IL-6 and TNF-α contributes to endothelial dysfunction in type 2 diabetic mouse hearts. *PLoS One*. 2017;12(11):e0187189.

doi: 10.1371/journal.pone.0187189

46. Ajuwon KM, Spurlock ME. Palmitate activates the NF-κB transcription factor and induces IL-6 and TNFα expression in 3T3-L1 adipocytes. *J Nutr*. 2005;135(8):1841-1846.

doi: 10.1093/jn/135.8.1841

47. Volpe CM, Abreu LF, Gomes PS, Gonzaga RM, Veloso CA, Nogueira-Machado JA. The Production of nitric oxide, IL-6, and TNF-alpha in palmitate-stimulated PBMNCs is enhanced through hyperglycemia in diabetes. *Oxidat Med Cell Longev*. 2014;2014(1):479587.

doi: 10.1155/2014/479587

48. Nordmann TM, Dror E, Schulze F, *et al*. The Role of inflammation in β-cell dedifferentiation. *Sci Rep*. 2017;7:6285.

doi: 10.1038/s41598-017-06731-w

49. King GL. The role of inflammatory cytokines in diabetes and its complications. *J Periodontol*. 2008;79(8S)1527-1534.

doi: 10.1902/jop.2008.080246

50. Martin SS. 3 Myths about cholesterol-lowering statin drugs. In: *Home Health Conditions and Diseases*, United States: John Hopkins Medicine; 2024.

ACCSCIENCE PUBLISHING

Global Translational Medicine

ORIGINAL RESEARCH ARTICLE

Hepatocyte-specific angiotensinogen deficiency inhibits Western diet-induced liver steatosis with suppression of cell division in mice

Alex C. Pettey[1,2,3], Dien Ye[1,2], Sohei Ito[1,2], Alan Daugherty[1,2,3], Hong S. Lu[1,2,3]*, and Hisashi Sawada[1,2,3]*

[1]Saha Cardiovascular Research Center, College of Medicine, University of Kentucky, Lexington, Kentucky, United States of America

[2]Saha Aortic Center, College of Medicine, University of Kentucky, Lexington, Kentucky, United States of America

[3]Department of Physiology, College of Medicine, University of Kentucky, Lexington, Kentucky, United States of America

Abstract

Liver steatosis is a common cause of chronic liver disease. To investigate the molecular basis of hepatic steatosis, low-density lipoprotein receptor-deficient (LDLR -/-) mice were fed a Western diet (WD, 42% of calories from fat) for 5, 14, or 42 days and evaluated against mice fed a normal laboratory diet. Histological analyses revealed that steatosis was detected as early as 14 days of WD feeding. Bulk RNA sequencing demonstrated that WD feeding altered liver transcriptomes related to inflammation and cell adhesion consistent with the progression of liver steatosis. Previous studies determined that hepatocyte-specific deficiency of angiotensinogen (AGT), the unique substrate of the renin-angiotensin system (RAS), alleviates WD-induced hepatic steatosis in mice. However, the effects of hepatic AGT deficiency were not mimicked by pharmacological inhibition of the RAS, and the molecular mechanisms by which AGT deficiency protects against WD-induced steatosis is unknown. Therefore, liver transcriptomes were compared between hepatocyte-specific AGT-deficient mice (hepAGT -/-) and their wild-type littermates (hepAGT +/+) after 14 days of WD feeding. Gene ontology analyses showed that upregulated genes in hepAGT -/- mice were enriched for metabolic processes and downregulated genes were enriched for cell division pathways. The integration analysis of the two RNA sequencing data identified 5 key genes, *Smpd3*, *Dtl*, *Cdc6*, *Mki67*, and *Top2a*, which were primarily associated with cell division processes in hepAGT +/+ mice and were suppressed in hepAGT -/- mice. In conclusion, hepatic AGT deficiency downregulated genes related to cell division during the progression of liver steatosis.

Keywords: Angiotensinogen; Liver steatosis; Obesity; Transcriptomic analysis

***Corresponding author:**
Hong S. Lu
(hong.lu@uky.edu)
Hisashi Sawada
(hisashi.sawada@uky.edu)

Citation: Pettey AC, Ye D, Ito S, Daugherty A, Lu HS, Sawada H. Hepatocyte-specific angiotensinogen deficiency inhibits Western diet-induced liver steatosis with suppression of cell division in mice. *Global Transl Med*. 2025;4(2):71-85.
doi: 10.36922/gtm.6027

Received: November 16, 2024

1st revised: February 12, 2025

2nd revised: March 24, 2025

Accepted: March 25, 2025

Published online: April 10, 2025

1. Introduction

Liver steatosis, characterized by excess lipid accumulation within hepatocytes, is a common hepatic disease that is prevalent worldwide.[1-5] Liver steatosis represents an independent risk factor for chronic liver diseases and many cardiovascular diseases.[6]

Multiple studies have shown that consumption of a diet rich in saturated fats has a significant positive correlation with steatosis in humans.[7,8] Furthermore, there is compelling preclinical evidence that feeding with Western diet (WD), a laboratory diet enriched in saturated fats, induces liver steatosis in mice.[9] Thus, WD feeding in combination with genetic mouse models provides a valuable approach to investigate specific molecular targets involved in the initiation and progression of liver steatosis.

Angiotensinogen (AGT) is the unique substrate of the renin-angiotensin system (RAS) and is derived predominantly from hepatocytes.[10-12] AGT exerts a key role in WD-induced steatosis.[11,13] Previous preclinical studies demonstrated that global and hepatocyte-specific AGT deficiency ameliorated WD-induced liver steatosis in both hypercholesteremic and normolipidemic mice.[11,14] AGT hypomorphic mice had a drastic reduction of AGT plasma concentrations and were resistant to WD-induced increases in body weight, liver weight, and liver triglycerides.[11] Hepatocyte-specific AGT deficiency decreased plasma AGT concentrations comparable to AGT hypomorphic mice and also conferred resistance to diet-induced body weight gain and liver steatosis.[11,14] Of note, the effect of AGT deficiency on liver steatosis was not mimicked by inhibition of renin or the angiotensin II type 1 receptor (AT1R), which indicates that the effect is independent of angiotensin II stimulation of AT1R.[11,14,15] Furthermore, in hepatocyte-specific AGT-deficient mice, restoration of plasma AGT concentrations by infection with an adeno-associated virus expressing des(AngI)AGT, a cleaved form of AGT that lacks the portion corresponding to angiotensin I (AngI), resulted in restoration of WD-induced body weight gain and liver steatosis comparable to expression of full-length AGT.[11] Importantly, despite the clear contribution of hepatic AGT to development of WD-induced steatosis, few studies have investigated functions of AGT outside of the production of RAS peptides, and the mechanism by which hepatocyte-specific AGT deletion inhibits liver steatosis remains unclear. Therefore, it is critical to identify potential molecules driving WD-induced liver steatosis through AGT.

In the present study, to identify target pathways and molecules, we employed a two-armed bulk RNA sequencing approach in mice. First, the temporal alteration of hepatic transcriptomes in response to WD was evaluated at different intervals of WD feeding in a hypercholesterolemic mouse model. Second, hepatic transcriptomes of hypercholesterolemia were compared between mice with AGT deletion in hepatocytes and their wild-type littermates. Last, the two RNA sequencing datasets were integrated to determine key processes that were altered by hepatic AGT deficiency during initiation of WD-induced steatosis.

2. Materials and methods

2.1. Mice

AGT floxed mice, with and without a transgene expressing Cre under the control of the albumin promoter (Alb-Cre; hepAGT -/- and hepAGT +/+, respectively), on a low-density lipoprotein-receptor deficient (LDLR -/-, #002207, The Jackson Laboratory, USA) background were developed and bred as described previously.[11] Since liver steatosis is often observed during childhood, with the mean age of diagnosis being 11 – 13 years old in pediatric cases, the present study used mice at 7 weeks of age, comparable to humans at approximately 13 years of age.[16-20] Mice were maintained in a barrier facility on a light: dark cycle of 14:10 h (ambient temperature of 21°C) and fed a normal mouse laboratory diet (fat 6.2% wt/wt; Diet #2918; Inotiv, USA). Littermates were used for all experiments. Male mice were used based on our previous study that found no sex-specific differences in hepAGT mice.[11] To induce hypercholesterolemia, mice at 7 weeks of age were fed a diet supplemented with saturated fat (milk fat 21% wt/wt) and cholesterol (0.2% wt/wt; Diet #TD.88137, Inotiv, termed "Western diet") for 5, 14, or 42 days. Mice were euthanized using a ketamine/xylazine cocktail (90 mg/kg #11695-6840-1, 10 mg/kg #11695-4024-1, respectively; Covetrus, USA). To minimize transcriptomic alterations following euthanasia, cold saline (8 – 10 mL) was perfused from the left ventricle, and livers were harvested immediately.

2.2. Histological analyses

Liver portions from the left lobe were collected and processed for histological analysis. For hematoxylin and eosin (H&E) staining, samples were fixed in paraformaldehyde (4% w/v), incubated with ethanol (70% v/v) for 24 h, embedded in paraffin, and sectioned (5 μm). Sections were subsequently deparaffinized using limonene (#183164, Millipore Sigma, Germany) followed by two washes with ethanol (100% v/v). Sections were then stained with Eosin Y (#ES709, Azer Scientific) for 2 min and counterstained with Mayer's hematoxylin for 10 s (#26043-06, Electron Microscopy Sciences). Coverslips were applied using Permount (#SP-15, Fisher Scientific, USA). For Oil Red O staining, liver samples were embedded in optimal cutting temperature compound (#4585, Fisher Scientific), frozen at −20°C, and sectioned (10 μm). Sections were fixed in neutral-buffered formalin (10% w/v) and dehydrated in isopropanol (60% v/v) for 5 min. Next, sections were stained with filtered Oil Red O (#O0625, Millipore Sigma; 0.15% w/v in 60% isopropanol) for 10 min, destained in isopropanol (60% v/v) for 2 min,

and counterstained in Mayer's hematoxylin (#26043-06, Electron Microscopy Sciences, USA) for 30 s. Coverslips were applied with warmed glycerol gelatin (#GG1, Millipore Sigma). Representative microscopic images were captured using an Eclipse NI microscope with a DS-Ri2 camera (Nikon, Japan). For quantification of Oil Red O, whole liver sections were imaged using a Z7 slide scanner (Zeiss, Germany). Oil Red O staining was quantified using an RGB color threshold (red: 0 – 255, green: 0 – 255, blue: 0 – 185) and normalized against total tissue area, defined by total pixels – white background pixels (red: 250 – 255, green: 250 – 255, blue: 250 – 255), using NIS-Elements AR (v4.51.00, Nikon).

2.3. Bulk RNA sequencing

Liver samples were snap-frozen in a homogenization solution (#Z305H, Promega, USA) containing 1-thioglycerol (#A208B, Promega). Subsequently, messenger RNA (mRNA) was extracted using Maxwell RSC simplyRNA Tissue Kits (#AS1340, Promega) according to the manufacturer's protocol. Samples were processed individually for bulk RNA sequencing, with single mice representing independent experimental replicates. RNA samples were shipped to Novogene (USA) for bulk mRNA sequencing. The sequencing library was generated from total mRNA (1 μg) using NEBNext Ultra™ RNA Library Prep Kits for Illumina (New England BioLabs, USA). cDNA libraries were then sequenced by a Next Generation NovaSeq platform, (HWI-ST1276, Illumina, USA), in a pair-end fashion to reach more than 1,500,000 reads. FASTQ sequence data were mapped to the reference mouse genome using STAR (v2.6.1d; https://academic.oup.com/bioinformatics/article/29/1/15/272537?login=false) and quantified using FeatureCounts (v1.5.0-p3; https://academic.oup.com/bioinformatics/article/30/7/923/232889?login=false). Bulk RNA sequencing data (raw FASTQ and aligned data) are publicly available at the gene expression omnibus repository (GEO accession number: GSE291082).

2.4. Statistical analysis

Data are presented as median and 25th/75th percentiles. Down triangles represent biological replicates. Statistical analyses of Oil Red O quantification and individual target differentially expressed genes (DEGs) were performed using SigmaPlot (v15.0, SYSTAT Software Inc., USA). Normality and homogeneity of variance were assessed by Shapiro–Wilk and Brown–Forsythe tests, respectively. Data with confirmed normal distribution and homogeneous variance were analyzed by one-way analysis of variance (ANOVA) followed by Holm–Sidak test. Data that failed tests for normality or homogeneity of variance were analyzed by Kruskal–Wallis one-way ANOVA on Ranks with Dunn's method. $p<0.05$ was considered statistically significant.

Bulk RNA sequencing data were analyzed on R (v4.1.0).[21,22] Ensembl gene identifiers with no detected read counts in any sample were excluded. Read count data were normalized using the TMM method in edgeR package (v3.36.0) to adjust for biases in library size and composition. P-values were calculated using either "glmQLFTest" for multi-group or "exactTest" for two-group comparisons in edgeR. Since the present study aimed to profile genes with a high potential for interaction with AGT, miscellaneous transcripts such as duplicated, unnamed, ribosomal, and mitochondrial genes were removed. Criteria for removal was based on searches within Ensembl gene identifiers for "NA," duplicated identifiers, or identifiers containing: "Gm[0 – 9]," "[0 – 9]Rik," "RP[2 – 9]," or "mt-." Subsequently, *p*-values were adjusted using the false discovery rate (FDR) method. FDR-adjusted $p<0.05$ was considered statistically significant. Gene ontology (GO) enrichment analysis of biological processes was performed using the clusterProfiler package (v4.2.2) after mapping Entrez gene identifiers with the org.Mm.eg.db package (v3.14.0) on R (v4.1.0).[23-25] Chord plot illustration was performed using the SRplot online tool.[26]

3. Results

3.1. Macrovesicular liver steatosis was present after 14 days of WD feeding in hepAGT +/+ mice

We first determined the temporal evolution of WD-induced liver steatosis in LDLR -/- mice. WD-induced liver steatosis is closely associated with body weight gain,[27,28] and our previous study revealed that WD-induced body weight gain begins after 14 days of WD feeding.[14] We therefore harvested liver tissues from LDLR -/- mice at selected intervals of WD feeding, including baseline and day 14 (Figure 1A). H&E staining did not detect discernable pathologies in livers at baseline and 5 days of WD feeding. At 14 days of WD feeding, intracellular vacuoles were detectable in a substantial portion of hepatocytes, indicating macrovesicular steatosis. At 42 days of WD feeding, intrahepatic vacuoles of increased size were present abundantly (Figure 1B). Oil Red O staining was then performed to assess neutral lipid accumulation in livers. Neutral lipids were minimally detected in baseline livers. At 5 days of WD feeding, punctate lipid droplets were diffusely present within hepatocytes without evident displacement of nuclei. However, we did not detect a statistically significant difference in the extent of Oil

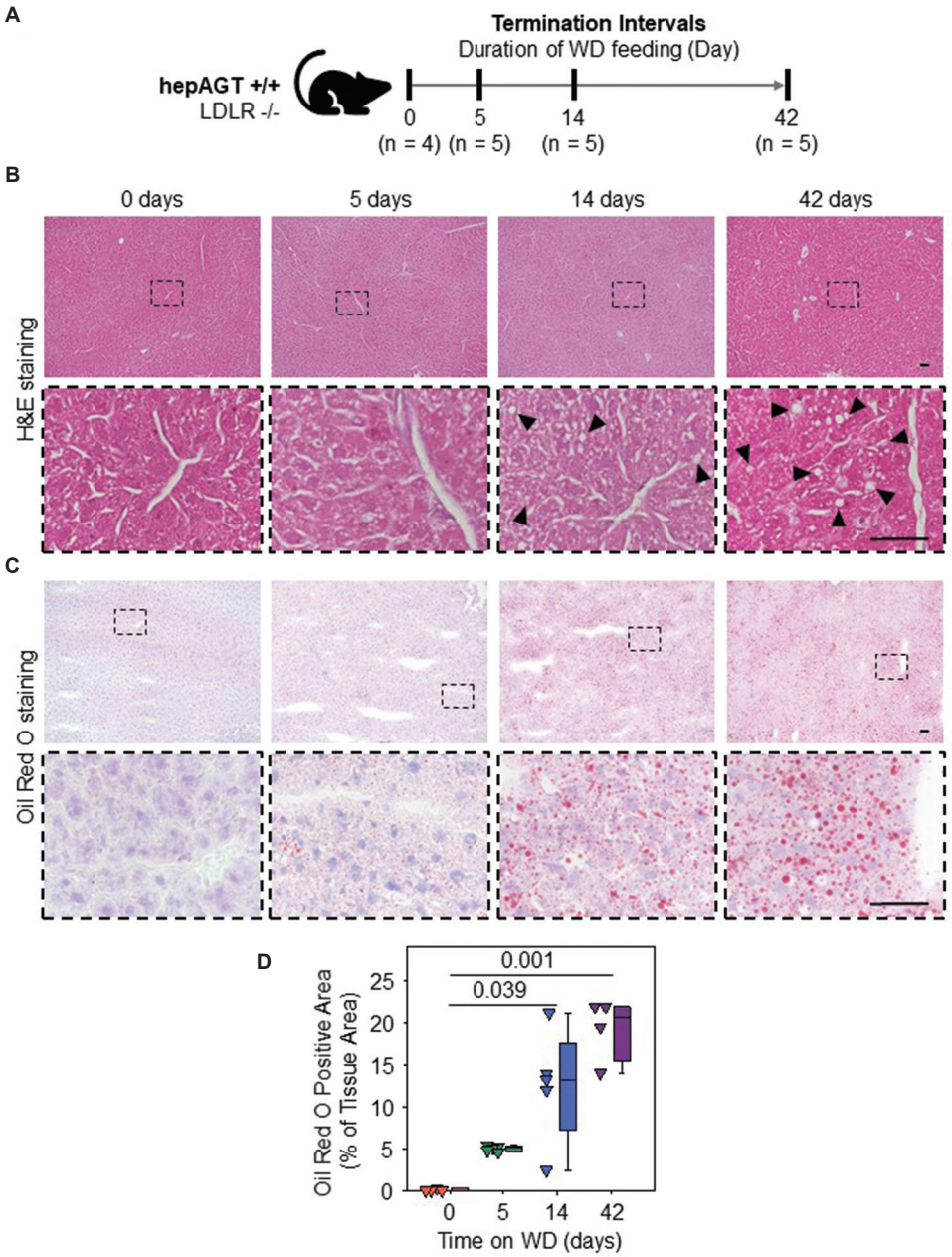

Figure 1. Macrovesicular liver steatosis was present after 14 days of WD feeding in hepAGT +/+ mice. (A) Albumin-Cre 0/0; angiotensinogen floxed (f/f) mice (hepAGT +/+) on an LDLR -/- background were fed WD for 0 (n = 4), 5 (n = 5), 14 (n = 5), or 42 (n = 5) days. (B) Representative images of H&E and (C) Oil Red O staining in livers. Black arrowheads indicate large intrahepatic vacuoles. Scale bars = 50 μm. (D) Quantification of Oil Red O staining-positive area. Numbers in the panel (D) are p-values calculated by Kruskal–Wallis test followed by Dunn's method.
Abbreviations: H&E: Hematoxylin and eosin; LDLR: Low-density lipoprotein receptor; ND: Normal laboratory diet; WD: Western diet.

Red O-positive area between baseline and 5 days of WD feeding (Figure 1C and D). At 14 days of WD feeding, a subset of hepatocytes displayed large neutral lipid droplets surrounded by apparently displaced nuclei, indicative of macrovesicular steatosis. At 42 days of WD feeding, macrovesicular steatosis was apparent in most hepatocytes (Figure 1C). Oil Red O-positive areas were increased significantly at 14 and 42 days of WD feeding compared to baseline (Figure 1D). These data suggest that 5, 14, and 42 days of WD feeding induce liver steatosis corresponding to pre-pathological, initiation, and advanced phases, respectively, in hypercholesterolemic mice.

3.2. WD altered the liver transcriptome related to inflammation consistent with the progression of steatosis

To identify key molecules driving WD-induced liver steatosis, bulk RNA-sequencing was performed in livers from LDLR -/- mice fed WD for 0, 5, 14, or 42 days. The bulk RNA sequencing identified 31,403 genes. Principal component analysis using unfiltered transcriptomes revealed distinct transcriptomic alterations in mice fed WD for 14 or 42 days compared to those fed WD for 5 days or baseline controls (Figure 2A), with the first two principal components explaining 26.5% of the variance among samples (15.4% + 11.1%). These data suggest that WD induces a transcriptomic shift within 14 days of feeding. Then, DEG analyses were performed among all four groups. There were 5,256 DEGs, and hierarchical clustering identified four distinct clusters in the DEGs (Figure 2B). Cluster 1 contained DEGs that were increased transiently by WD feeding at the initiation phase of liver steatosis. Meanwhile, DEGs in Cluster 2 were decreased by WD feeding. DEGs in Cluster 3 were increased transiently by WD feeding before the initiation phase of steatosis. Of note, Cluster 4 was composed of genes that were increased by WD feeding concurrent with steatosis development. GO enrichment analysis for biological processes was then performed to characterize the DEGs within each cluster. DEGs in Cluster 1 were associated mainly with epithelial tube morphogenesis and cell-

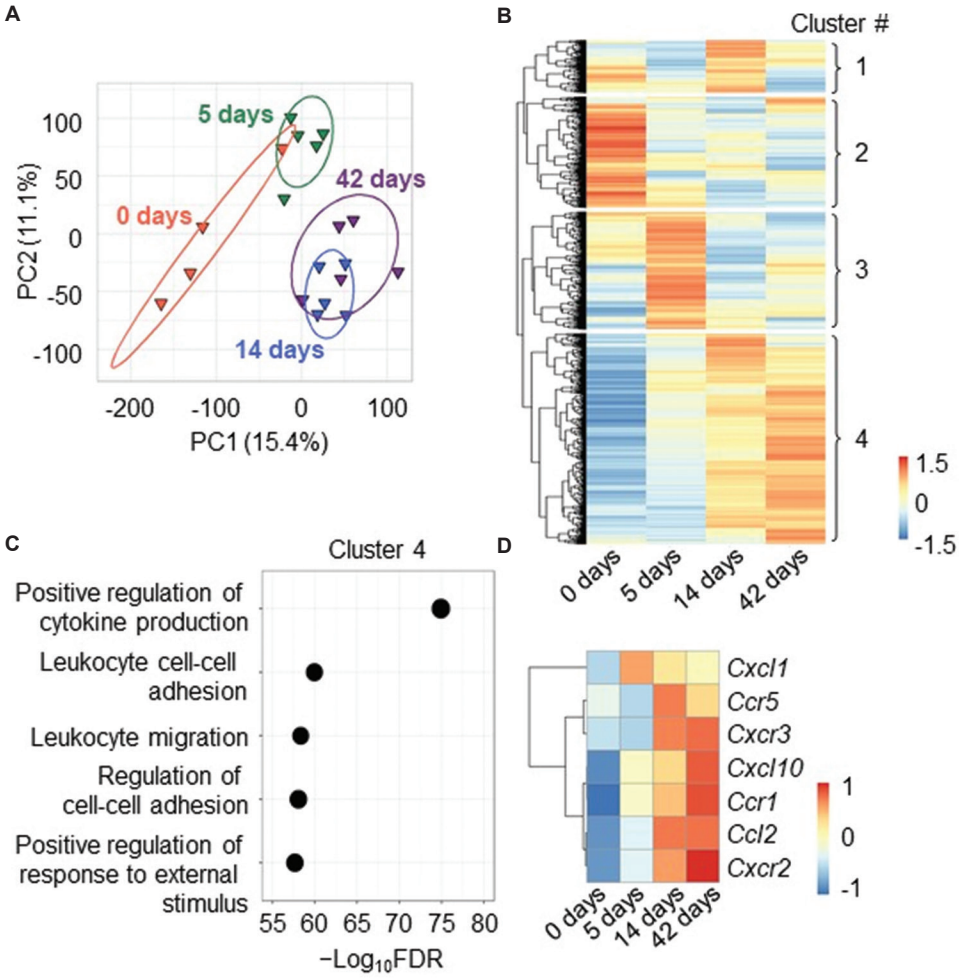

Figure 2. WD altered the liver transcriptome related to inflammation consistent with the progression of steatosis. (A) Principal component analysis of liver transcriptomes of hepAGT +/+ mice fed WD for 0, 5, 14, or 42 days. Numbers in parentheses indicate the percent of variation explained by the graphed PCs. (B) Z-scored heatmap of all DEGs. DEG cluster numbers were assigned by hierarchical clustering analysis. (C) Top five annotations in gene ontology analysis for biological processes using DEGs in Cluster 4. (D) Z-scored heatmap of key inflammatory cytokines and chemokines within detected DEGs. $n = 4 – 5$ mice/group.

Abbreviations: DEG: Differentially expressed gene; FDR: False discovery rate; hepAGT +/+: Albumin-Cre 0/0 angiotensinogen floxed (f/f) low-density lipoprotein-receptor-deficient background; PC: Principal component; WD: Western diet.

substrate adhesion (Figure A1[A]). DEGs in Cluster 2 were related to sterol and secondary alcohol biosynthetic processes as well as fatty acid and steroid metabolic processes (Figure A1[B]). DEGs in Cluster 3 were related to catabolic processes (Figure A1[C]). Interestingly, in Cluster 4 which was consistent with the progression of liver steatosis, DEGs were related to inflammation and included major cytokines and chemokines, such as *Ccl2* and *Cxcl1* (Figure 2C and D).

3.3. Hepatocyte-specific AGT deficiency increased the hepatic transcriptome related to metabolic processes and suppressed cell division processes at 14 days of WD feeding

We next investigated the impact of hepAGT-/- on WD-induced transcriptomic alterations in liver. H&E and Oil Red O staining revealed that WD-induced liver steatosis becomes discernible after 14 days of WD feeding (Figure 1B-D). Therefore, to determine molecular mechanisms by which hepatocyte-derived AGT contributes to disease initiation, additional bulk RNA sequencing was performed using livers from hepAGT -/- mice after 14 days of WD feeding. DEG analyses were conducted by comparing these newly generated data with the previously sequenced transcriptomes of hepAGT +/+ mice after the same interval of 14 days of WD feeding (Figure 3A). *Agt* mRNA deletion was verified by reduction of mRNA reads aligned to exon 2 of *Agt* in hepAGT -/- mice (Figure 3B). Despite the significant reduction, only 128 DEGs were detected between genotypes. Sixty-two DEGs were upregulated and 66 DEGs were downregulated in hepAGT -/- mice compared to wild-type (Figure 3C). GO enrichment analysis revealed that genes upregulated in hepAGT -/- mice were related to metabolic and biosynthetic processes (Figure 3D). Meanwhile, downregulated genes were related to cell division processes (Figure 3E).

3.4. Cell division-related genes elevated by WD feeding were suppressed in hepatocyte-specific AGT-deficient mice at 14 days of WD

To define key molecules mediating the attenuation of WD-induced liver steatosis in hepAGT -/- mice, the two RNA sequencing data were integrated (Figure 4A). We sought to isolate genes that were both increased in association with WD-feeding and altered in hepAGT -/- mice at the initiation phase of steatosis. Since Cluster 4 contained DEGs that were increased in abundance consistent with continued WD-feeding, DEGs in Cluster 4 were compared against all DEGs identified by comparing hepAGT +/+ and -/- mice at 14 days of WD-feeding (Figure 4B). Twenty-four DEGs were overlapped between the two sequencing datasets (Figure 4C). GO enrichment analysis within the overlapped DEGs highlighted six DEGs that were present in the top five biological processes, all of which related to cell division (Figure 4D). These six DEGs represented potential target genes relating to the contribution of AGT to diet-induced steatosis. Among these genes, *Smpd3*, *Mki67*, and *Top2a* demonstrated the highest normalized read count expression (Figure 4E).

3.5. mRNA abundance of target cell division genes increased concurrently with steatosis in hepAGT +/+ mice

To verify that the abundance of potential target genes was increased during feeding of WD in hepAGT +/+ mice, normalized read count data for each DEG were analyzed separately. *Plk1* displayed a statistically significant increase in abundance only after 14 days of WD feeding compared to baseline (0 days of WD). Increased abundances of *Smpd3, Dtl, Cdc6, Mki67,* and *Top2a* were detected after 14 and 42 days of feeding WD, which was consistent with the initiation and advanced phases of steatosis in hepAGT +/+ mice (Figure 5).

4. Discussion

In the present study, we performed two bulk RNA sequencing analyses to explore the molecular basis underlying the inhibition of WD-induced liver steatosis and protective effects of hepatocyte-specific AGT deletion. We found that genes related to inflammatory biological processes were increased consistently with the progression of steatosis. The mRNA abundance of several key inflammatory cytokines was maximal at an advanced stage of steatosis. Surprisingly, despite the established protective effect against WD-induced steatosis, hepatocyte-specific AGT deficiency altered a select portion of the liver transcriptome, particularly genes related to metabolic and cell division processes, during the initiation phase of steatosis. By integrating data from the two RNA sequencing analyses, we identified five molecules related to cell division: *Smpd3*, *Dtl*, *Cdc6*, *Mki67*, and *Top2a*, as key mediators in suppressing WD-induced steatosis in hepAGT -/- mice.

In this study, liver steatosis was defined histologically by the presence of intrahepatocellular lipid droplet accumulation. Macrovesicular steatosis, a defining feature of metabolic dysfunction-associated fatty liver disease (MAFLD),[29-33] was observed after 14 days of WD feeding, but not after 5 days, suggesting that 14 days of feeding represents the initiation phase of pathology. This finding is consistent with a previous study reporting hepatic triglyceride content increased in mice after 14 days of a high-fat diet.[34] In the present study, progressive macrovesicular steatosis was noted after 42 days of WD

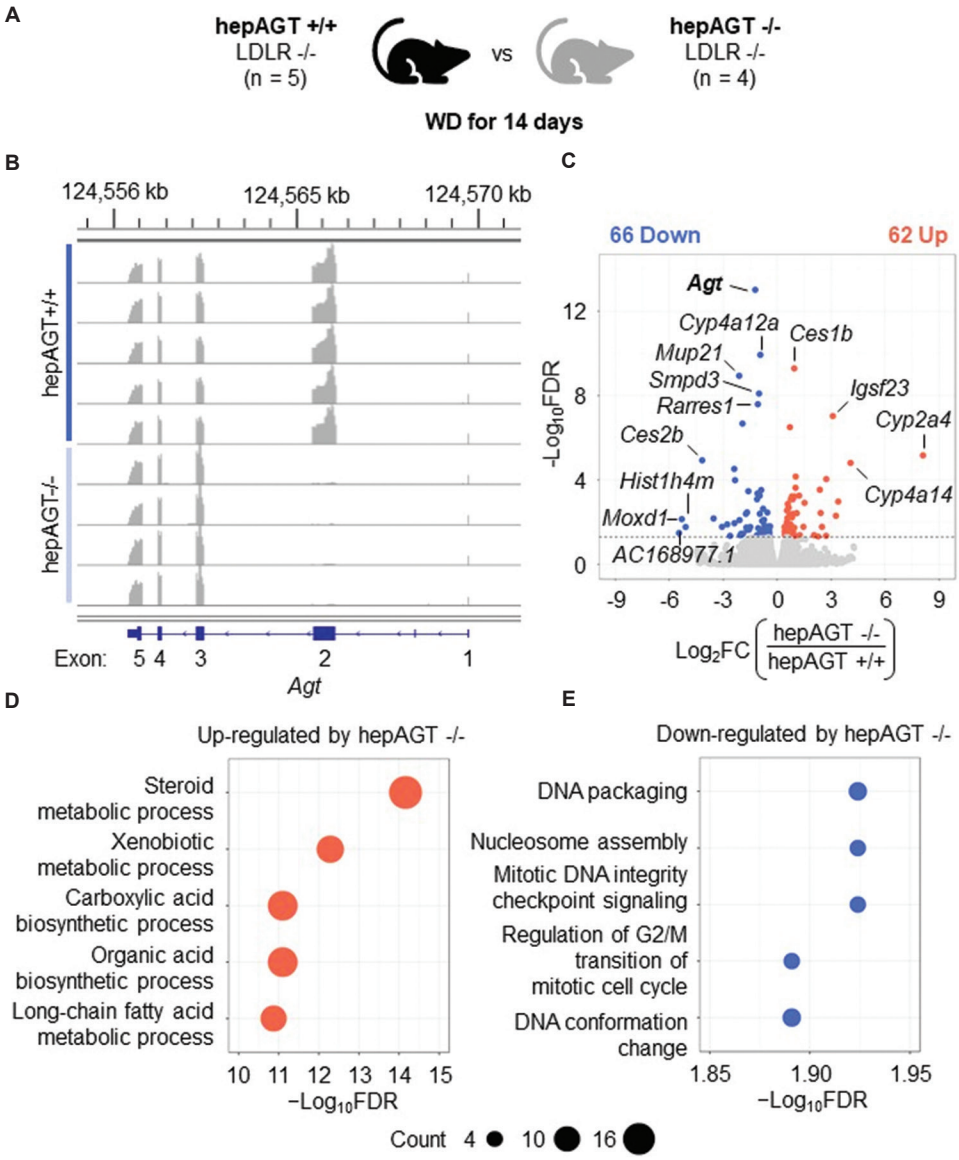

Figure 3. Hepatocyte-specific AGT deficiency increased the hepatic transcriptome related to metabolic processes and suppressed cell division processes at 14 days of WD feeding. (A) Livers of albumin-Cre 0/0; angiotensinogen floxed (f/f) mice (hepAGT +/+) and albumin-Cre 1/0; angiotensinogen floxed (f/f) mice (hepAGT -/-) on a low-density lipoprotein-receptor deficient (LDLR -/-) background fed WD for 14 days were analyzed by bulk RNA sequencing. (B) Visualization of read coverage on mouse *Agt* in hepAGT +/+ and -/- mice fed WD for 14 days. (C) Volcano plot of all DEGs between hepAGT +/+ versus -/- mice at 14 days of WD. Top 5 annotations in gene ontology analysis for biological processes within (D) upregulated and (E) downregulated DEGs. $n = 4 – 5$ mice/group.
Abbreviations: AGT: Angiotensinogen; DEG: Differentially expressed gene; FC: Fold change; FDR: False discovery rate; WD: Western diet.

feeding, consistent with previous studies reporting the presence of macrovesicular steatosis in mice after 56 days of WD or high-fat diet feeding.[28,34] These observations suggest that 14 days of WD feeding is an optimal interval for investigating the mechanisms underlying liver steatosis that relate to the initiation of this disease.

The primary aim of this study was to identify previously unknown molecules that may interact with AGT during the initiation phase of steatosis. The combination of a time-course RNA sequencing analysis in WD-fed hepAGT +/+ mice and another sequencing analysis comparing hepatocyte-specific AGT genotypes at the initiation phase of steatosis allowed us to isolate target genes with potential roles in both interaction with AGT and development of steatosis. We identified 128 DEGs between hepAGT +/+ and -/- mice at the initiation

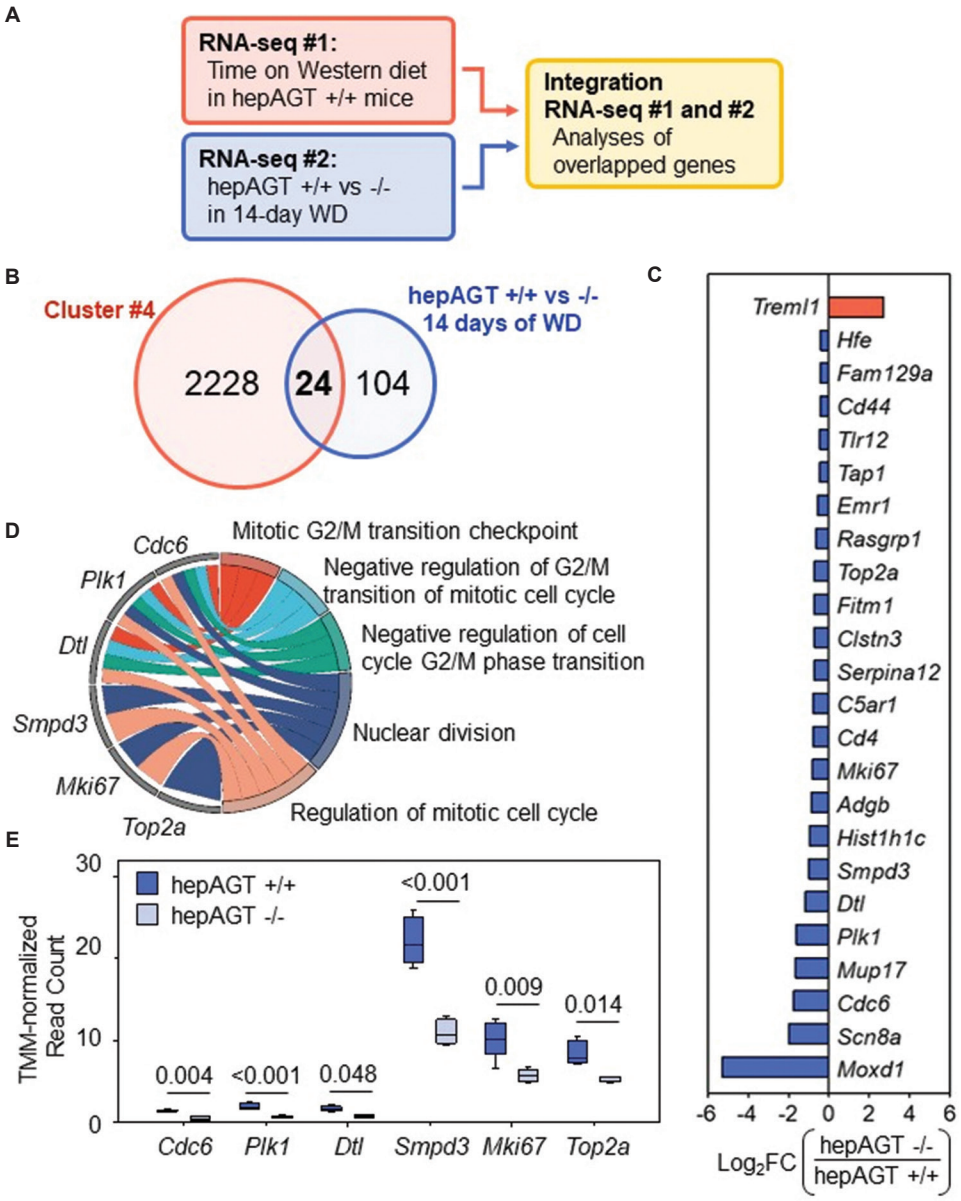

Figure 4. Cell division-related genes elevated by WD feeding were suppressed in hepatocyte-specific AGT-deficient mice at 14 days of WD. (A) Flowchart of two-armed bulk RNA sequencing. WD-induced liver transcriptomic alterations were analyzed in hepAGT +/+ mice after 5, 14, and 42 days of WD feeding compared against 0 days of WD. Liver transcriptomic alterations due to hepatic AGT deficiency were analyzed after 14 days of WD feeding by comparing hepAGT -/- mice against hepAGT +/+ mice. Both RNA sequencing data were integrated to identify target genes. (B) Venn diagram for overlapped DEGs from combined transcriptomic analyses. Cluster 4 represents DEGs with upregulation consistent with steatotic progression in hepAGT +/+ mice. hepAGT -/- versus +/+ represents DEGs altered in hepAGT -/- mice at 14 days of WD. (C) Log_2FC alteration in hepAGT -/- mice at 14 days of WD within overlapped DEGs. (D) Chord graph representing overlapped DEGs corresponding to the top five terms in gene ontology analysis. (E) Normalized read count expression of six target DEGs in hepAGT +/+ and -/- mice after 14 days of WD feeding. False discovery rate-adjusted *p*-values are represented above for each DEG.

Abbreviations: AGT: Angiotensinogen; DEG: Differentially expressed gene; FC: Fold change; hepAGT +/+: albumin-Cre 0/0 AGT floxed (f/f) low-density lipoprotein-receptor-deficient background; hepAGT -/-: Albumin-Cre 1/0 AGT floxed (f/f) low-density lipoprotein-receptor-deficient background; WD: Western diet.

of steatosis. The integration of the two sequencing data highlighted 24 DEGs. Despite the small number of DEGs, by focusing on the initiation phase, we gain insights into the regulation of potentially causative genes with less interference from genes altered as a consequence of steatosis.

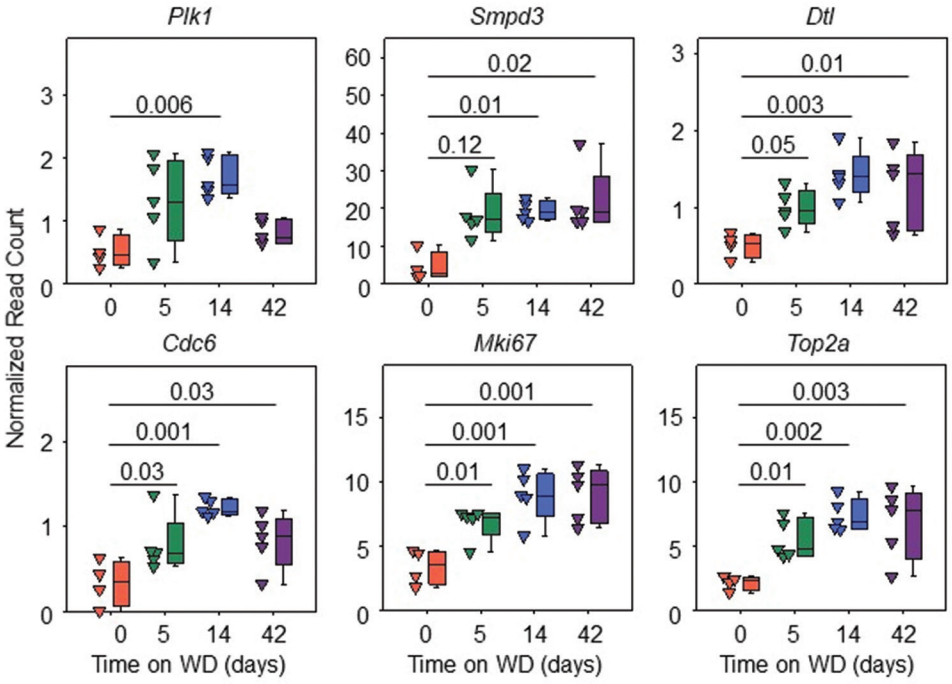

Figure 5. mRNA abundance of target cell division genes increased concurrently with steatosis in hepAGT +/+ mice. Normalized read count expression of target DEGs after 5, 14, and 42 days of WD feeding compared to 0 days in hepAGT +/+ mice. *p-values* compared against 0 days were calculated by Kruskal–Wallis with Dunn's method for *Plk1* and *Smpd3* or one-way analysis of variance with Holm–Sidak test for *Dtl, Cdc6, Mki67,* and *Top2a*. $n = 4 – 5$ mice/group.
Abbreviations: DEG: Differentially expressed gene; hepAGT +/+: Albumin-Cre 0/0 AGT floxed (f/f) low-density lipoprotein-receptor-deficient background; WD: Western diet.

The present study identified five genes (*Smpd3*, *Dtl*, *Cdc6*, *Top2a*, and *Mki67*) as potential mediators in the development of WD-induced liver steatosis. *Smpd3*, encoding neutral sphingomyelinase 2, catalyzes the hydrolysis of the biochemically inert lipid sphingomyelin, leading to an increased abundance of ceramide. Excess ceramide has been implicated in liver inflammation and steatosis, potentially by enhancing endoplasmic reticulum stress, lipid uptake, and triglyceride production in the liver.[35-39] Both pro- and anti-proliferative functions of ceramide have been reported, explained in part by contextual differences of cell type, subcellular localization, and fatty-acid chain length.[40-43] The contribution of *Smpd3* and ceramide to liver cell proliferation in the context of WD-induced steatosis remains unclear. However, inhibition of *Smpd3* by genetic or pharmacologic methods attenuates hepatocyte lipid accumulation and pathologic features of MAFLD *in vitro*.[36,39] *Dtl*, which encodes denticleless E3 ubiquitin protein ligase homolog, plays a key role in the cell cycle as a substrate receptor for cullin-RING ligases and regulates replication licensing, cell cycle control, and chromatin modification-associated proteins.[44,45] Overexpression of *Dtl* promotes hepatocellular carcinoma (HCC) proliferation and invasion *in vitro* and *in vivo*, while its knockdown attenuates both phenotypes.[46-48] *Dtl* has been shown to relieve transcriptional repression in HCC cell lines, indicating that *Dtl* may be a causative mediator in liver cell proliferation.[47] *Cdc6* (encoding cell division cycle 6), *Top2a* (encoding DNA topoisomerase II alpha), and *Mki67* (encoding Ki67) play critical roles in the cell cycle. *Cdc6* functions in the assembly of prereplicative complexes at origins of replication and participates in checkpoint control before mitosis. Increased expression of *Cdc6* may promote DNA hyperreplication or oncogenesis.[49] Overexpression of *Cdc6* in HCC cells promoted cell proliferation and metastatic markers.[50] *Top2a* is a crucial part of the DNA replisome and regulates chromatin topology by catalyzing transient DNA double-stranded breaks and facilitating the relief of super-helical stress.[51] *In vitro* and *in vivo* knockdown and overexpression of *Top2a* can inhibit or promote HCC proliferation and metastasis, respectively.[52] Ki67 is a well-known marker of cellular proliferation and plays a key role in mitosis by preventing aggregation of mitotic chromosomes.[53-57] Despite its universal expression in proliferative cells, Ki67 is dispensable for proliferation using several established cancer cell lines, yet its knockdown reduced tumorigenesis potentially through altered chromatin accessibility.[58]

However, *in vitro* studies investigating the role of *Dtl*, *Cdc6*, *Top2a*, and *Mki67* in lipid-treated hepatocytes are needed to investigate their potential causative roles in liver steatosis.

Elevated mRNA abundances of *Dtl*, *Top2a*, *Cdc6*, and *Mki67* are associated with highly proliferative phenotypes in HCC, a disease that can emerge as a long-term consequence of liver steatosis.[48,50,59-63] We detected increased mRNA abundance of *Dtl*, *Top2a*, *Cdc6*, and *Mki67* in liver before development of macrovesicular steatosis in hepAGT +/+ mice, suggesting that cell proliferation precedes WD-induced liver pathology. This observation is consistent with several recent reports which indicate that early liver proliferation is a key driver of hepatic steatosis.[56,64,65] Expression of *Top2a*, *Cdc6*, and *Mki67* is dynamically regulated within the cell cycle,[57,66,67] suggesting that the upregulation of these genes by WD feeding may occur subsequent to proliferative intracellular signaling. *Dtl* relieves transcriptional repression through ubiquitination of several transcriptional modulators.[47,68] These data suggest that *Dtl* may promote cell proliferation and downstream upregulation of *Top2a*, *Cdc6*, and *Mki67*.[69] Interestingly, *Smpd3* is often reported as a tumor-suppressing gene in HCC. Overexpression of *Smpd3* in HCC reduced cell proliferation.[70] *In vitro*, overexpression of *Smpd3* has been shown to promote palmitate-induced insulin resistance.[39] Disruption of PI3K/Akt signaling and enhanced stress responses resulting from insulin resistance suggest a potential opposing relationship between *Smpd3* and *Dtl* in the context of WD-induced steatosis. While our findings and previous literature suggest potential mechanisms by which *Smpd3*, *Dtl*, *Cdc6*, *Top2a*, and *Mki67* contribute to liver steatosis, further study is needed to clarify their precise roles. Taken together, it is important to understand the complex interplay between WD, AGT, and hepatocyte proliferation in the pathophysiology of liver steatosis.

In the present study, bulk RNA sequencing was performed to determine transcriptomic alterations in livers. A key limitation of bulk RNA sequencing is its inability to resolve cellular heterogeneity, which precludes the identification of cell-specific changes in gene expression.[71] The responses of heterogenous liver cell populations to WD-feeding, particularly in respect to hepatocyte zonality and the regulatory roles of parenchymal cells, remain critical areas of interest in understanding the link between AGT and liver steatosis. As such, single-cell, single-nuclei, and spatial transcriptomic approaches represent promising tools for future investigations into the relationship between the target genes identified in this study and their potential contributions to AGT-mediated liver steatosis.

The present study used a ketamine/xylazine cocktail to euthanize mice that has the potential to impact metabolic organs, such as the liver.[72] However, in the present study, mice were rapidly perfused with cold saline by left ventricular puncture, and livers were immediately processed for RNA extraction. Furthermore, all study mice were euthanized and processed in the same manner in a random order. Therefore, we infer that any variation in liver transcriptomes due to the euthanasia method would not interfere with data analyses and interpretation.

5. Conclusion

Our integrated transcriptomic analyses identified five target genes related to cell division that may contribute to the development of liver steatosis mediated by WD and AGT. This study provides insights into the role of the RAS in WD-induced hepatic steatosis.

Acknowledgments

None.

Funding

This research work is supported by the National Institutes of Health (R01HL139748, R35HL155649, and TL1TR001997) and a MERIT award from the American Heart Association (23MERIT1036341). The content in this article is solely the responsibility of the authors and does not necessarily represent the official views of the National Institutes of Health.

Conflict of interest

Alan Daugherty is an Honorary Editor-in-Chief, and Hong S. Lu is an Editorial Board Member of this journal, but they were not in any way involved in the editorial and peer-review process conducted for this paper, directly or indirectly. Separately, other authors declared that they have no known competing financial interests or personal relationships that could have influenced the work reported in this paper.

Author contributions

Conceptualization: Alan Daugherty, Hong S. Lu, Hisashi Sawada
Formal analysis: Alex C. Pettey, Hisashi Sawada
Investigation: Alex C. Pettey, Dien Ye, Sohei Ito
Methodology: Alan Daugherty, Hong S. Lu, Hisashi Sawada
Writing–original draft: Alex C. Pettey
Writing–review & editing: Dien Ye, Sohei Ito, Alan Daugherty, Hong S. Lu, Hisashi Sawada

Ethics approval and consent to participate

All experiments were performed according to a protocol approved by the Institutional Animal Care and Use Committee at the University of Kentucky (Protocol #2015-2050) in accordance with the guidelines of the National Institutes of Health.

Consent for publication

Not applicable.

Availability of data

RNA sequencing data (raw FASTQ and aligned data) are publicly available at the gene expression omnibus (GEO) repository (GSE291082). The data that support the findings of this study are also available from the corresponding authors on reasonable request.

Further disclosure

The findings which are presented in the current manuscript in Figure 2A and Figure 3C were previously presented at the following conferences:

1. 09/2022 Pettey, AC, Sawada, H, Ye, D, Wu, C, Daugherty, A, Lu, HS. Hepatocyte-specific angiotensinogen deficiency prevents Western diet-induced fatty liver in mice. Fredrickson Lipid Research Conference, Durham, NC, USA. *Poster presentation by Pettey AC.*
2. 10/2022 Pettey, AC, Sawada, H, Amioka, N, Ye, D, Wu, C, Daugherty, A, Lu, HS. Hepatocyte-specific deletion of angiotensinogen ameliorates Western diet-induced hepatic steatosis with a suppression of the transcriptome related to inflammation. Kentucky Chapter of the American Physiological Society Annual Meeting, University of Kentucky. *Oral and poster presentations by Pettey AC.*
3. 10/2022 Pettey, AC, Sawada, H, Amioka, N, Ye, D, Wu, C, Daugherty, A, Lu, HS. Western diet-induced hepatic steatosis is ameliorated by hepatocyte-specific angiotensinogen deletion with suppression of complement component C4. Saha Cardiovascular Research Day, Lexington, KY, USA. *Poster presentation by Pettey AC.*
4. 5/2023 Pettey AC, Sawada H, Ye D, Wu C, Daugherty A, Lu HS. Complement component C4 suppression accompanies abatement of steatosis in hepatocyte-specific angiotensinogen deficient mice. Vascular Discovery. Boston, MA, USA. *Poster presentation by Pettey AC.*

References

1. Younossi ZM, Koenig AB, Abdelatif D, Fazel Y, Henry L, Wymer M. Global epidemiology of nonalcoholic fatty liver disease-Meta-analytic assessment of prevalence, incidence, and outcomes. *Hepatology*. 2016;64:73-84.

   doi: 10.1002/hep.28431

2. Cotter TG, Rinella M. Nonalcoholic fatty liver disease 2020: The state of the disease. *Gastroenterology*. 2020;158:1851-1864.

   doi: 10.1053/j.gastro.2020.01.052

3. Loomba R, Sanyal AJ. The global NAFLD epidemic. *Nat Rev Gastroenterol Hepatol*. 2013;10:686-690.

   doi: 10.1038/nrgastro.2013.171

4. Teng ML, Tan DJH, Ng CH, Huang DQ. Hepatocellular carcinoma surveillance in non-alcoholic fatty liver disease-who and how? *Clin Mol Hepatol*. 2023;29:404-407.

   doi: 10.3350/cmh.2023.0069

5. Gwaltney-Brant SM. In: Gupta RC, editor. *Nutraceuticals in Renal Diseases*. Ch. 8. United States: Academic Press; 2016. p. 101-108.

6. Ma W, Wu W, Wen W, *et al*. Association of NAFLD with cardiovascular disease and all-cause mortality: A large-scale prospective cohort study based on UK Biobank. *Ther Adv Chronic Dis*. 2022;13:20406223221122478.

   doi: 10.1177/20406223221122478

7. Engin A. Non-alcoholic fatty liver disease. *Adv Exp Med Biol*. 2017;960:443-467.

   doi: 10.1007/978-3-319-48382-5_19

8. Yki-Jarvinen H, Luukkonen PK, Hodson L, Moore JB. Dietary carbohydrates and fats in nonalcoholic fatty liver disease. *Nat Rev Gastroenterol Hepatol*. 2021;18:770-786.

   doi: 10.1038/s41575-021-00472-y

9. Stephenson K, Kennedy L, Hargrove L, *et al*. Updates on dietary models of nonalcoholic fatty liver disease: Current studies and insights. *Gene Expr*. 2018;18:5-17.

   doi: 10.3727/105221617X15093707969658

10. Matsusaka T, Niimura F, Shimizu A, *et al*. Liver angiotensinogen is the primary source of renal angiotensin II. *J Am Soc Nephrol*. 2012;23:1181-1189.

    doi: 10.1681/ASN.2011121159

11. Lu H, Wu C, Howatt DA, *et al*. Angiotensinogen exerts effects independent of Angiotensin II. *Arterioscler Thromb Vasc Biol*. 2016;36:256-265.

    doi: 10.1161/ATVBAHA.115.306740

12. Kukida M, Cai L, Ye D, *et al*. Renal angiotensinogen is predominantly liver derived in nonhuman primates. *Arterioscler Thromb Vasc Biol*. 2021;41:2851-2853.

    doi: 10.1161/atvbaha.121.316590

13. Daugherty A, Sawada H, Sheppard MB, Lu HS. Angiotensinogen as a therapeutic target for cardiovascular

and metabolic diseases. *Arterioscler Thromb Vasc Biol*. 2024;44:1021-1030.

doi: 10.1161/ATVBAHA.124.318374

14. Tao XR, Rong JB, Lu HS, *et al*. Angiotensinogen in hepatocytes contributes to Western diet-induced liver steatosis. *J Lipid Res*. 2019;60:1983-1995.

doi: 10.1194/jlr.M093252

15. Ye D, Wu C, Cai L, *et al*. Antisense oligonucleotides targeting hepatic angiotensinogen reduce atherosclerosis and liver steatosis in hypercholesterolemic mice. *Glob Transl Med*. 2023;2:288.

doi: 10.36922/gtm.288

16. Dutta S, Sengupta P. Men and mice: Relating their ages. *Life Sci*. 2016;152:244-248.

doi: 10.1016/j.lfs.2015.10.025

17. Temple JL, Cordero P, Li J, Nguyen V, Oben JA. A guide to non-alcoholic fatty liver disease in childhood and adolescence. *Int J Mol Sci*. 2016;17:947.

doi: 10.3390/ijms17060947

18. Boyraz M, Hatipoglu N, Sari E, *et al*. Non-alcoholic fatty liver disease in obese children and the relationship between metabolic syndrome criteria. *Obes Res Clin Pract*. 2014;8:e356-363.

doi: 10.1016/j.orcp.2013.08.003

19. Berardis S, Sokal E. Pediatric non-alcoholic fatty liver disease: An increasing public health issue. *Eur J Pediatr*. 2014;173:131-139.

doi: 10.1007/s00431-013-2157-6

20. Ratziu V, Bellentani S, Cortez-Pinto H, Day C, Marchesini G. A position statement on NAFLD/NASH based on the EASL 2009 special conference. *J Hepatol*. 2010;53:372-384.

doi: 10.1016/j.jhep.2010.04.008

21. Team RC. R: A language and environment for statistical computing. *R Foundation for Statistical Computing*; 2021. Available from: https://www.r-project.org [Last accessed on 2022 Dec 16].

22. Robinson MD, McCarthy DJ, Smyth GK. edgeR: A Bioconductor package for differential expression analysis of digital gene expression data. *Bioinformatics*. 2010;26:139-140.

doi: 10.1093/bioinformatics/btp616

23. Carlson M. Genome wide annotation for Mouse. R package version 3.14.0; 2021. Available from: https://bioconductor.org/packages/release/data/annotation/html/org.Mm.eg.db.html [Last accessed on 2021 Jun 15].

24. Wu T, Hu E, Xu S, *et al*. clusterProfiler 4.0: A universal enrichment tool for interpreting omics data. *Innovation* (*Camb*). 2021;2:100141.

doi: 10.1016/j.xinn.2021.100141

25. Yu G, Wang LG, Han Y, He QY. clusterProfiler: An R package for comparing biological themes among gene clusters. *OMICS*. 2012;16:284-287.

doi: 10.1089/omi.2011.0118

26. Tang D, Chen M, Huang X, *et al*. SRplot: A free online platform for data visualization and graphing. *PLoS One*. 2023;18:e0294236.

doi: 10.1371/journal.pone.0294236

27. Gaemers IC, Stallen JM, Kunne C, *et al*. Lipotoxicity and steatohepatitis in an overfed mouse model for non-alcoholic fatty liver disease. *Biochim Biophys Acta*. 2011;1812:447-458.

doi: 10.1016/j.bbadis.2011.01.003

28. Spooner MH, Garcia-Jaramillo M, Apperson KD, Lohr CV, Jump DB. Time course of western diet (WD) induced nonalcoholic steatohepatitis (NASH) in female and male Ldlr-/-mice. *PLoS One*. 2023;18:e0292432.

doi: 10.1371/journal.pone.0292432

29. Rinella ME, Neuschwander-Tetri BA, Siddiqui MS, *et al*. AASLD Practice Guidance on the clinical assessment and management of nonalcoholic fatty liver disease. *Hepatology*. 2023;77:1797-1835.

doi: 10.1097/HEP.0000000000000323

30. Milic S, Stimac D. Nonalcoholic fatty liver disease/steatohepatitis: Epidemiology, pathogenesis, clinical presentation and treatment. *Dig Dis*. 2012;30:158-162.

doi: 10.1159/000336669

31. Basaranoglu M, Neuschwander-Tetri BA. Nonalcoholic fatty liver disease: Clinical features and pathogenesis. *Gastroenterol Hepatol (N Y)*. 2006;2:282-291.

32. Brunt EM, Tiniakos DG. Histopathology of nonalcoholic fatty liver disease. *World J Gastroenterol*. 2010;16:5286-5296.

doi: 10.3748/wjg.v16.i42.5286

33. Khoonsari M, Mohammad Hosseini Azar M, Ghavam R, *et al*. Clinical manifestations and diagnosis of nonalcoholic fatty liver disease. *Iran J Pathol*. 2017;12:99-105.

34. Li X, Wang Z, Klaunig JE. Modulation of xenobiotic nuclear receptors in high-fat diet induced non-alcoholic fatty liver disease. *Toxicology*. 2018;410:199-213.

doi: 10.1016/j.tox.2018.08.007

35. Park WJ, Song JH, Kim GT, Park TS. Ceramide and sphingosine 1-phosphate in liver diseases. *Mol Cells*. 2020;43:419-430.

doi: 10.14348/molcells.2020.0054

36. Al-Rashed F, Arefanian H, Madhoun AA, *et al*. Neutral sphingomyelinase 2 inhibition limits hepatic steatosis and inflammation. *Cells*. 2024;13:463.

doi: 10.3390/cells13050463

37. Nikolova-Karakashian M, Karakashian A, Rutkute K. Role of neutral sphingomyelinases in aging and inflammation. *Subcell Biochem*. 2008;49:469-486.

doi: 10.1007/978-1-4020-8831-5_18

38. Summers SA. Ceramides: Nutrient signals that drive hepatosteatosis. *J Lipid Atheroscler*. 2020;9:50-65.

doi: 10.12997/jla.2020.9.1.50

39. El-Amouri S, Karakashian A, Bieberich E, Nikolova-Karakashian M. Regulated translocation of neutral sphingomyelinase-2 to the plasma membrane drives insulin resistance in steatotic hepatocytes. *J Lipid Res*. 2023;64:100435.

doi: 10.1016/j.jlr.2023.100435

40. Geilen CC, Wieder T, Orfanos CE. Ceramide signalling: regulatory role in cell proliferation, differentiation and apoptosis in human epidermis. *Arch Dermatol Res*. 1997;289:559-566.

doi: 10.1007/s004030050240

41. Hajduch E, Lachkar F, Ferre P, Foufelle F. Roles of ceramides in non-alcoholic fatty liver disease. *J Clin Med*. 2021;10:792.

doi: 10.3390/jcm10040792

42. Raichur S, Brunner B, Bielohuby M, *et al*. The role of C16:0 ceramide in the development of obesity and type 2 diabetes: CerS6 inhibition as a novel therapeutic approach. *Mol Metab*. 2019;21:36-50.

doi: 10.1016/j.molmet.2018.12.008

43. Saddoughi SA, Ogretmen B. Diverse functions of ceramide in cancer cell death and proliferation. *Adv Cancer Res*. 2013;117:37-58.

doi: 10.1016/B978-0-12-394274-6.00002-9

44. Rossi M, Duan S, Jeong YT, *et al*. Regulation of the CRL4(Cdt2) ubiquitin ligase and cell-cycle exit by the SCF(Fbxo11) ubiquitin ligase. *Mol Cell*. 2013;49:1159-1166.

doi: 10.1016/j.molcel.2013.02.004

45. Huh J, Piwnica-Worms H. CRL4(CDT2) targets CHK1 for PCNA-independent destruction. *Mol Cell Biol*. 2013;33: 213-226.

doi: 10.1128/MCB.00847-12

46. Liu Z, Yang G, Yi X, *et al*. Osteopontin regulates the growth and invasion of liver cancer cells via DTL. *Oncol Lett*. 2023;26:476.

doi: 10.3892/ol.2023.14064

47. Chen ZX, Mu MY, Yang G, *et al*. Hypoxia-induced DTL promotes the proliferation, metastasis, and sorafenib resistance of hepatocellular carcinoma through ubiquitin-mediated degradation of SLTM and subsequent Notch pathway activation. *Cell Death Dis*. 2024;15:734.

doi: 10.1038/s41419-024-07089-4

48. Dong R, Zhang D, Han B, *et al*. DTL is a novel downstream gene of E2F1 that promotes the progression of hepatocellular carcinoma. *Curr Cancer Drug Targets*. 2023;23:817-828.

doi: 10.2174/1568009623666230511100246

49. Borlado LR, Mendez J. CDC6: From DNA replication to cell cycle checkpoints and oncogenesis. *Carcinogenesis*. 2008;29:237-243.

doi: 10.1093/carcin/bgm268

50. Shi Y, Yan F, Wang F, Pan L. MiR-128-3p suppresses tumor proliferation and metastasis via targeting CDC6 in hepatocellular carcinoma cells. *Tissue Cell*. 2021;72:101534.

doi: 10.1016/j.tice.2021.101534

51. Uuskula-Reimand L, Wilson MD. Untangling the roles of TOP2A and TOP2B in transcription and cancer. *Sci Adv*. 2022;8:eadd4920.

doi: 10.1126/sciadv.add4920

52. Wang T, Lu J, Wang R, Cao W, Xu J. TOP2A promotes proliferation and metastasis of hepatocellular carcinoma regulated by miR-144-3p. *J Cancer*. 2022;13:589-601.

doi: 10.7150/jca.64017

53. Assy N, Minuk GY. Liver regeneration: methods for monitoring and their applications. *J Hepatol*. 1997; 26:945-952.

doi: 10.1016/s0168-8278(97)80266-8

54. Huang Z, Zhou P, Li S, Li K. Prediction of the Ki-67 marker index in hepatocellular carcinoma based on dynamic contrast-enhanced ultrasonography with sonazoid. *Insights Imaging*. 2022;13:199.

doi: 10.1186/s13244-022-01320-6

55. Trauner M, Fuchs CD. Novel therapeutic targets for cholestatic and fatty liver disease. *Gut*. 2022;71:194-209.

doi: 10.1136/gutjnl-2021-324305

56. Cast A, Kumbaji M, D'Souza A, *et al*. Liver proliferation is an essential driver of fibrosis in mouse models of nonalcoholic fatty liver disease. *Hepatol Commun*. 2019;3:1036-1049.

doi: 10.1002/hep4.1381

57. Sun X, Kaufman PD. Ki-67: More than a proliferation marker. *Chromosoma*. 2018;127:175-186.

doi: 10.1007/s00412-018-0659-8

58. Mrouj K, Andres-Sanchez N, Dubra G, *et al*. Ki-67 regulates global gene expression and promotes sequential stages of carcinogenesis. *Proc Natl Acad Sci U S A*. 2021;118:e2026507118.

doi: 10.1073/pnas.2026507118

59. Li Z, Wang R, Qiu C, *et al*. Role of DTL in hepatocellular carcinoma and its impact on the tumor microenvironment. *Front Immunol*. 2022;13:834606.

doi: 10.3389/fimmu.2022.834606

60. Chen YC, Chen IS, Huang GJ, *et al*. Targeting DTL induces cell cycle arrest and senescence and suppresses cell growth and colony formation through TPX2 inhibition in human hepatocellular carcinoma cells. *Onco Targets Ther*. 2018;11:1601-1616.

doi: 10.2147/OTT.S147453

61. Jia W, Liu X, Zhang Z. Role of TOP2A and CDC6 in liver cancer. *Medicine (Baltimore)*. 2023;102:e35604.

doi: 10.1097/MD.0000000000035604

62. Wang K, Jiang X, Jiang Y, *et al*. EZH2-H3K27me3-mediated silencing of mir-139-5p inhibits cellular senescence in hepatocellular carcinoma by activating TOP2A. *J Exp Clin Cancer Res*. 2023;42:320.

doi: 10.1186/s13046-023-02855-2

63. Ramos-Santillan V, Oshi M, Nelson E, Endo I, Takabe K. High Ki67 gene expression is associated with aggressive phenotype in hepatocellular carcinoma. *World J Oncol*. 2024;15:257-267.

doi: 10.14740/wjon1751

64. Jin J, Valanejad L, Nguyen TP, *et al*. Activation of CDK4 triggers development of non-alcoholic fatty liver disease. *Cell Rep*. 2016;16:744-756.

doi: 10.1016/j.celrep.2016.06.019

65. Denechaud PD, Lopez-Mejia IC, Giralt A, *et al*. E2F1 mediates sustained lipogenesis and contributes to hepatic steatosis. *J Clin Invest*. 2016;126:137-150.

doi: 10.1172/JCI81542

66. Chen T, Sun Y, Ji P, Kopetz S, Zhang W. Topoisomerase IIalpha in chromosome instability and personalized cancer therapy. *Oncogene*. 2015;34:4019-4031.

doi: 10.1038/onc.2014.332

67. El Dika M, Dudka D, Kloc M, Kubiak JZ. CDC6 as a key inhibitory regulator of CDK1 activation dynamics and the timing of mitotic entry and progression. *Biology (Basel)*. 2023;12:855.

doi: 10.3390/biology12060855

68. Fesler A, Zhang N, Ju J. The expanding regulatory universe of p53 in gastrointestinal cancer. *F1000Res*. 2016;5:756.

doi: 10.12688/f1000research.8363.1

69. Song B, Wang Y, Titmus MA, *et al*. Molecular mechanism of chemoresistance by miR-215 in osteosarcoma and colon cancer cells. *Mol Cancer*. 2010;9:96.

doi: 10.1186/1476-4598-9-96

70. Revill K, Wang T, Lachenmayer A, *et al*. Genome-wide methylation analysis and epigenetic unmasking identify tumor suppressor genes in hepatocellular carcinoma. *Gastroenterology*. 2013;145:1424-1435.e1421-1425.

doi: 10.1053/j.gastro.2013.08.055

71. Jovic D, Liang X, Zeng H, Lin L, Xu F, Luo Y. Single-cell RNA sequencing technologies and applications: A brief overview. *Clin Transl Med*. 2022;12:e694.

doi: 10.1002/ctm2.694

72. Tobar Leitao SA, Soares DDS, Carvas Junior N, Zimmer R, Ludwig NF, Andrades M. Study of anesthetics for euthanasia in rats and mice: A systematic review and meta-analysis on the impact upon biological outcomes (SAFE-RM). *Life Sci*. 2021;284:119916.

doi: 10.1016/j.lfs.2021.119916

Appendix

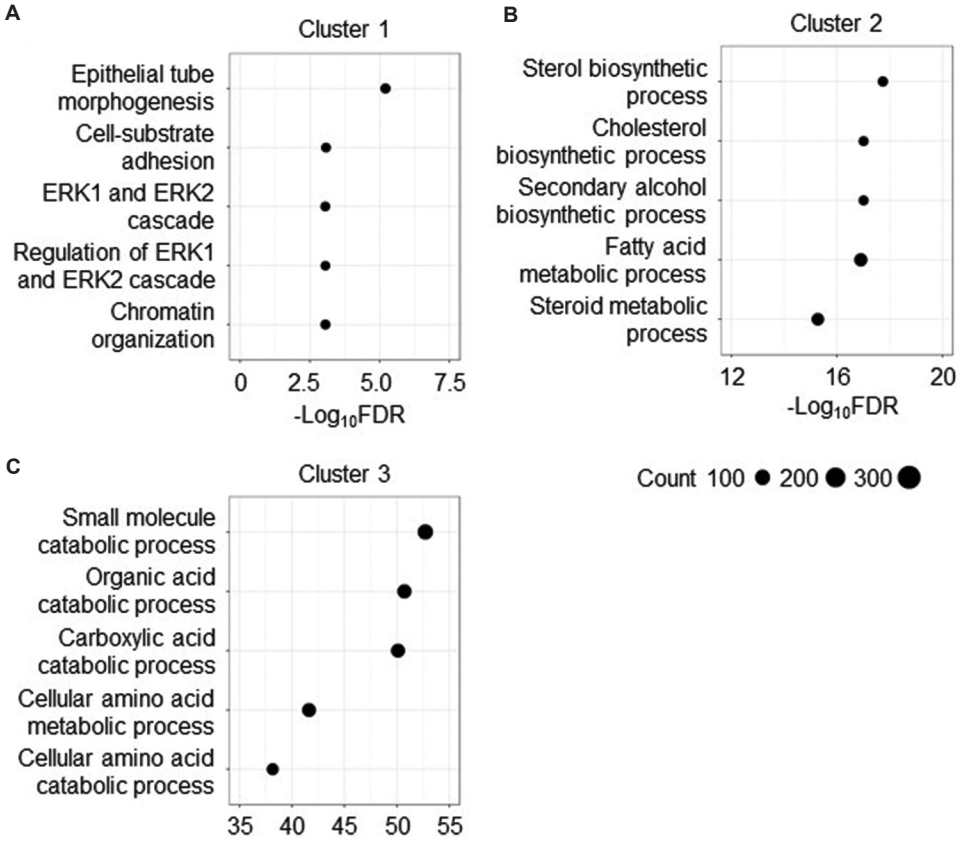

Figure A1. Gene ontology enrichment analysis for biological processes within subclustered DEGs of hepAGT +/+ mice fed WD for 5, 14, or 42 days and compared against mice fed for 0 days. DEG clusters were assigned by hierarchical clustering analysis. Top five annotations in gene ontology analysis for biological processes using DEGs in Cluster 1 (A), Cluster 2 (B), and Cluster 3 (C). n = 4 – 5 mice/group.
Abbreviations: DEG: Differentially expressed gene; FDR: False discovery rate; hepAGT +/+: Albumin-Cre 0/0 angiotensinogen floxed (f/f) low-density lipoprotein-receptor-deficient background; WD: Western diet.

ACCSCIENCE PUBLISHING

Global Translational Medicine

ORIGINAL RESEARCH ARTICLE

Thyroid morphology and functional alterations in male and female rats with diet-induced visceral obesity

Tatyana A. Mityukova*, Anastasia A. Basalai*, Tatyana E. Kuznetsova, Olga Y. Poluliakh, and Mikita S. Kastsiuchenka

Department of Laboratory of Biomedical Technologies and Medical Rehabilitation, Institute of Physiology, National Academy of Sciences of Belarus, Minsk, Republic of Belarus

Abstract

With obesity reaching epidemic proportions worldwide, its impact on thyroid function is gaining increasing attention. Epidemiological studies show an association between obesity, hypothyroidism, and circulating thyroid antibodies but experimental research is needed to investigate the mechanisms underlying these associations. This study aimed to investigate thyroid function indicators in male and female rats subjected to a high-calorie diet for 16 weeks. We assessed mass-metric indices, blood biochemical markers, thyroid morphometry, and tissue concentrations of triglycerides, malonic dialdehyde (MDA), and thyroperoxidase (TPO) activity. The results revealed biochemical features of metabolic syndrome, including elevated thyroxine (T4) levels in peripheral blood. Morphological analysis indicated steatosis and thyroid hypofunction, with increased triglyceride accumulation, decreased TPO activity, and lower MDA levels in the thyroid tissue. These findings suggest that visceral obesity in male and female rats promotes early signs of thyroid dysfunction, potentially leading to hypothyroidism.

Keywords: High-calorie diet; Visceral obesity; Rats; Thyroid function; Thyroid hormones; Morphological changes

***Corresponding authors:**
Tatyana A. Mityukova (mityukovat@gmail.com)
Anastasia A. Basalai (anastasiya.basalay@gmail.com)

Citation: Mityukova TA, Basalai AA, Kuznetsova TE, Poluliakh OY, Kastsiuchenka MS. Thyroid morphology and functional alterations in male and female rats with diet-induced visceral obesity. *Global Transl Med*. 2025;4(2):86-95. doi: 10.36922/GTM025080020

Received: February 22, 2025

Revised: March 28, 2025

Accepted: April 1, 2025

Published online: April 16, 2025

1. Introduction

The link between obesity and endocrine dysfunction, including thyroid pathology, has been well established in many studies. As obesity reaches epidemic proportions worldwide, this relationship has gained increasing clinical relevance.[1] Thyroid hormones are known to play an important role in the regulation of metabolism. Elevated blood levels of thyroxine (T4) and triiodothyronine (T3) increase resting energy expenditure (REE), reducing fat accumulation. These hormones increase REE through sodium-potassium adenosine triphosphatase activity and activate the adrenergic nervous system to enhance thermogenesis, particularly in cold conditions.[2] This process, called "adaptive thermogenesis," occurs in brown adipose tissue through the thyroid hormone receptors TRα and TRβ.[2]

Obese individuals usually exhibit slightly elevated thyroid-stimulating hormone (TSH) levels, which correlate positively with body mass index (BMI).[3] A characteristic

hormonal pattern in obesity includes reduced free T4 (fT4) levels and moderately elevated levels of total or free T3 (fT3) levels. In addition, the fT3/fT4 ratio has been positively associated with waist circumference and BMI in obese patients.[3] The mechanisms underlying these changes remain controversial.

Leptin, an adipose tissue hormone, plays an important role in the regulation of the hypothalamic-pituitary-thyroid axis. It activates this system in response to excess caloric intake. This adaptive response to overnutrition results in a moderate increase in blood levels of thyrotropin-releasing hormone (TRH) and TSH. This is accompanied by a slight increase in circulating thyroid hormone levels within or slightly above the upper limit of normal.[2]

One theory explaining the relationship between obesity and thyroid function is increased deiodinase activity, leading to enhanced conversion of T4 to T3.[2] This may serve as a compensatory mechanism to counteract fat accumulation by increasing energy expenditure.[2] Another hypothesis suggests that obesity-induced reductions in TSH receptor expression in the thyroid and T4/T3 receptor expression in adipocytes drive compensatory increases in TSH and fT3 secretion.[2] In addition, leptin influences thyroid function by stimulating the central conversion of prothyroliberin to TRH and, consequently, the synthesis of TSH. Leptin also increases the activity of deiodinases. Pro-inflammatory cytokines secreted by adipose tissue – such as tumor necrosis factor-alpha, interleukin-1 (IL)1, and IL-6 – may also contribute to thyroid dysfunction by inhibiting sodium/iodide symporter Na+/I- symporter (NIS) mRNA expression and iodide uptake.[2]

Epidemiological studies suggest that the risk of obesity is associated with elevated TSH levels and reduced concentrations of the free T4 and T3 hormones.[4,5] These data suggest that reduced levels of circulating thyroid hormones are a predictor of obesity. Hypothyroidism and thyroperoxidase antibodies (TPO-Ab) are highly prevalent in people with excess fat mass.[6] A meta-analysis of 22 studies showed that obesity is associated with an increased risk of clinical and subclinical hypothyroidism.[6] Symptoms of hypothyroidism, including reduced physical activity, fatigue, sleepiness, memory loss, cold intolerance, weight gain, and constipation, often develop gradually. Another meta-analysis found that obesity was significantly associated with Hashimoto's thyroiditis, but not with Graves' disease. Weight gain correlated with TPO-Ab positivity but not with thyroglobulin antibodies (TG-Ab).[6] However, some studies have reported associations between subclinical hypothyroidism and both TPO-Ab and TG-Ab. A survey of 2,505 subjects showed that 11.5% of the subjects (289/2505) were obese, of whom 165 (57%) had subclinical hypothyroidism. Thyroid autoantibodies (TPO-Ab and TG-Ab) were found in 17.64% of the obese subjects.[7] Thus, a large body of data in the literature highlights the role of autoimmune processes in obesity-related thyroid glands. However, alternative mechanisms influencing thyroid hormone synthesis remain to be fully elucidated and warrant further investigation.

The aim of this study was to investigate indices of thyroid functional activity in diet-induced visceral obesity in male and female rats.

2. Materials and methods

2.1. Animals and diets

This study was conducted on 2-month-old sexually mature male and female Wistar rats. These rats were bred in-house in a certified vivarium at the Institute of Physiology of the National Academy of Sciences of Belarus. The rats were kept under controlled conditions (12/12 h light/dark cycle, 22 ± 2°C temperature, and 60 – 65% humidity). The male (n = 27) and female (n = 27) Wistar rats were randomly divided into two experimental groups: control and high-calorie diet (HCD). The control group, consisting of 13 male and 14 female rats, received a standard diet (StD; the normal diet at the vivarium), while the HCD group, comprising 14 male and 13 female rats, was given an HCD for 16 weeks.

The HCD consisted of StD supplemented with animal fats (lard), consisting of 45% of daily caloric intake, along with a 10% fructose solution provided *ad libitum* in place of water.[8] The caloric intake was 150 kcal/day for StD and 228 kcal/day for HCD.

This study was approved by the Bioethics Committee of the Institute of Physiology, National Academy of Sciences of Belarus (Protocol No.1, January 22, 2021; Protocol No.2, February 2, 2022) and conducted in accordance with the guidelines set forth by the European Convention for the Protection of Vertebrate Animals (ETS No. 123).

Euthanasia was performed through decapitation under sodium thiopental anesthesia. Female rats were euthanized during the diestrus phase of the estrous cycle, determined by the type of cells present in vaginal swabs.[9]

Body weight of the rats was measured using a weighing scale (Saturn ST-KS7230, China). After euthanasia, the visceral fat was collected and weighed on a laboratory weighing scale (Scout Pro, China). For male rats, the visceral fat mass included paranephral and epididymal fat deposits, while for female rats, it included paranephral and periovarian fat deposits. The mass coefficient (MC) of the visceral fat was calculated using the following formula: (Visceral fat mass/body weight) ×100%.

2.2. Morphological analysis

At necropsy, the thyroid gland was extracted from the animals for morphologic examination. Thyroid tissue fragments were subjected to rapid freezing in an HM 525 cryostat (MICROM International GmbH, Germany). Cryostat sections (7 μm) were stained with hematoxylin-eosin for structural analysis. Microstructure examination, morphometry, and microphotography were performed using a light microscope (Altami LUM-1, Altami LLC, Russia) equipped with a digital camera (1300D EOS Body, Canon, Japan).

Images were analyzed using ImageJ software (National Institutes of Health, USA). For thyroid follicles counted in ten fields of view at ×400 magnification, we measured follicle area (in μm^2), inner follicle diameter (in μm), and follicular epithelium height (in μm). The colloid accumulation index (CAI) was calculated as the ratio of the inner follicle diameter to twice the follicular epithelium height.

2.3. Biochemical and hormonal parameters

Biochemical parameters in blood serum and thyroid homogenates (diluted 1:80 in 0.05 M PBS) were determined using a BS-200 biochemical automatic analyzer (Shenzhen Mindray Bio-Medical Electronics, China) and commercial kits (Production Unitary Enterprise "Diasens," Belarus). Quality control was performed using control sera (Randox Laboratories, UK). Malonic dialdehyde (MDA) levels in thyroid homogenates were determined using the spectrophotometric method by reaction with thiobarbituric acid.[10] Thyroid peroxidase (TPO) activity was estimated based on iodide oxidation reaction in the presence of hydrogen peroxide, producing molecular iodine and I_3^- (periodide ion).[11] The periodide concentration, determined spectrophotometrically at 353 nm, was used to estimate TPO activity in thyroid tissue.[12] The triiodothyronine (T3) and thyroxine (T4) levels in blood serum were determined by enzyme immunoassay using commercial kits (Xema Co., Russia).

2.4. Statistical analysis

Statistical analysis was performed using Statistica 10.0 (Tibco, USA). Normality was assessed with the Shapiro–Wilk test. Parametric variables were expressed as mean ± standard deviation and analyzed with Student's t-test. Non-parametric variables were expressed as 25th percentiles, median, and 75th percentiles and analyzed using the Mann–Whitney U-test. Correlation analysis was performed using the Pearson correlation coefficient. A $p<0.05$ was considered statistically significant for all tests.

3. Results

3.1. Mass-metric parameters

At the start of the experiment, male and female rats (2 months old) weighed approximately 220 – 230 g. After 16 weeks, the mean body weight of males in the control group was 433.46 ± 48.38 g, while those in the HCD group reached 471.14 ± 94.11 g. The mean body weight of females in the control group was 310.93 ± 25.43 g, while that of the HCD group was 316.31 ± 72.07 g. No significant differences in final body weight were observed between the control and HCD groups of the same sex.

Male rats in the control group had visceral adipose tissue that weighed 7.99 ± 2.64 g and had an MC of 1.82 ± 0.49%. In the HCD group, these values increased significantly to 22.99 g ± 11.97 g ($p<0.001$) and 4.64 ± 1.67% ($p<0.0001$), respectively (Figure 1A and B). In female rats, visceral fat mass was 8.86 ± 4.86 g in the control group (MC: 2.78 ± 1.31%) and significantly higher than in the HCD group (17.22 ± 9.07 g, $p=0.006$; MC: 5.15 ± 2.11%; $p=0.002$) (Figure 1A and B). These data indicate the development of visceral obesity in rats of both sexes following HCD administration.

3.2. Morphological analysis of the thyroid gland

The examination of thyroid gland preparations from control male and female rats revealed a well-developed follicular structure with thin connective tissue septa separating gland lobules (Figure 2A and C). The follicles were round or angular, lined with single-layer cuboidal epithelium, and larger at the gland periphery compared to the center. The follicular cavities contained colloid, including thyroglobulin. Thyrocytes had a cubic shape, with nuclei located in the basal part of the cell (Figure 2B and D). Their cytoplasm appeared oxyphilic, and the cells were tightly adherent. Interfollicular islets, consisting of poorly differentiated thyrocytes, were observed between follicles. These features indicate that the thyroid glands of rats maintained on a balanced diet were within physiological norms.

In the HCD group, male rats maintained the thyroid gland's lobular structure (Figure 3A), but follicles enlarged with colloid accumulation (Figure 3A). The walls of follicles were thinned (Figure 3B) and thyrocytes appeared flattened, revealing pyknotic nuclei surrounded by a thin rim of cytoplasm. The number of interfollicular islets was insignificant, and moderate diffuse leukocytic infiltration was observed. Large lipid inclusions were frequently visualized near blood vessels (Figure 3A and B). Morphometric analysis relative to the control males showed a statistically significant increase

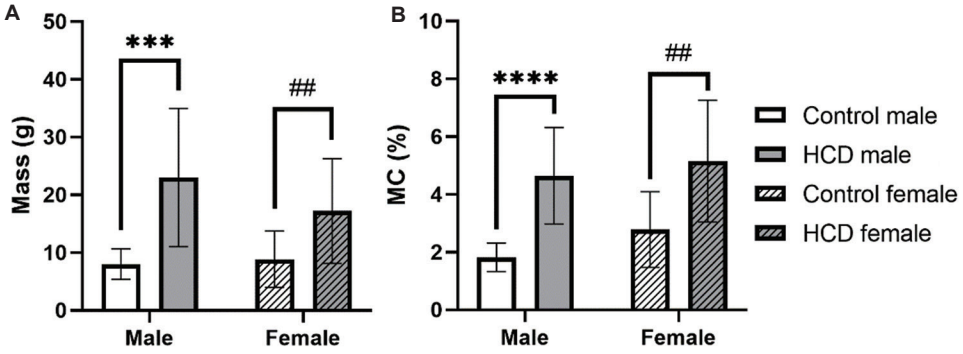

Figure 1. Mass-metric indices of visceral adipose tissue in experimental animals. Mass (A) and MC (B) of visceral adipose tissue in male and female rats. Data are presented as mean ± standard deviation. Statistically significant differences: ***p<0.001, ****p<0.0001 between male HCD and male control groups; ##p<0.01 between female HCD and female control groups.
Abbreviations: HCD: High-calorie diet; MC: Mass coefficient.

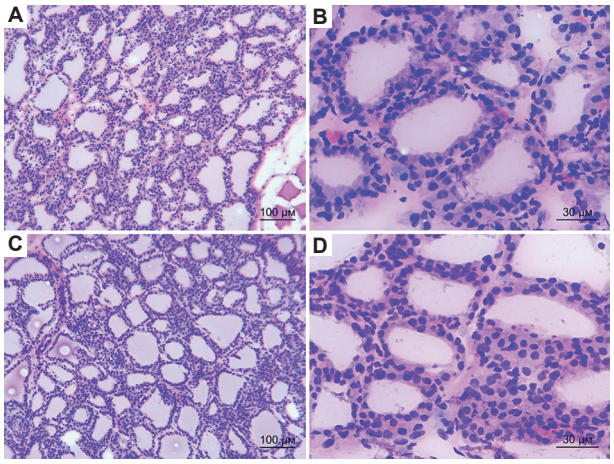

Figure 2. Histological structure of hematoxylin-eosin-stained thyroid glands of control male rats (A and B) and female (C and D) rats. Magnification: A and C: ×100; B and D: ×400.

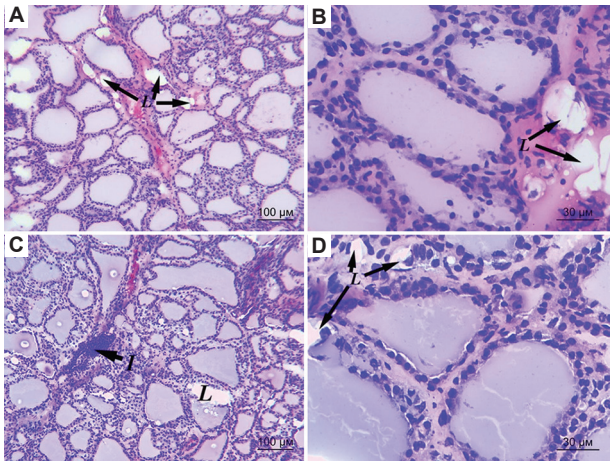

Figure 3. Histological structure of hematoxylin-eosin-stained thyroid glands in HCD male (A and B) and female (C and D) rats. Magnification: A and C: ×100; B and D: ×400.
Abbreviations: HCD: High-calorie diet; I: Inflammatory infiltration; L: Lipid inclusions.

in follicle area (50.7%, p<0.0001), follicle inner diameter (14.0%, p=0.043), and CAI (67.9%, p<0.0001). The height of follicular epithelium was reduced by 37.0% (p<0.0001) (Table 1). These histological and morphometric changes are characteristic of thyroid hypofunction.

In the HCD female rats, the follicular structure of the thyroid was also preserved, with follicles enlarged, colloid accumulation, and flattened thyrocytes (Figure 3C). Moderate diffuse inflammatory infiltration was also evident, with large foci of lymphocytic infiltrate in some regions (Figure 3C). Large lipid inclusions were observed in connective tissue septa and perivascular spaces (Figure 3C and D). Morphometric analysis relative to the control revealed a statistically significant increase in follicular area (73.3%, p<0.0001), follicle inner diameter (36.6%, p<0.0001), and CAI (1.9-fold, p<0.0001). The height of follicular epithelium was reduced by 24.0% (p<0.0001) (Table 1). Similar to HCD male rats, these histological and morphometric alterations suggest thyroid hypofunction.

3.3. Biochemical and hormonal parameters of blood serum and thyroid gland

Biochemical analysis of blood serum from male rats in the HCD group revealed changes associated with liver dysfunction (Table 2). Compared to the control group, a statistically significant change in four liver function markers was observed: urea concentration (−36.3%, p<0.0001), aspartate aminotransferase activity (−12.2%, p=0.019), alkaline phosphatase activity (+80.8%, p=0.009), and total bilirubin level (+71.4%, p=0.007). The HCD female showed similar statistically significant alterations in urea concentration (−42.4%, p<0.0001), alanine aminotransferase activity (−33.3%, p=0.002), alkaline

Table 1. Morphometric indices of thyroid tissue in experimental animals

Index	Male rats		Female rats	
	Control (*n*=13)	HCD (*n*=14)	Control (*n*=14)	HCD (*n*=13)
Follicle area (μm²)	3694.67 (2629.37, 5529.83)	5566.28 (4039.65, 7748.07)****	2513.43 (1737.55, 3932.96)	4355.28 (2677.50, 6265.74)####
Inner follicle diameter (μm)	44.30 (33.27, 56.00)	50.51 (36.27, 65.20)*	39.84 (32.62, 51.49)	54.41 (41.15, 74.41)####
Follicle epithelium height (μm)	7.52 (6.47, 8.32)	4.74 (4.28, 5.27)****	6.63 (6.15, 7.18)	5.04 (4.65, 5.53)####
Colloid accumulation index	3.08 (2.34, 4.05)	5.17 (3.69, 7.07)****	2.95 (2.54, 3.83)	5.58 (4.27, 7.25)####

Note: Data are presented as median (25th percentile, 75th percentile). Statistically significant differences: *p<0.05, ****p<0.0001 between male HCD and male control groups; ####p<0.0001 between female HCD and female control groups.
Abbreviation: HCD: High-calorie diet.

Table 2. Biochemical indices of serum in experimental animals

Index	Male rats		Female rats	
	Control (*n*=13)	HCD (*n*=14)	Control (*n*=14)	HCD (*n*=13)
Total bilirubin (μmol/L)	1.40 (1.20, 1.60)	2.40 (1.60, 3.00)**	2.30 (2.10, 2.90)	3.60 (2.40, 4.20)#
Aspartate aminotransferase (U/L)	196.00 (181.00, 217.00)	172.00 (146.00, 189.00)*	162.00 (144.00, 185.00)	159.00 (129.00, 164.00)
Alanine aminotransferase (U/L)	65.00 (62.00, 74.00)	57.50 (51.00, 68.00)	54.00 (43.00, 67.00)	36.00 (33.00, 41.00)##
Alkaline phosphatase (U/L)	373.00 (333.00, 423.00)	674.50 (371.00, 850.00)**	276.50 (219.00, 392.00)	496.00 (365.00, 661.00)###
Urea (mmol/L)	6.83 (6.45, 8.40)	4.35 (3.45, 4.77)****	6.35 (5.83, 6.73)	3.66 (3.37, 4.21)####
Glucose (mmol/L)	5.81 (5.61, 7.37)	7.54 (7.10, 8.21)**	6.88 (6.07, 7.21)	7.80 (7.24, 8.03)#
Alpha amylase (U/L)	1508 (1426, 1712)	1940 (1788, 2124)***	1556 (1418, 1748)	1758 (1580, 1860)#
Cholesterol (mmol/L)	1.43 (1.23, 1.61)	1.88 (1.50, 1.95)**	1.62 (1.47, 1.77)	1.67 (1.36, 1.90)
Triglycerides (mmol/L)	0.88 (0.63, 1.18)	1.18 (0.94, 2.21)*	1.37 (0.84, 1.80)	0.96 (0.66, 2.47)

Note: Data are presented as median (25th percentile, 75th percentile). Statistically significant differences: *p<0.05, **p<0.01, ***p<0.001, and ****p<0.0001 between male HCD and male control groups; #p<0.05, ##p<0.01, ###p<0.001, and ####p<0.0001.
Abbreviation: HCD: High-calorie diet.

phosphatase activity (+79.4%, p<0.001), and total bilirubin level (+56.5%, p=0.037).

Rats with HCD-induced visceral obesity also showed abnormalities in carbohydrate metabolism and pancreatic function. In relation to control animals, HCD rats exhibited a statistically significant increase in serum glucose concentration (male: 29.8%, p=0.003; female: 13.4%, p=0.047) and alpha-amylase activity (male: 28.6%, p<0.001; female: 13.0%, p=0.036) (Table 2).

In male rats with HCD-induced visceral obesity, a statistically significant increase in serum cholesterol concentration (31.5%, p=0.003), serum triglycerides (61.8%, p=0.029) (Table 2), and thyroid tissue triglycerides (2.5-fold, p=0.020) were observed compared to the control (Figure 4). Notably, these lipid disturbances were absent in female rats.

A statistically significant decrease in TPO activity in the thyroid tissue was observed in the HCD group compared to the controls: by 53.0% (p=0.018) in male rats and by 26.5% (p=0.017) in female rats (Figure 5A). Similarly, MDA content in thyroid tissue was lower in the HCD group

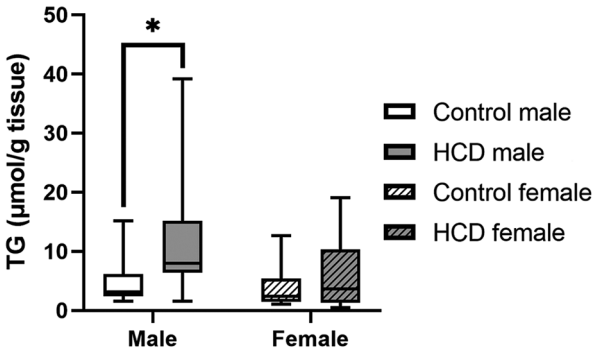

Figure 4. TG content in the thyroid tissue of experimental animals. Data are presented in boxplots showing the 25th percentile, median, and 75th percentile. *p<0.05 indicates a statistically significant difference between male HCD and male control groups.
Abbreviations: HCD: High-calorie diet; TG: Triglyceride.

(male: 30.4%, p=0.005; female: 36.0%, p=0.020) compared to the corresponding controls (Figure 5B). Correlation analysis showed a moderate positive correlation between TPO activity and MDA levels in male rats (r=0.54, p=0.014) but not in female rats.

After 16 weeks of HCD, a statistically significant increase in serum T4 levels by 34.2% (p=0.002) and 29.5% (p=0.020) was observed in male and female rats, respectively, compared with the corresponding control groups (Figure 6A). No differences in serum T3 levels were observed between the experimental groups (Figure 6B).

4. Discussion

Our findings demonstrate that 16 weeks of HCD consumption resulted in a significant increase in visceral fat mass in both male and female rats, with male rats exhibiting an almost threefold increase and females a twofold increase compared to their respective controls. With increasing visceral fat mass, triglyceride levels in both serum and thyroid tissues increased in male but not in female rats. Analysis of serum biochemical parameters further indicated liver and pancreatic dysfunction in HCD-fed rats, consistent with our previous morphological studies, which confirmed fatty liver degeneration following prolonged HCD consumption.[13] These findings align with established models of diet-induced visceral obesity[8] and are comparable to those of Shao *et al.*,[14] who observed similar metabolic and hepatic alterations in rats fed a high-fat diet for 24 – 30 weeks.

Shao *et al.*[14] also found an enlarged thyroid with lower echotexture and relatively heterogeneous features in ultrasound imaging of rats fed a high-fat diet. The authors showed that rats fed a high-fat diet exhibited focal colloid goiter, flattened follicular epithelium, and distended follicles, which are consistent with our data. Electron microscopy revealed dilated endoplasmic reticulum and twisted nuclei, as well as fewer microvilli and secretory vesicles, all of which indicate thyroid hypofunction.[14] Steatosis and reduced thyroid function have also been reported in diet-induced obese mice and genetically obese ob/ob and db/db mouse models.[15]

Our evaluation of TPO activity revealed a more than twofold reduction in HCD males and a 1.4-fold reduction in HCD females. Shao *et al.* further investigated the molecular mechanisms of thyroid hormone synthesis and showed that a high-fat diet downregulated the expression of thyroid transcription factor 1 and NIS, both of which

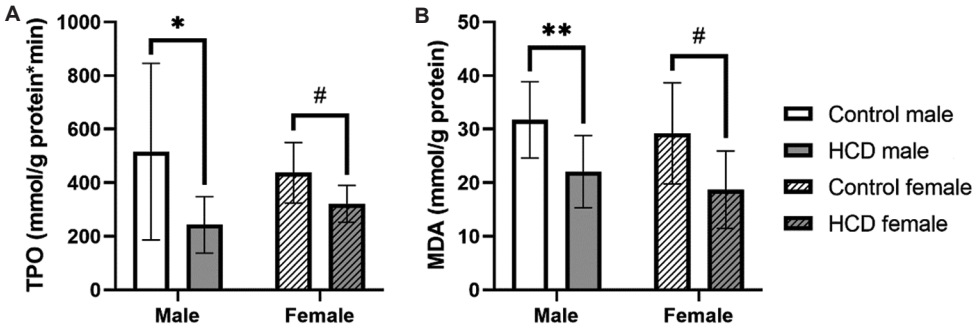

Figure 5. TPO activity and MDA content in the thyroid tissue of experimental animals. TPO activity (A) and MDA content (B) in male and female rats. Data are presented as mean ± standard deviation. Statistically significant differences: *p<0.05, **p<0.01 between male HCD and male control groups; #p<0.05 between female HCD and female control groups.
Abbreviations: HCD: High-calorie diet; TPO: Thyroperoxidase; MDA: Malonic dialdehyde.

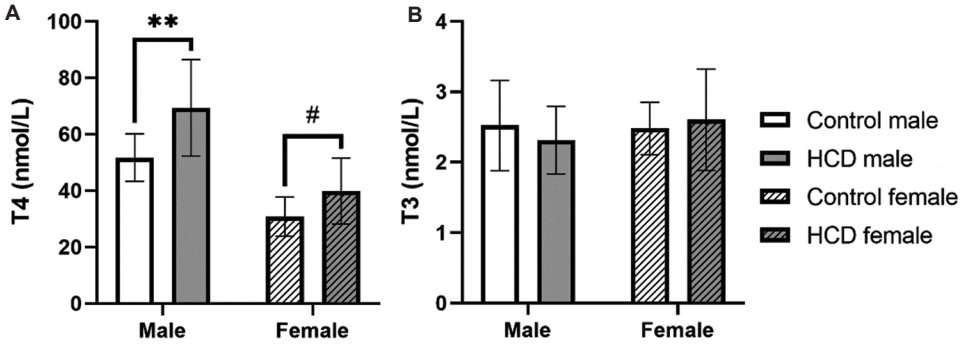

Figure 6. Thyroid hormone levels in the serum of experimental animals. Serum levels of T4 (A) and T3 (B) in male and female rats. Data are presented as mean ± standard deviation. Statistically significant differences: **p<0.01 between male HCD and male control groups; #p<0.05 between female HCD and female control groups.
Abbreviations: HCD: High-calorie diet; T4: Thyroxine; T3: Triiodothyronine.

are essential for thyroid hormone synthesis.[14] The authors suggested that the decrease in NIS activity could be due to lipotoxicity. The decrease in TPO activity in obesity may also be attributable to proinflammatory IL, including IL-6.[2] Our previous studies revealed that IL-6 levels in thyroid tissue were significantly reduced almost twofold in HCD-fed rats compared to the control. However, upon switching to StD, IL-6 levels began to normalize, with the most substantial recovery observed in rats subjected to a combined intervention of StD and moderate treadmill exercise ("HCD/StD + running").[16] IL-6 is known to play a pleiotropic role in activating intracellular signaling pathways, including phosphatidylinositol 3-kinase, AMP-activated protein kinase, and Janus kinase pathways, all of which are necessary for the regulation of intracellular metabolism.[17] This suggests that IL-6 reduction may contribute to metabolic suppression in the thyroid gland, while dietary and physical interventions can restore metabolic function. Interestingly, our data indicate that exercise alone (even without dietary changes) led to partial normalization of IL-6 levels, suggesting that physical activity may directly stimulate energy metabolism within the thyroid gland, potentially mitigating HCD-induced hypofunction.

Our findings indicate that the decrease in TPO activity in thyroid tissue occurs against a background of reduced MDA levels, a fact that deserves special attention. Generally, obesity is associated with increased lipid peroxidation, leading to elevated MDA levels in various tissues. We previously demonstrated this phenomenon in muscle tissue homogenates of rats subjected to a 16-week HCD.[18] However, in the thyroid gland, we observed the opposite trend—a decrease in MDA levels despite visceral obesity. This paradox can be explained by the specificity of TPO, a hemin peroxidase. Only the oxidized form of this enzyme can oxidize the substrate.[19] Efficient thyroid hormone synthesis depends on the adequate production of hydrogen peroxide (H_2O_2), which serves as an oxidant in the synthesis of T4 and T3. H_2O_2 is produced by a member of the NADPH oxidase (NOX) family—double oxidase 2 (DUOX2). Studies indicate that a deficient reactive oxygen species production, due to insufficient NOX/DUOX activity, can lead to thyroid hypofunction in rodent models.[20] In this study, the observed reduction in MDA content in thyroid tissue and the positive correlation between TPO activity and MDA levels in males suggest a potential decrease in H_2O_2 production at the apical membrane of thyrocytes. However, the precise mechanisms underlying reduced TPO activity in obesity remain poorly understood.

Analysis of thyroid status parameters revealed a statistically significant increase in blood T4 levels in rats receiving HCD. Previously, we demonstrated that 16 weeks of HCD led to increased serum TSH levels and heightened 5′-deiodinase type 1 (DI-1) activity in the liver.[21] Since DI-1 catalyzes the conversion of T4 to the active hormone T3, these findings suggest an adaptive response to prolonged overnutrition, aimed at increasing metabolic activity under excessive caloric intake.[22]

Notably, thyroid follicles store large amounts of thyroid hormones,[23] which can be released into the blood circulation under the influence of TSH, despite the inhibition of T4 and T3 synthesis. However, a decrease in TPO activity, along with morphological signs of thyroid hypofunction, indicates an incipient trend towards hypothyroidism. A prolonged high-fat diet may eventually lead to overt thyroid dysfunction, as demonstrated by Shao *et al.*, who reported decreased T4 levels and persistently high TSH levels in rats fed a high-fat diet for 24 – 30 weeks.[14] This reduction in T4 was accompanied by downregulation of thyroid hormone synthesis-related proteins in thyroid tissue, suggesting a progressive decline in thyroid function. Similarly, studies in genetically obese mouse models reveal pronounced thyroid dysfunction with reduced circulating thyroid hormone levels.[15] Thyroid hypofunction has also been reported in obese rats with streptozotocin-induced type 2 diabetes (T2DM).[24] Patients with T2DM often manifest hypothyroidism.[25] Insulin resistance has been shown to play a crucial role in both T2DM and thyroid dysfunction.[26]

Several molecular mechanisms underlie the interplay between insulin resistance and thyroid dysfunction. Insulin resistance in subclinical hypothyroidism is linked to decreased insulin-stimulated glucose transport, likely caused by impaired translocation of glucose transporter type 2. The Thr92Ala polymorphism in the gene encoding DI-2 reduces T3 activation, leading to intrathyroidal deiodination defects and contributing to insulin resistance.[27]

According to Shpakov,[28] altered adenylate cyclase signaling is the most important mechanism linking thyroid disorders to T2DM; in T2DM, there is reduced sensitivity of the thyrocyte adenylate cyclase signaling system in thyrocytes to TSH, along with decreased thyroid hormone receptor expression in peripheral tissues and dysregulated deiodinase activity. A decreased activity of DI-2, a deiodinase that converts T4 into the active form of T3, is associated with insulin resistance. A decreased activity of DI-3, a deiodinase that catalyzes T3 inactivation in pancreatic β-cells, suppresses insulin secretion and leads to insulin deficiency.[28] Together, these findings highlight the bidirectional relationship between thyroid dysfunction and insulin resistance, where thyroid hormone imbalances

contribute to metabolic dysregulation, and insulin resistance exacerbates thyroid dysfunction.

From a clinical point of view, these findings underscore the long-term risk of developing hypothyroidism in obesity. Given the strong link between obesity, insulin resistance, and thyroid dysfunction, overweight individuals should undergo regular thyroid function assessments, including an ultrasound examination of the thyroid gland and determination of the thyroid hormonal status.

5. Conclusion

Our findings confirm the adaptive changes in the thyroid function in response to 16 weeks of HCD consumption in rats. While serum T4 increased, there was a concurrent trend toward thyroid hypofunction, as evidenced by a decrease in TPO activity. Morphological studies of the thyroid gland further support this emerging hypothyroid state, revealing lipid inclusions, enlarged follicles with colloid accumulation, and flattened thyrocytes in both male and female rats.

Acknowledgments

None.

Funding

This work was supported by the State Program for Scientific Research of the National Academy of Sciences of Belarus (No.: 4.1.1.5).

Conflict of interest

The authors declare that they have no competing interests.

Author contributions

Conceptualization: Tatyana A. Mityukova
Formal analysis: All authors
Investigation: Anastasia A. Basalai, Tatyana E. Kuznetsova, Olga Y. Poluliakh, Mikita S. Kastsiuchenka
Methodology: Anastasia A. Basalai, Tatyana E. Kuznetsova, Olga Y. Poluliakh, Mikita S. Kastsiuchenka
Writing – original draft: Tatyana A. Mityukova, Anastasia A. Basalai, Tatyana E. Kuznetsova
Writing – review & editing: All authors

Ethics approval and consent to participate

This study was approved by the Bioethics Committee of the Institute of Physiology, National Academy of Sciences of Belarus (Protocols No.1 on January 22, 2021; Protocols No.2 on February 2, 2022) and conducted in accordance with the guidelines set forth by the European Convention for the Protection of Vertebrate Animals (ETS No. 123).

Consent for publication

Not applicable.

Availability of data

The datasets used and/or analyzed are available from the Institute of Physiology of the National Academy of Sciences of Belarus, upon reasonable and justifiable request in accordance with the rules and procedures of the institute (https://physiology.by/or biblio@fizio.bas-net.by).

References

1. Okunogbe A, Nugent R, Spencer G, Powis J, Ralston J, Wilding J. Economic impacts of overweight and obesity: Current and future estimates for 161 countries. *BMJ Glob Health*. 2022;7(9):e009773.

   doi: 10.1136/bmjgh-2022-009773

2. Reinehr T. Obesity and thyroid function. *Mol Cell Endocrinol*. 2010;316(2):165-171.

   doi: 10.1016/j.mce.2009.06.005

3. Sanyal D, Raychaudhuri M. Hypothyroidism and obesity: An intriguing link. *Indian J Endocrinol Metab*. 2016;20(4):554-557.

   doi: 10.4103/2230-8210.183454

4. Du FM, Kuang HY, Duan BH, Liu DN, Yu XY. Associations between thyroid hormones within the euthyroid range and indices of obesity in obese Chinese women of reproductive age. *Metab Syndr Relat Disord*. 2019;17(8):416-422.

   doi: 10.1089/met.2019.0036

5. Alevizaki M, Saltiki K, Voidonikola P, Mantzou E, Papamichael C, Stamatelopoulos K. Free thyroxine is an independent predictor of subcutaneous fat in euthyroid individuals. *Eur J Endocrinol*. 2009;161(3):459-465.

   doi: 10.1530/EJE-09-0441

6. Song RH, Wang B, Yao QM, Li Q, Jia X, Zhang JA. The impact of obesity on thyroid autoimmunity and dysfunction: A systematic review and meta-analysis. *Front Immunol*. 2019;10:2349.

   doi: 10.3389/fimmu.2019.02349

7. Yan Y, Xu M, Wu M, *et al*. Obesity is associated with subclinical hypothyroidism in the presence of thyroid autoantibodies: A cross-sectional study. *BMC Endocr Disord*. 2022;22(1):94.

   doi: 10.1186/s12902-022-00981-0

8. Gancheva S, Zhelyazkova-Savova M, Galunska B, Chervenkov T. Experimental models of metabolic syndrome in rats. *Scr Sci Med*. 2015;47(2):14-21.

   doi: 10.14748/ssm.v47i2.1145

9. Marcondes FK, Bianchi FJ, Tanno AP. Determination of the

estrous cycle phases of rats: Some helpful considerations. *Braz J Biol*. 2002;62(4A):609-614.

doi: 10.1590/s1519-69842002000400008

10. Khoubnasabjafari M, Ansarin K, Jouyban A. Reliability of malondialdehyde as a biomarker of oxidative stress in psychological disorders. *Bioimpacts*. 2015;5(3):123-127.

doi: 10.15171/bi.2015.20

11. Alexander NM. A spectrophotometric assay for iodide oxidation by thyroid peroxidase. *Anal Biochem*. 1962;4: 341-345.

doi: 10.1016/0003-2697(62)90097-0

12. Митюкова ТА, Чудиловская ЕН, Мигалевич АС. Определение активности тиреопероксидазы в ткани щитовидной железы (экспериментальное исследование). Лабораторная диагностика. *Восточная Европа*. (Mityukova TA, Chudilovskaya EH, Mihalevich AC. Determination of thyroid peroxidase activity in the thyroid tissue of rats [experimental study]. Laboratory diagnostics. *East Eur*). 2020;9(3):285-293. [In Russ].

doi: 10.34883/PI.2020.9.3.009

13. Басалай АА, Кузнецова ТЕ, Митюкова ТА, *и др*. Морфофункциональное состояние печени крыс-самцов линии Вистар при диет-индуцированном ожирении и его коррекции. Известия Национальной Академии Наук Беларуси. *Серия Медицинских Наук*. (Basalai AA, Kuznetsova TE, Mityukova TA, *et al.* Morphofunctional state of the liver of male Wistar rats during diet-induced obesity and its correction. *Proc Natl Acad Sci Belarus Med Ser*). 2022;19(3):308-320. [In Russ].

doi: 10.29235/1814-6023-2022-19-3-308-320

14. Shao SS, Zhao YF, Song YF, *et al*. Dietary high-fat lard intake induces thyroid dysfunction and abnormal morphology in rats. *Acta Pharmacol Sin*. 2014;35(11):1411-1420.

doi: 10.1038/aps.2014.82

15. Lee MH, Lee JU, Joung KH, *et al*. Thyroid dysfunction associated with follicular cell steatosis in obese male mice and humans. *Endocrinology*. 2015;156(3):1181-1193.

doi: 10.1210/en.2014-1670

16. Митюкова ТА, Кузнецова ТЕ, Басалай АА, *и др*. Морфологические и функциональные характеристики щитовидной железы при диет-индуцированном ожирении и его коррекции у крыс самцов Вистар. *Патологическая Физиология и Экспериментальная Терапия*. (Mityukova TA, Kuznetsova TE, Basalai AA, *et al*. Morphological and functional characteristics of the thyroid gland in diet-induced obesity and its correction in male Wistar rats. *Pathol Physiol Exp Ther*). 2023;67(4):47-55. [In Russ].

doi: 10.25557/0031-2991.2023.04.47-55

17. Kistner TM, Pedersen BK, Lieberman DE. Interleukin 6 as an energy allocator in muscle tissue. *Nat Metab*. 2022;4(2): 170-179.

doi: 10.1038/s42255-022-00538-4

18. Mityukova TA, Basalai AA, Chudilovskaya KN, Poluliakh OE, Shcherbakov YV, Kastiuchenka MS. Decrease in muscle mass in diet-induced visceral obesity in male wistar rats: Relationship with hormonal and metabolic parameters. *J Evol Biochem Physiol*. 2023;59(4):1277-1286.

doi: 10.1134/S0022093023040208

19. Carvalho DP, Dupuy C. Thyroid hormone biosynthesis and release. *Mol Cell Endocrinol*. 2017;458:6-15.

doi: 10.1016/j.mce.2017.01.038

20. Szanto I, Pusztaszeri M, Mavromati M. H_2O_2 metabolism in normal thyroid cells and in thyroid tumorigenesis: Focus on NADPH oxidases. *Antioxidants* (*Basel*). 2019;8(5):126.

doi: 10.3390/antiox8050126

21. Митюкова ТА, Чудиловская ЕН, Басалай АА. Активность 5'-дейодиназы йодотиронина I типа в печени у крыс, получающих высококалорийную диету (экспериментальное исследование). Лабораторная диагностика. *Восточная Европа*. (Mityukova TA, Chudilovskaya EH, Basalai AA. Activity of type I iodothyronine 5'-deiodinase in the liver in rats receiving a high-calorie diet [experimental study]. laboratory diagnostics. *East Eur*). 2022;11(1):60-68. [In Russ].

doi: 10.34883/PI.2022.11.1.016

22. Gereben B, Zeöld A, Dentice M, Salvatore D, Bianco AC. Activation and inactivation of thyroid hormone by deiodinases: Local action with general consequences. *Cell Mol Life Sci*. 2008;65(4):570-590.

doi: 10.1007/s00018-007-7396-0

23. Chawla S, Jena S. The anatomy and physiology of laboratory rat. In: *Essentials of Laboratory Animal Science: Principles and Practices*. Vol. 1. Singapore: Springer; 2021. p. 187-209.

doi: 10.1007/978-981-16-0987-9_9

24. Rizk FH, Barhoma RAE, El-Saka MH, *et al*. Exercise training and spexin ameliorate thyroid changes in obese type 2 diabetic rats: The possible interlaying mechanisms. *Am J Physiol Endocrinol Metab*. 2024;327(3):E313-E327.

doi: 10.1152/ajpendo.00213.2024

25. Biondi B, Kahaly GJ, Robertson RP. Thyroid dysfunction and diabetes mellitus: Two closely associated disorders. *Endocr Rev*. 2019;40(3):789-824.

doi: 10.1210/er.2018-00163

26. Mohammed Hussein SM, AbdElmageed RM. The relationship between type 2 diabetes mellitus and related

thyroid diseases. *Cureus*. 2021;13(12):e20697.

doi: 10.7759/cureus.20697

27. Butler PW, Smith SM, Linderman JD, *et al*. The Thr92Ala 5' type 2 deiodinase gene polymorphism is associated with a delayed triiodothyronine secretion in response to the thyrotropin-releasing hormone-stimulation test: A pharmacogenomic study. *Thyroid*. 2010; 20(12):1407-1412.

doi: 10.1089/thy.2010.0244

28. Shpakov AO. Molecular mechanisms of the relationship between thyroid dysfunctions and diabetes mellitus. *J Evol Biochem Physiol*. 2018;54:257-266.

doi: 10.1134/S0022093018040014

ACCSCIENCE PUBLISHING

Global Translational Medicine

BRIEF REPORT

A comparison of pathology examination and immunohistochemistry in studying pituitary adenomas

Ach Taieb[1,2,3*], El Arem Marwa[1,2], Abdessaied Nihed[1,4], and Ach Koussay[1,2]

[1]Department of Endocrinology, Faculty of Medicine, University of Sousse, Sousse, Tunisia

[2]Department of Diabetology, University Hospital of Farhat Hached, Sousse, Tunisia

[3]Laboratory of Exercise Physiology and Pathophysiology; L.R.19ES09, Faculty of Medicine, University of Sousse, Sousse, Tunisia

[4]Department of Pathology, University Hospital of Farhat Hached, Sousse, Tunisia

Abstract

The integration of clinical, biochemical, radiological, and pathological data is crucial for diagnosing and managing pituitary adenomas (PAs). The objective of the study is to compare the clinical and biochemical classifications of PAs with their histopathological findings to improve diagnosis and treatment. This study characterized the clinical, hormonal, and pathological profiles of 40 patients with histologically confirmed PAs. Histopathological analysis identified eosinophilic adenomas in 75% of cases, amphophilic adenomas in 15%, and basophilic adenomas in 10%. Hormonal profiling revealed 22.5% prolactinomas, 15% somatotroph adenomas, 0.5% Cushing disease, and 57.5% non-functioning adenomas. Morphologically, tumors exhibited solid (55%), trabecular (30%), and papillary (15%) growth patterns. Immunohistochemical (IHC) analysis revealed monohormonal secretion in 31.5%, mixed growth hormone/prolactin secretion in 39.4%, and plurihormonal secretion in 28.9% of cases. In conclusion, this study highlights prolactinomas as the most prevalent subtype, underscoring the critical role of integrating histopathological and IHC findings for accurate diagnosis and classification of adenomas.

Keywords: Adenomas; Pathology; Immunohistochemistry; Hormones; Pituitary

***Corresponding author:**
Ach Taieb
(ach.taieb@gmail.com)

Citation: Taieb A, Marwa EA, Nihed A, Koussay A. A comparison of pathology examination and immunohistochemistry in studying pituitary adenomas. *Global Transl Med*. 2025;4(2):96-102. doi: 10.36922/gtm.8474

Received: January 9, 2025

Revised: February 9, 2025

Accepted: February 24, 2025

Published online: March 24, 2025

1. Introduction

Pituitary adenomas (PAs) are the most common pituitary neoplasms, accounting for approximately 10 – 15% of all intracranial tumors.[1] According to the 2017 World Health Organization (WHO) classification, pituitary tumors are defined as neoplasms originating within the sella turcica, arising from adenohypophysial cells, and presenting with varying clinical manifestations based on their hormonal activity and size.[2] Clinically significant pituitary tumors remain relatively rare, with an estimated prevalence of 200/1,000,000 and an annual incidence of approximately two per 100,000.[3] However, many adenomas are asymptomatic and are often discovered incidentally during neuroimaging for unrelated reasons, a phenomenon referred to as pituitary incidentalomas.

PAs are broadly categorized into two types: functioning PAs (FPAs) and non-FPAs (NFPAs). FPAs are characterized by excess hormone production, often leading to distinct clinical syndromes such as acromegaly, Cushing disease, or prolactinomas, depending on the type of hormone secreted.[4] In contrast, NFPAs do not cause hormone hypersecretion and are typically diagnosed due to mass effects, such as visual disturbances or headaches.[4] Larger NFPAs may compress nearby structures, including the optic chiasm, leading to neuro-ophthalmologic symptoms.

The 2017 WHO classification incorporates immunohistochemical (IHC) staining and ultrastructural features, categorizing PAs into five subtypes based on hormone immunostaining: prolactin (PRL)-secreting, growth hormone (GH)-secreting, adrenocorticotropic hormone (ACTH)-secreting, thyroid-stimulating hormone (TSH)-secreting, and gonadotroph adenomas expressing follicle-stimulating hormone (FSH) and luteinizing hormone (LH).[5-7] Non-functioning adenomas may express hormone markers without clinical signs of hormone overproduction, whereas null cell adenomas exhibit no detectable hormone production.[4]

Recent research has highlighted that tumor behavior, including growth potential and recurrence risk, can be better predicted through the integration of clinical, biochemical, radiological, and IHC profiles with molecular and genetic markers. Atypical adenomas, characterized by more aggressive clinical behavior, often exhibit features such as a high mitotic rate, increased Ki-67 proliferation index, and p53 overexpression.[2] This comprehensive approach is crucial in enhancing diagnostic precision and optimizing therapeutic strategies, including surgery, pharmacological treatment, and radiation therapy.

Previous studies have emphasized the complementary roles of histopathology and IHC in diagnosing PAs. Histopathology evaluates cellular morphology and growth patterns, while IHC facilitates precise identification of hormone expression, even in clinically silent or ambiguous cases. For instance, NFPA, which constitutes a significant proportion of pituitary tumors, often exhibits immunoreactivity for pituitary hormones without associated clinical syndromes. Despite these diagnostic advancements, discrepancies between histopathological classifications and IHC profiles persist, underscoring the need for an integrated diagnostic approach.

This study aimed to characterize the clinical and hormonal profiles of PAs and compare their clinical and biochemical classifications with histopathological findings to improve diagnostic and management approaches.

2. Materials and methods

2.1. Patients

A total of 40 patients diagnosed with PAs were included in the study. These patients were followed up in the Endocrinology and Diabetology Department of Farhat Hached University Hospital, Sousse. Each patient underwent pituitary neurosurgery, and the surgical specimens were analyzed in the Pathology Department of the same hospital. Only cases that were histologically confirmed as PAs after a complete pathological examination were included in the study. Written informed consent was obtained from all participants for the use of their clinical data and specimens. Patients with histologically confirmed pituitary carcinomas or other non-adenoma pituitary diseases were excluded from the study. All procedures were conducted in accordance with the ethical standards of the Declaration of Helsinki and approved by the Institutional Ethics Committee.

2.2. Clinical identification of PAs

Patients were classified into two groups based on their clinical and biochemical profiles. FPAs were identified in cases with clinical and biochemical evidence of endocrine syndromes associated with hormone hypersecretion. NFPAs were diagnosed in patients without clinical or biochemical signs of hormone overproduction and were primarily identified through neuro-ophthalmological or radiological manifestations. Tumor size was assessed using magnetic resonance imaging and classified as microadenomas (<10 mm in diameter) or macroadenomas (≥10 mm). Tumor invasiveness was graded according to Hardy's classification, with Grade I-III being non-invasive and Grade IV classified as invasive.[8]

2.3. Hormonal assessment

Serum levels of FSH, LH, PRL, and TSH were measured using a chemiluminescence immunoassay (Diasorin, Italy). ACTH and GH levels were determined using immunoradiometric assay techniques with commercially available kits (Beckman Coulter, United States).

2.4. Pathological examination

The pathological examination of the tumor specimens consisted of two main steps: tissue processing and histopathological examination. In the tissue processing phase, tumor specimens were fixed in 10% buffered formalin for 48 h to preserve tissue integrity, followed by embedding in paraffin blocks to facilitate sectioning.

For histopathological examination, serial sections of 4 μm in thickness were cut from each paraffin block and mounted onto glass slides. Hematoxylin and eosin staining

was performed on these sections for routine histological examination, allowing assessment of cellular morphology, growth patterns (solid, trabecular, or papillary), and tumor classification (eosinophilic, amphophilic, or basophilic). Based on their staining properties, PAs are categorized as: (i) eosinophilic, typically associated with GH or PRL secretion, (ii) basophilic, which is often linked to ACTH secretion, or (iii) amphophilic, which may show mixed hormonal profiles.

The growth patterns of PAs (solid, trabecular, and papillary) are linked to specific tumor subtypes and clinical behaviors:

(i) Solid: These are NFPAs that are less aggressive but may cause mass effects.
(ii) Trabecular: These are GH-secreting (somatotroph) adenomas and prolactinomas.GH adenomas are linked to acromegaly (50% invasive), while prolactinomas are often invasive (43%).
(iii) Papillary: These are ACTH-secreting (corticotroph) adenomas and plurihormonal adenomas. ACTH adenomas are associated with Cushing disease and are often invasive, while plurihormonal adenomas have variable behavior.

IHC staining was conducted using a panel of primary antibodies targeting pituitary hormones, including GH, PRL, ACTH, TSH, FSH, and LH. The IHC protocol involved antigen retrieval, blocking of non-specific binding, and application of the primary antibodies, followed by detection using standardized staining. IHC results were semi-quantitatively scored based on the number of positively stained cells: 0 (Negative), 1+ (1 – 4 cells), 2+ (5 – 20 cells), 3+ (21 – 50 cells), and 4+ (>51 cells). This approach ensured a systematic evaluation of hormone expression and correlation with histopathological findings.

2.5. Categories of PAs

2.5.1. Functioning adenomas

These tumors secrete one or more pituitary hormones, leading to specific clinical syndromes. They are further classified based on the hormone they produce:

(i) Prolactin-secreting adenomas: These can cause hyperprolactinemia, leading to symptoms such as galactorrhea, menstrual irregularities, and infertility
(ii) GH-secreting adenomas: These result in acromegaly or gigantism due to excessive GH production
(iii) ACTH-secreting adenomas: These lead to Cushing disease, characterized by hypercortisolism
(iv) TSH-secreting adenomas: These can cause hyperthyroidism due to excessive TSH
(v) FSH/LH-secreting adenomas: These are often asymptomatic but may cause hormonal imbalances.

2.5.2. Non-functioning adenomas

Non-functioning adenomas do not secrete hormones at clinically significant levels. They are typically asymptomatic until they grow large enough to cause mass effects, such as headaches, visual disturbances, or hypopituitarism.

2.6. Statistical analysis

Data analysis was performed using IBM Statistical Package for Social Sciences for Windows, Version 23.0 (IBM Inc., United States). Continuous variables such as age and tumor size were presented as mean ± standard deviation. Descriptive statistics were used to summarize the clinical, biochemical, and histopathological features of the PAs.

3. Results

The cohort consisted of 40 patients (24 men and 16 women) with a mean age of 45 ± 6.5 years. The average tumor size was 13.2 ± 5.8 mm, with 87.5% classified as macroadenomas (>10 mm) and 12.5% as microadenomas (<10 mm). Among the patients, 30% required a second surgery due to tumor recurrence, while 17.5% underwent adjuvant radiotherapy. Eighty percentages of the patients received medical therapy postoperatively, targeting hormonal control and tumor recurrence. Invasiveness, defined by Hardy Grade IV, was identified in 40% of cases, while 60% were non-invasive or localized to intrasellar or extrasellar regions (Hardy Grades I-III) (Table 1).

Clinical symptoms varied according to the type of PA. In prolactinomas (22.5%), women presented with amenorrhea, galactorrhea, and infertility in 75% of the cases. Patients with somatotroph adenomas (15%) exhibited

Table 1. Clinical baseline characteristics of patients and pituitary adenomas

Characteristics	Results (%)
Age (years)	45±6.5
Gender	
Men	24
Woman	16
Diameter (mm)	13.2±5.8
Second surgery, *n* (%)	12 (30)
Radiotherapy, *n* (%)	7 (17.5)
Medical treatment, *n* (%)	32 (80)
Invasiveness extension (Hardy), *n* (%)	
Non- invasive	
Intrasellar (I-II)	11 (27.5)
Extrasellar (III)	13 (32.5)
Invasive (IV)	16 (40)

typical features of acromegaly, such as enlarged extremities in 90% of the cases. Two patients (0.5%) with Cushing disease had symptoms of weight gain, central obesity, hypertension, and purple striae. NFPAs represented 57.5% of cases, and 60% of them were diagnosed due to mass effects, causing headaches, visual field defects, and optic chiasm compression.

Histopathological analysis revealed that 75% of adenomas were eosinophilic, 15% amphophilic, and 10% basophilic. Solid growth patterns were observed in 55% of tumors, with 30% displaying a trabecular structure and 15% a papillary pattern (Figures 1 and 2). Eosinophilic adenomas were primarily associated with PRL and GH secretion, while basophilic adenomas were linked to ACTH production.

Immunohistochemistry profiling revealed monohormonal secretion in 31.5% of adenomas, with the following distribution: 10% were prolactinomas, 5% GH-secreting, 5% ACTH-secreting, 5% TSH-secreting, and 5% gonadotroph adenomas. Mixed GH/PRL adenomas comprised 37.5% of cases, while plurihormonal adenomas accounted for 27.5%, and null-cell adenomas represented 5%.

Eosinophilic adenomas exhibited higher rates of invasiveness (50% invasive) compared to amphophilic and basophilic adenomas (20% invasive) (Figure 3). This was particularly evident in prolactinomas (43% invasive) and somatotroph adenomas (50% invasive). IHC findings closely correlated with clinical presentations in FPAs, with acromegaly and Cushing disease confirmed by hormone overproduction in GH and ACTH adenomas, respectively.

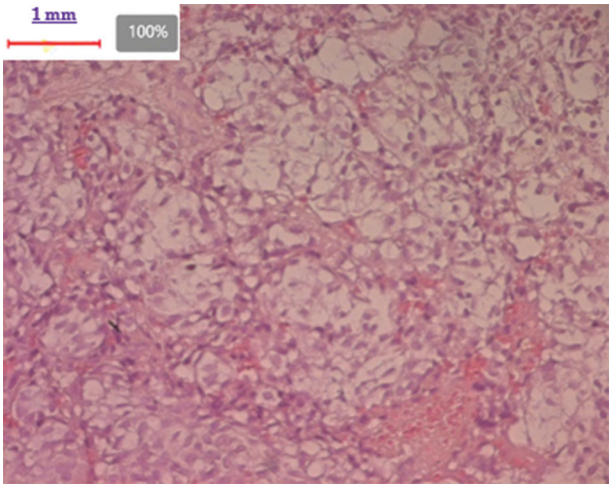

Figure 1. Pituitary adenoma showing solid pattern in hematoxylin and eosin staining. The solid pattern is characterized by densely packed tumor cells forming sheets or nests without distinct organizational structures, such as trabeculae or papillae. Scale bar: 1 mm, magnification: ×200.

NFPAs, despite lacking endocrine symptoms, exhibited significant mass effects, with 65% of patients presenting with neuro-ophthalmological complications and 45% requiring surgery for compression-related symptoms. Most NFPAs were macroadenomas (85%), underlining the importance of timely surgical intervention to prevent further neurological damage.

Statistical analysis revealed a significant correlation between tumor size and invasiveness, with larger adenomas (>12 mm) more frequently exhibiting Hardy Grade IV invasion ($p < 0.05$). This association was particularly pronounced in eosinophilic adenomas, suggesting that

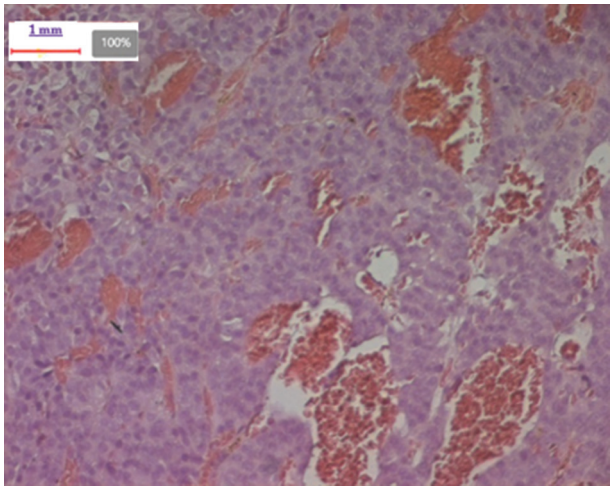

Figure 2. Pituitary adenoma with trabecular pattern in hematoxylin and eosin staining. The trabecular architecture is characterized by elongated, ribbon-like structures of tumor cells separated by fibrous stroma or vascular channels. Scale bar: 1 mm, magnification: ×200.

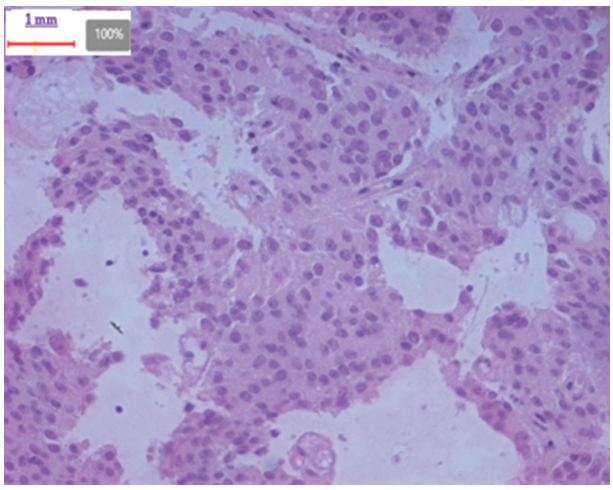

Figure 3. The predominant type of pituitary adenomas according to cell features: acidophilic pituitary adenoma with hematoxylin and eosin. The acidophilic cells are characterized by their pink-staining cytoplasm, which is indicative of hormone-producing cells, such as those secreting growth hormone or prolactin. Scale bar: 1 mm, magnification: ×200.

both tumor size and histological subtype serve as key predictors of aggressive behavior and clinical outcomes.

4. Discussion

In this study, we conducted a comparative analysis of histological examination and immunohistochemistry to characterize PAs. A notable strength of this research is the comprehensive inclusion of radio-clinical, hormonal, and IHC assessments for all patients, all performed in a single laboratory. Despite numerous publications on PAs, there is a scarcity of large-scale studies scrutinizing both morphologic and IHC features. However, a key limitation of our study is the absence of molecular analysis, which could provide further insights into tumor behavior.

NFPAs often present as macroadenomas and can exhibit invasiveness. The primary therapeutic approach involves surgery, with radiotherapy employed in cases of recurrence or persistence.[9] In contrast to FPAs, medical interventions for NFPAs are generally less effective, as their management often focuses on alleviating mass effects rather than hormonal control.[4] The prognosis for NFPAs depends on the efficacy of these treatments. Although most PAs are benign and slow-growing, clinical follow-up is infrequent when no residual tumor is evident post-surgery or irradiation.[10]

Our hormonal findings revealed that prolactinomas, somatotroph adenomas, Cushing disease, and NFPAs accounted for 57.5% of the cohort, aligning with existing literature that highlights prolactinomas as the most common pituitary tumors.[11] Interestingly, our IHC analysis showed that LH and TSH adenomas each represented only 5% of cases. This lower prevalence may be attributed to the fact that gonadotroph adenomas are often not surgically removed due to their indolent nature.[9] In addition, certain assays, such as alpha subunit measurement, may be necessary to accurately detect these adenomas, which could contribute to discrepancies.[9]

Histologically, eosinophilic adenomas are traditionally associated with acromegaly, basophilic adenomas with Cushing syndrome, and chromophobe adenomas with non-functionality.[11] However, our findings suggest that not all acidophilic tumors produce GH, nor are all GH-producing tumors eosinophilic. Similarly, some basophilic tumors may not cause Cushing syndrome, and many chromophobic tumors exhibit hormonal activity.[11,12] These results align with findings in recent literature that emphasize the need for a nuanced understanding of PA classification.[13]

The IHC classification of PAs has several limitations. Despite its advancements in tumor classification, the technique is semi-quantitative and is subjected to observer-dependent variations.[14] This variability, along with its reliance on specific antibodies, introduces bias into IHC results.[7] The effectiveness of IHC is compromised in cases where adenomas secrete hormone isoforms that are not recognizable by the chosen antibodies.[15] Petrus *et al.*[16] noted the potential underestimation of FSH levels when using monoclonal antibodies, particularly in altered isoform balances.[16]

Plurihormonal adenomas are characterized by the production of multiple hormones, with combinations such as GH-PRL or GH-TSH being common.[17] Our study identified a plurihormonal frequency of 28.9%, which aligns with findings from other studies where over 30% of adenomas expressed multiple hormones.[18] The cytogenesis of these tumors remains poorly understood, but they can significantly impact clinical management, especially in somatotroph adenomas, where up to 50% may exhibit plurihormonal activity.[13]

In a study of 143 plurihormonal PAs, 29 IHC subtypes were recognized, highlighting the complexity of tumor classification.[19] In another study by Balinisteanu *et al.*,[11] only 9.1% of adenomas were found to be plurihormonal.[11] The differences in reported frequencies may arise from variations in quantification methods for hormone immunoreactivity, emphasizing the need for standardized protocols in IHC analysis.[11]

This study has several limitations, including the absence of molecular analyses, which restricts the ability to explore genetic and epigenetic alterations that could provide deeper insights into the pathogenesis and heterogeneity of PAs, particularly plurihormonal tumors. Without techniques such as next-generation sequencing or RNA sequencing, the study was not able to identify potential biomarkers or therapeutic targets.

Overall, our findings contribute to the evolving understanding of PAs, underscoring the importance of integrating histopathological and IHC data for accurate diagnosis and management. Further research, particularly incorporating molecular analyses, is needed to enhance our understanding of the pathogenesis and behavior of these tumors.

5. Conclusion

The comparison between pathology examination and IHC in our study highlights that prolactinomas are the most prevalent pituitary tumors in our cohort. The critical role of comprehensive IHC staining for all pituitary hormones is underscored, as it is essential for accurately characterizing the secretory or non-secretory behavior of tumors,

particularly in assessing plurihormonality. Our findings indicate a plurihormonal frequency of 28.9%, suggesting a significant overlap in hormone production among various adenoma types.

The integration of molecular profiling techniques may enhance the diagnostic precision of PA subtypes beyond the ability of traditional IHC. This advancement could lead to a reevaluation of the known prevalence of PAs, with important clinical implications for treatment strategies and patient management. The emerging understanding of the molecular landscape of these tumors has the potential to inform tailored therapeutic approaches, ultimately improving patient outcomes.

Acknowledgments

None.

Funding

None.

Conflict of interest

The authors declare no conflicts of interest.

Author contributions

Conceptualization: Taieb Ach
Investigation: Nihed Abdessaied
Methodology: Koussay Ach
Writing–original draft: Ach Taieb
Writing–review & editing: All authors

Ethics approval and consent to participate

The Institutional Review Board Statement obtained from University Hospital of Sousse Tunisia. Approval number: 15/2023. Informed consent was obtained from all subjects involved in the study.

Consent for publication

Patients consented on the publication of their data.

Availability of data

Data will be made available on reasonable request to the corresponding author.

References

1. Tritos NA, Miller KK. Diagnosis and management of pituitary adenomas: A review. *JAMA*. 2023;329(16):1386-1398.

   doi: 10.1001/jama.2023.5444

2. Lloyd RV, Osamura RY, Klöppel G, Rosai J. WHO classification of tumours: Pituitary tumours. In: *Pathology and Genetics of Tumours of Endocrine Organs*. Lyon, France: IARC; 2022. p. 10-15.

3. Saeger W, Lüdecke DK, Buchfelder M, Fahlbusch R, Quabbe HJ, Petersenn S. Pathohistological classification of pituitary tumors: Experience from the German pituitary tumor registry. *Eur J Endocrinol*. 2017;176(2):193-201.

4. Sanchez-Tejada L, Moreno-Perez O, Alfayate R, *et al*. Contribution of molecular analysis to the typification of non-functioning pituitary adenomas. *PLoS One*. 2019;14(8):e0221268.

5. Dineen R, Stewart PM, Sherlock M, *et al*. The evolving role of molecular profiling in the management of pituitary adenomas. *Cancers* (*Basel*). 2020;12(6):1628.

6. Fuchsberger C, Flannick J, Teslovich TM, *et al*. The genetic architecture of type 2 diabetes. *Nature*. 2016;536(7614):41-47.

   doi: 10.1038/nature18642

7. DeStephano DB, Lloyd RV, Pike AM, Wilson BS. Pituitary adenomas. An immunohistochemical study of hormone production and chromogranin localization. *Am J Pathol*. 1984;116(3):464-472.

8. Molitch ME. Diagnosis and treatment of pituitary adenomas: A review. *JAMA*. 2017;317(5):516-524.

   doi: 10.1001/jama.2016.19699

9. Zargar AH, Laway BA, Masoodi SR, *et al*. Clinical and endocrine aspects of pituitary tumors. *Saudi Med J*. 2004;25(10):1428-1432.

10. Trouillas J. In search of a prognostic classification of endocrine pituitary tumors. *Endocr Pathol*. 2014;25(2):124-132.

    doi: 10.1007/s12022-014-9322-y

11. Balinisteanu, B, Ceauşu RA, Cîmpean AM, *et al*. Conventional examination versus immunohistochemistry in the prediction of hormone profile of pituitary adenomas. An analysis on 142 cases. *Rom J Morphol Embryol*. 2011;52(3 Suppl):1041-1045.

12. Sen A, Das C, Mukhopadhyay M, Mukhopadhyay S, Deb S, Mukhopadhyay B. Cytohistological correlation in pituitary tumor and immunological assessment with the help of Ki-67. *J Postgrad Med*. 2017;63(2):96-99.

    doi: 10.4103/0022-3859.192797

13. Brito J, Cortés ME, Rodríguez F. Immunohistochemistry for pituitary hormones and Ki-67 in growth hormone producing pituitary adenomas. *Rev Med Chil*. 2008;136(7):831-836.

14. Liu DG. Immunohistochemical and ultrastructural study of plurihormonal pituitary adenomas. *Zhonghua Yi Xue Za Zhi*. 1993;73(4):223-225, 254.

15. Kontogeorgos G. Classification and pathology of pituitary tumors. *Endocrine*. 2005;28(1):27-35.

    doi: 10.1385/ENDO:28:1:027

16. Petrus M, Rittie JL, Causse JE, *et al*. Turner's syndrome and

isoforms of LH and FSH. Value of polyclonal enzymatic techniques. *Arch Pediatr*. 1996;3(3):245-247.

doi: 10.1016/0929-693x(96)81302-9

17. Ho DM, Hsu CY, Ting LT, *et al*. Plurihormonal pituitary adenomas: The necessity of immunostaining for accurate classification. *Histopathology*. 2020;76(3):422-430.
18. Lopes MBS. The current role of immunohistochemistry in the diagnosis and management of pituitary adenomas. *Neuroendocrinology*. 2021;111(5):459-469.
19. Wang Y, Li J, Zhang X, *et al*. Advances in molecular biology and pathology of pituitary tumors: A review. *Front Endocrinol*. 2022;13:795983.

ACCSCIENCE PUBLISHING

Global Translational Medicine

BRIEF REPORT

Platelet aggregation inhibition by fluorophenyl-substituted 2-isoxazoline-5-carboxylic acids and their derivatives

Mikalai M. Kauhanka*, Marharita E. Parkhach, Svetlana N. Borisevich, Stanislava V. Glinnik, and Elena N. Haluk

Department of General Chemistry, Career Guidance and Pre-University Training Faculty, Belarusian State Medical University, Minsk, Belarus

(This article belongs to the *Special Issue: Special Issue of Global Translational Medicine in the Fourth RCCCDT-2024*)

Abstract

Platelets perform many important bodily functions, with their primary task being the prevention of bleeding by facilitating hemostasis. While platelets protect the body from blood loss, they also contribute to the development of serious diseases, such as atherosclerosis and its complications. Understanding the dual role of platelets is crucial for developing new treatments aimed at reducing thrombotic risk while improving the prognosis for patients with cardiovascular diseases. Specifically, elucidating the mechanisms underlying platelet activation may facilitate the development of selective agents that inhibit pathological platelet activity without compromising their protective function. In this context, the present study evaluated the antiplatelet activity of newly synthesized fluorophenyl-substituted 2-isoxazoline-5-carboxylic acids and their derivatives. Results showed that all compounds demonstrated the ability to suppress platelet aggregation. Increasing the concentration of the active substance from 1 to 25 mmol/L enhanced the inhibitory effect of the compounds. Methyl esters, compared to derivatives with a free carboxyl group, exhibited a stronger ability to suppress the activation of platelet receptors glycoprotein (GP) IIa/IIIb, thereby inhibiting their binding to fibrinogen and subsequent aggregation. The half-maximal inhibitory concentration values for two of the studied compounds were 7.5 mmol/L (methyl ester of 3-[3]-fluorophenyl]-2-isoxazoline carboxylic acid) and 12.5 mmol/L (methyl ester of 3-[2]-fluorophenyl]-2-isoxazoline carboxylic acid), respectively. In conclusion, the findings of this study indicate that 3-aryl-2-isoxazoline-5-carboxylic acids and their methyl esters, containing a single fluorine atom in the aryl group, effectively suppress the activation of platelet receptors GPIIa/IIIb.

Keywords: Antiplatelet agent; Heterocycle; 2-isoxazoline; Platelet; Flow cytometry

***Corresponding author:**
Mikalai M. Kauhanka
(mikalai44@tut.by)

Citation: Kauhanka MM, Parkhach ME, Borisevich SN, Glinnik SV, Haluk EN. Platelet aggregation inhibition by fluorophenyl-substituted 2-isoxazoline-5-carboxylic acids and their derivatives. *Global Transl Med.* 2025;4(2):103-108.
doi: 10.36922/gtm.8147

Received: December 23, 2024

1st revised: February 24, 2025

2nd revised: February 26, 2025

Accepted: March 20, 2025

Published online: April 4, 2025

1. Introduction

Platelets, or thrombocytes, are essential components of the hemostatic system, playing a key role in preventing blood loss during trauma. However, their function extends beyond merely protecting the body against bleeding. Platelets are also involved in pathological mechanisms, leading to thrombus formation, which can cause acute vascular diseases,

such as acute coronary syndromes, unstable angina, myocardial infarction, ischemic attack, and peripheral arterial disease.[1] Platelet activation occurs under the influence of various agonists, such as arachidonic acid, adenosine diphosphate (ADP), thrombin, thromboxane A2, and collagen. These substances activate platelets, leading to their aggregation and thrombus formation, which are necessary to stop bleeding. However, in atherosclerotic conditions, platelets begin to aggressively interact with the vascular wall when an atheromatous plaque ruptures, leading to the formation of pathogenic thrombi that block blood flow and cause ischemic tissue damage.[2] In recent years, researchers have discovered that platelets are not only involved in thrombus formation but also play a role in the inflammatory processes associated with atherogenesis. For example, molecules such as soluble CD40 ligand, C-C chemokine ligand 5, and soluble P-selectin mediate platelet interactions with other cells, contributing to the progression of atherosclerotic disease.[3] These interactions highlight the versatility of platelet functions, which can both protect and harm the vascular wall. Following an atheromatous plaque rupture, platelets adhere to the damaged vessel area, releasing granule contents that activate platelets and form thrombi. This process can cause intermittent or persistent obstruction of blood flow, resulting in ischemic tissue injury and organ dysfunction with serious clinical consequences.[4]

Acetylsalicylic acid (aspirin) has traditionally been used to combat platelet hyperactivity and reduce the risk of serious ischemic events, such as stroke and myocardial infarction. This drug has become the standard of care for many patients with cardiovascular disease, including those who have undergone coronary artery bypass grafting. Acetylsalicylic acid acts by inhibiting the enzyme cyclooxygenase, which leads to a decrease in the synthesis of thromboxane A2, a potent agonist of platelet aggregation. However, despite its effectiveness, the use of aspirin is associated with some limitations and risks. For example, some patients may develop resistance to aspirin, which reduces its effectiveness. In addition, long-term use may lead to an increased risk of gastrointestinal bleeding. In this regard, new antiplatelet drugs, such as clopidogrel and ticlopidine, are being studied, which can be combined with aspirin to increase the effectiveness of treatment and reduce the risk of thrombosis.[5] In recent years, there has also been interest in studying the role of platelets in other pathological aspects, including their role in immune responses. Platelets can interact with immune cells, such as neutrophils and monocytes, promoting inflammation and modulating the immune response. This opens new horizons for understanding their role in the pathogenesis of various diseases, including infectious and autoimmune diseases. Thus, platelets are multifunctional cells that play a key role in maintaining hemostasis and the development of multiple pathologies. They can protect the body from blood loss and contribute to serious diseases like atherosclerosis and its complications. Understanding the mechanisms of platelet activation and their interactions with other cells and molecules is important for developing new therapeutic strategies to reduce the risk of thrombosis and improve the prognosis for patients with cardiovascular diseases.

This work aimed to study the ability of synthesized fluorophenyl-substituted 2-isoxazoline-5-carboxylic acids and their derivatives in inhibiting ADP-dependent platelet aggregation. The preparation of platelet aggregation inhibitors based on compounds containing an isoxazole ring with aromatic substituents in positions 3 and 5 of the heterocyclic fragment has been previously described.[6] Among the compounds obtained, some were found to slow down platelet aggregation. However, a limitation of the previously described compounds is the absence of functional groups in the aromatic substituents, which could increase the affinity of the inhibitor molecules to platelet receptors. Therefore, the present work investigated the activity of compounds containing only one aromatic fragment in positions 3 and 5, a carboxyl group either in a free state or in the form of its methyl ester. Compounds containing an aromatic fragment linked by bridging groups to the isoxazole ring have also been studied.[7] It was assumed that the absence of conjugation in the heterocyclic fragment of 2-isoxazoline and the rigidity imparted to the molecule by the second aromatic fragment would increase the inhibitory ability of the compounds under study. It should be noted that work is currently ongoing to obtain new isoxazole- and 2-isoxazoline-containing substances to assess their potential for medical use.[8-10] The novelty of the compounds studied in this work lies in their fluorine-substituted nature conjugated with the 2-isoxazoline cycle, which has not been explored as substances that promote the inhibition of platelet aggregation.

2. Materials and methods

2.1. Compounds of study

Infrared (IR) spectra were recorded using a Specord 75 IR instrument (Carl Zeiss Jena, Germany). Ultraviolet (UV) spectra of the solutions were obtained using a Specord M40 instrument (Carl Zeiss Jena, Germany). Nuclear magnetic resonance (NMR) spectra of solutions were recorded on a Bruker NMR spectrometer, Avance 400 (400 MHz) (Bruker, USA) in deuterochloroform, with chemical shifts (δ) reported relative to tetramethylsilane as the internal standard. Reaction progress and the characteristics of the obtained compounds were monitored using thin-

layer chromatography on Silufol UV-254 plates (Merck, Germany).

The target compounds 1 – 6 were synthesized using the following method (Figure 1). A solution of oxime (10 mmol) in dichloromethane (20 mL) at 0°C was added dropwise to a mixture of acrylic acid (or methyl acrylate) (10 mmol), 1.5 mL triethylamine (11 mmol), and 5% aqueous sodium hypochlorite solution (20 mL). The reaction mixture was stirred for 60 min and then extracted with dichloromethane (3 – 15 mL) in ice water. The aqueous layer was separated, and the combined organic extracts were dried over sodium sulfate. The solvent was distilled off under reduced pressure. The resulting solid was recrystallized from propan-2-ol. The purified products were then characterized using analytical techniques, as detailed below.

(i) Compound 1: 3-(2-Fluorophenyl)-2-isoxazoline carboxylic acid. The compound has a yield of 83% and a melting point between 181 and 183°C. The IR spectrum (KBr, cm^{-1}) shows peaks at 3100, 3093 (C-H aromatic), 1807, 1260 (COO), 1649 (C = N), and 1600, 1508 (C = C aromatic). The UV spectrum (EtOH, λ_{max}, nm) is 277. The ^{1}H NMR shows the following shifts: δ 2.96 (2H, dd, J = 15.5, 7.4 Hz), 5.31 (1H, dd, J = 7.9, 6.8 Hz), 7.14 – 7.35 (2H, 7.20 (ddd, J = 8.3, 1.1, 0.5 Hz), 7.28 (ddd, J = 7.9, 7.3, 1.1 Hz), 7.43 – 7.59 (2H), 7.49 (ddd, J = 7.9, 1.5, 0.5 Hz), and 7.52 (ddd, J = 8.3, 7.3, 1.5 Hz). The ^{13}C NMR shows: δ 41.8 (1C, s), 81.2 (1C, s), 115.5 (1C, s), 126.7 (1C, s), 128.4 (1C, s), 129.3 (1C, s), 131.3 (1C, s), 155.5 (1C, s), 159.7 (1C, s), and175.2 (1C, s).

(ii) Compound 2: 3-(3-Fluorophenyl)-2-isoxazoline carboxylic acid. The compound has a yield of 85 % and a melting point between 191 and 193°C. The IR spectrum (KBr, cm^{-1}) shows peaks at 3095, 3085 (C-H aromatic), 1805, 1265 (COO), 1651 (C = N), and 1605, 1510 (C = C aromatic). The UV spectrum (EtOH, λ_{max}, nm) is 275. The ^{1}H NMR shows the following shifts: δ 2.79 – 3.04 (2H, 2.87 (dd, J = 15.5, 6.8 Hz), 2.96 (dd, J = 15.5, 7.9 Hz)), 5.26 (1H, dd, J = 7.9, 6.8 Hz), 7.04 – 7.27 (2H, 7.10 [ddd, J = 8.1, 1.4, 1.2 Hz], 7.22 [ddd, J = 1.7, 1.4, 0.5 Hz]), 7.45 (1H, ddd, J = 8.1, 7.7, 0.5 Hz), and 7.65 (1H, ddd, J = 7.7, 1.7, 1.2 Hz). The ^{13}C NMR shows δ 41.8 (1C, s), 81.2 (1C, s), 115.0 – 115.1 (2C, 115.0 [s], 115.1 [s]), 127.3 (1C, s), 130.2 (1C, s), 132.1 (1C, s), 155.7 (1C, s), 161.2 (1C, s), and 175.2 (1C, s).

(iii) Compound 3: 3-(4-Fluorophenyl)-2-isoxazoline carboxylic acid. The compound has a yield of 82% and a melting point between 217 and 219°C. The IR spectrum (KBr, cm^{-1}) shows peaks as 3105, 3085 (CH aromatic), 1800, 1255 (COO), 1645 (C = N), and 1605, 1,515 (C = C aromatic). The UV spectrum (EtOH, λ_{max}, nm) is 272. The ^{1}H NMR shows the following shifts: δ 2.94 (2H, dd, J = 15.5, 7.4 Hz), 5.30 (1H, dd, J = 7.9, 6.8 Hz), 7.04 (2H, ddd, J = 8.7, 1.0, 0.6 Hz), and 7.93 (2H, ddd, J = 8.7, 1.6, 0.6 Hz). The ^{13}C NMR shows δ 41.8 (1C, s), 81.2 (1C, s), 115.4 (2C, s), 125.3 (1C, s), 128.6 (2C, s), 155.7 (1C, s), 162.5 (1C, s), and 175.2 (1C, s).

(iv) Compound 4: Methyl ester of 3-(2-fluorophenyl)-2-isoxazoline carboxylic acid. The compound has a yield of 87% and a melting point between 158°C and 160°C. The IR spectrum (KBr, cm^{-1}) shows peaks at 3110, 3090 (C-H aromatic), 1798, 1271 (COO), 1653 (C = N), and 1603, 1504 (C = C aromatic). The UV spectrum (EtOH, λ_{max}, nm) is 275. The ^{1}H NMR shows δ 2.97 (2H, dd, J = 15.5, 7.4 Hz), 3.75 (3H, s), 5.29 (1H, dd, J = 7.9, 6.8 Hz), 7.14 – 7.35 (2H, 7.20 [ddd, J = 8.3, 1.1, 0.5 Hz], 7.28 [ddd, J = 7.9, 7.3, 1.1 Hz]), 7.52 (1H, ddd, J = 8.3, 7.3, 1.5 Hz), and 7.72 (1H, ddd, J = 7.9, 1.5, 0.5 Hz). The ^{13}C NMR shows δ 41.8 (1C, s), 52.2 (1C, s), 77.8 (1C, s), 115.5 (1C, s), 126.7 (1C, s), 128.4 (1C, s), 129.3 (1C, s), 131.3 (1C, s), 155.5 (1C, s), 159.7 (1C, s), and 170.2 (1C, s).

(v) Compound 5: Methyl ester of 3-(3-fluorophenyl)-2-isoxazoline carboxylic acid. The compound has a yield of 86% and a melting point between 165 and 167°C. The IR spectrum (KBr, cm^{-1}) shows peaks at 3107, 3096 (C-H aromatic), 1802, 1263 (COO), 1653 (C = N), and 1607, 1509 (C = C aromatic). The UV spectrum (EtOH, λ_{max}, nm) is 273. The ^{1}H NMR shows the following shifts: δ 2.92 (2H, dd, J = 15.5, 7.4 Hz), 3.75 (3H, s), 5.28 (1H, dd, J = 7.9, 6.8 Hz), 7.04 – 7.27 (2H, 7.10 [ddd, J = 8.1, 1.4, 1.2 Hz], 7.22

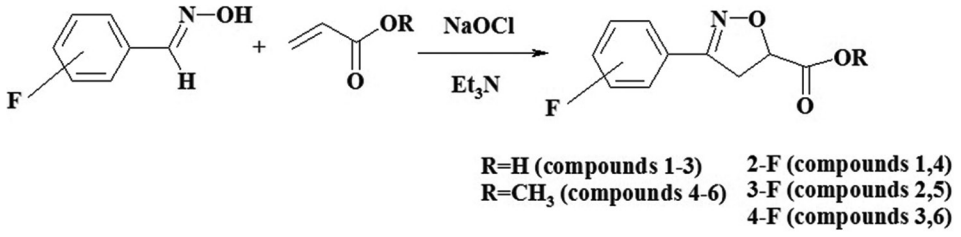

Figure 1. Synthesis of the compounds

[ddd, J = 1.7, 1.4, 0.5 Hz]), 7.45 (1H, ddd, J = 8.1, 7.7, 0.5 Hz), and 7.64 (1H, ddd, J = 7.7, 1.7, 1.2 Hz). ^{13}C NMR: δ 41.8 (1C, s), 52.2 (1C, s), 77.8 (1C, s), 115.0 – 115.1 (2C, 115.0 (s), 115.1 (s)), 127.3 (1C, s), 130.2 (1C, s), 132.1 (1C, s), 155.7 (1C, s), 161.2 (1C, s), and 170.2 (1C, s).

(vi) Compound 6: Methyl ester of 3-(4-fluorophenyl)-2-isoxazoline carboxylic acid. The compound has a yield of 84% and a melting point between 171 and 173°C. The IR spectrum (KBr, cm^{-1}) shows the following peaks: 3101, 3092 (C-H aromatic), 1806, 1263 (COO), 1651 (C = N), and 1603, 1507 (C = C aromatic). The UV spectrum (EtOH, λ_{max}, nm) is 271. The ^{1}H NMR shows the following: δ 2.94 (2H, dd, J = 15.5, 7.4 Hz), 3.75 (3H, s), 5.27 (1H, dd, J = 7.9, 6.8 Hz), 7.04 (2H, ddd, J = 8.7, 1.0, 0.6 Hz), and 7.93 (2H, ddd, J = 8.7, 1.6, 0.6 Hz). The ^{13}C NMR shows δ 41.8 (1C, s), 52.2 (1C, s), 77.8 (1C, s), 115.4 (2C, s), 125.3 (1C, s), 128.6 (2C, s), 155.7 (1C, s), 162.5 (1C, s), and 170.2 (1C, s).

2.2. Light transmission method

To assess platelet aggregation in our study, we used a Solar 2111 aggregometer (Solar, Republic of Belarus), which allows monitoring platelet aggregation using the light transmission method. This technique is based on the change in light transmission in the sample when platelets aggregate and form larger structures, leading to a decrease in the light intensity passing through the sample. The experiment used 480 µL of platelet-rich plasma (PRP) with a concentration of 200 × 10^9 platelets per liter. In the reaction vessel, the plasma was pre-incubated with 20 µL of physiological saline, which served as a control sample, and with the test substance. After 3 min of incubation, 20 µL of ADP solution with a concentration of 8 µM was added to the mixture. ADP is a potent activator of platelet aggregation, and its addition initiated the aggregation process, which was then measured for 6 min.

2.3. Flow cytometry method

The ability to inhibit platelet aggregation was studied using flow cytometry according to the method proposed by Vinholt *et al.*[11] A solution of ADP (final concentration 12 µmol/L) and the corresponding synthesized substance in 10 µL of dimethyl sulfoxide (DMSO) was added to 100 µL of PRP, prepared with the integrity PRP Kit (PRP-62621) (Integrity PRP, United States). A control sample was prepared by adding 10 µL of DMSO without the test compound to PRP. The activation of platelets by ADP induces conformational changes in glycoprotein (GP) IIa/IIIb receptors, which are responsible for further aggregation. Samples of PRP with added effectors were kept at room temperature for 15 min, followed by the addition of labeled antibodies: CD41a-fluorescein isothiocyanate (FITC) and CD61-phycoerythrin (PE). Further analysis of platelet surface markers GPIIa (CD41a) and GPIIIb (CD61) was performed using a flow cytometer Perlong FC2060 (Perlong Medical Equipment, China). The gating strategy was based on determining the number of double positive ($CD41a^+$ $CD61^+$) cells on the cytogram. Methyl ester of (+)-(S)-alpha-(o-chlorophenyl)-6,7-dihydrothieno[3.2-c]pyridine-5(4H)-acetic acid (Clopidogrel), which is currently used as an antiplatelet agent (final concentration 5 and 10 mmol/L, respectively) was used as a positive control.

2.4. Statistical analysis

To ensure the reliability of the results, all measurements were performed in triplicate, which eliminated random errors and increased the reliability of the data. The platelet aggregation results were determined as the maximum amplitude expressed as a percentage. This indicator was calculated using specialized software (version 2.1, MedCalc) that analyzed the data obtained during the experiment. Inhibition of maximum platelet aggregation was estimated as a percentage compared to the control, which made it possible to determine to what extent the test substance affected aggregation compared to saline. The data were expressed as mean ± standard error of the mean.

3. Results and discussion

All the studied compounds showed the ability to suppress the aggregation ability of platelets. Increasing the concentration of the substance from 1 to 25 mmol/L led to an increase in the inhibitory effect of the compounds. We studied the ability of the obtained compounds to inhibit platelet aggregation in two ways. The first is the classical method of determining the ability of platelets to aggregate using the light transmission method (Figure 2).[11]

The second method was based on flow cytometry. Specific GP receptors GPIIa/IIIb expressed on the platelet surface are known to be involved in platelet aggregation.[5]

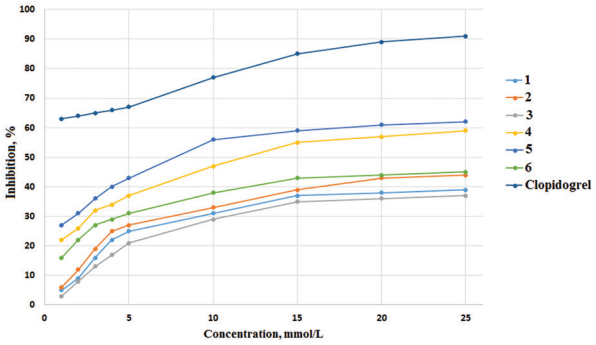

Figure 2. Inhibition of platelet aggregation (light transmission method)

The activation of platelets by adding ADP leads to a change in the conformation of membrane receptors, and GPIIa/IIIb is responsible for further aggregation. Samples of PRPR with added effectors were kept at room temperature, followed by an addition of a solution of labeled antibodies CD41a-FITC (antibodies to the GPIIa receptor) and CD61-PE (antibodies to the GPIIIb receptor). Subsequently, an analysis was performed, and the number of double-positive cells ($CD41a^+$ $CD61^+$) was counted and compared with the number of the same cells in the control sample, which did not contain any inhibitors. The obtained data on the ability to inhibit platelet aggregation is shown in Figure 3.

A comparison of both methods based on the graphs obtained for the dependence of the inhibition capacity indicates the similarity of the results obtained. It should be noted that methyl esters, compared to substances with a free carboxyl group, showed a stronger ability to suppress the transition of platelet GPIIa/IIIb receptors to an active state, in which they are then able to bind to fibrinogen and, subsequently, undergo further aggregation. This is evident from the position of the inhibition curves in the graphs in Figures 2 and 3. Noticeably, at a concentration of 1 mmol/L of the studied compounds, the degree of inhibition is 15 – 27% and gradually increases thereafter. Unlike methyl esters 4 – 6, compounds with a free carboxyl group at a concentration of 1 mmol/L exhibit the ability to inhibit platelet aggregation in the 5 – 7% range. A further increase in concentration also leads to an improvement in the ability to suppress platelet fusion. However, the growth is more gradual, and even at a concentration of 25 mmol/L, it does not reach 50%.

A comparison with the currently used antiplatelet agent clopidogrel indicates the need for further research into new compounds, which may result in modifying the aromatic substituent in the structure of new substances. The activity of compounds containing the isoxazole ring[7] turned out to be higher (≥60%) than the inhibitory capacity of the compounds synthesized in this study. A comparison of our results with other compounds containing a similar heterocycle[6] showed a relatively equal ability to inhibit platelet aggregation. The degree of inhibition of the compounds we obtained was 21 – 43% at 5 mmol/L and 29 – 56% at 10 mmol/L. The inhibitory ability of the previous compounds was in the range of 35 – 65% at a concentration of 4.4 – 4.5 mmol/L.

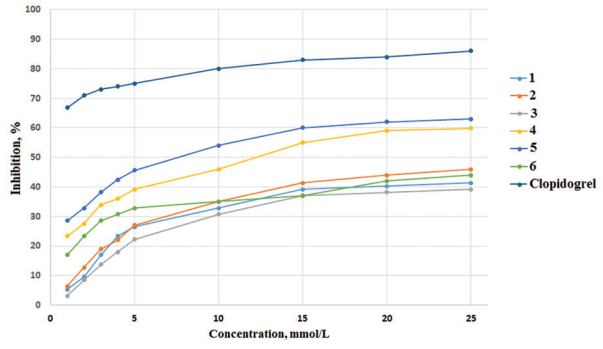

Figure 3. Inhibition of platelet aggregation (flow cytometry method)

While the simplicity of the obtained compounds may not suggest the presence of exceptional properties in platelet aggregation, we believe the data hold significant value. They provide insights into the establishment of a "structure-properties" relationship in the obtained compounds.

4. Conclusion

It has been established that 3-aryl-2-isoxazoline-5-carboxylic acids and their methyl esters containing one fluorine atom in the aryl group effectively suppress the activation of platelet receptors GPIIa/IIIb. This opens up prospects for using these compounds as synthetic fragments in designing the structure and synthesis of new antiplatelet agents. Ongoing research focuses on synthesizing new derivatives of 2-isoxazoline, particularly those incorporating an N-substituted amide group in position 5 of the heterocyclic fragment. The results of this work indicate that fluorine atoms located in the ortho- and meta-positions of the aromatic substituent (compounds 4 and 5) are more effective than fluorine in the para-position. The current efforts are directed toward synthesizing compounds with this arrangement of substituents, with results to be reported in the future.

Acknowledgments

None.

Funding

The work was carried out with financial support from the Ministry of Health of the Republic of Belarus, grant 2.2.2/20240516.

Conflict of interest

The authors declare that they have no competing interests.

Author contributions

Conceptualization: Mikalai M. Kauhanka, Marharita E. Parkhach

Investigation: Mikalai M. Kauhanka, Marharita E.Parkhach, Svetlana N. Borisevich,
Stanislava V. Glinnik, Elena N. Haluk

Methodology: Mikalai M. Kauhanka

Writing – original draft: Mikalai M. Kauhanka, Svetlana N. Borisevich, Stanislava V. Glinnik

Writing – review & editing: Mikalai M. Kauhanka, Marharita E.Parkhach

Ethics approval and consent to participate

This research involved the use of platelet-rich plasma from healthy donors. All donors gave written voluntary consent to participate in the study.

Consent for publication

Donors consented to the publication of their data.

Availability of data

Data will be made available upon request to the corresponding author.

References

1. Jennings LK. Mechanisms of platelet activation: Need for new strategies to protect against platelet-mediated atherothrombosis. *Thromb Haemost*. 2009;102(2):248-257.

   doi: 10.1160/TH09-03-0192

2. Angiolillo DJ, Capodanno D, Goto, S. Platelet thrombin receptor antagonism and atherothrombosis. *Eur Heart J*. 2010;31(1):17-28.

   doi: 10.1093/eurheartj/ehp504

3. Fuentes QE, Fuentes QF, Andrés V, Pello OM, Font de Mora J, Palomo GI. Role of platelets as mediators that link inflammation and thrombosis in atherosclerosis. *Platelets*. 2013;24(4):255-262.

   doi: 10.3109/09537104.2012.690113

4. Viallard JF, Solanilla A, Gauthier B, *et al*. Increased soluble and platelet-associated CD40 ligand in essential thrombocythemia and reactive thrombocytosis. *Blood*. 2002;99(7):2612-2614.

   doi: 10.1182/blood.v99.7.2612

5. Ruggeri ZM. Mechanisms initiating platelet thrombus formation. *Thromb Haemost*. 1997;78(1):611-616.

   doi: 10.1055/s-0038-1657598

6. Gutiérrez M, Amigo J, Fuentes E, Palomo I, Astudillo L. Synthetic isoxazole as antiplatelet agent. *Platelets*. 2014;25(4):234-238.

   doi: 10.3109/09537104.2013.807335

7. Xue CB, Roderick J, Mousa S, Olson RE, DeGrado WF. Synthesis and antiplatelet effects of an isoxazole series of glycoprotein IIb/IIIa antagonists. *Bioorg Med Chem Lett*. 1998;8(24):3499-3504.

   doi: 10.1016/s0960-894x(98)00637-4

8. Yogesh W, Pravin M, Pramod K. Application, reactivity and synthesis of isoxazole derivatives. *Mini-Rev Org Chem*. 2021;18(1):55-77.

   doi: 10.2174/1570193x17999200511131621

9. Shanshan L, Yiou M, Luchen J, Xueyan Y, Wei Z, Yunfei D. Oxazole and isoxazole-containing pharmaceuticals: Targets, pharmacological activities, and their SAR studies. *RSC Med Chem*. 2025;16(4):1461-1469.

   doi: 10.1039/D4MD00777H

10. Mohan K, Vikul K, Meenakshi S. A review of isoxazole biological activity and present synthetic techniques. *Int J Pharm Chem Anal*. 2024;11(4):307-317.

    doi: 10.18231/j.ijpca.2024.045

11. Vinholt PJ, Frederiksen H, Hvas AM, Sprogøe U, Nielsen, C. Measurement of platelet aggregation, independently of patient platelet count: A flow-cytometric approach. *J Thromb Haemost*. 2017;15(6):1191-1202.

    doi: 10.1111/jth.13675

Our Journals

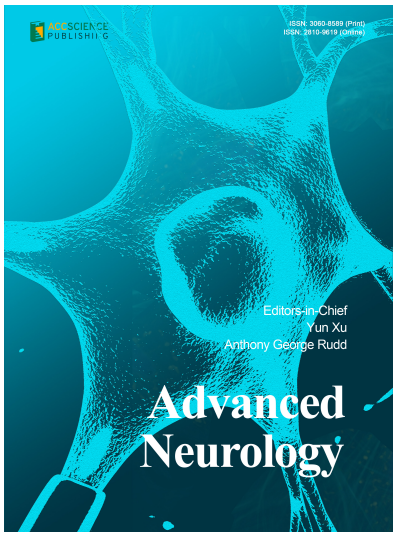

Advanced Neurology is a peer-reviewed and open-access journal that aims to publish and disseminate novel research in the breadth of neurology and neuroscience. The journal aims to advance our understanding in the nervous system and provide a platform to neuroscientists and physicians to showcase their findings in original fundamental and clinical research as well as to present new ideas that highlight the changes in the neurological clinical practice.

Advanced Neurology covers subject areas, including but not limited to the following:

- Neurological disorders
- Neurodegenerative disease
- Cerebrovascular disease
- Epilepsy and movement disorders
- Neuroimmune disease
- Neurological infections
- Muscle disease
- Molecular and cellular neuroscience
- Systems neuroscience
- Cognitive neuroscience
- Computational modeling of nervous system

Gene & Protein in Disease publishes rigorously peer-reviewed and high quality original articles and authoritative reviews that focus on the latest development in multidisciplinary areas in biology and biomedicine, with an emphasis on gene and protein research. The journal has worldwide authorship, and a broad scope in basic and translational biomedical research of genetics, biochemistry, biophysics, oncology, immunology, cell biology, molecular biology, developmental biology, microbiology, neuroscience, stem cell, protein science, structural biology, regenerative medicine and translational medicine.

Start a new journal

Write to us via email if you are interested to start a new journal with AccScience Publishing. Please attach your CV, professional profile page and a brief pitch proposal in your email. We shall inform you of our decision whether we are interested to collaborate in starting a new journal.

Contact: info@accscience.com

https://accscience.com/journal/GTM

Contact
www.accscience.com
9 Raffles Place, Republic Plaza 1 #06-00 Singapore 048619
Email: editorial@accscience.com
Phone: +65 8182 1586